Faculty of Mechanical Engineering

Departamnent of Mechanical Machines, Equipments and Transportations

HABILITATION THESIS

-PhD Domain: Mechanical Engineering-

Conf.univ.dr.ing. Adrian Ciprian STUPARU

Timișoara

-2021-

Faculty of Mechanical Engineering

Departamnent of Mechanical Machines, Equipments and Transportations

-Habilitation thesis-

Research in the domain of turbomachines hydrodynamics

Author: Conf.univ.dr.ing. Adrian Ciprian STUPARU

Timișoara

-2021-

Contents

Abstract

In the year 2009 I publicly defended my PhD thesis entitled „Numerical and experimental modelling of the flow in the centrifugal pumps” under the coordination of acad.prof.dr.ing. Ioan ANTON, being one of the first PhD thesis from Romania in which is investigated, with the help of numerical simulation, the complex flow from the impellers of large power pumps.

In the year 2003 I was starting my university career at Politehnica University Timisoara, Faculty of Mechanical Engineering, department of Hydraulic Machines, initially as a university preparator and starting from the year 2005 as a university assistant. In the year 2012 I promoted as a lecturer and starting from the year 2017 I have the position of associated professor. Along my university career, alongside my colleagues, I published 3 support books for my courses, 3 support books for the seminars and laboratories and I was involved in the activity for modernizing the Laboratory of Fluid Mechanics, the Laboratory of Hydraulic Machines and the Laboratory of Numerical Simulation. The courses that I taught, eight in number, were with a specific for the domain of Mechanical Engineering, *Hydraulic and Pneumatic Machines and Systems*, bachelor engineer degree, and *Hydrodynamics of Machines and Hydromechanical Systems*, master’s degree.

I have coordinated more than 50 bachelor and master thesis, as single coordinator or together with other colleagues. Starting from the year 2011 I am one of the coordinators of the Practice activity of the students from the 3rd year of the domain Mechanical Engineering. Another component of my activity was to attract students to attend our bachelor’s degree of *Hydraulic and Pneumatic Machines and Systems* and our master’s degree of *Hydrodynamics of Machines and Hydromechanical Systems*. For doing this I organised study trips to a number of hydropower plants (Iron Gates 1, Iron Gates 2, Baile Herculane, Raul Mare-Retezat) and I had direct discussion with the students emphasising the useful things they would learn if they would attend our two specializations and so they would be able to get hired as engineers in the companies from Romania and abroad.

Since I defend my PhD thesis I participated, as a manger or member of the research team, to the implementation of 4 research grants and 9 research contracts with industrial partners. After the progress of this type of research activity I published 23 research papers that were presented at international conferences or were published in international journals, 18 of them being indexed in international data bases ISI and SCOPUS.

For my professional and academic activity, I will continue to update other courses and to upgrade the laboratories.

I will continue to attract research funding by applying to the research competitions and I will extend my collaboration with the companies that are acting in my domain of research. The results of my future research I will publish them in international journals and present them at international conferences.

All my academic, professional and scientific experience and the research infrastructure that I developed I will employ in the activity that I will carry out with my PhD students. I will seek that the research themes that I will propose to be part of research

subjects of some research grants or research contracts, so that the practical component of the PhD student's research activity to be significant and to ensure a supplementary income.

Rezumat

În anul 2009 am susținut public teza de doctorat intitulată „Modelarea numerică și experimentală a curgerii în pompele centrifuge" sub conducerea domnului acad.prof.dr.ing. Ioan ANTON, fiind una din primele teze de doctorat din România care au investigat curgerea complexă din interiorul rotoarelor de pompe de mare putere cu ajutorul simulării numerice.

În anul 2003 îmi începeam cariera universitară la Universitatea Politehnica Timișoara, Facultatea de Mecanică, catedra de Mașini Hidraulice, ocupând inițial poziția de preparator universitar și apoi în anul 2005 pe cea de asistent universitar. În anul 2012 am promovat pe poziția de șef de lucrări, iar din anul 2017 ocup poziția de conferențiar universitar. De-a lungul carierei universitare împreună cu colegii din catedră am redactat un număr de 3 manuale suport pentru cursuri, 3 manuale suport pentru activitatea practică de laborator și seminar și am participat la modernizarea Laboratorului de Mecanica fluidelor, a Laboratorului de Mașini hidraulice și a Laboratorului de Simulare numerică. Materiile predate de-a lungul timpului, în număr de opt, au fost cele specifice domeniului de Inginerie mecanică, specializarea *Mașini și Sisteme Hidraulice și Pneumatice*, respectiv specializării de master *Hidrodinamica Mașinilor Sistemelor Hidromecanice*.

Am coordonat peste 50 de lucrări de licență și disertație fie singur, fie în colaborare cu alți colegi. De asemenea, începând cu anul 2011, mă ocup de coordonarea activității de Practică a studenților. O altă coordonată a activității didactice a fost atragerea studenților la specializarea de licență *Mașini și Sisteme Hidraulice și Pneumatice* și la cea de master *Hidrodinamica Mașinilor și Sistemelor Hidromecanice.* Acest lucru l-am realizat prin excursii de studiu la hidrocentralele (Porțile de Fier 1, Porțile de Fier 2, Băile Herculane, Râul Mare-Retezat) și prin discuții directe în care am evidențiat lucrurile utile care le vor învăța în cadrul celor două specializări și care astfel le vor asigura accesul la o poziție de inginer în companiile din România și străinătate.

După susținerea tezei de doctorat am participat, ca manager sau membru al echipei de cercetare, la derularea a peste 4granturi de cercetare și peste 9 de contracte de cercetare cu industria. În urma derulării acestei activități de cercetare științifică am publicat un număr de 23 de articole științifice prezentate la conferințe internaționale sau publicate în jurnale internaționale, 18 fiind indexate în bazele de date internaționale ISI și SCOPUS.

Pentru dezvoltarea activității mele profesionale și didactice voi continua să îmbunătățesc materialul cursurilor ce le voi preda și voi continua modernizarea laboratoarelor.

Voi continua să atrag fonduri de cercetare prin aplicarea la competițiile de cercetare și voi intensifica colaborarea cu firmele ce își desfășoară activitatea în domeniul meu de cercetare. Rezultatele ce le voi obține din activitatea de cercetare le voi publica în jurnale internaționale și le voi prezenta în cadrul conferințelor internaționale la care voi participa.

Toată această experiență acumulată și infrastructură de cercetare dezvoltată o voi folosi în activitatea ce o voi desfășură cu viitorii studenți doctoranzi. Voi căuta ca temele de cercetare propuse să fie parte a unor subiecte de cercetare ale unor granturi de cercetare sau

contracte de cercetare, astfel încât componenta practică a activității de cercetare a doctorandului să fie semnificativă și să poată asigura chiar și un venit suplimentar.

1. Overview of the author's professional, academic and scientific achievements

1.1. Professional and academic achievements

In the year 2009 I defended my PhD thesis „Numerical and experimental modelling of the flow in the centrifugal pumps", [1], under the coordination of acad.prof.dr.ing. Ioan ANTON. It was one of the first PhD thesis in Romania that investigated the flow phenomena in a storage centrifugal pump with the help of numerical simulation software ANSYS Fluent. The results obtained in my thesis permitted to identify the causes of the poor operation of the storage pump: cavitation generated by the particular shape of the inlet section of the pump.

In the following years, a number of PhD thesis under the coordination of prof.dr.ing. Liviu ANTON, prof.dr.ing. Romeo SUSAN-RESIGA and CS I.dr.ing. Sebastian MUNTEAN, continued the investigations started by my thesis and developed several solutions for a better operation of similar storage pump: a couple of new designed impellers, a new designed inducer, an optimised shape of the inlet section of the pump.

I started my university career at the Politehnica University Timisoara, Faculty of Mechanical Engineering, department of Hydraulic Machines in the year 2003 as university preparator and in the year 2005 I was promoted to the position of university assistant. The main professional achievements, after defending my PhD thesis, represent the promotion to the position of lecturer in the year 2012 and to the current position of associated professor, in the year 2017.

During the period of 2009-2021 my teaching activity included the following study subjects:

- Pumps and fans,
- Numerical simulations in hydraulic machines and equipment,
- Hydrodynamics,
- Fluid mechanics and hydraulic machines (including teaching activity in English language),
- Numerical methods for heat and fluid flow,
- Numerical optimisation of the turbomachines design,
- Real time monitoring and measurement of hydrodynamic data,
- Hydraulic turbines.

In order to offer a support for the students who attends my lectures, together with colleagues from Politehnica University Timisoara, I published several books:

- Stuparu Adrian Ciprian, Bosioc Alin, *Pompe centrifuge*, Editura Politehnica, 2021, [2],
- Stuparu Adrian Ciprian, Anton Liviu, *Hidrodinamica*, Editura Orizonturi universitare, Timișoara, 2018, [3],

All the above-mentioned books were written with the intention to increase the interest of students for this study subjects and to allow the students to easily understand the theoretical and practical concepts presented. All the books are available in physical format in a sufficient number at the library of the university and they are also available in electronic format on the Virtual Campus, so that they are very easy to access by the students.

Since the year of 2005 I begun coordinating bachelor's degree thesis and starting from 2012 I also coordinated master's degree thesis. After defending my PhD thesis, I coordinated, alone or together with other colleagues, a number of 37 bachelor's thesis and a number of 24 master's thesis. The thesis covers a wide range of subjects from the domain of fluid mechanics and hydraulic machines:

- Designing of the blades of the impellers of pumps,
- Designing of the blades of the rotors of turbines,
- Experimental measurements concerning operation of centrifugal pumps,
- Experimental measurements concerning operation of an inducer,
- Experimental investigations of methods for measuring the flow rate,
- Experimental investigations of local hydraulic losses,
- Numerical investigations of the flow in a cascade of hydrodynamic profiles,
- Numerical investigation of the flow and thermal performance of a cooling device.

Starting from 2009 I also was offering guidance and support for the research performed by a number of 10 PhD students who were preparing their thesis under the coordination of prof.univ.dr.ing. Liviu ANTON and prof.univ.dr.ing. Romeo SUSAN-RESIGA. I was member of the guidance committee for five PhD students who are coordinated by the above-mentioned professors. The PhD thesis covers the following research subjects:

- Numerical and experimental investigations of large centrifugal pumps
- Numerical investigations of the flow in the draft tube of a Francis turbine
- Numerical and experimental investigation of the floe with thermal transfer for cooling down electronic components from automotive industry

Prof.univ.dr.ing. Liviu ANTON has implemented two grants of 15.000 USD and 160.804 EUR, „Modernizarea și dezvoltarea învățării Mecanicii fluidelor și Hidraulicii", for the modernisation of the Fluid Mechanics laboratory, where I, together with prof.dr.ing. Alexandru BAYA, participated to the commissioning of the following equipment from the laboratory:

- Multifunctional test rig for determining the operating curves of a centrifugal pump,
- Test rig for flow rate measurements,
- Test rig for flow through orifices and nozzles,
- Test rig for the Bernoulli equation,
- Test rig for determining local hydraulic losses,
- Test rig for the study of the operation of an axial turbine,
- Test rig for the study of the operation of an axial fan,

- Test rig for determining the operation curves of a centrifugal pump
- Test rig for the study of the operation of two pumps coupled in series or parallel,
- Test rig for the study of the operation of a Pelton turbine.

Starting from that period I was designated to take care of the good operation of all the experimental test rigs from the Fluid Mechanics laboratory.

Prof.univ.dr.ing. Liviu ANTON also purchased a very performant and rare equipment, based on the thermodynamic method, for determining the efficiency of hydraulic machines. I was designated, together with prof.univ.dr.ing. Alexandru BAYA, for the commissioning of this equipment.

For increasing the high-performance measuring equipment available in our laboratory, I purchased in the year 2017 a portable ultrasonic flow rate meter manufactured by FLUXUS company.

I also participate to the modernisation of three laboratories for numerical simulation. My task was to ensure that all 50 computers are operating and have the appropriate software installed. Still today I ensure the functionality of all the computers from the three laboratories.

I was member of the implementation team for 4 POSDRU grants that aim to improve the knowledge of the students in the domain of Fluid Mechanics and to improve the method for the practice sessions of students.

From 2010 to 2013 I was a member of the team that implemented the project "*Fluid Engineering Informatics Platform Project*" (i.e., PiiF Project) that was developed in Romania, within the ESF Sectoral Operational Programme Human Resources Development 2007-2013. It started in September 2010 and ended in August 2013. The purpose of the PiiF Project was to renew and modernize the Romanian education system dealing with Fluid Engineering. This objective was achieved by a collaborative effort performed by 7 departments, each having different names from the Fluid Engineering field, coming from 6 Romanian technical universities, namely: the Technical University of Civil Engineering Bucharest (PiiF Project Coordinator), University "Politehnica" of Bucharest, Politehnica University of Timisoara, Technical University of Cluj-Napoca, "Dunarea de Jos" University Galati, and "Gheorghe Asachi" Technical University of Iasi.

The PiiF web-based platform was mainly composed of four databases linked together in order to assess the major idea of the project, that is: "basic concepts + correct scientific or engineering logic = solving applications". The four components of the PiiF platform were:

- A database with basic concepts and sample scientific or engineering logic,
- A database with interactive applications of the basic concepts and/or scientific logic,
- A virtual database of significant laboratory experiments,
- A database containing flow visualizations and numerical simulations of flow phenomena.

Each of the partner departments involved in the PiiF project dealt, in addition to general concepts, with the concepts, sample engineering logic, applications, laboratory experiments, flow visualizations and numerical simulations in its own line of expertise. The four databases were linked together so that any teacher to be able to use any of the resources on the platform to build up his own course or to indicate to students a given path through the existing information on the platform.

My role in the project was to develop several basic concepts and to upgrade two laboratory test rigs so that they can be operated remote by students from all the six universities:

- Multifunctional test rig for determining the operation curves of a centrifugal pump and the hydraulic losses coefficients in a pipe system
- Test rig for visualising the piezometric and energetic lines across a pipe network

I wrote the necessary material needed by the students to handle remotely the test rigs and I coordinated a several group of students from the six universities to perform the experimental measurements.

From 2011 to 2016 I was a member of the team that implemented two projects, funded by the European Union, concerning the improvement of the method the students are making their practice:

- THE EUROPEAN SOCIAL FUND, The Sectorial Operational Programme for the Development of Human Resources 2007 – 2013, Priority axis 2 "Lifelong Correlation of Learning with the Labour Market" Major intervention field 2.1. "Transition from School to Active Life" Project title: Transnational Educational Network for Career Guidance, Counseling and Practice Correlated with the Labour Market, in the Society of Knowledge – PRACTICOR, Contract no. POSDRU/90/2.1/S/48816,
- FONDUL SOCIAL EUROPEAN, Investeste in OAMENI!, Programul Operational Sectorial Dezvoltarea Resurselor Umane 2007 – 2013, Axa prioritara 2 "Corelarea invatarii pe tot parcursul vietii cu piata muncii", Domeniul major de interventie 2.1. "Tranzitia de la scoala la viata activa", Titlul proiectului: Parteneriat regional si euro-regional pentru tranzitia spre piata muncii prin consiliere pentru cariera si stagii de practica la angajator - PRACTICOR ® EURO-REGIO, Contract nr. POSDRU/161/2.1/G/132889, cod SMIS: 51563.

One of my tasks in these projects was to coordinate the practice sessions of the students from our Politehnica University Timisoara in the renowned research institute Fraunhofer from Stuttgart, Germany, where I went with three different groups of students, and also in different companies from Timisoara (Continental Automotive, Casa Auto Timișoara, Berg Banat, Azur, MaschinnenTehnich, DosetImpex, Rio Bucovina). Another task was to teach the students how to fill in their CV and how to prepare for a job interview.

In the year 2015 I participated to the project with the title "Cresterea atractivitatii si performantei programelor de formare doctorala si postdoctorala pentru cercetatori in stiinte inginerești - ATRACTING", priority axis 1, „Educația şi formarea profesională în sprijinul creşterii economice şi dezvoltării societății bazate pe cunoaştere", major domain of intervention 1.5, „Programe doctorale şi postdoctorale în sprijinul cercetării”, contract number POSDRU/159/1.5/S/137070 and the beneficiary was Politehnica University Timisoara. During my activity in this project, I developed a material for one of the thematic workshops entitled “AT-18_S-Modern experimental methods in hydrodynamics” and, together with prof.univ.dr.ing. Romeo SUSAN-RESIGA, I presented the material to the students involved in the project.

During this time, I participated abroad to a number of 7 international conferences and workshops where I presented my research results and I kept informed about the recent results obtained by researchers from all over the world in the domain of hydraulic machines:

- International Symposium on Fluid Dynamics associated with the International Conference of Computational Methods in Sciences and Engineering 2019 (ICCMSE’2019), Rhodos, Greece,
- 29th IAHR Symposium on Hydraulic Machinery and Systems, 2018, Kyoto, Japan,
- PROCEEDINGS OF THE INTERNATIONAL CONFERENCE ON NUMERICAL ANALYSIS AND APPLIED MATHEMATICS 2017 (ICNAAM-2017), Salonic, Greece,
- IOP Conference Series: Earth and Environmental Science, Proceeding of 28th IAHR Symposium on Hydraulic Machinery and Systems, 2016, Grenoble, France,
- Cavitation and dynamic problems, Proceedings of the 6th IAHR meeting of the working group, IAHRWG 2015, Ljubljana, Slovenia,
- 10th German-Romanian Workshop on Turbomachinery Hydrodynamics, Stuttgart, Germany, 2014,
- „6th International Conference on Diffusion in Solids and Liquids: Mass Transfer, Heat Transfer and Microstructure and Properties, DSL-2010, Paris, France,

When I attended the 29th IAHR Symposium on Hydraulic Machinery and Systems, 2018, Kyoto, Japan, I was also nominated as a co-chairman to one of the sessions of the conference, Pumps 7, together with the professor Jun Matsui from the Yokohama National University.

Another part of my professional activities consists in being part of the organising team for several conferences and workshops organized by Politehnica University Timisoara:

- 25th IAHR Symposium on Hydraulic Machinery and Systems, 2010,
- Conference „Diaspora în Cercetarea Ştiinţifică şi Învăţământul Superior din România - Diaspora şi prietenii săi”, 2016.

Since 2017 I started to review scientific papers for several conferences and international journals indexed in the Web of Science and Scopus:

- CIEM 2017, 8th International Conference on Energy and Environment, Bucharest, Romania,
- EENVIRO 2018, 5th International Conference on Sustainable Solutions for Energy and Environment, Cluj-Napoca, Romania,
- Facta Universitatis, Series: Mechanical Engineering, University of Nis, Serbia, 2017,
- Energies, MDPI, Basel, Switzerland, ISSN 1996-1073, Impact Factor 3.004,

- Processes, MDPI, Basel, Switzerland, ISSN 2227-9717, Impact Factor 2.847,
- Ocean Engineering, Elsevier, ISSN 0029-8018, Impact Factor 3.795.

My professional activity also contains my involvement as a coordinator in the accreditation process for both specializations managed by our collective:

- 2015, Hydraulic and pneumatic machines and systems, bachelor engineer degree,
- 2019, Hydrodynamics of machines and hydromechanical systems, master's degree.

For this activity I had to collect all the necessary documents from all the professors teaching to both programs and to compose and write the final report and all the annexes.

1.2. Scientific achievements

My scientific area of research is divided in the following main categories:

- Hydraulic pumps,
- Hydraulic turbines,
- Chemical reactors,
- Flow around heated elements.

My scientific research work was carried out as part of numerous grants and contracts with industrial partners. For two of these grants and contracts I was the manager of the research team:

- BRIDGE grant, *Creşterea competitivității COLTERM prin optimizarea tehnologiei de antrenare cu turație variabilă a pompelor centrifuge de termoficare de mare putere*, number 69BG, 2016-2018, UEFISCDI, value 100,000 Euro,
- Research contract, *Determinarea parametrilor de performanță garantați pentru două ansambluri pompă-motor-convertizor de frecvență ce funcționează la CET Centru şi CET Sud*, number 30/18.03.2015, 2015, beneficiary Compania locală de termoficare COLTERM S.A., value 2,050 Euro,

A list of the research grants for which I was a member of the research team is presented next:

- *Free Runner for Swirling Flow Control at the Outlet of Hydraulic Turbines "FreeRunnerFlowContr,* number TE 179/2020, period 2020-2022, UEFISCDI, value 23,460 Euro,
- *Soluție inovatoare de dispozitiv magneto - reologic pentru îmbunătățirea performanțelor pompelor centrifuge, IRheoDev,* number TE-62, period 2015-2017, UEFISCDI, value 121,874 Euro,
- *Instabilități autoinduse ale curgerii cu rotație în turbine hidraulice la regimuri departe de regimul optim*, number PNII-17, period 2013-2016, UEFISCDI, value 327,111 Euro,

A list of the research contracts for which I was a member of the research team is presented next:

- *Servicii expert-asistenta tehnica, emitere rapoarte , participare sedinte de lucru si audieri in cadrul actiunii de arbitraj international ICC22482/MHM*, number 26, period 2020-2021, beneficiary S.C. Hidroelectrica S.A., value 110,000 Euro,
- *Identificarea soluției optime pentru înlocuirea hidroagregatelor de la stația de pompare Cenad*, number 19, period 2018, beneficiary S.C. Emiliana West Rom S.R.L., value 3,053 Euro,
- *Proiectare și verificare a sistemului de agitare din reactor în vederea conversiei instalației DOF în instalație de obținere a DOTP*, number 50, period 2017, beneficiary Oltchim S.A., value 7,761 Euro,
- *Numerical simulation of flow with heat convection and radiation for a dryer heating system in two different configurations*, number 49, period 2012, beneficiary S.C. Zoppas Industries Romania S.R.L., value 4,346 Euro,
- *Cercetări şi experimentări privind îmbunătățirea performanțelor energetice şi cavitaționale ale pompelor PRO 10-195 de la stația de pompe Jidoaia, etapa a II-a*, number BC 119, period 2009, beneficiary S.C. Hidroelectrica S.A., Sucucrsala Râmnicu Vâlcea, value 33,378 Euro,
- *Cercetări şi experimentări privind creşterea performanțelor turbinelor Francis 57.5-128.5 CHE Brădişor, etapa a II-a*, number BC 120, period 2009, beneficiary S.C. Hidroelectrica S.A., Sucursala Râmnicu Vâlcea, value 41,505 Euro,

The scientific results, obtained from the research carried out in the above-mentioned grants and research contracts, were published in scientific papers published in international journals and presented to international conferences:

- Stuparu Adrian Ciprian, Susan-Resiga Romeo, Tanasa Constantin, *CFD Assessment of the Hydrodynamic Performance of Two Impellers for a Baffled Stirred Reactor*, Applied Sciences, Special Issue Application of Computational Fluid Dynamics in Mechanical Engineering/2076-3417, vol. 11 (11), 2021, pp. 13, impact factor 2.679, [7],
- Stuparu Adrian Ciprian, Susan-Resiga Romeo, Bosioc Alin, *Improving the Homogenization of the Liquid-Solid Mixture Using a Tandem of Impellers in a Baffled Industrial Reactor*, Applied Sciences, Special Issue Application of Computational Fluid Dynamics in Mechanical Engineering/2076-3417, vol. 11 (12), 2021 , pp.11, impact factor 2.679, [8],
- Stuparu Adrian Ciprian, Susan-Resiga Romeo, Bosioc Alin, *CFD Simulation of Solid Suspension for a Liquid–Solid Industrial Stirred Reactor,* Applied Sciences, Special Issue Application of Computational Fluid Dynamics in Mechanical Engineering/2076-3417, vol. 11 (12), 2021, pp. 15, impact factor 2.679, [9],
- Stuparu Adrian Ciprian, Alexandru Baya, Alin Bosioc, Liviu Anton, Daniel Mos, *Experimental investigation of a pumping station from CET power plant Timisoara*, IOP Conference Series: Earth and Environmental Science, Proceeding of 29th IAHR Symposium on Hydraulic Machinery and Systems/1755-1307, vol. 240, 2019, pp. 10, [10],
- Stuparu Adrian Ciprian, Alexandru Baya, Alin Bosioc, Liviu Anton, Daniel Mos, *Modelling the operation curves of two similar high power centrifugal pumps,*

PROCEEDINGS OF THE INTERNATIONAL CONFERENCE ON NUMERICAL ANALYSIS AND APPLIED MATHEMATICS 2017 (ICNAAM-2017)/0094-243X, vol. 1978, 2018, pp. 4, [11],

- Stuparu Adrian Ciprian, Susan-Resiga Romeo, *The Complex Dynamics of the Precessing Vortex Rope in a Straight Diffuser*, IOP Conference Series: Earth and Environmental Science, Proceeding of 28th IAHR Symposium on Hydraulic Machinery and Systems/1755-1307, vol. 49, 2016, pp. 10, [12],
- Stuparu Adrian Ciprian, Sorin Holotescu, *Influence of Geometry on the Position and the Intensity of Maximum Kinetic Energy in a Combustion Chamber*, Defect and Diffusion Forum, Diffusion in Solids and Liquids VI/1012-0386, vol. 312-315, 2011, pp. 6 (725-730), [13],
- Stuparu Adrian Ciprian, Sorin Holotescu, *Numerical simulation of the 3D unsteady turbulent flow in a combustion chamber*, Central European Journal of Engineering/1896-1541, vol. 1 (2), 2011, pp. 6 (189-194), [14],
- Stuparu Adrian Ciprian, Susan-Resiga Romeo, Anton Liviu, Muntean Sebastian, *Numerical investigation of the cavitational behaviour into a storage pump operating at off design operating points*, IOP Conference Series: Earth and Environmental Science, Proceedings of the 25th IAHR Symposium on Hydraulic Machinery and Systems/1755-1307, vol. 12(1), 2010, pp. 10, [15],
- Romeo Susan-Resiga, Popescu Constantin, Szakal Raul, Sebastian Muntean, Stuparu Adrian Ciprian, *A benchmark test case for swirling flows: design of the swirl apparatus, experimental data, and numerical challenges,* IOP Conference Series: Earth and Environmental Science, Proceeding of 29th IAHR Symposium on Hydraulic Machinery and Systems/1755-1307, vol. 240, 2019, pp. 10, [16],
- Romeo Susan-Resiga, Sebastian Muntean, Stuparu Adrian Ciprian, Alin Bosioc, Constantin Tanasa, Cosmin Ighişan, *A variational model for swirling flow states with stagnant region*, European Journal of Mechanics B-Fluids/0997-7546, vol. 55, 2016, pp. 12 (104-115), impact factor 1.418, [17],
- Constantin Tanasa, Romeo Susan-Resiga, Sebastian Muntean, Stuparu Adrian Ciprian, Alin Bosioc, Tiberiu Ciocan, *Numerical Assessment of a Novel Concept for Mitigating the Unsteady Pressure Pulsations Associated to Decelerating Swirling Flow with Precessing Helical Vortex*, International Conference of Computational Methods in Science and Enginnering, AIP Conference Proceedings/0094-243X, vol. 1702, 2015, pp. 4, [18],
- Susan-Resiga Romeo, Muntean Sebastian, Bosioc Alin, Stuparu Adrian Ciprian, *Stabilisation of the swirl exiting a Francis runner far from the best efficiency point*, IOP Conference Series: Earth and Environmental Science, Proceeding of 30th IAHR Symposium on Hydraulic Machinery and Systems/1755-1307, vol. 774(1), 2021, pp. 9, [19],
- Nemet Octavian, Stuparu Adrian Ciprian, Susan-Resiga Romeo, *Design and optimization of an axial expension turbine for energy recovery*, Proceedings of the 9th

International Conference on Energy and Environment 2019/978-1-7281-1532-0, 2019, pp. 5, [20],
- Tănasă Constantin, Stuparu Adrian Ciprian, Bosioc Alin, Susan-Resiga Romeo, *Numerical Analysis of Pulsating Water Jet Method for Mitigating the Vortex Rope,* Proceedings of the 9th International Conference on Energy and Environment 2019/978-1-7281-1532-0, 2019, pp. 6, [21],
- Tănasă Constantin, Stuparu Adrian Ciprian, Stroiță Cătălin, Popescu Constantin, Susan-Resiga Romeo, *3D Numerical Analysis of Pulsating Water Jet in the Draft Tube Cone of Hydraulic Machinery,* PROCEEDINGS OF THE INTERNATIONAL CONFERENCE OF COMPUTATIONAL METHODS IN SCIENCES AND ENGINEERING 2019 (ICCMSE-2019)/978-0-7534-1933-9, vol. 2186, 2019, pp. 4, [22],
- Romeo Susan-Resiga, Sebastian Muntean, Stuparu Adrian Ciprian, *Francis turbine with tandem runners: a proof of concept*, IOP Conference Series: Earth and Environmental Science, Proceeding of 29th IAHR Symposium on Hydraulic Machinery and Systems/1755-1307, vol. 240, 2019, pp. 8, [23],
- Alin I. Bosioc, Stuparu Adrian Ciprian, Romeo Susan-Resiga, *Numerical Analysis of Temperature and Torque in A Magneto-Rheological Clutch*, PROCEEDINGS OF THE INTERNATIONAL CONFERENCE ON NUMERICAL ANALYSIS AND APPLIED MATHEMATICS 2016 (ICNAAM-2016)/0094-243X, vol. 1863(1), 2017, pp. 4, [24].

The research work conducted also to one international patent:
- Susan-Resiga Romeo Florin, Tanasa Constantin, Bosioc Alin Ilie, Ciocan Tiberiu, Stuparu Adrian Ciprian, Muntean Sebastian, *Method and equipment for controlling the swirling flow through the conical diffuser of hydraulic turbines*, 2017.

1.2.1. Scientific achievements in the domain of hydraulic pumps

A first paper that I published together with other colleagues, was in the International Journal of Fluid Machinery and Systems, which at that time was not indexed in the Web of Science or Scopus database, but shortly after was indexed in the Scopus data base. The results presented in this paper generated a large number of citations, [25].

The paper presents a new method for the analysis of the cavitation behaviour of hydraulic turbomachines. This new method allows determining the coefficient of the cavitation inception and the cavitation sensitivity of the turbomachines. By plotting in semi-logarithmic coordinates, the vapour volume versus the cavitation coefficient, we show that all numerical data collapse in an exponential manner. By analysis of the slope of the curve describing the evolution of the vapour volume against the cavitation coefficient we determine the cavitation sensitivity of the pump for each operating point. The computational domain includes the impeller of the first stage of the storage pump. For the numerical investigation only one inter-blade channel is used because of the symmetry of the geometry:

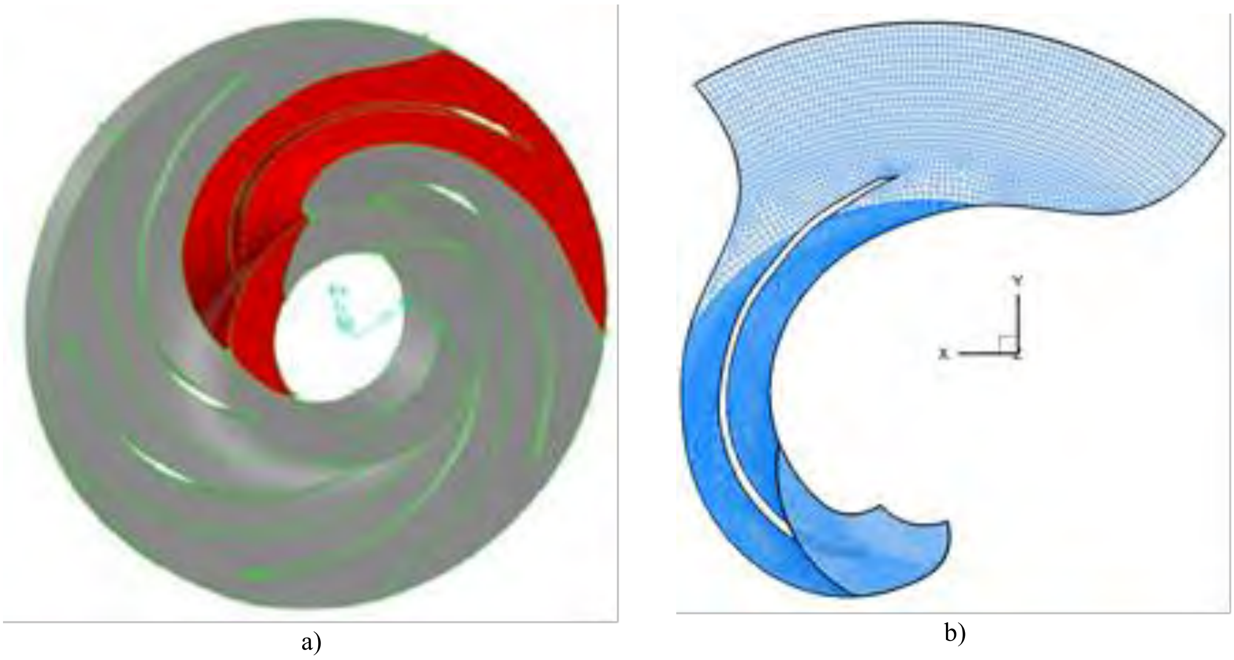

Figure 1. a) Impeller of the storage pump with highlighted inter blade channel, b) Mesh generated on the 3D computational domain of the inter-blade channel, [25].

We found that the connection between the relative volume of vapour, representing the ratio between the volume of vapour from the inter-blade channel and the volume of the inter-blade channel, and the flow rate is given by the following equation:

$$\frac{V_V}{V} = A \cdot e^{B \cdot \sigma_{inst}}, \quad V = 0.010417187\ m^3 \qquad (1)$$

where A, B are two coefficients specific for every operating point. According to our new approach, the interdependency between the relative volume of vapour and the flow rate can be represented using a semi-logarithmic plot, meaning that on the 0Y axis we represent $ln\left(\frac{V_V}{V}\right)$, but the values on the axis of the plot are in fact the value of the $\frac{V_V}{V}$. From the numerical simulation of the multiphase flow for the 5 operating points of the first stage of the storage pump we obtained the following results describing the variation of the relative volume of vapour as a function of the cavitation number of the installation for a single inter-blade channel:

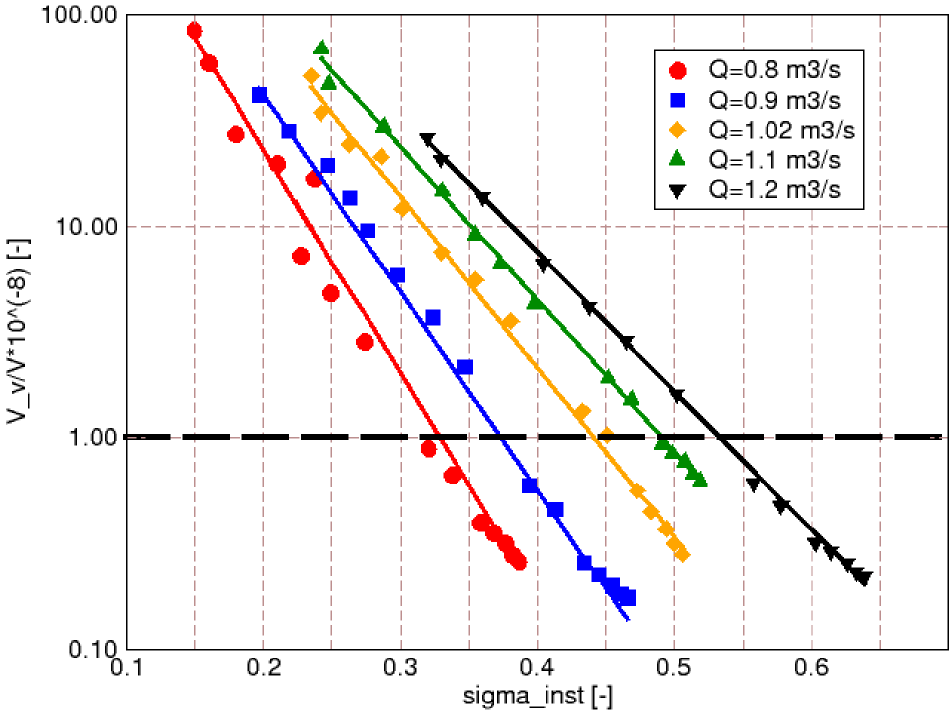

Figure 2. Variation of the volume of vapour against the cavitation number for the investigated operating points, [25].

In order to determine the cavitation inception coefficient, it was considered that the relative volume of vapour of 10^{-8} corresponds to the volume of the first bubble, so the cavitation coefficient corresponding to this value of the relative volume of vapour represents the cavitation inception coefficient. The advantage of this method is that the value of the relative volume of vapour could be considered different of 10^{-8} if a more accurate result is needed and the corresponding value of the cavitation inception coefficient can be easily determined from the curves represented in Figure 2. It is our opinion that by adopting a clear quantitative criterion instead of the rather qualitative (the "first bubble") or mesh dependent (void present in at least one cell) approaches would be preferable. Moreover, the exponential variation of the relative volume of vapour versus the cavitation number allows us to consider a fit that accounts for a whole range of σ_{inst} values, instead of looking only for a particular (and rather sensitive) value of σ_i.

This new approach allows us also to compare the cavitation behaviour of the same turbo machine operating at variable discharge or of different turbomachines operating at the same discharge by comparing the slope of the curves represented in. A higher value of the slope of the curve represents a higher cavitation sensitivity of the turbo machine, while a smaller value of the slope of the curve predicts lower cavitation sensitivity. So, if one has obtained the curves describing the cavitation behaviour of a hydraulic turbomachines, not just a pump, it can easily determine, by comparison of these curves, which turbomachines has a better cavitation behaviour.

For the centrifugal pump investigated it results from Figure 1 that the slope of the curve increases with the decrease of the flow rate. That shows that the cavitation behaviour of the investigated pump is getting worse while the flow rate decreases.

From Figure 2 it results the following values for the cavitation inception coefficient presented in Figure 3 :

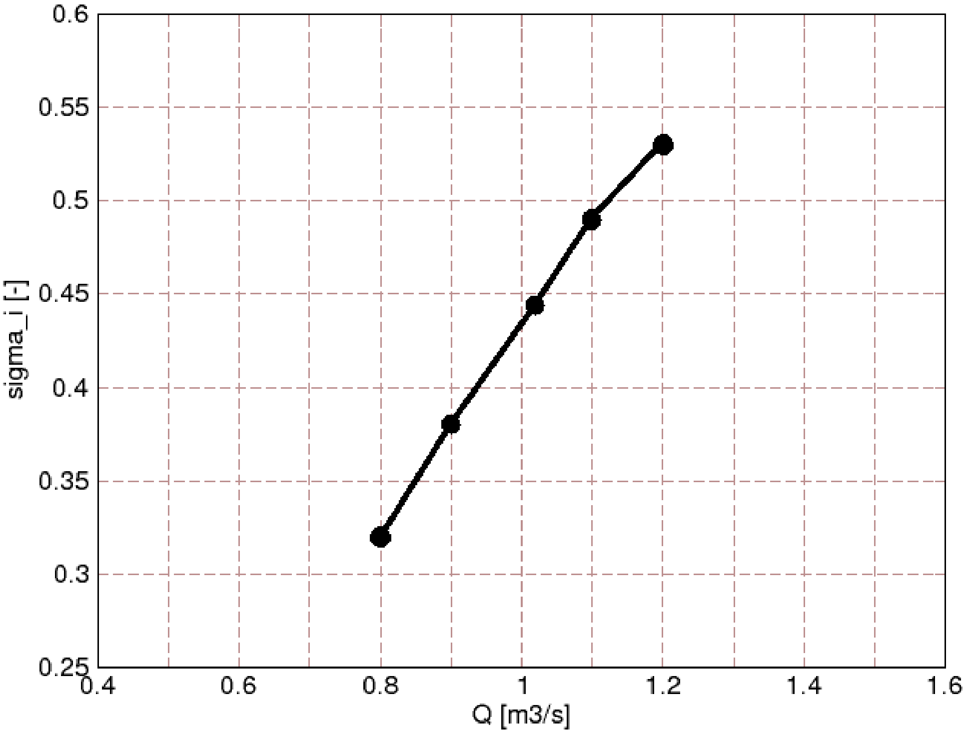

Figure 3. Evolution of the cavitation inception coefficient as a function of flow rate, [25].

From Figure 3 it results that the value of the cavitation inception coefficient increases with the value of the flow rate.

Dividing the pumping head with the value of the pumping head corresponding to the zero cavitation situation and representing the result as a function of $\frac{V_V}{V}$ for all the investigated operating points in a semi-logarithmic plot, where the 0X axis is the logarithmic one, Figure 4, the following equation was obtained for the curve which fits best the data obtained:

$$\frac{H}{H_0} = 1 - 0.0100374 \cdot \left(\frac{V_V}{V_L} - 0.176596 \right)^{0.489854} \tag{2}$$

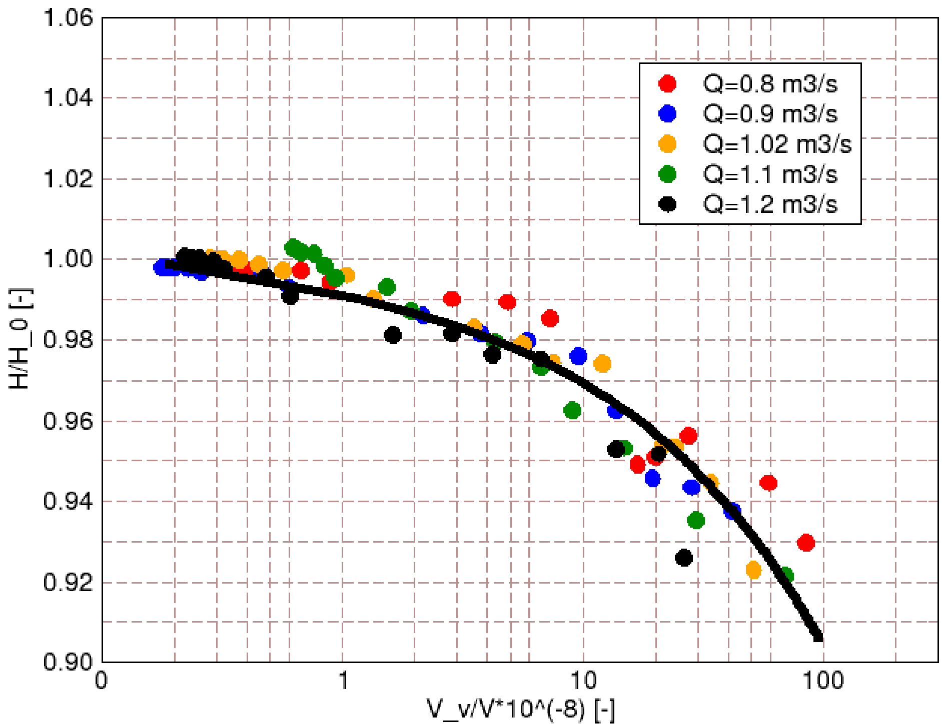

Figure 4. Variation of the pumping head ratio against the volume of vapour for the investigated operating points, [25].

Figure 4, representing the master curve of relative head drop as the dimensionless vapour volume increases, and Equation (2) underlines the fact that the pumping head drop is dependent and caused mainly by the increase of the volume of vapour inside the inter-blade channel of the turbo machine.

In the interval 2009-2011 I was part of the research team that investigated the operation of a large storage pump from the pumping station Jidoaia. The project was carried out by a team of researchers from Politehnica University Timisoara and The Romanian Academy-Timisoara Branch. The manager of the project was prof.dr.ing. Liviu ANTON and I was the manager of the team of researchers from Politehnica University Timisoara. My role in the project was to ensure that all the tasks of my research team are performed on time, and to perform numerical and experimental investigations for the operating of the pump impeller.

The operating problems of the investigated pump were:

- The pump did not supply the required flow rate and pumping head,
- The cavitation phenomena were present over the accepted limits so that the performances of the pump were affected, and the erosion of the material conducted to significant damages of the blades of the impeller,
- There are two types of pumps, one manufactured by a French company and one manufactured by UCM Resita, and although they were supposed to be identical, they were operating at different operating points.

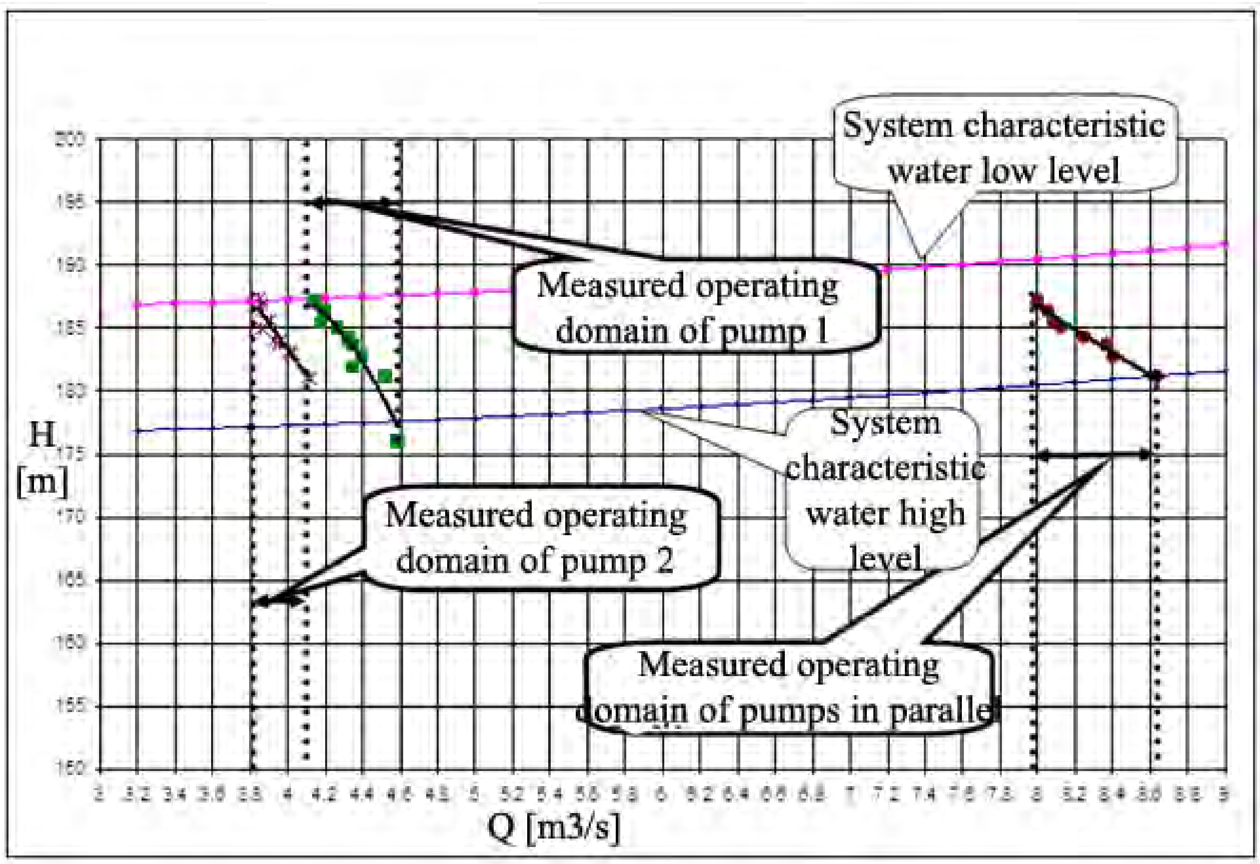

Figure 5. Operating characteristics for the pumps from Jidoaia pumping station.

Figure 6. Erosion due to cavitation of the blades of the impeller of the pumps from Jidoaia pumping station.

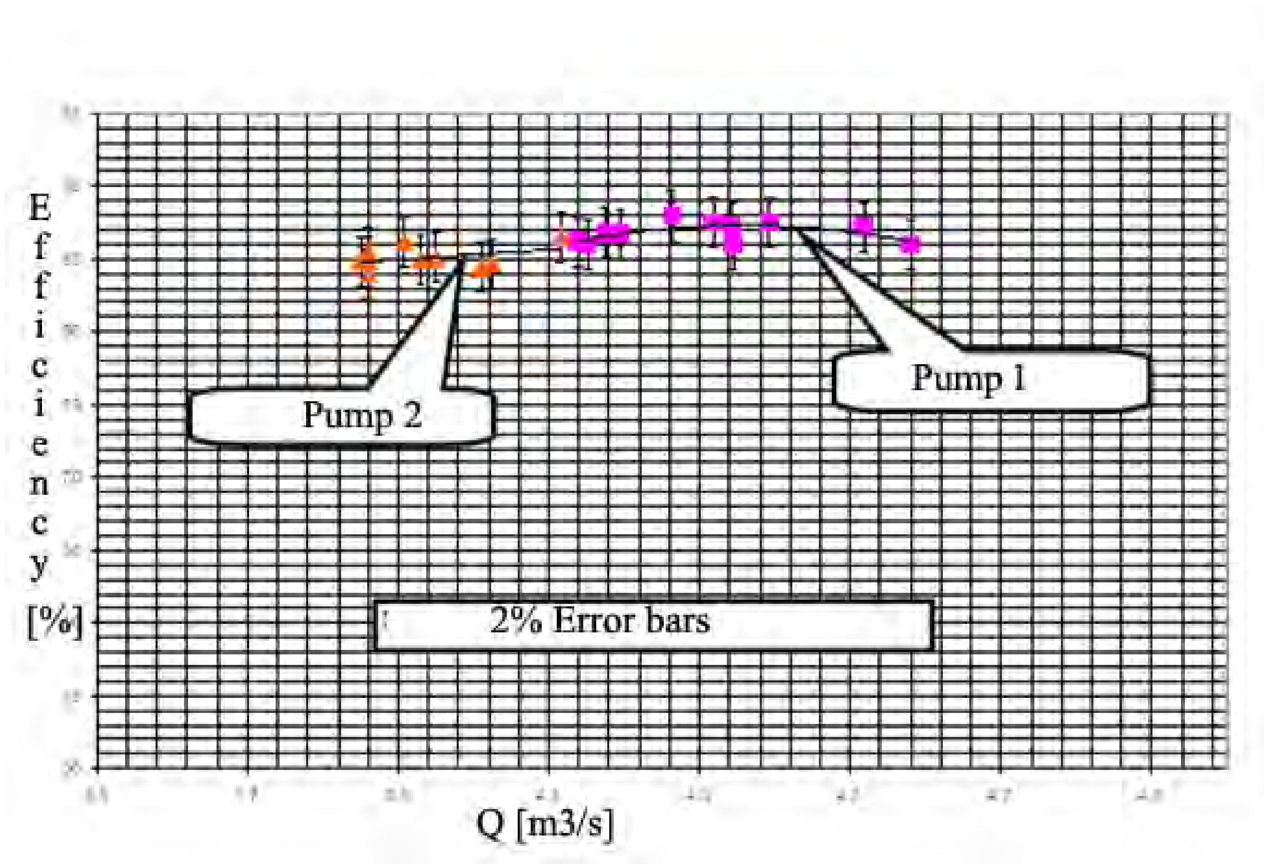

Figure 7. Efficiency curves of the pumps from Jidoaia pumping station.

The objectives of the research project were:

- Analysing, with the help of numerical simulation, the operation and the hydrodynamic of the flow inside the pump manufactured by ICM Resita in order to understand the causes of the poor operation,
- Design of a new impeller with improved operating characteristics and cavitation behaviour,
- Manufacturing of a small-scale model of the new designed impeller
- Designing and manufacturing of the experimental test rig for the testing of the model of the new designed impeller,
- Testing of the model of the new designed impeller on the experimental test rig from our laboratory.

The numerical investigation was performed for one blade channel of the impeller and for the suction elbow for 5 operating points. The results of the numerical investigations allowed to determine the operation curves of the pump and to analyse the pressure coefficient distribution on the blades of the impeller and the velocity coefficients distribution on the outlet section of the suction elbow.

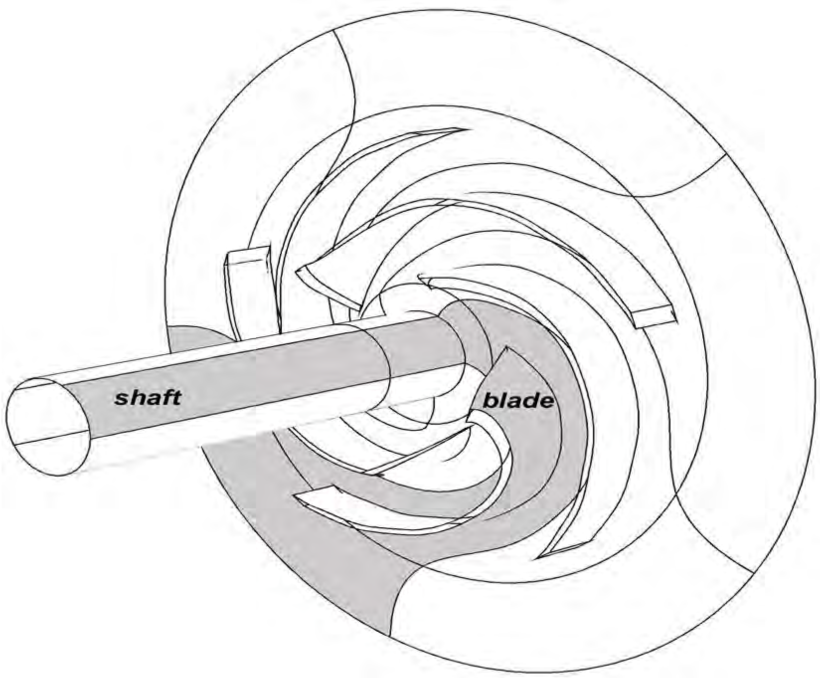

Figure 8. Numerical investigation domain of the impeller of the pump PRO-195.

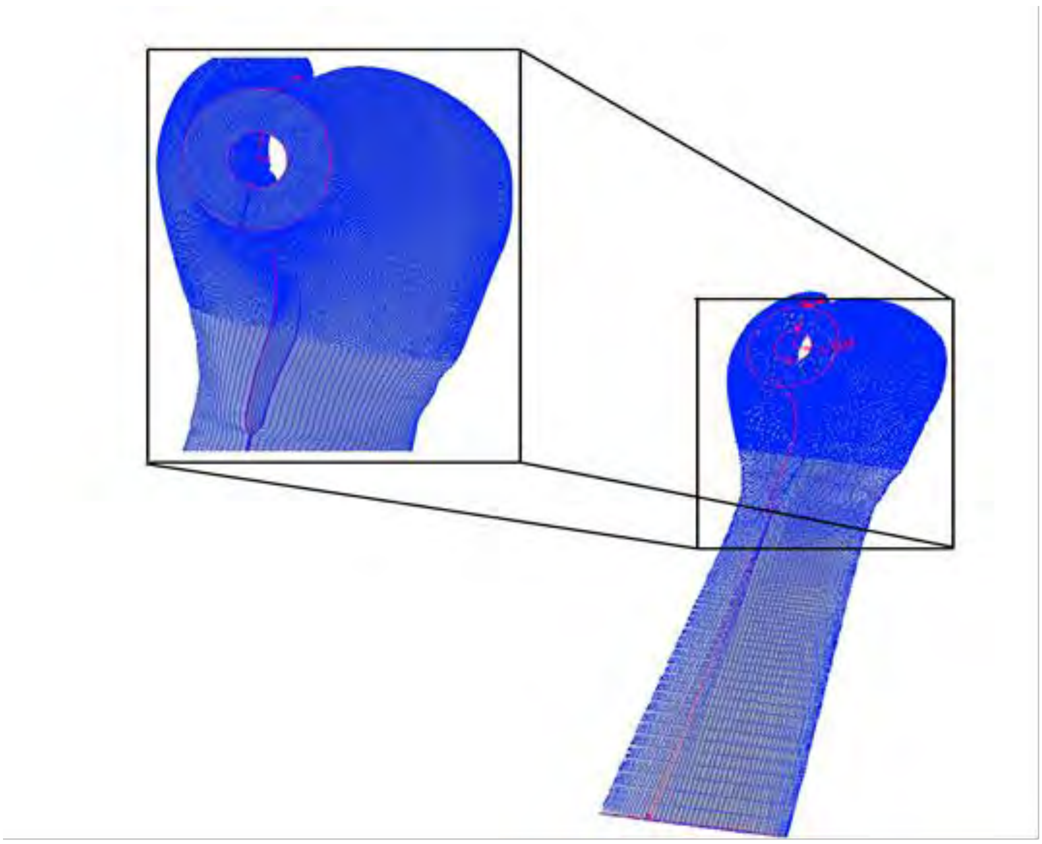

Figure 9. Numerical investigation domain of the suction elbow of the pump PRO-195.

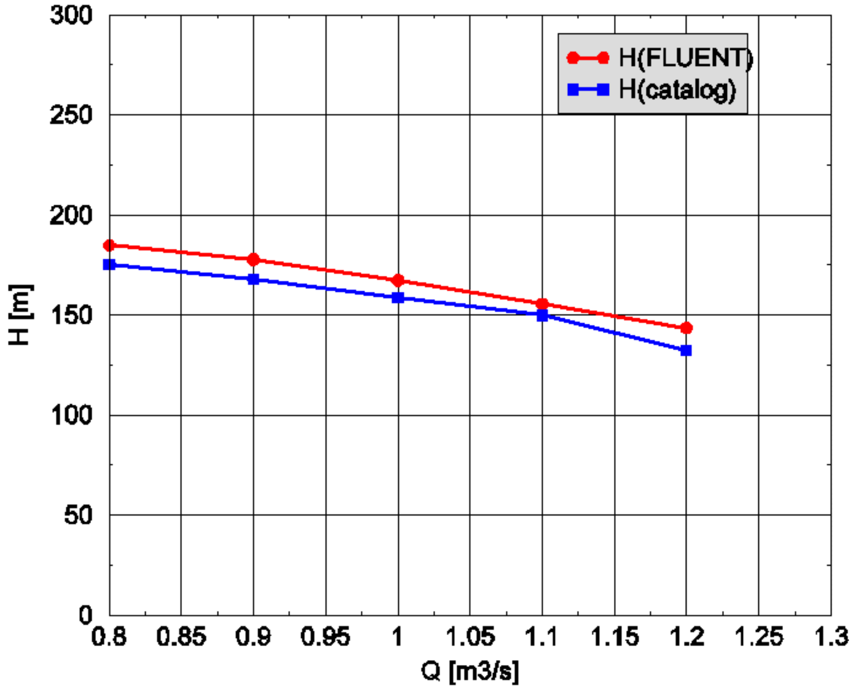

Figure 10. Pumping head vs. flow rate for the pump PRO-195.

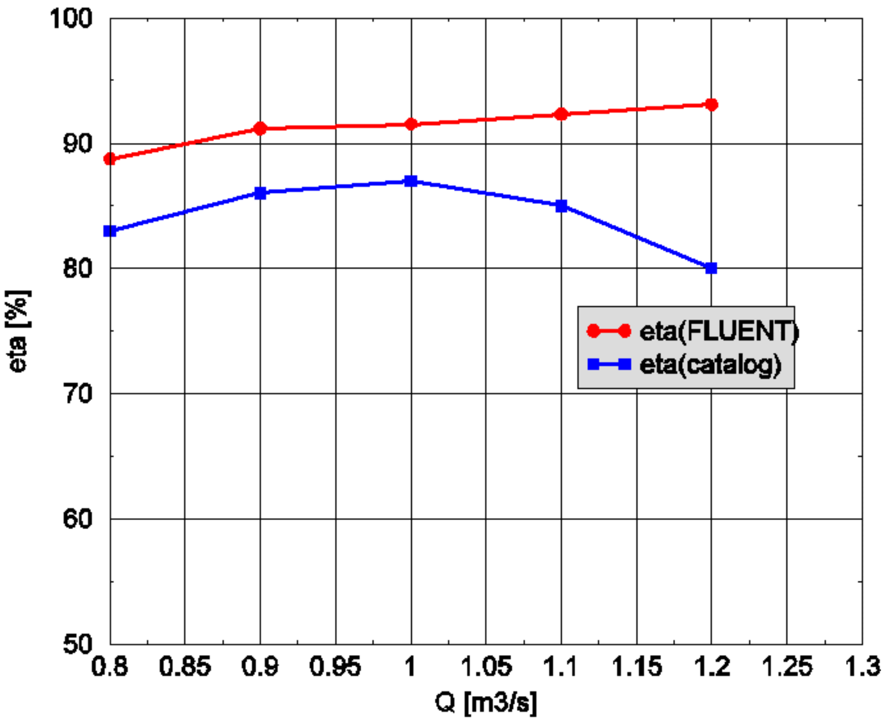

Figure 11. Hydraulic efficiency vs. flow rate for the pump PRO-195.

The pumping head and the hydraulic efficiency obtained from numerical simulation had higher values because we did not calculate the flow in all the pump components (we did not take into consideration the spiral case) and just one impeller was considered, the real pump had two back-to-back impellers, and the values from the catalogue of the manufacturer represented the values for the entire pump.

The pressure coefficient is defined as following:

$$c_p = \frac{p - p_{IN}}{\rho g H} \tag{3}$$

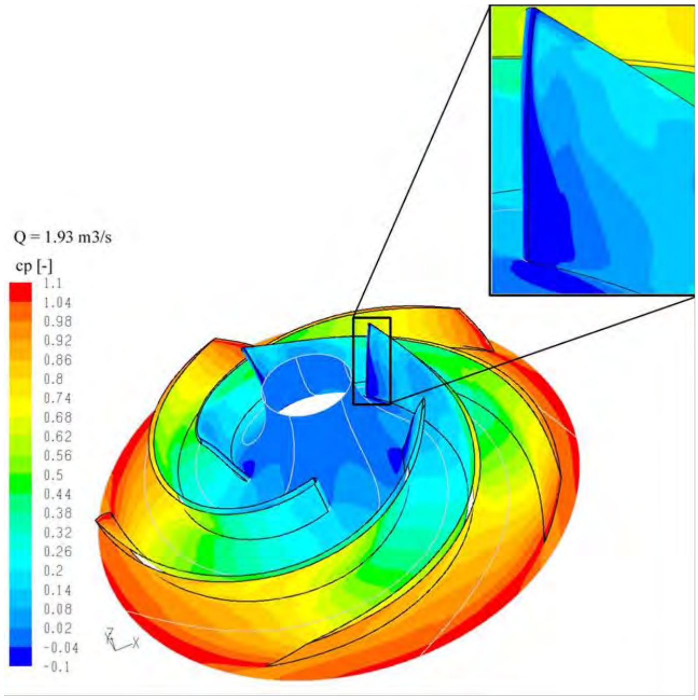

Figure 12. Pressure coefficient distribution for the pump PRO-195, Q=1.93 m³/s.

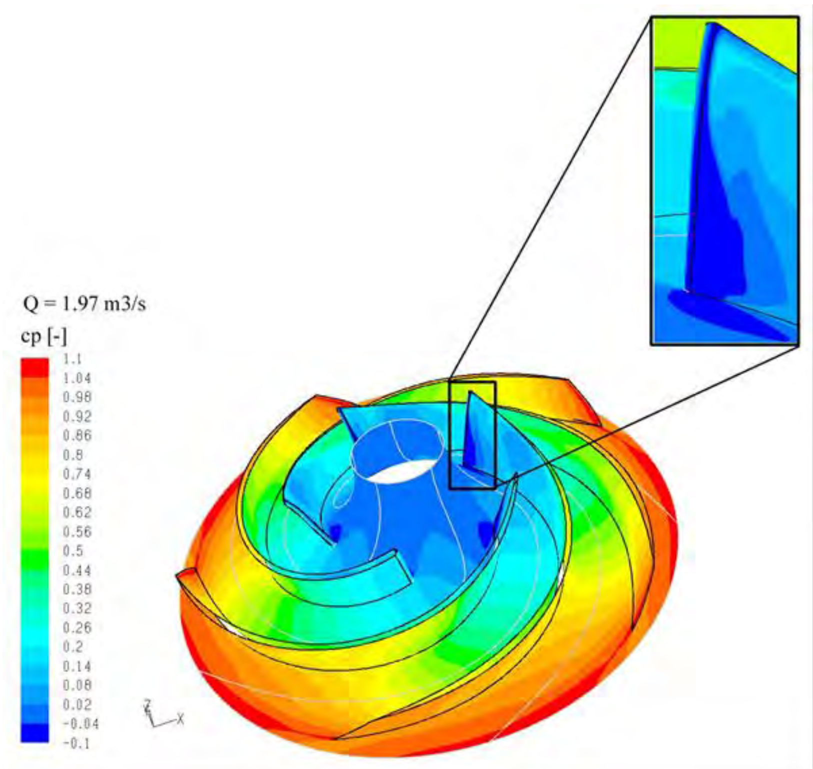

Figure 13. Pressure coefficient distribution for the pump PRO-195, Q=1.97 m³/s.

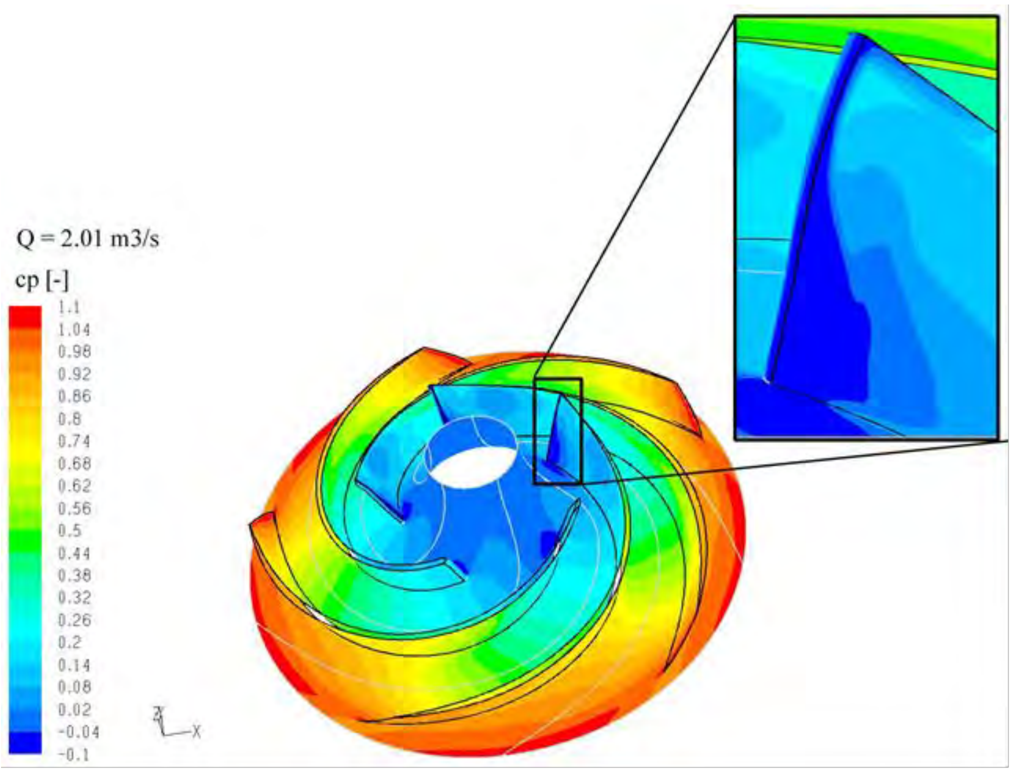

Figure 14. Pressure coefficient distribution for the pump PRO-195, Q=2.01 m³/s.

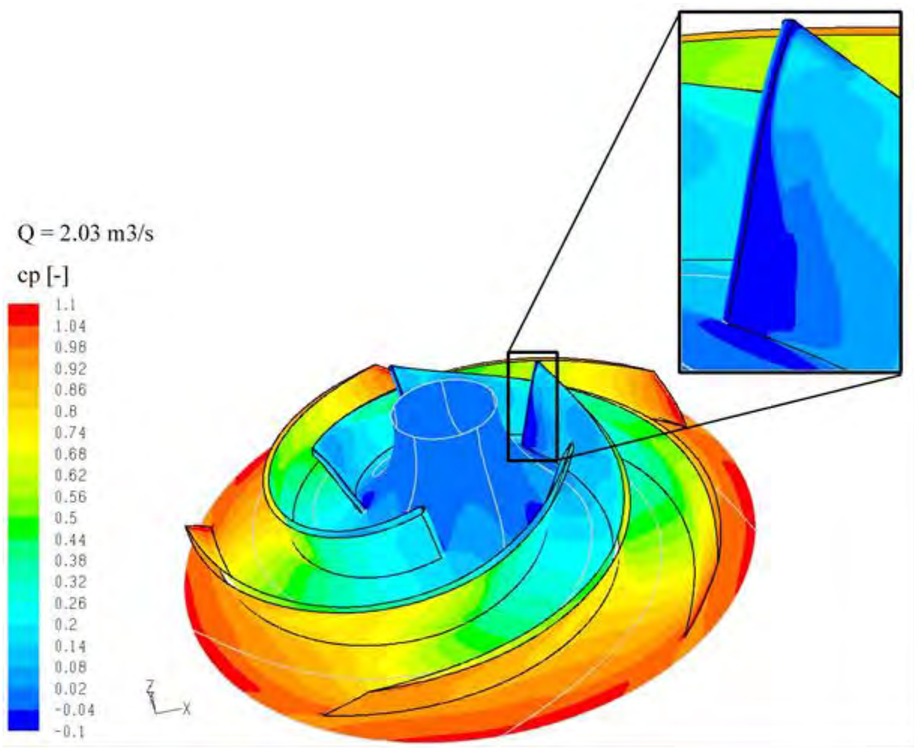

Figure 15. Pressure coefficient distribution for the pump PRO-195, Q=2.03 m³/s.

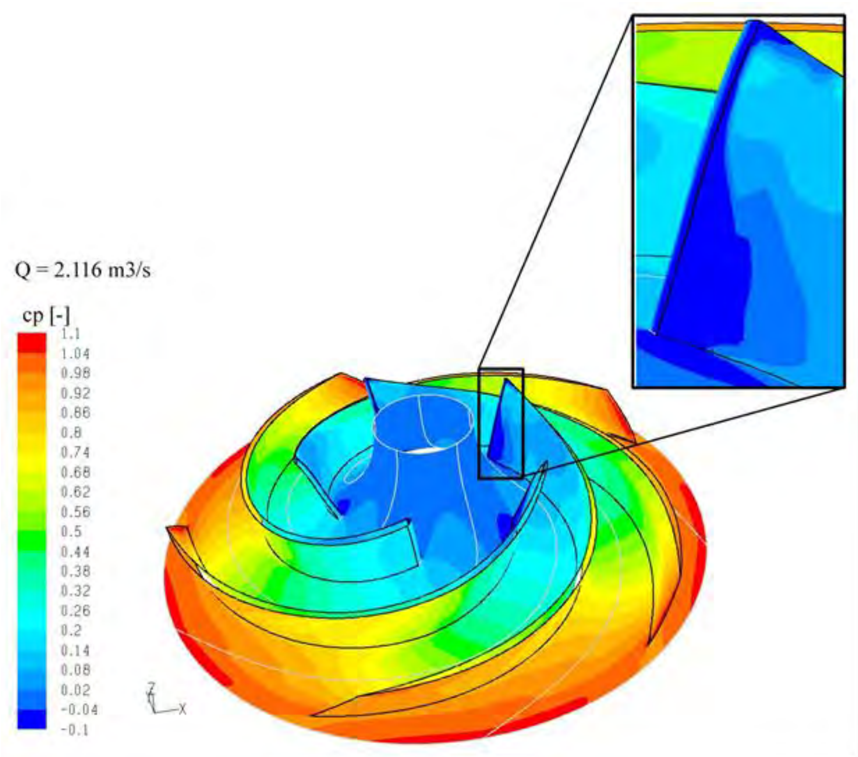

Figure 16. Pressure coefficient distribution for the pump PRO-195, Q=2.116 m³/s.

From analysing the results, it is underlined that the minimum value of the coefficient was on the suction side of the blade and the zone with lower values was quite large, extending also on the hub of the impeller. The zones of the blades with lower values of the pressure coefficient were the zones where the cavitation phenomena occurred. Also, because the investigated operating points were so close to another, the distribution of the pressure coefficient was very similar for all five investigated operating points.

The velocity coefficients are calculated with the next equations and the distribution of these coefficients on the outlet section of the suction elbow was presented:

$$c_r = \frac{v_r}{\sqrt{2gH}} \tag{4}$$

$$c_u = \frac{v_u}{\sqrt{2gH}} \tag{5}$$

$$c_a = \frac{v_a}{\sqrt{2gH}} \tag{6}$$

The distribution of the axial velocity coefficient underlines the presence of a hydrodynamic trail at the position of 180° because of the shape of the suction elbow.

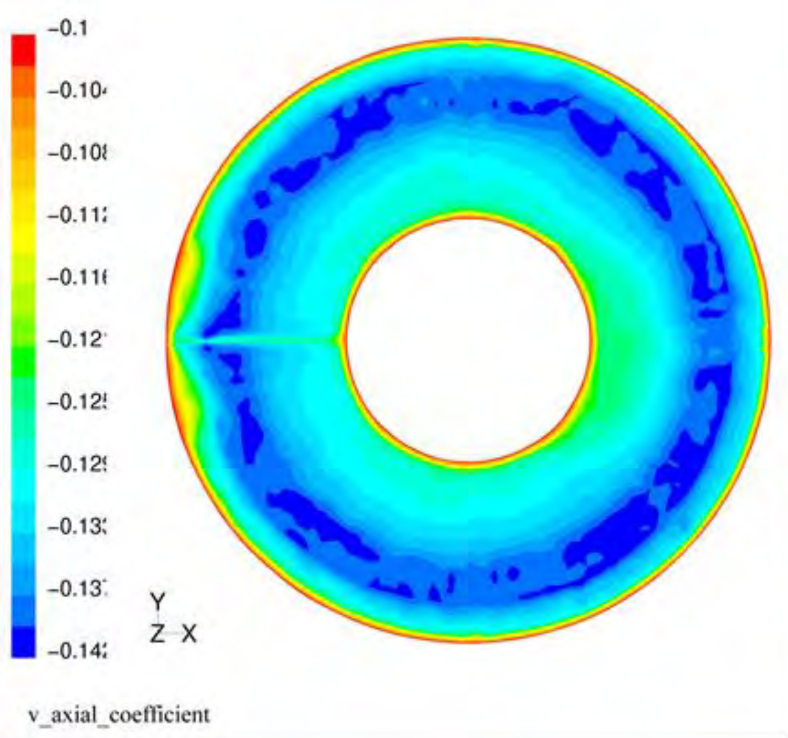

Figure 17. Axial velocity coefficient distribution for the outlet section of the suction elbow of the pump PRO-195, Q=1.97 m³/s.

The radial velocity coefficient distribution shows the presence of two zones, at 30° and 330°, where the radial velocity is almost zero because two counter rotating swirls are intersecting there.

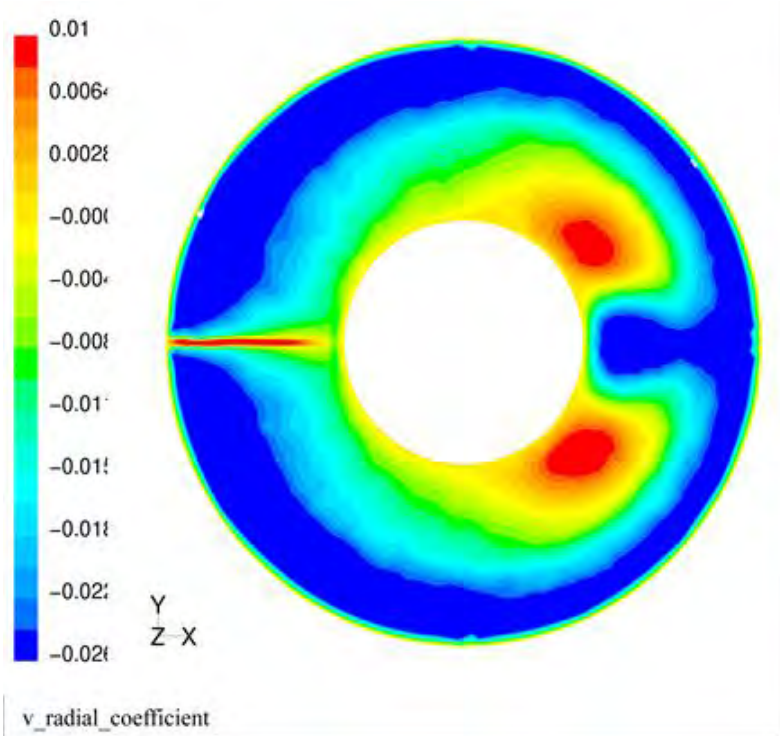

Figure 18. Radial velocity coefficient distribution for the outlet section of the suction elbow of the pump PRO-195, Q=1.97 m³/s.

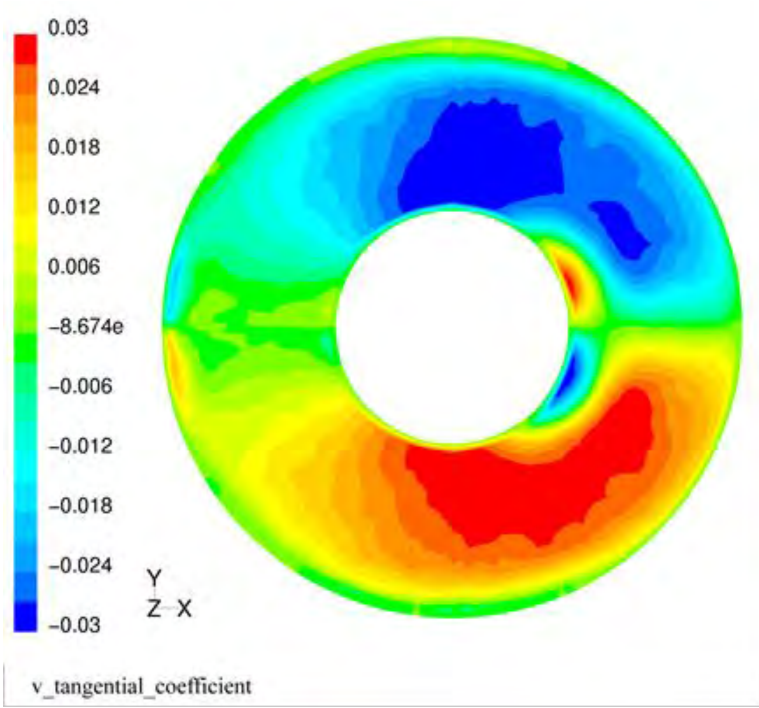

Figure 19. Tangential velocity coefficient distribution for the outlet section of the suction elbow of the pump PRO-195, Q=1.97 m³/s.

The analysis of the tangential velocity coefficient distribution reveals a large variation of the tangential component of the velocity over the outlet section, with two extreme values at the positions of 90° and 270°.

From analysing all three velocity coefficients distribution it resulted that the flow at the inlet section of the pump is severely unsteady and because of this, the cavitation phenomena appeared on the blades of the impeller.

The next step was to choose a new solution and design a new impeller with better cavitation characteristics, by taking into account the following recommendations from the literature:

- The increase of the diameter from the inlet section,
- Changing the shape of the leading edge of the blade,
- Reducing the curvature of the hub,
- Reducing the number of blades on the inlet section,
- Optimizing the geometry shape of the entire blade of the impeller,
- Adding an inducer in the front of the impeller.

Considering all the above-mentioned recommendations, three solutions of the new impeller were designed:

- A new impeller with 5 long blades,
- A new impeller with 3 long blades and 3 short blades,
- A new impeller with 3 long blades and 3 short blades and an inducer.

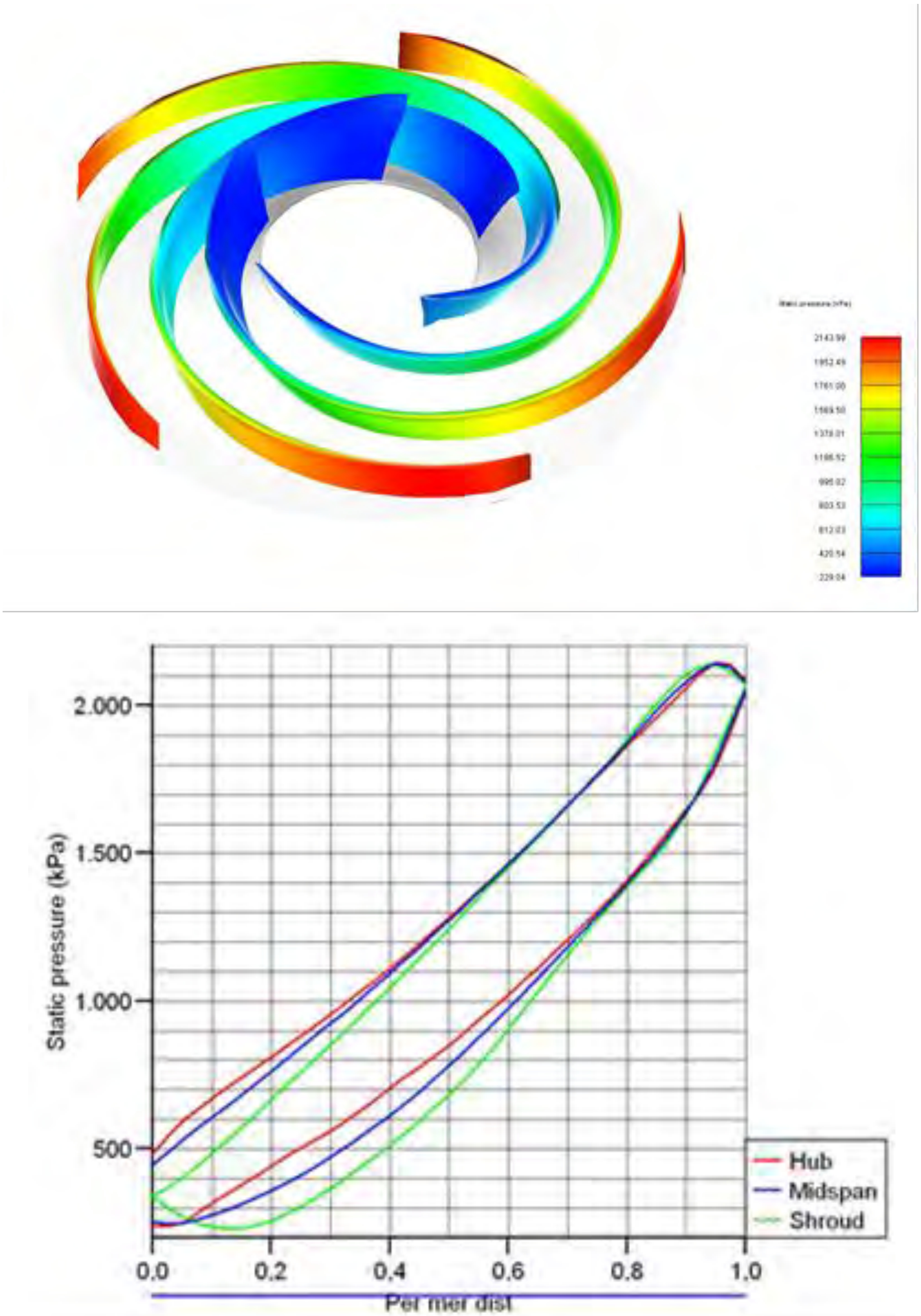

Figure 20. Pressure distribution for the new designed impeller with 5 long blades: a) for NNR=1180 m.

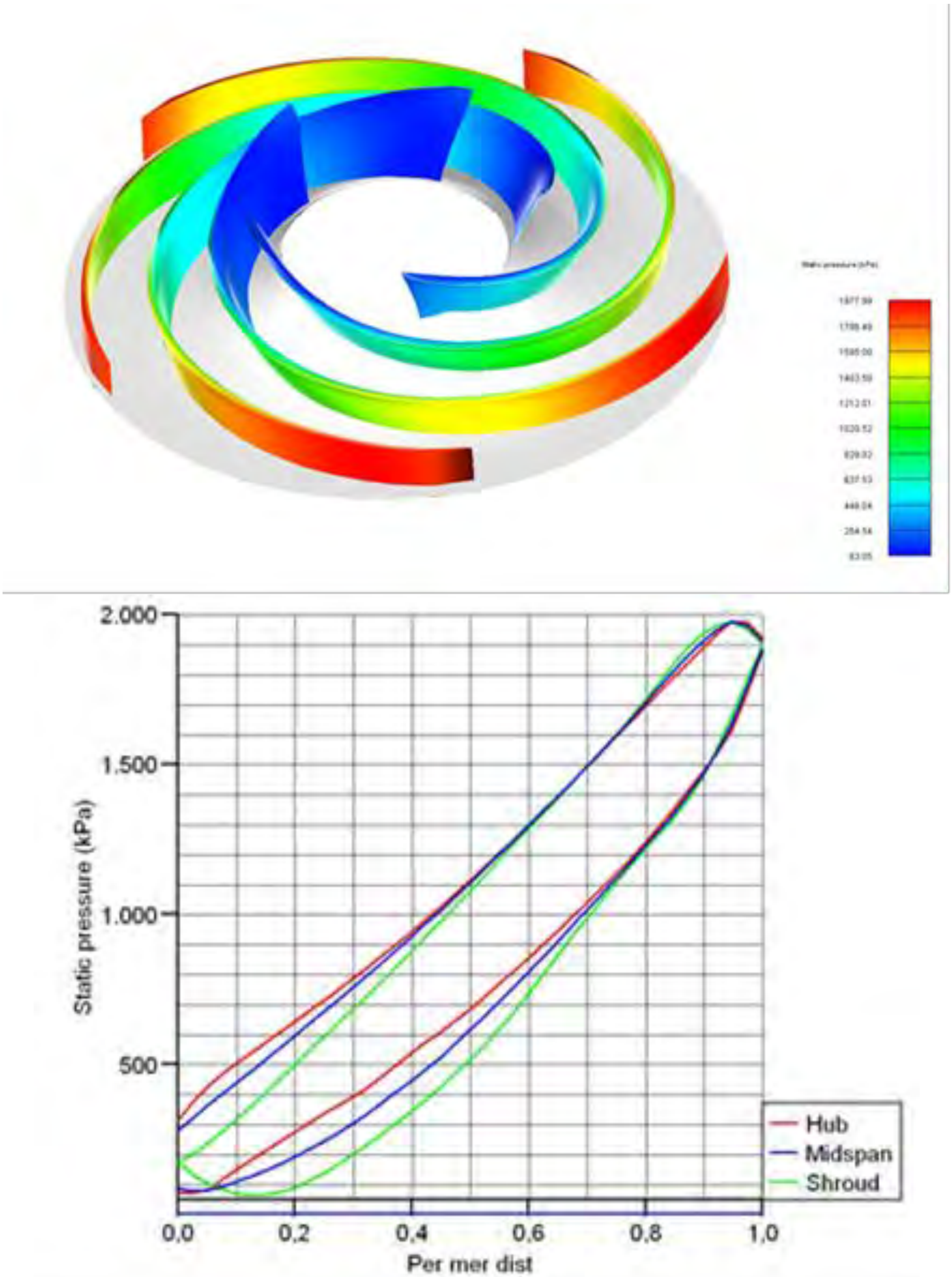

Figure 21. Pressure distribution for the new designed impeller with 5 long blades for NNR=1163 m.

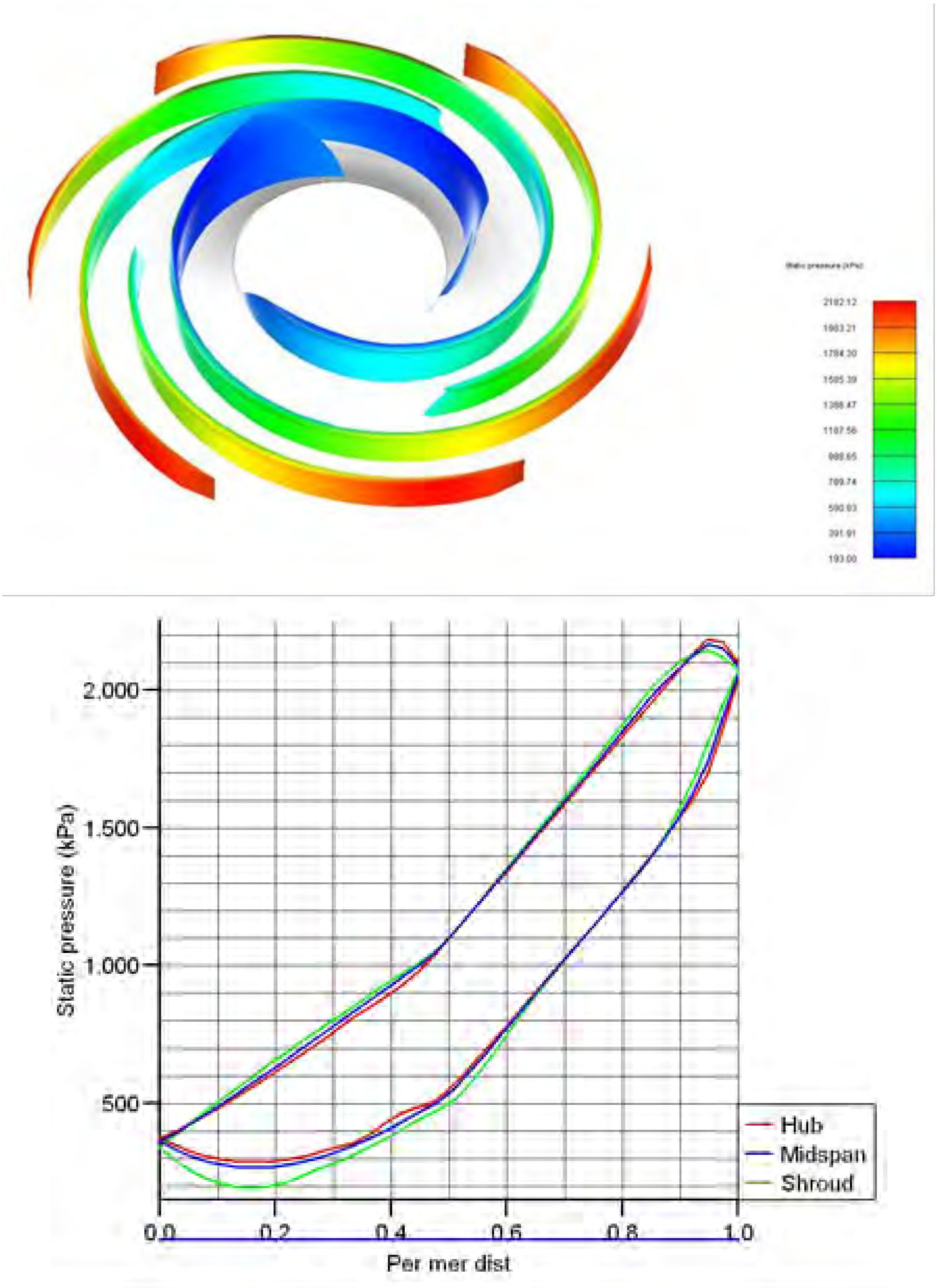

Figure 22. Pressure distribution for the new designed impeller with 3 long blades and 3 short blades for NNR=1180 m.

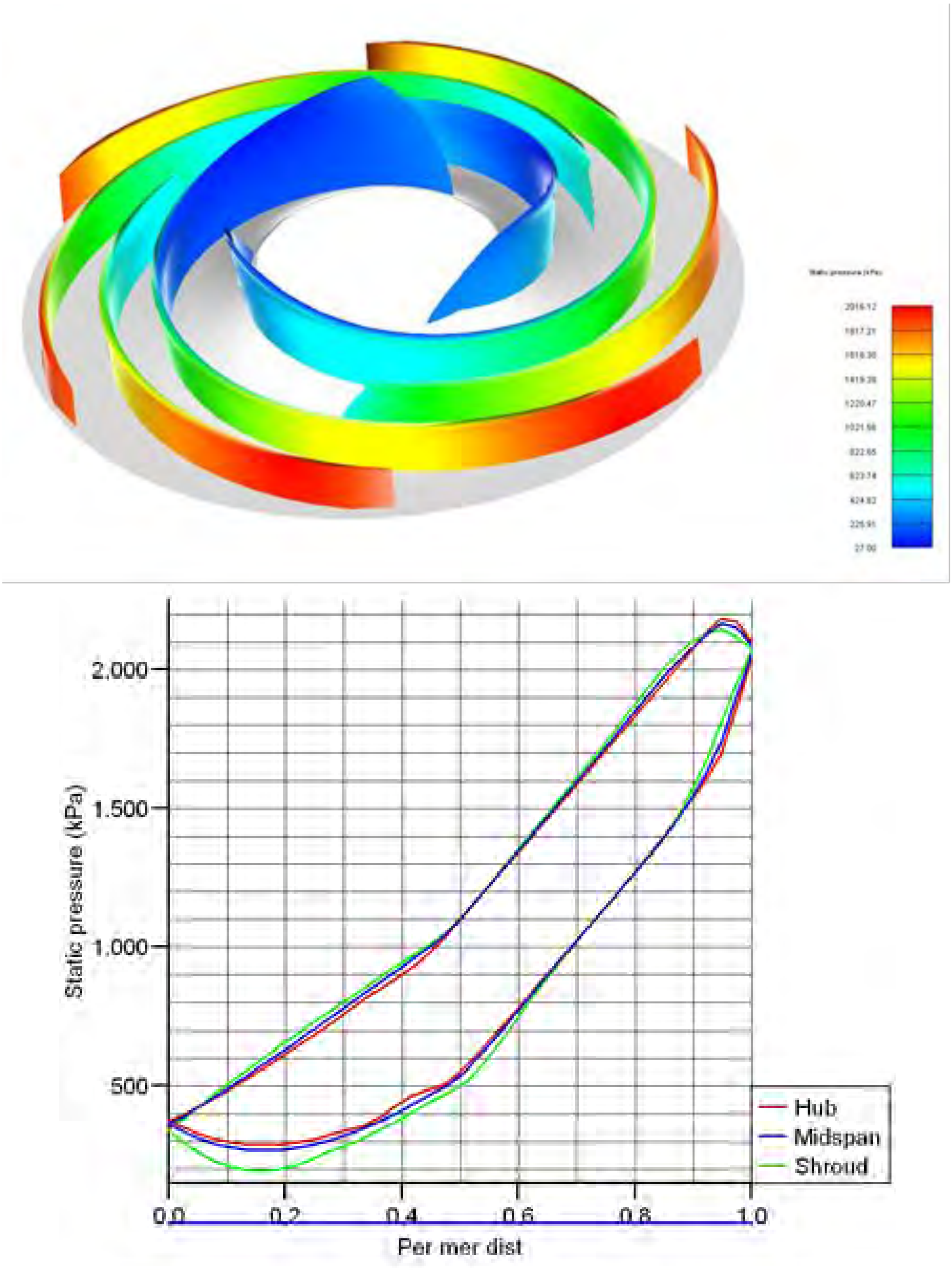

Figure 23. Pressure distribution for the new designed impeller with 3 long blades and 3 short blades for NNR=1163 m.

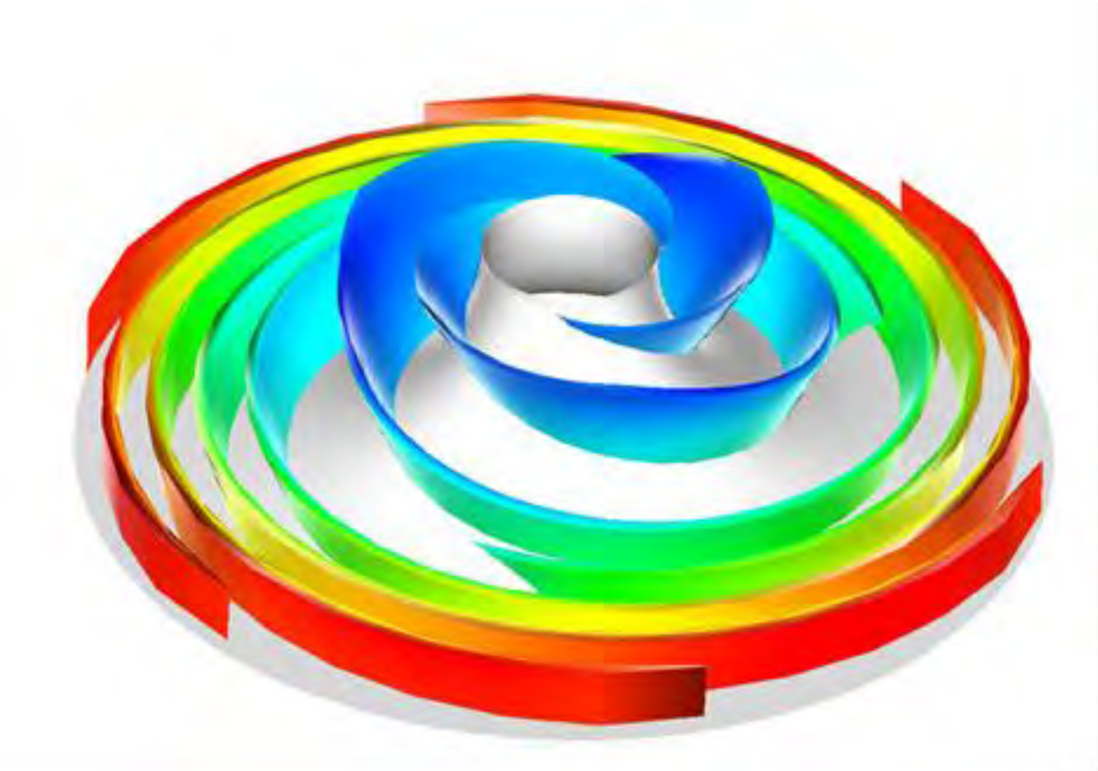

Figure 24. Pressure distribution for the new designed impeller with 3 long blades and 3 short blades and an inducer.

The following step of the research was represented by the development of an experimental test rig necessary to test the existing impeller and the new designed solutions for the pumping station Jidoaia, which had the following components:

- Two reservoirs manufactured from stainless steel,
- Pipes manufactured from stainless steel,
- Measuring equipment.

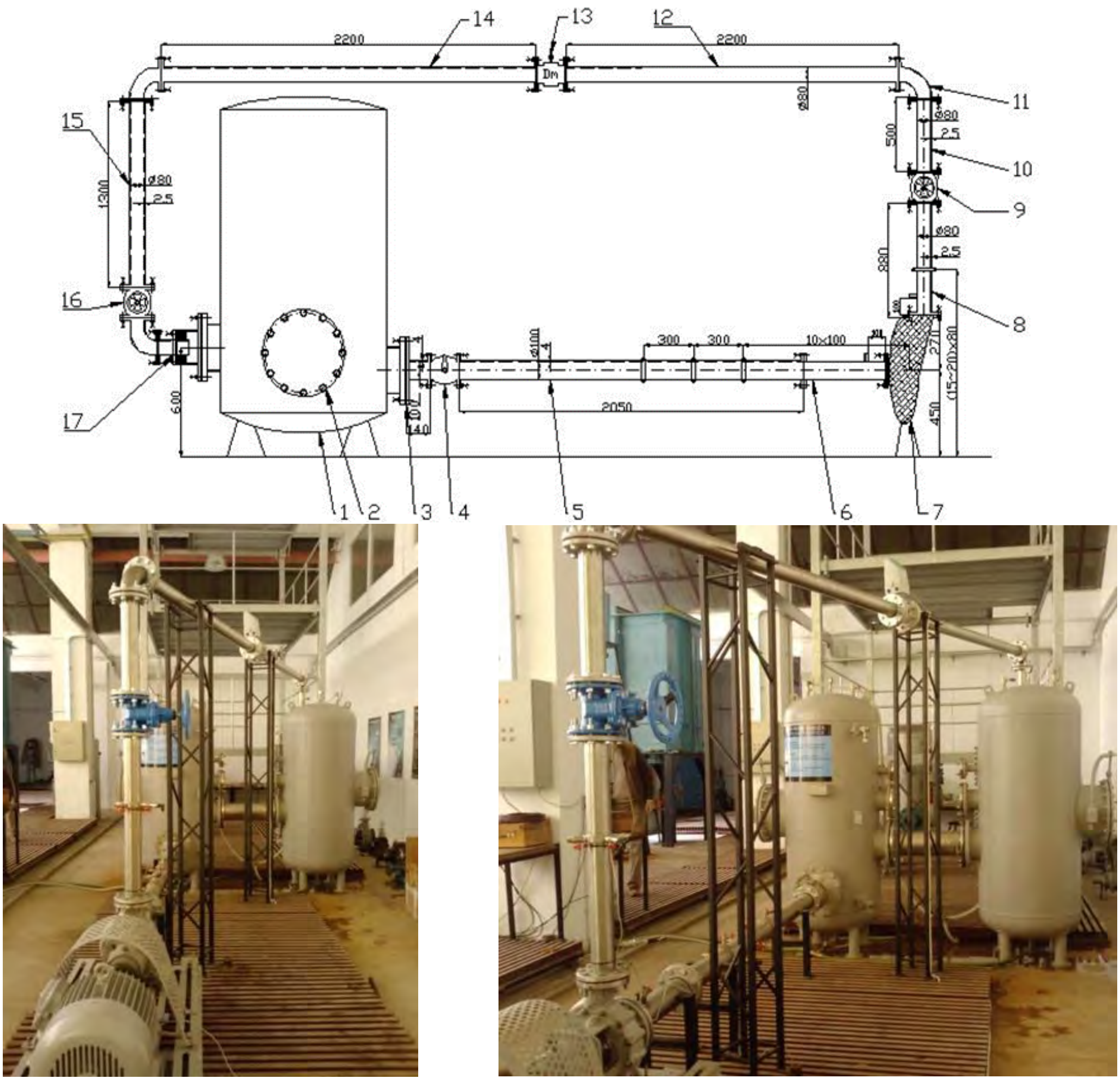

Figure 25. Closed loop experimental test rig for determining operation and cavitation characteristics of the centrifugal pumps.

The measuring equipment has the following components:

- Two pressure transducers, one with the range of -1 up to 2.5 bar and one with the range from 0 to 6 bar,
- One electromagnetic flow rate meter with the range from 0 to 50 l/s,
- A temperature pressure transducer,
- A power transducer for measuring the electric power consumed by the electric motor that drives the pump,
- A transducer for measuring the rotational speed of the impeller of the pump,
- One data acquisition system for automated measurements.

Figure 26. Measuring equipment for the closed loop experimental test rig for determining operation and cavitation characteristics of the centrifugal pumps.

A small-scaled model of the impeller of the pump PRO-195 was designed to fit an existing spiral case and was manufactured by rapid prototyping at Technical University Cluj-Napoca.

a) b)

Figure 27. Impeller of the pump PRO-195: a) small-scale model; b) prototype of pump from the pumping station Jidoaia.

In order to calibrate the measuring equipment from the new test rig, experimental measurements were performed on an existing impeller with the code PCN 80-200. For this pump there were available a set of results from previous measurements regarding the operating and cavitation characteristics. Also, for the calibration of the measuring equipment, another measuring equipment, based on thermodynamic method, was employed in order to determine the operating characteristics of the pump. Another set of experimental data was measured with classical manometers in order to determine the pumping head and a classical wattmeter for measuring the electric power consumed by the driving electric motor.

Figure 28. Measuring equipment P22f based on thermodynamic method for determining the operating curves of the pump.

After the measurements were performed, the results were calculated with the following equations and were compared with previous existing results and the overlapping was considered good, for both operation curves and cavitation curves.

$$H = \frac{p_r - p_a}{\rho g} + z_r - z_a + \frac{v_r^2 - v_a^2}{2g} \quad (7)$$

$$P_h = \rho g H Q \quad (8)$$

$$\eta = \frac{P_h}{P_e} \quad (9)$$

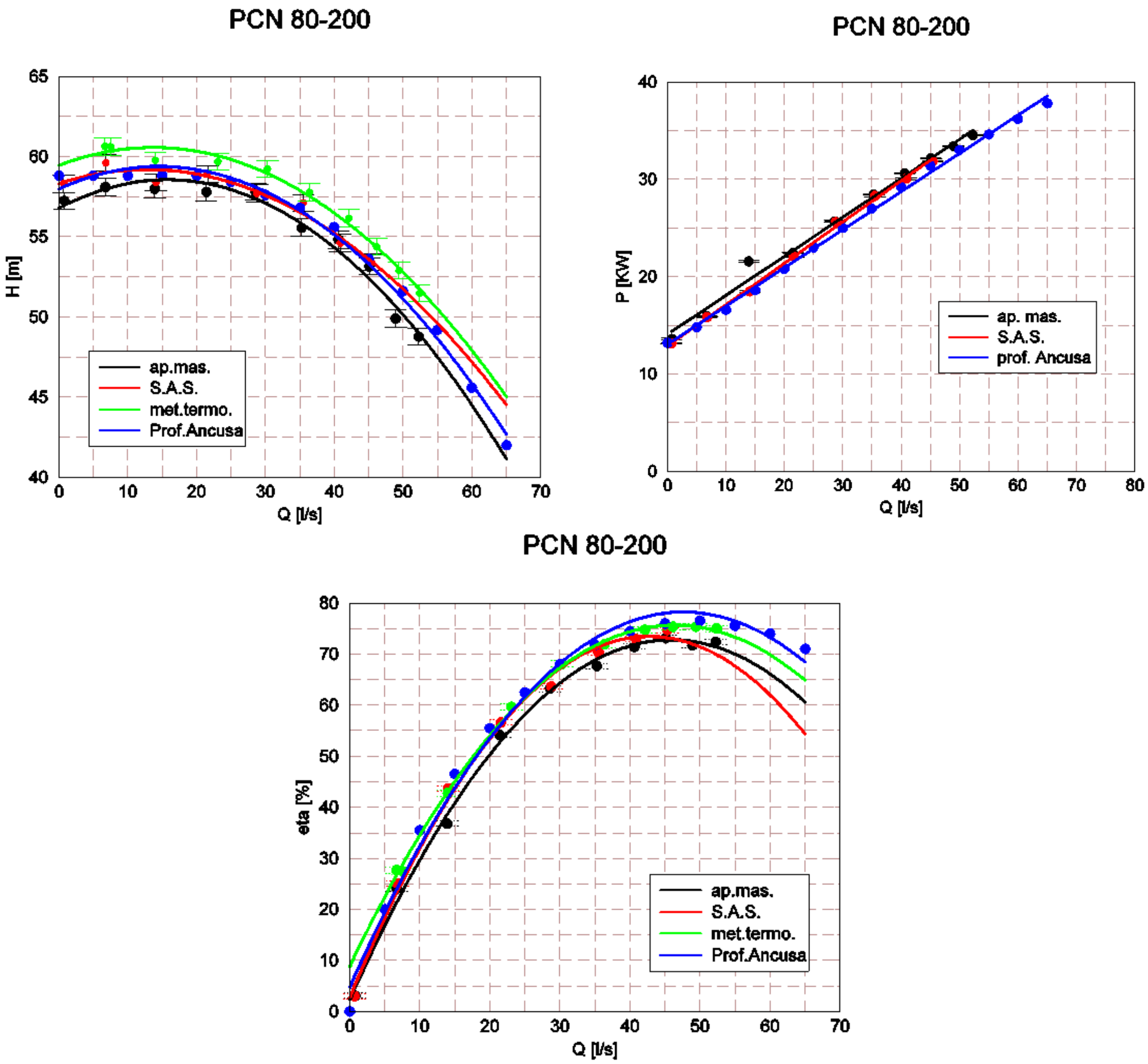

Figure 29. Operation curves of the pump PCN 80-200.

For the experimental measuring of the cavitation curves there was also tested a case where an inducer was fitted in front of the impeller in order to improve the cavitation behaviour. The comparison of the experimental results with the previous results, proved a very good overlapping. For the calculation of the cavitation curve the following equation was applied:

$$\Delta h_e = \frac{p_a}{\rho g} + \frac{v_a^2}{2g} - \frac{p_{vap}}{\rho g} \tag{10}$$

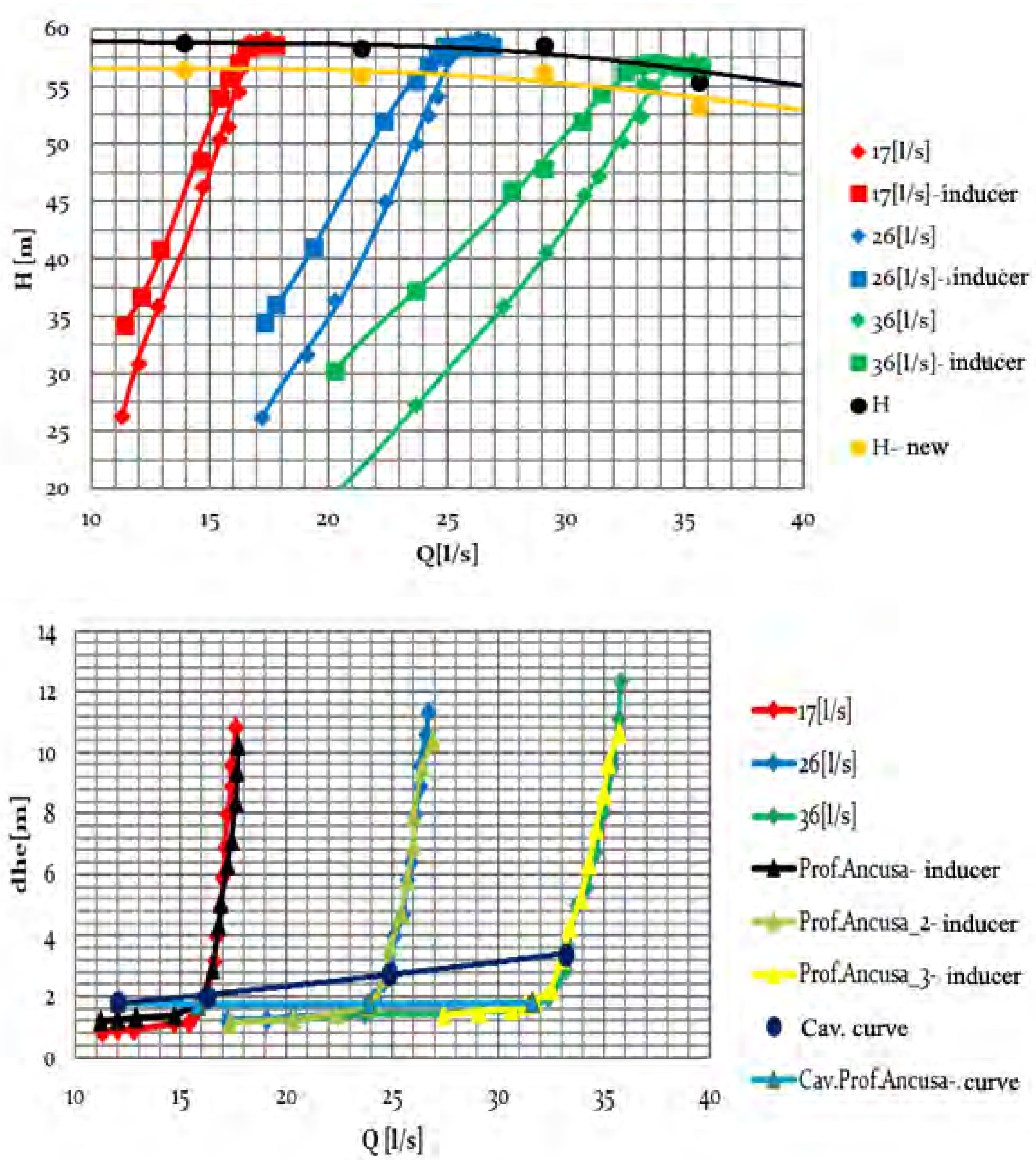

Figure 30. Cavitation curves of the pump PCN 80-200.

After the calibration of the measuring equipment was performed, the experimental tests were carried out for the small-scale model of impeller for the existing pump PRO-195. At that moment, for the measurements performed it was considered that the inlet section of the pump is axial, the suction elbow was not taken into consideration. Both types of tests were performed: for the determination of the operating curves and for determining the cavitation curves.

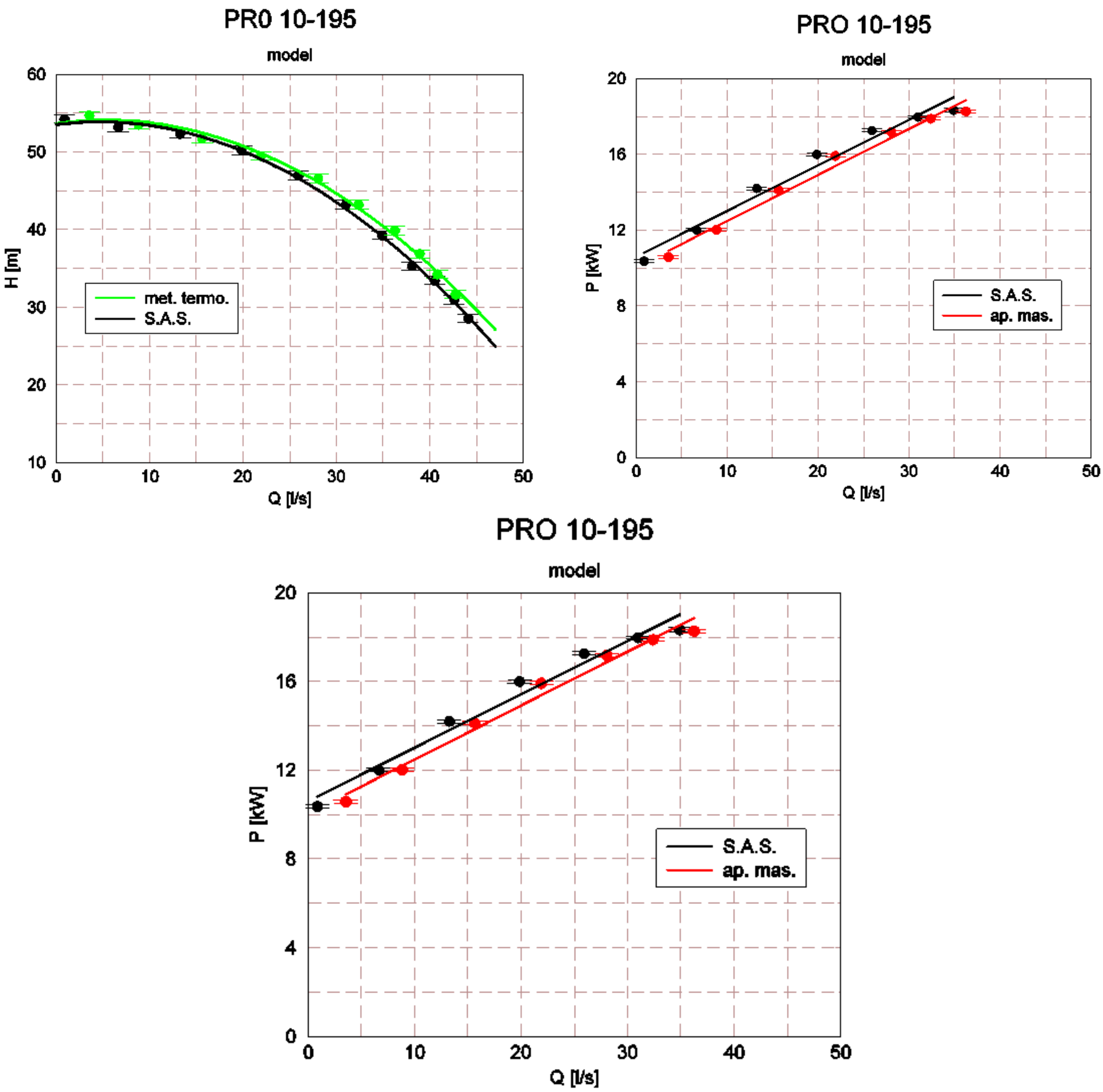

Figure 31. Operation curves of the small-scale model of the pump PRO-195.

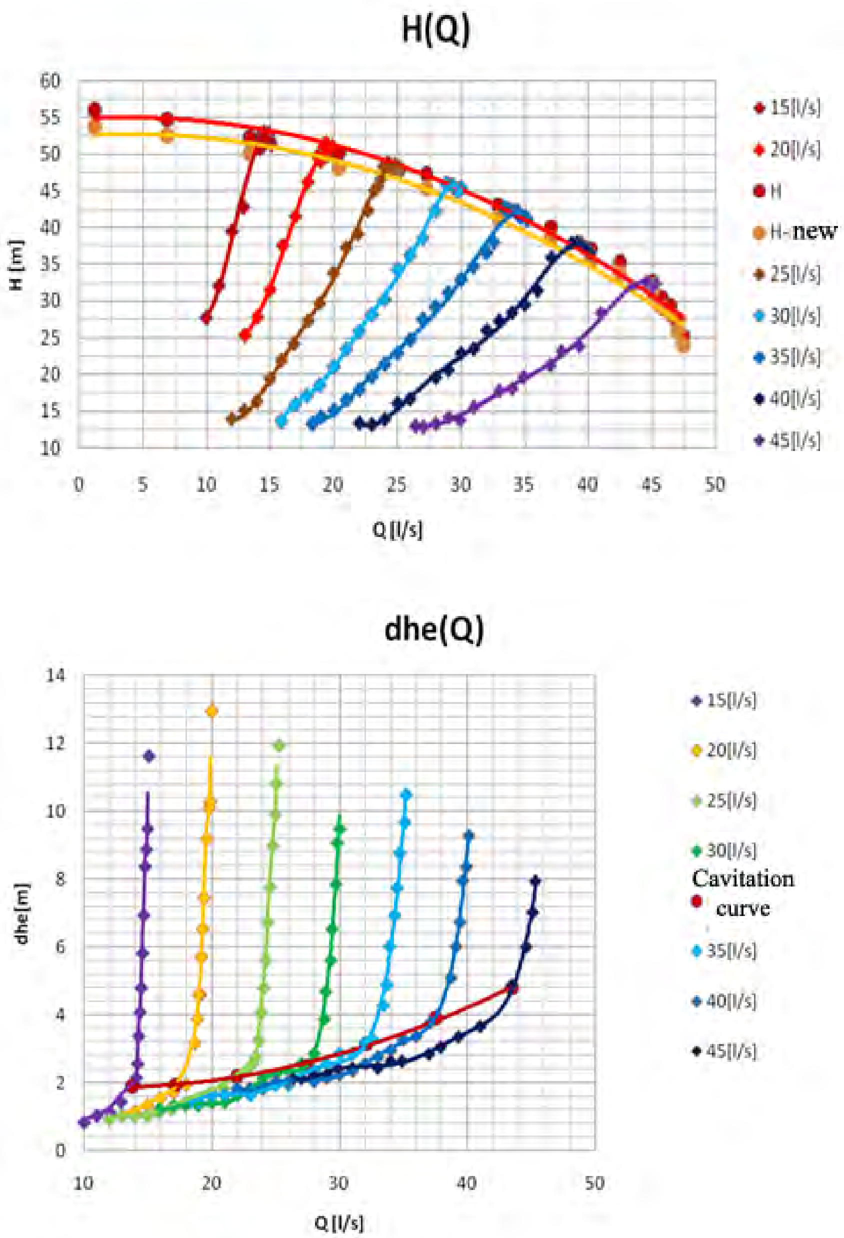

Figure 32. Cavitation curves of the small-scale model of the pump PRO-195.

In order the transpose the experimental results obtained for the small-scale model of the pump PRO-195 to the full-scale prototype of the pump, the following equations were applied corresponding to the affinity laws of the pumps:

$$\frac{Q_m}{Q_p} = \left(\frac{D_m}{D_p}\right)^3 \cdot \frac{n_m}{n_p} \tag{11}$$

$$\frac{H_m}{H_p} = \left(\frac{D_m}{D_p}\right)^2 \cdot \left(\frac{n_m}{n_p}\right)^2 \tag{12}$$

$$\frac{P_m}{P_p} = \left(\frac{D_m}{D_p}\right)^5 \cdot \left(\frac{n_m}{n_p}\right)^3 \tag{13}$$

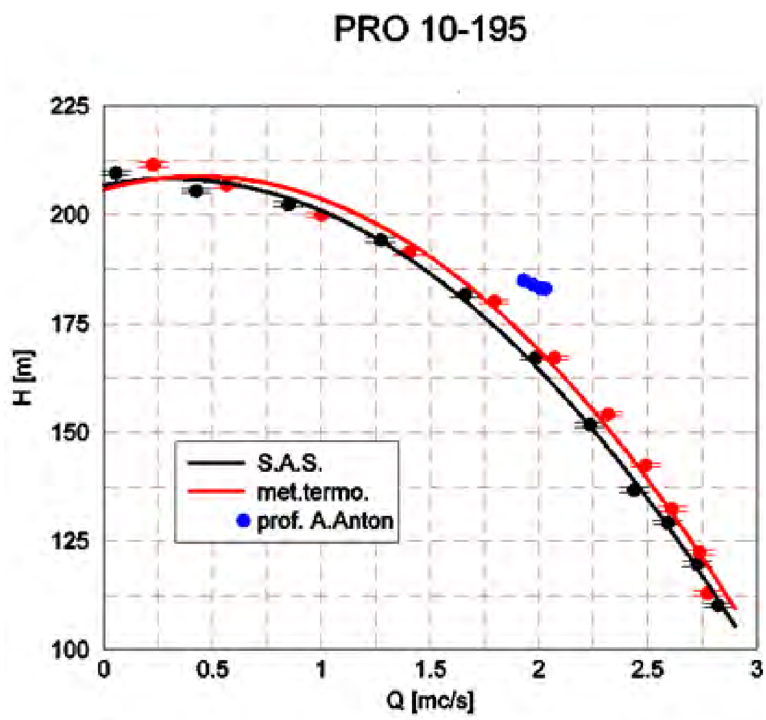

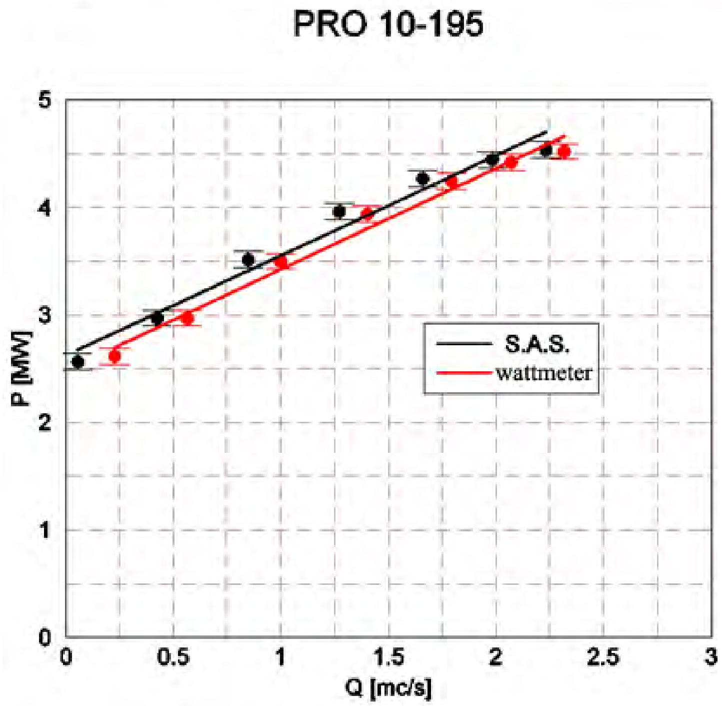

Figure 33. Operation curves of the full-scale prototype of the pump PRO-195, obtained with affinity laws of the pumps.

The research project continued for the next years, but I was no longer part of the research team, and some of the solutions proposed were analysed and tested in the laboratory.

In the year 2015 the local company for heat and hot water from Timisoara, S.C. Colterm S.A., required our expertise for determining the operation points for two new large centrifugal pumps. These two pumps, together with other existing pumps, were operating at CET-Centre and CET-South providing the hot water and heat for the citizens of

Timisoara. For this research project I had the position of manager and I also perform the experimental measurements, the data processing and the writing of the technical report.

The two pumps were manufactured by Pentair Fairbanks Nijhuis:

- the pump from CET Centre, Venus1-250.650, has an impeller with a diameter of 626 mm, the inlet section diameter is 300 mm and the outlet section diameter of 250 mm. The nominal operating point of this pump is characterized by a maximum flow rate of 1200 m^3/h and a pumping head of 144 m at a rotational speed of 1490 rpm. This pump has variable speed,
- the pump from CET South, Venus1-350.650, has an impeller with a diameter of 673 mm, the inlet section diameter is 400 mm and the outlet section diameter of 350 mm. The nominal operating point of this pump is characterized by a maximum flow rate of 3250 m^3/h and a pumping head of 164 m at a rotational speed of 1490 rpm. This pump has variable speed.

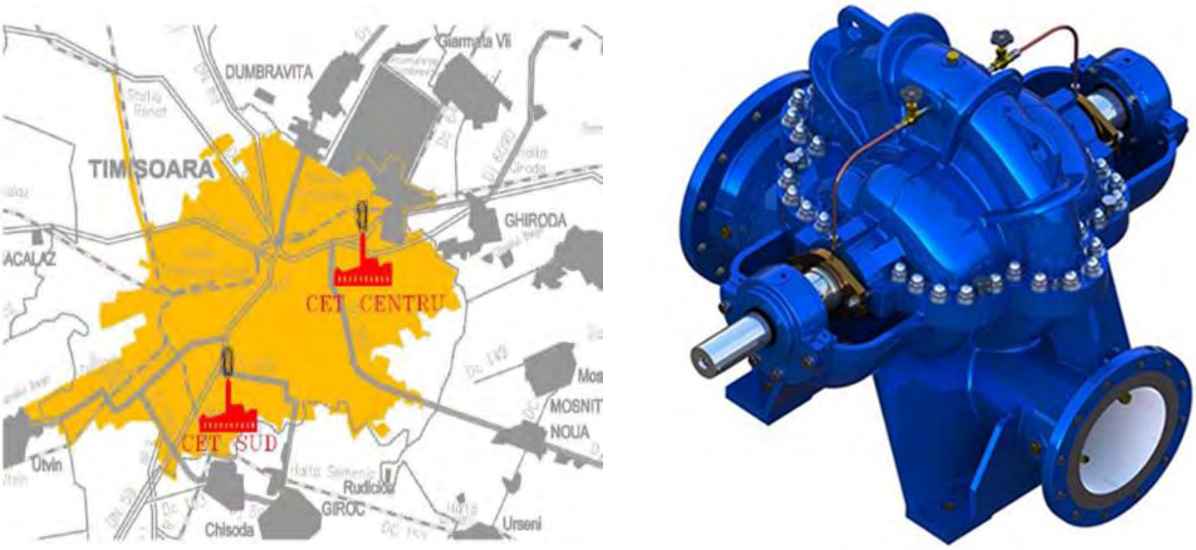

Figure 34. Position of the CET-Centre and CET-South and the centrifugal pump of type Venus.

In order to determine the current operating curves of the two pumps, the measurement of the pressure, flow rate and the efficiency is needed. For the measuring of these parameters a portable ultrasonic flow rate meter was employed together with an equipment based on thermodynamic method for measuring the pumping head and the hydraulic efficiency of the pumps.

The P22F equipment based on the thermodynamic method is produced by Robertson Technology and allows the measurement of the pumping head and the efficiency of the pump. In the thermodynamic method, pump efficiency is measured by means of temperature and pressure probes fitted to tapping points on the inlet and outlet section of the pump. The critical parameter is the differential temperature across the pump, which must be measured to an accuracy of typically 1 mK. This is achieved with Robertson Technology’s CoolTip™ technology incorporated into the P22F to provide accurate and stable measurement of pump efficiency. On-site constraints make it difficult to accurately measure pump efficiency under installed conditions by the same method that pump manufacturers traditionally use for work tests. The advent of the thermodynamic method has provided a solution to this problem. Now accurate measurements can be made on installed pumps. That is because the thermodynamic technique requires measurement of only two parameters, temperature and pressure, to determine pump efficiency and energy difference is effectively being measured. A 5% error in the measurement of energy difference (typically 20%) leads to a corresponding error in the pump efficiency measurement of 1%, for a pump operating at 80% efficiency. However, with the traditional technique, and 5% instrumentation accuracy, the error in the pump efficiency measurement would also be 5%.

The equations for the thermodynamic method are:

$$\eta = \frac{E_h}{E_m} \tag{14}$$

$$E_h = \frac{p_2 - p_1}{\rho} \tag{15}$$

$$E_m = a \cdot \left(p_2 - p_1\right) + c_p \cdot \left(T_2 - T_1\right) \tag{16}$$

where E_h is the hydraulic energy per unit mass of fluid, E_m is the mechanical energy per unit mass of fluid, p_1, p_2 are the pressure of the fluid at the inlet and outlet section of the pump, T_1, T_2 are the temperature of the fluid at the inlet and outlet section of the pump, ρ is the density of the fluid, a is the isothermal coefficient of the fluid, c_p is the specific heat capacity of the fluid.

The pumping head is calculated with the following equation:

$$H = \frac{p_2 - p_1}{\rho \cdot g} + z_2 - z_1 + \frac{v_2^2 - v_1^2}{2 \cdot g} \tag{17}$$

where z_1, z_2 are the position of the tapping points at the inlet and outlet section of the pump and v_1, v_2 are the velocity of the fluid at the inlet and outlet section of the pump.

The theoretical background to the thermodynamic method for pumps is documented in ISO 5198 and other standards. The performance of an instrument employing this method is determined by the design, accuracy and stability of the temperature and pressure probes. The pump efficiency measured with the P22F equipment is measured by accurate and innovative temperature and pressure probes. The electronic circuits are contained in the probe handles, thus eliminating potential errors from connector and cable resistances. The design allows the self-contained calibration of each temperature and pressure probe, without reference to any external electronic components. This greatly simplifies operational use and maintenance. The probes are connected to each other and to the control computer by an RS485 serial interface (Modbus™ protocol), which provides high immunity to electromagnetic interference over long distances. The connecting cables only carry the digital signals and the power to the probes.

The standard setup for the components of the P22F equipment is presented in Figure 35. The temperature probes employ a novel design to ensure high sensitivity and long-term stability. Each temperature probe has dual sensors, to detect drift in an individual sensor. The sensor and signal conditioning electronics are stable over long time period. Experience over several years shows no observable drift, less than 0.25mK. the sensors give a high electrical signal, which minimises electronic noise. With the standard temperature probes

(0-60° C), the precision of each temperature point due to electronic noise is 0.11 mK. A set of 25 readings results in a standard error of 0.025 mK for the average temperature. The standard error in the average differential temperature due to electronic noise will then be 0.035 mK. The signal conditioning electronics minimises self-heating effects in the sensors. The probes are also designed to minimise the stem effects, which can otherwise occur due to differences between the fluid and ambient temperatures. The pressures probes allow measurement of pressure in the range of -1 to 25 bar. These probes have built-in temperature sensors and active temperature correction. The accuracy of 0.1% is maintained over a wide temperature range.

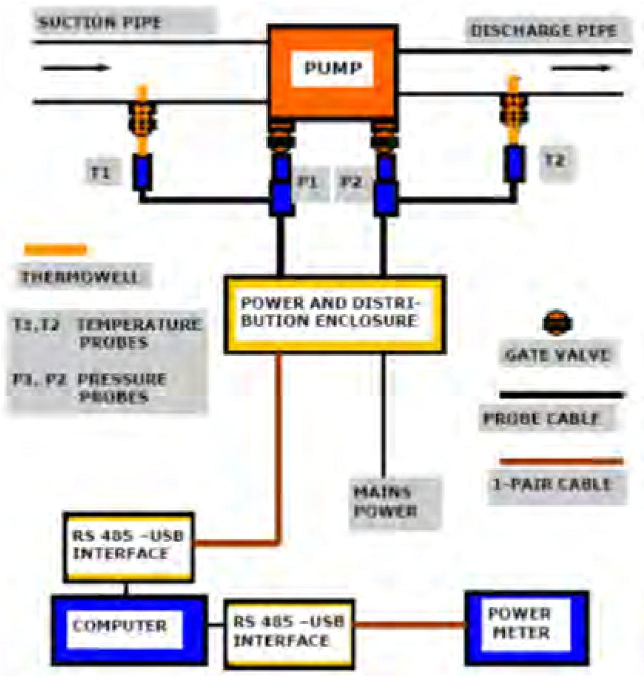

Figure 35. Configuration for the P22F equipment and on -site measurements at CET-Centre and CET-South.

Tapping points are required on the inlet and outlet of pump, ideally about two pipe diameters from the pump flanges, but one pipe diameter is sufficient if space is tight.

With the P22F, the accuracy of the pump efficiency measurement is typically ±1%. The temperature rise across the pump increases with head, so the higher the head, the more accurate the efficiency measurements. Also, the temperature rise is higher for less efficient pumps, as more energy is being lost in the pump, so the lower the pump efficiency, the more accurate are the measurements. The accuracy for this equipment, following international standard, is defined in terms of uncertainty, at the 95% confidence level. Thus, if the efficiency is 70%, with an uncertainty of 1%, there is a 95% probability that the pump efficiency lies between 69 and 71%.

Thea experimental investigations were carried out and the experimental data were compared with the operation curves given by the manufacturer of the pumps and with previous measurements performed by other teams of experts.

The main concern of the representatives of Colterm was that the two centrifugal pumps did not perform at the required operated point (ROP). The values for the required operating points for the two locations were:

- for CET-South, Q=2750 m^3/h, H=124 m
- for CET-Centre, Q=1000 m^3/h, H=125 m

After comparing the experimental data with the data provided by the pump manufacturer it resulted a good agreement. For CET-Centre it resulted that the measurement performed by the UPT research team was the most accurate in comparation with the results obtained by the previous two teams of experts.

By analysing the measured data for both pumps it resulted that neither of the two centrifugal pumps were performing at the required operated point.

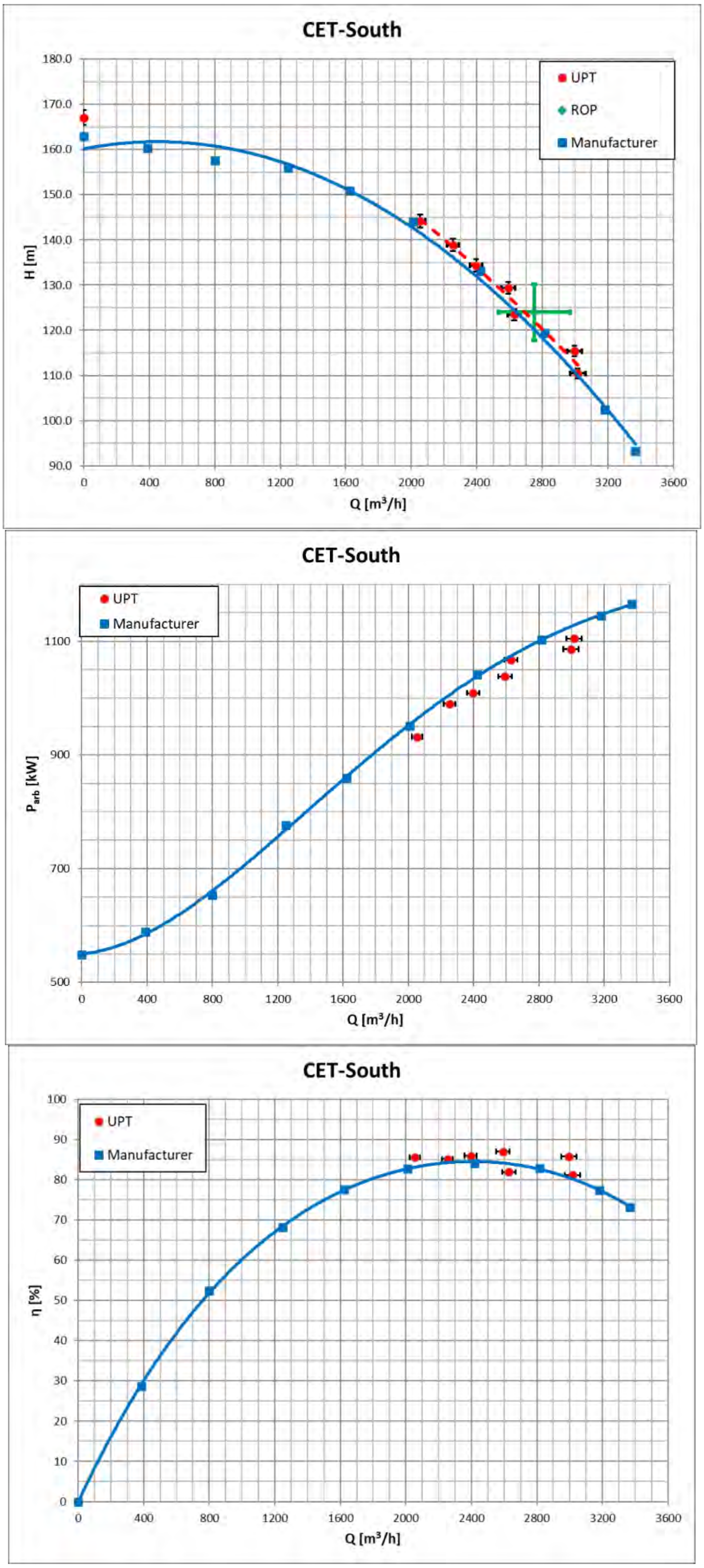

Figure 36. Operation curves of the centrifugal pump Venus 1-350.650 from CET-South.

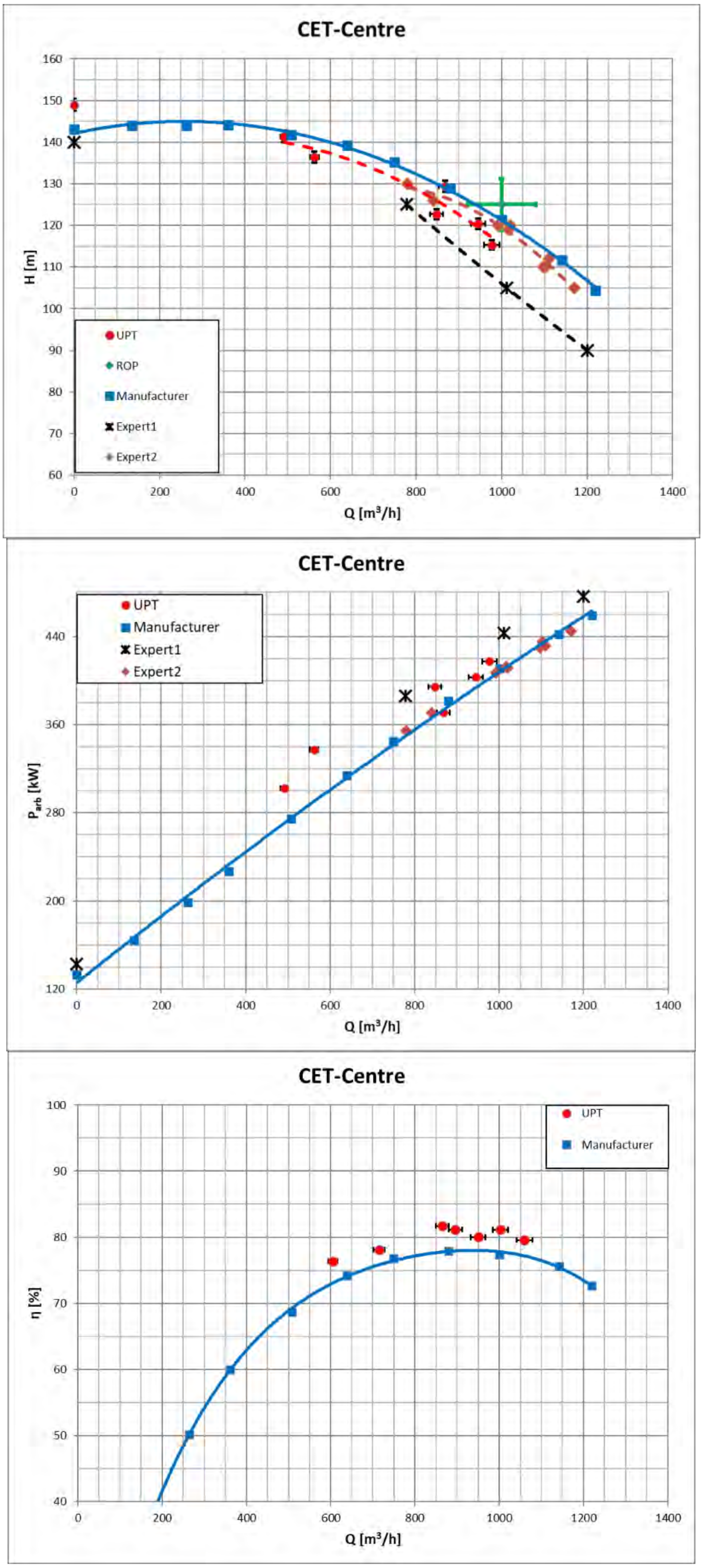

Figure 37. Operation curves of the centrifugal pump Venus 1-250.650 from CET-Centre.

In the year 2016 my proposal for a BRIDGE research grant was approved and for 2 years I managed and implemented this grant. My role in the research grant was to manage the project but I also participated to the experimental measurements, the data processing and to the writing of the research reports. The research subject was the study concerning the determination of the best operating scheme for the storage pumps of the local heat and hot water provider COLTERM S.A. The entire network for supplying heat and hot water for the citizens of the city of Timisoara consists of 118 distribution stations and 5 district heating stations. The CET-Centre power plant together with another power plant, CET-South, supplies the necessary heat and hot water for the cold season. This last power plant operates only during the cold season, while CET-Centre operates all year long.

CET-Centre power plant has been operating since 1884 and was the first power plant in Europe to produce and supply the energy for the street illumination, Timisoara being the first European city with streets illuminated by electric light. Nowadays this power plant is producing only heat and hot water. It contains five large boilers and in order to heat the water, natural gas and oil fuel is used. The water fed to the five boilers is supplied with the help of a pumping station that was refurbished first in the year 2004 and again in the year 2015. The pumping station from CET-Centre is equipped with three pumps (EPT1, EPT2 and EPT3) supplied by Grundfos in the year 2004 and one pump (EPT4) supplied by Pentair Fairbanks Nijhuis in the year 2015. These pumps have to operate in parallel, in different configuration depending on the demand of the network and to supply a prescribed flow rate and pressure for the consumers.

From the three pumps manufactured by Grundfos, two of them have constant speed (EPT1 and EPT2) and one has variable speed (EPT3). From the two pumps with constant speed, EPT1 has the diameter of the impeller equal with 585 mm and EPT2 has the diameter of the impeller equal with 590 mm. The diameter of the impeller for the pump EPT3 is also 590 mm. The nominal operating point of these three pumps is characterized by a flow rate of 1300 m3/h and a pumping head of 125 m at a rotational speed of 1485 rpm. This type of pumps has the inlet and outlet section on the same axis and the impeller is with a double suction section, Figure 38.

Figure 38. Centrifugal pump HS 300x350x590 manufactured by Grundfos.

The fourth pump, manufactured by Pentair Fairbanks Nijhuis, Venus1-2510.650 (EPT4), has an impeller with a diameter of 626 mm, the inlet section diameter is 300 mm and the outlet section diameter of 250 mm. A flow rate of 1200 m3/h and a pumping head of 144 m at a rotational speed of 1490 rpm, Figure 39, characterize the nominal operating point of this pump. This pump also has variable speed.

Figure 39. Centrifugal pump Venus1-250.650 manufactured by Pentair Fairbanks Nijhuis.

The position of the four pumps inside the pumping station is presented in Figure 40. During the spring, summer and autumn, when the CET has to deliver only hot water, the pumping station operates with maximum two pumps in parallel, usually one pump with variable speed and one pump with constant speed. During the winter, situations may occur when all the pumps have to operate in parallel configuration. The operating regimes cover a wide range for the flow rate and pumping head, the main concern being to supply optimal operating conditions for the most far distribution station.

Because the four pumps are of different types and also because over the years their operating characteristics may be altered by the operating cycles, the challenge is to find the operating regimes for each pump which allow smooth parallel operation.

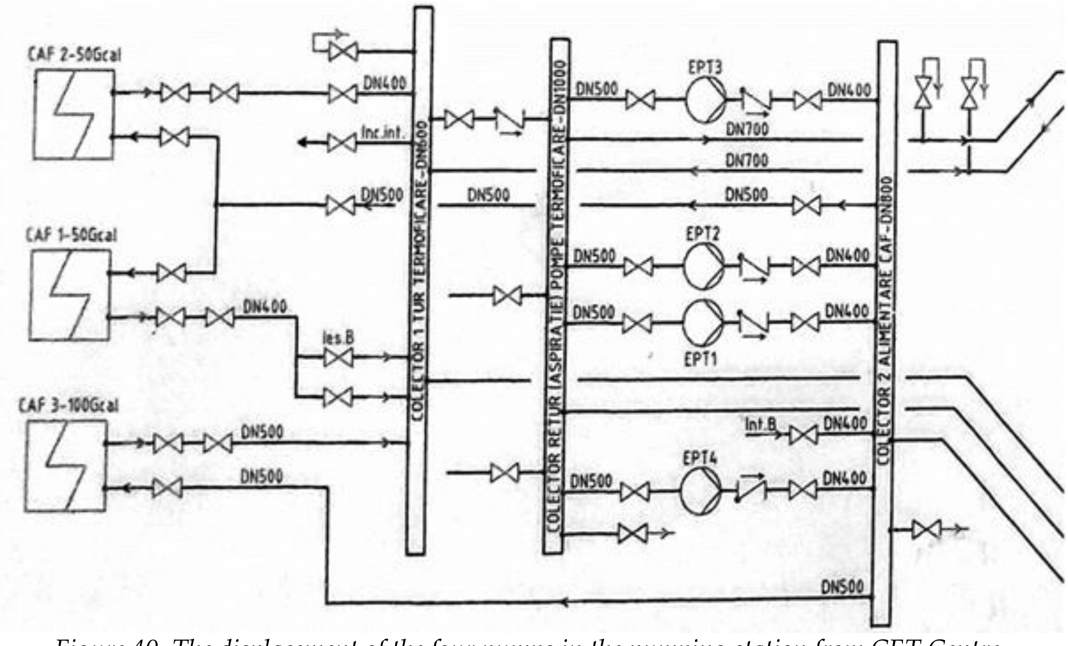

Figure 40. The displacement of the four pumps in the pumping station from CET Centre.

The experimental investigation of the operation of the four large centrifugal pumps was carried out for 4 days, on each day a single pump being investigated. For each pump, 8 operating points were measured. For every investigated operating point, three sets of measurements were performed, each containing 20 samples. The results of all those measurements were averaged and so the parameters (flow rate, pumping head and efficiency) for each investigated operating point for every pump were obtained. Each pump was operating at a constant rotational speed of 1490 rpm.

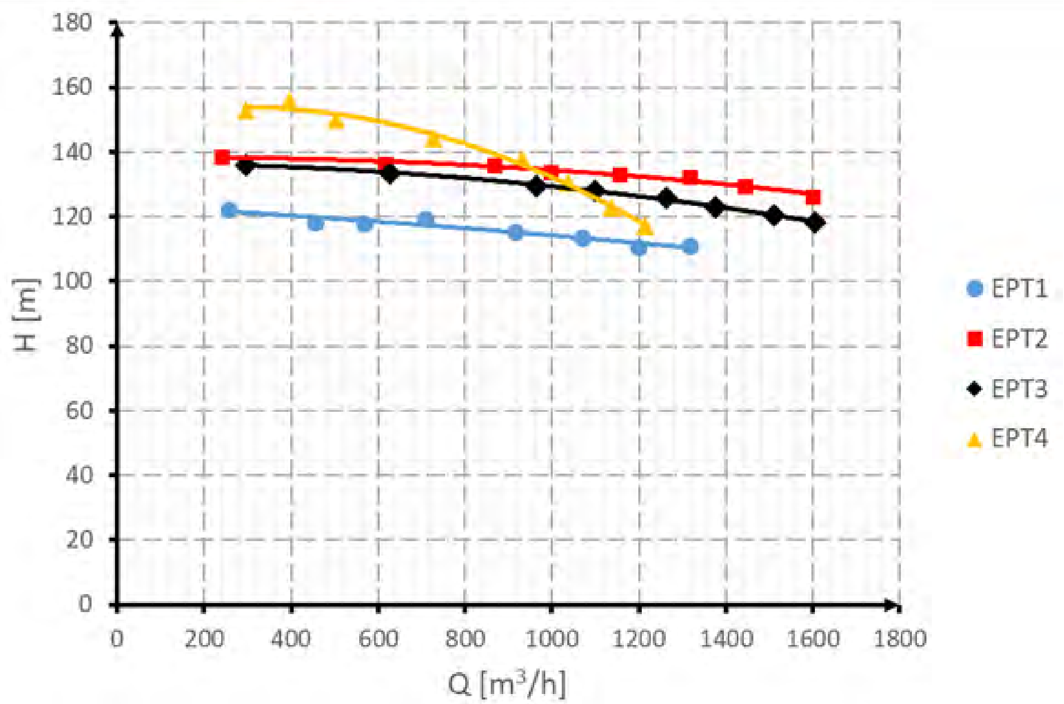

Figure 41. Pumping head vs. flow rate for the investigated centrifugal pumps from CET Centre, [10].

Analysing Figure 41, one can observe that even though the pumps EPT1, EPT2 and EPT3 are similar and manufactured by the same producer, there is a big difference between pump EPT1 and the other two pumps, EPT2 and EPT3 regarding the pumping head characteristic curve. The significant difference may be caused by the more unfavourable flow conditions from the inlet section of the pump EPT1 determined by the different geometry of the inlet piping. That can lead to a flow with pre-swirl on the inlet section and this can cause a reduced value for the pumping head. Also, a cause for the low values of the pumping head, might be some alteration of the impeller caused by cavitation. The presence of cavitation may be determined by the shape of the inlet piping system of this pump which is different from the other two similar pumps. An inspection of the impeller of the pump EPT1 is required in order to determine the presence of the effects of cavitation. The fourth pump, EPT4, being a totally different centrifugal pump than the other three, has a completely different pumping head curve. Because of the different pumping head curve characteristics, a stable parallel operation of these pumps will be difficult to obtain.

From the efficiency point of view, Figure 42, the centrifugal pump EPT4 achieves the best efficiency point for lower values of the flow rate and for higher values of the flow rate both pumps EPT2 and EPT3 achieve the best efficiency point. The centrifugal pumps EPT2 and EPT3 have similar efficiency values for almost the entire operating range. There is a slight difference in efficiency only between 1400 m^3/h and 1600 m^3/h. Because of the poor values of the pumping head, pump EPT1 has also low efficiency values compared to the other three pumps. When operating, this pump will consume more electrical power than the other two similar pumps (EPT2 and EPT3) leading to higher costs. A refurbishment of this pump is recommended.

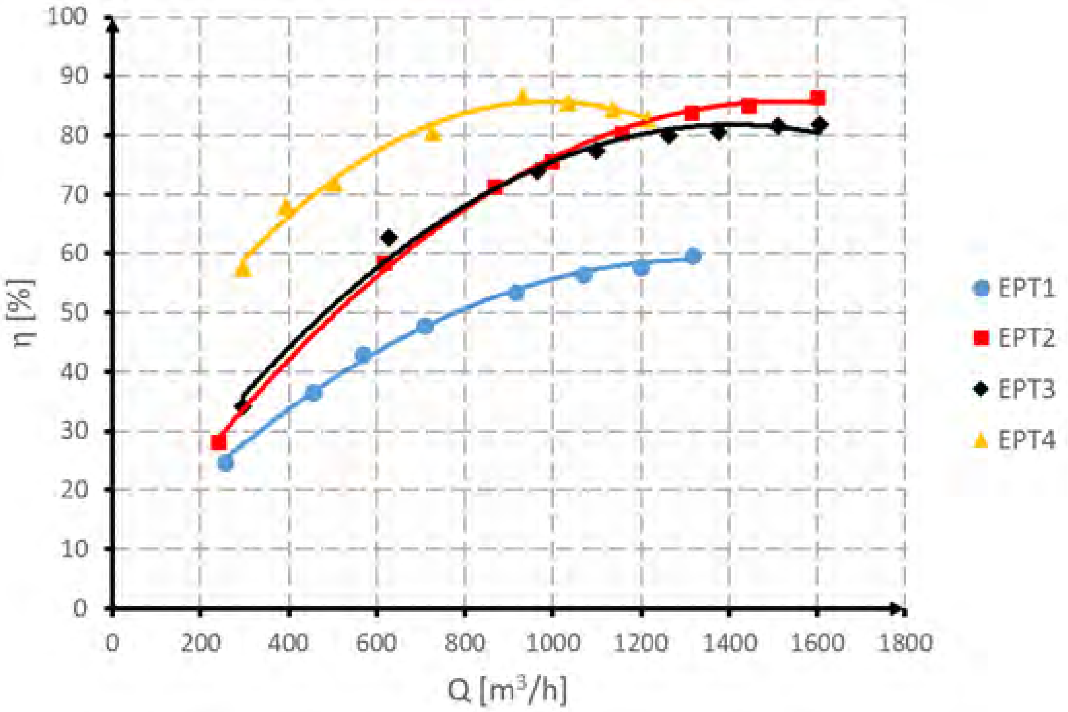

Figure 42. Efficiency vs. flow rate for the investigated centrifugal pumps from CET Centre, [10].

Gulich, [31], shows that for stable parallel operation, steadily falling Q-H-curves are required, because unambiguous intersection points between the combined pump characteristics and the system curve must be obtained. If the pump Q-H-curve is flat in the part load range, one pump can displace another during parallel operation, since the Q-H-curves of the individual pumps are not exactly identical due to manufacturing tolerances and wear. In this case, the Q-H-curves for the four pumps are very different which will lead to problems when they operate in parallel. Even pumps whose Q-H-curves are clearly different can be operated in parallel. In that case, the pump with the lower shut-off head should be started up only when the required head is lower than the shut-off pressure of the pump to be added. Similarly, the pump with the lower shut-off pressure must be shut down before the head required by the system exceeds the shut-off pressure of the smaller pump.

We analysed the possibility of operating these four centrifugal pumps in parallel configuration. Only two pumps are required to operate in parallel at a time. From this analysis, four possible scenarios were obtained, Figure 43, where one pump has constant speed and the other one has variable speed:

- pump EPT1 operating in parallel with pump EPT3 which has a rotational speed of 1400 rpm,
- pump EPT1 operating in parallel with pump EPT4 which has a rotational speed of 1325 rpm,
- pump EPT2 operating in parallel with pump EPT3 which has a rotational speed of 1490 rpm,

- pump EPT2 operating in parallel with pump EPT4 which has a rotational speed of 1400 rpm.

The best cases for parallel operation of the pumps are the last two, because the values of the pumping head are higher than the requested value of 125 m for all the flow rate domain. Of the two cases, the most favourable is that of pump EPT2 operating together with pump EPT3 because the range of the flow rate is the largest. Because the system curve changes a lot due to the variable demand from the network, an operating of these pumps only in the range of high values of the efficiency is not possible.

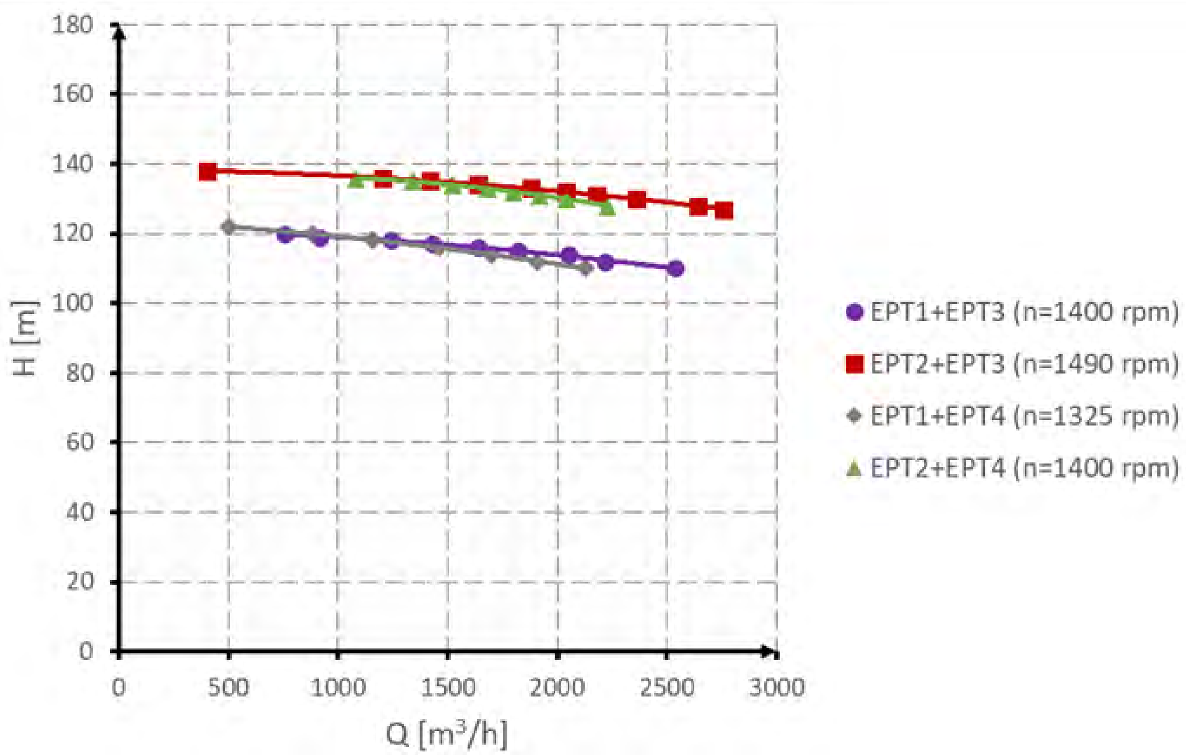

Figure 43. Pumping head vs. flow rate for the investigated centrifugal pumps from CET Centre, operating in parallel.

The pumping station from CET South has a large number of centrifugal pumps, but only three of them usually operate. Two pumps are old but refurbished (EPT1.1 and EPT 2.2) and one pump is new (EPT 1.2). The new pump was provided by the manufacturer Pentair Fairbanks Nihjuis and is of the type Venus1-350.650. The operating point has a flow rate of 3250 m^3/h and a pumping head of 164 m. These three storage pumps were investigated in order to obtain the operating curves. The measurements were performed using a the P22F equipment based on the thermodynamic method and a portable ultrasonic flow rate meter.

From the analysis of the operation curves, it results that the curves pumping head vs. flow rate have a flat shape and this is favourable for the parallel operation. Also, it results that pump EPT 1.2 has the best efficiency, so it is recommendable to operate with this pump as much as possible.

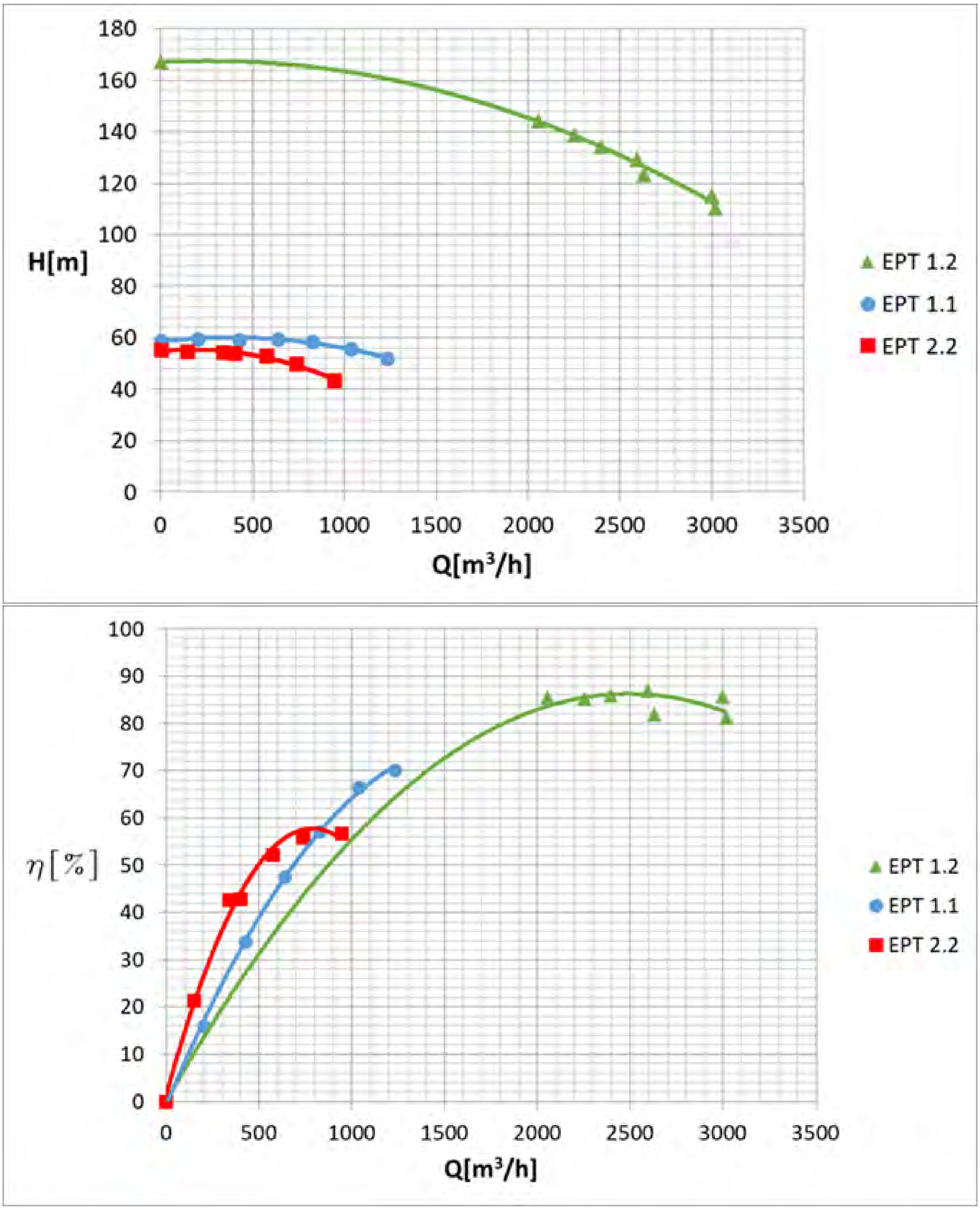

Figure 44. Operation curves for the three pumps from CET South.

In winter, the requirements for the pumping station from CET South is to deliver a pressure of 14 bar (142,71 m.c.a) for a flow rate domain of 1000 to 2000 m3/h. From Figure 45 it results that this demand is achieved by using only pump EPT1.2.

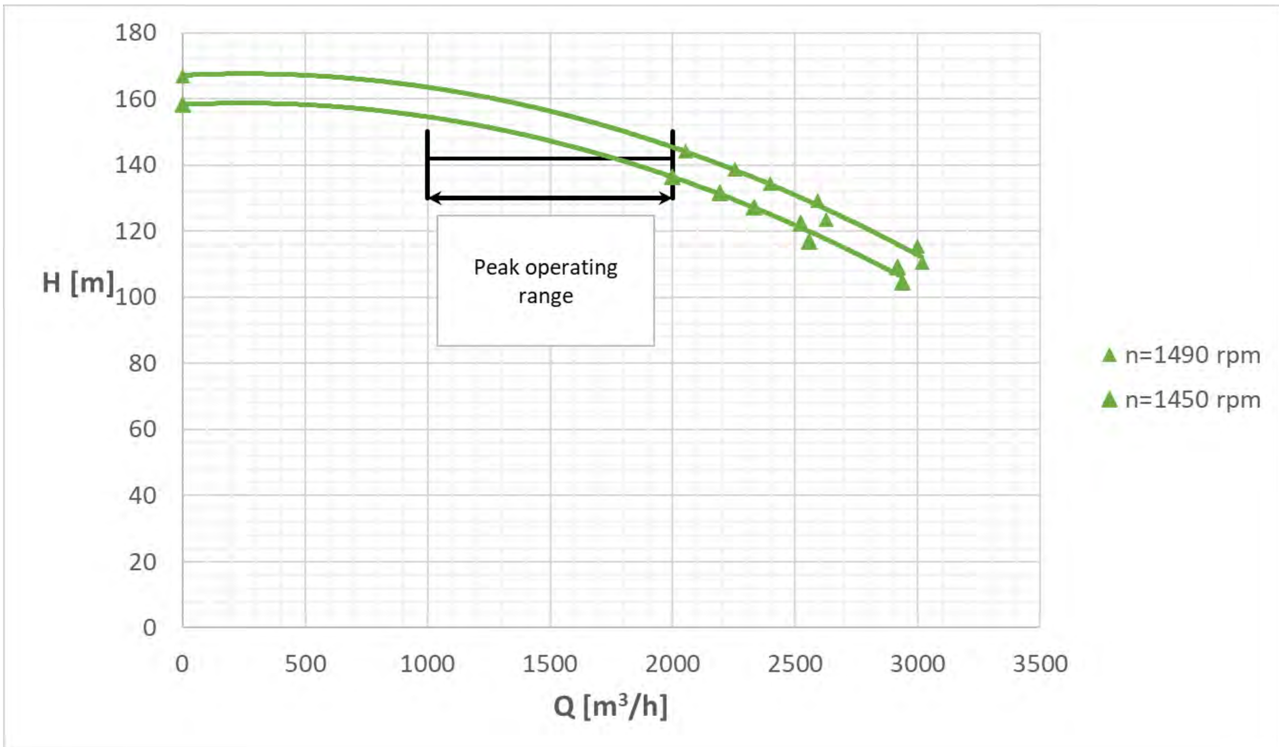

Figure 45. Pumping head vs. flow rate for storage pump EPT1.2 from CET South.

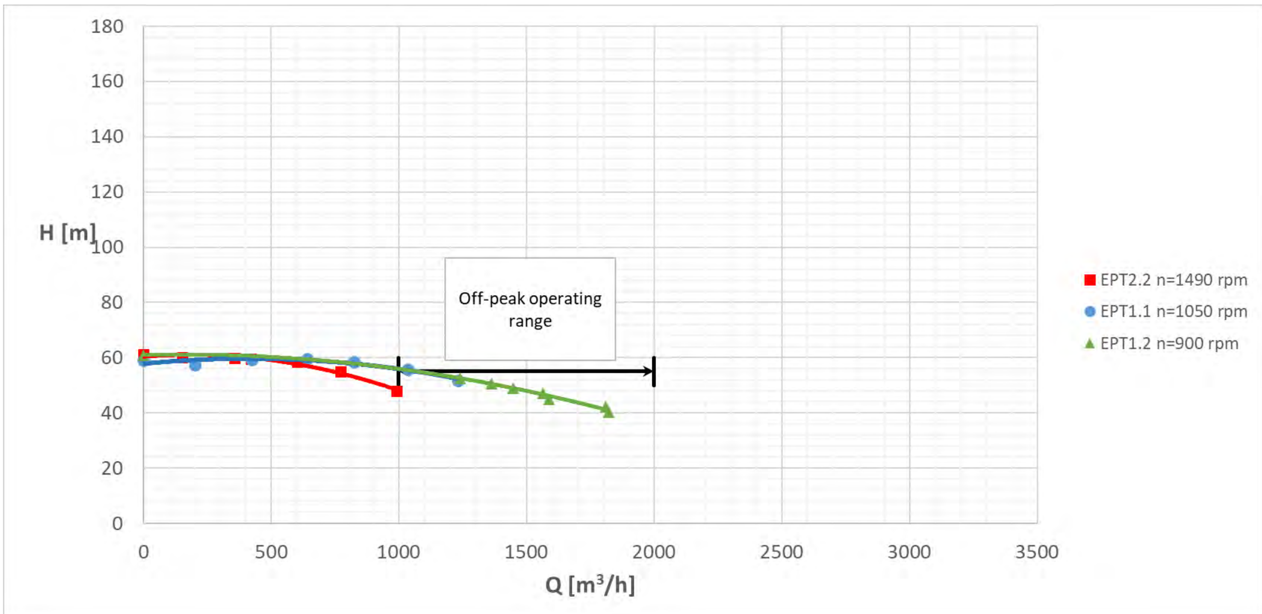

Figure 46. Pumping head vs. flow rate for storage pump EPT1.1, EPT1.2 and EPT2.2 from CET South.

There are also additional demands for the pumping station from CET South, so that it has to deliver a pressure of 5 bar (51 m.c.a) for the same flow rate domain. For this case, there are 4 operating solutions:

- EPT1.1+EPT1.2 operating at n=900 rot/min,
- EPT1.1+EPT2.2 operating at n=1050 rot/min,
- EPT1.2 operating at n=900 rot/min+EPT2.2 operating at n=1050 rot/min,
- EPT1.1+EPT1.2 operating at n=900 rot/min+EPT2.2 operating at n=1050 rot/min.

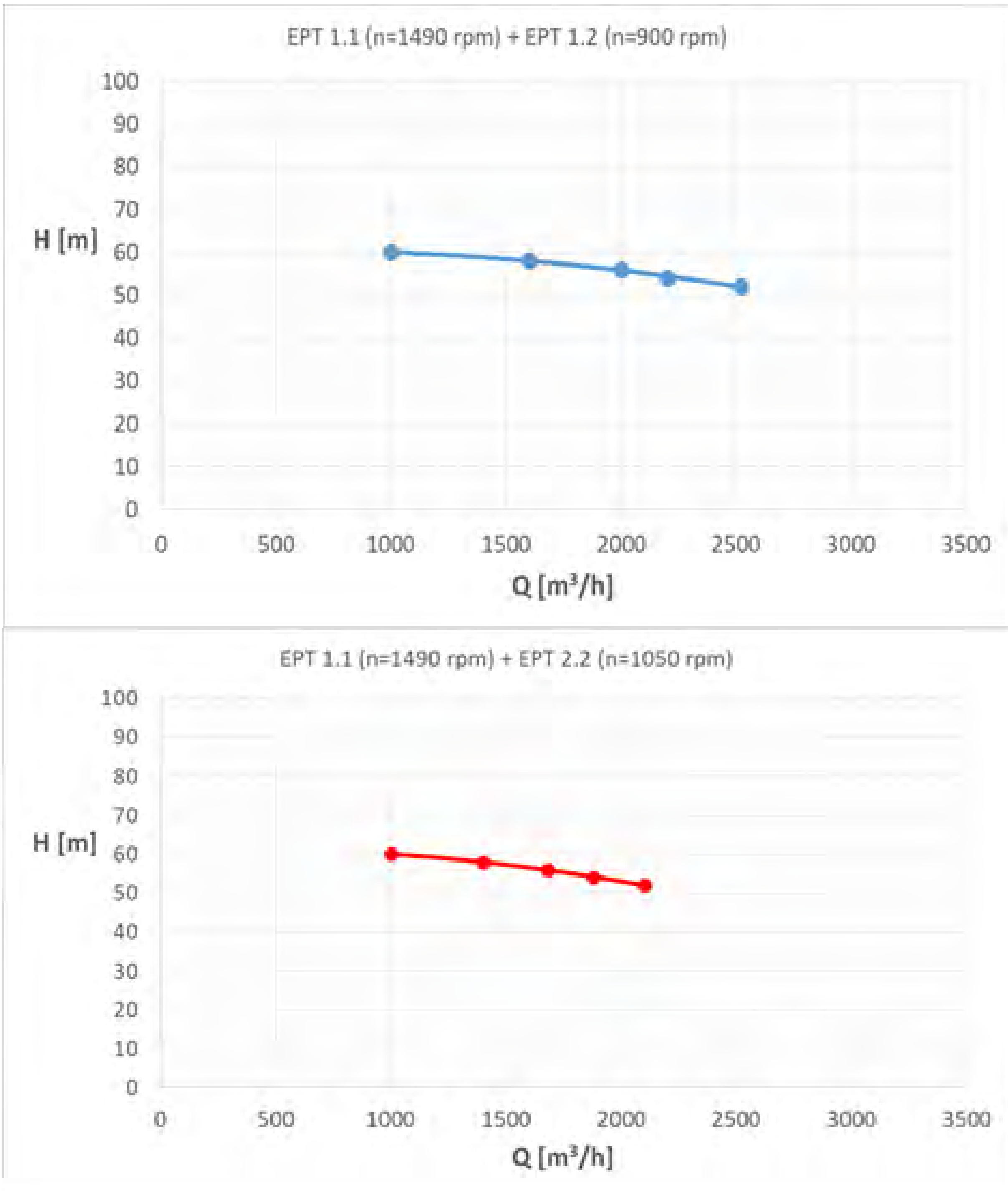

Figure 47. Operating curves for parallel operation of the storage pumps from CET South, first two solutions.

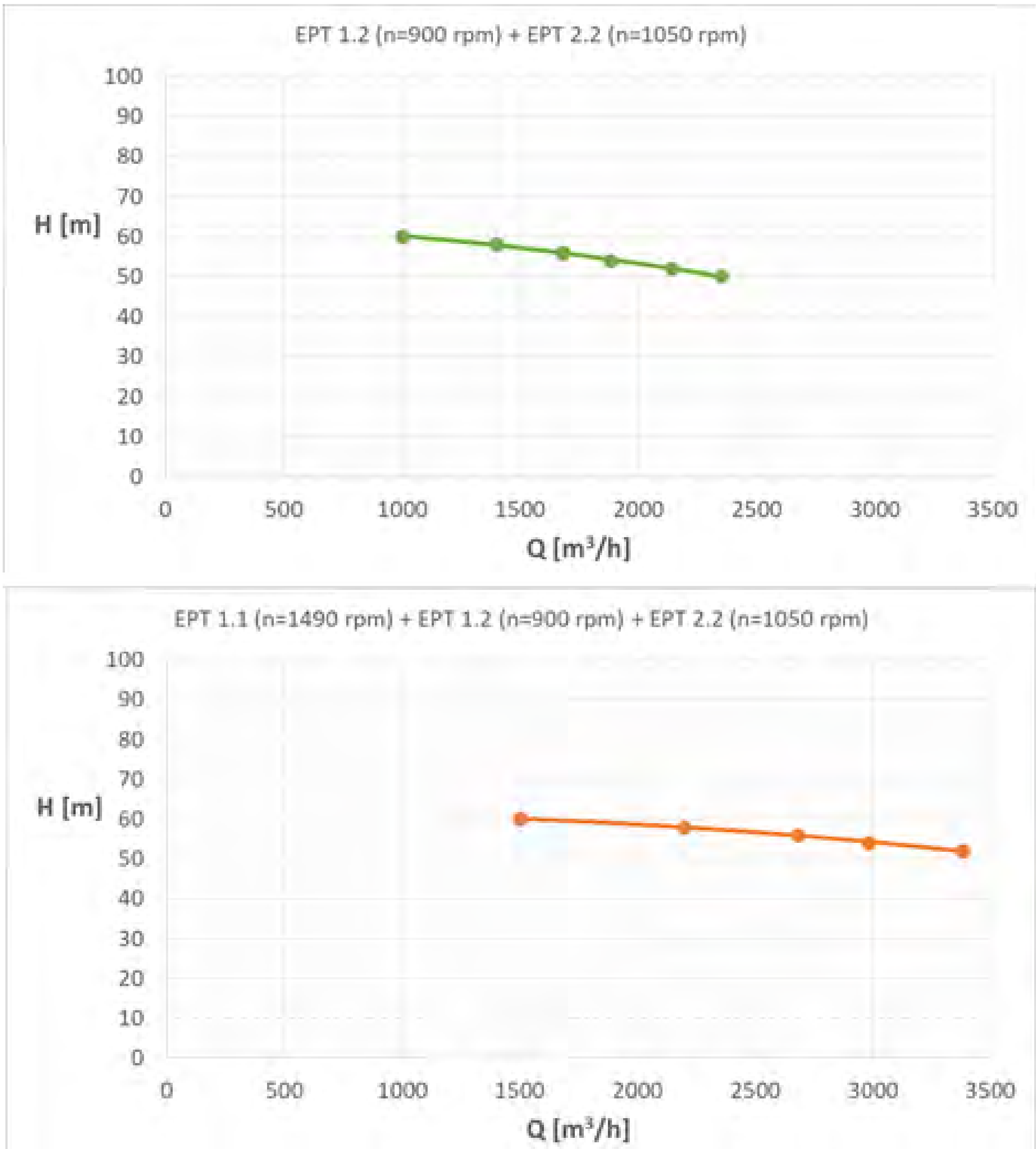

Figure 48. Operating curves for parallel operation of the storage pumps from CET South, second two solutions.

Analysing the operation curves from Figure 47 and Figure 48 it results that it is recommended to use the parallel operation of the pump EPT1.2 with one of the other two pumps because it has the highest values of efficiency. The operation of the pump EPT1.1 is allowed only if it operates in the domain of flow rates of 900 to 1250 m^3/h where it has high efficiency values and the pump EPT 2.2 is allowed to operate in the domain of the flow rate of 500 to 1000 m^3/h.

The most recent research in the domain of pumps was represented by the research project with an agricultural company, S.C. Emiliana West Rom S.R.L., for the replacement of an axial pump from the pumping station Cenad.

The pumping station Cenad had two axial pumps, each pump with the following operating characteristics: maximum flow rate of 1.5 m^3/s, pumping head of 7.5 m, a rotational speed of 585 rpm and an electric consumed power of 145 kW. The requirement of the company was to find a technical solution which implies minimum changes to the pumping station so that the flow rate to increase up to 4…5 m^3/s. The pumps that were equipping the pumping station had two roles:

- To ensure the necessary water for the irrigation system by pumping the water from the river Mures to the irrigation canals,
- To ensure the evacuation of water in the case of flooding and to pump the water from the irrigation canals back into the river

There were two solutions that were taken into consideration:

- The replacement of one of the existing pumps with one new pump with a higher value of the flow rate,
- The replacement of both existing pumps with two new pumps that could deliver the required flow rate.

For finding the best technical solution the first step was to calculate the characteristic curve of the piping system that would be connected to the pumping station.

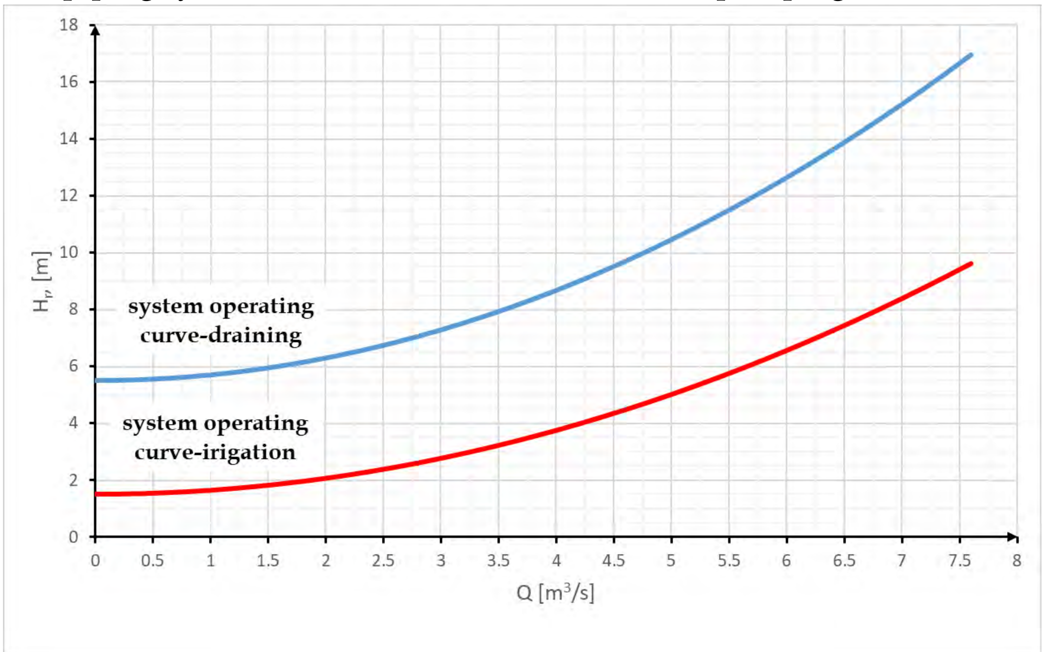

Figure 49. Characteristic curve of the pipe system form pumping station Cenad.

Then, to determine the operating points of the new pumps, the characteristic curve of the system was overlapped with the operating characteristics of each of the investigated pumps. Five cases were investigated:

- A single pump manufactured by Flygt of type PL7121/905-3-495N4,
- Two pumps manufactured by Flygt of type PL7081/766-3-990B4 that operates in parallel configuration,
- Two pumps manufactured by Grundfos, of type KWM.1400.350.12.T.50.M.40,
- A single pump manufactured by Flyght, of type P7105/865/230kW,
- A single or two pumps manufactured by Flygt, of type PL 7105/8653-1020.

From analysing the operation of the pump Flygt type PL7121/905-3-495N4 it resulted that the value of the supplied flow rate is high enough, but the price is too high and the acquisition of this type of pump would lead to civil engineering works and also to the replacement of the electrical transformer.

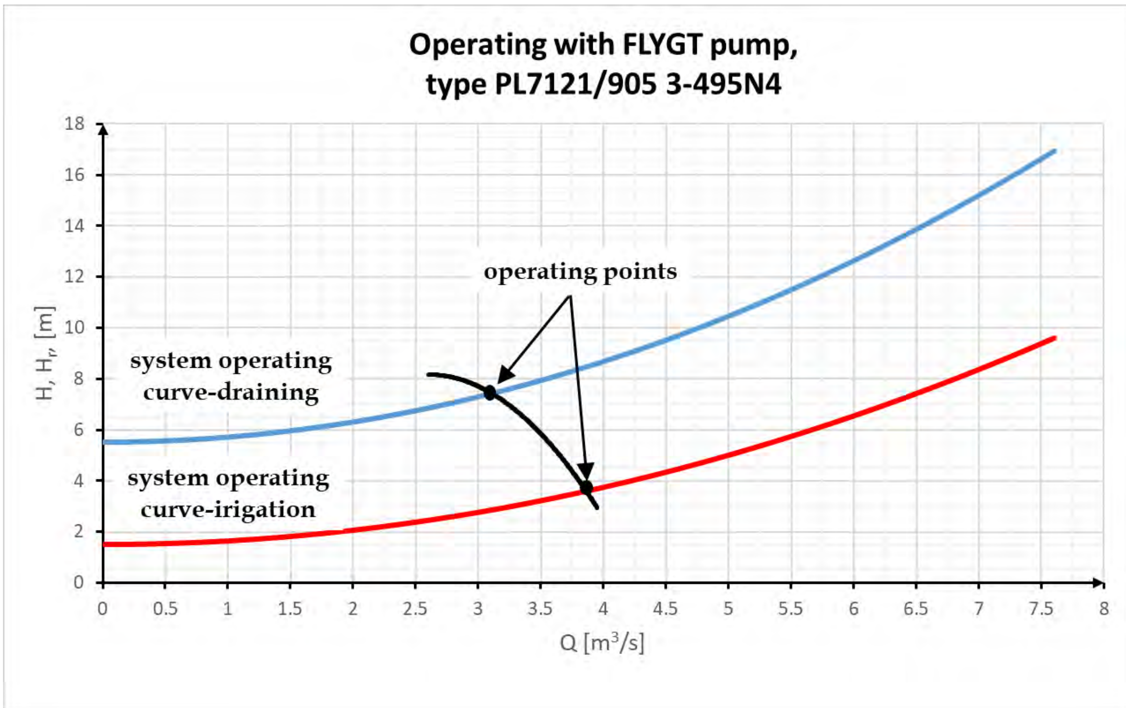

Figure 50. Operating points for the pump Flygt PL7121/905-3-495N4.

From analysing the operation of the two identical pumps Flygt of type PL7081/763 3-990B4, operating in parallel configuration, it resulted that the two pumps supply the required flow rate, for both irrigation and draining, the necessary civil work for fitting the new pumps are not so extended, but the electrical transformer has to be changed.

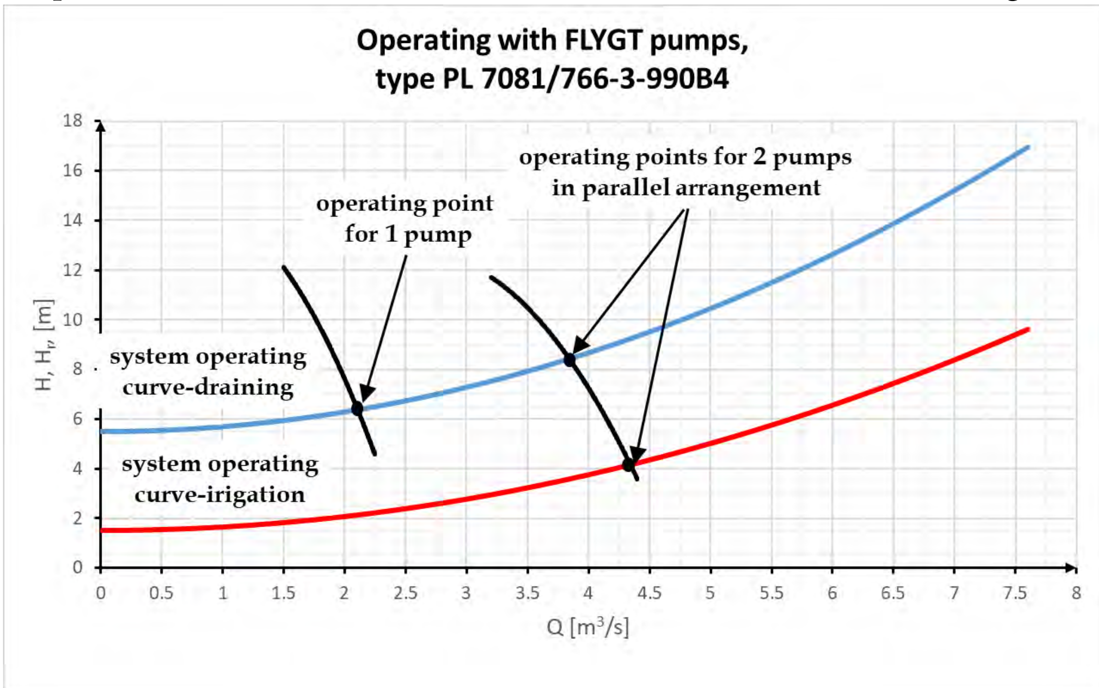

Figure 51. Operating points for the pump Flygt PL7081/766-3-990B4, single and parallel operation.

Analysing the third solution, two identical pumps of type KWM.1400.350.12.T.50.M.40, resulted that the required flow rate would be ensured, the electrical motors that drive the pumps consume a large quantity of electrical power and also the electrical transformer has to be replaced and the required civil works engineering are extensive.

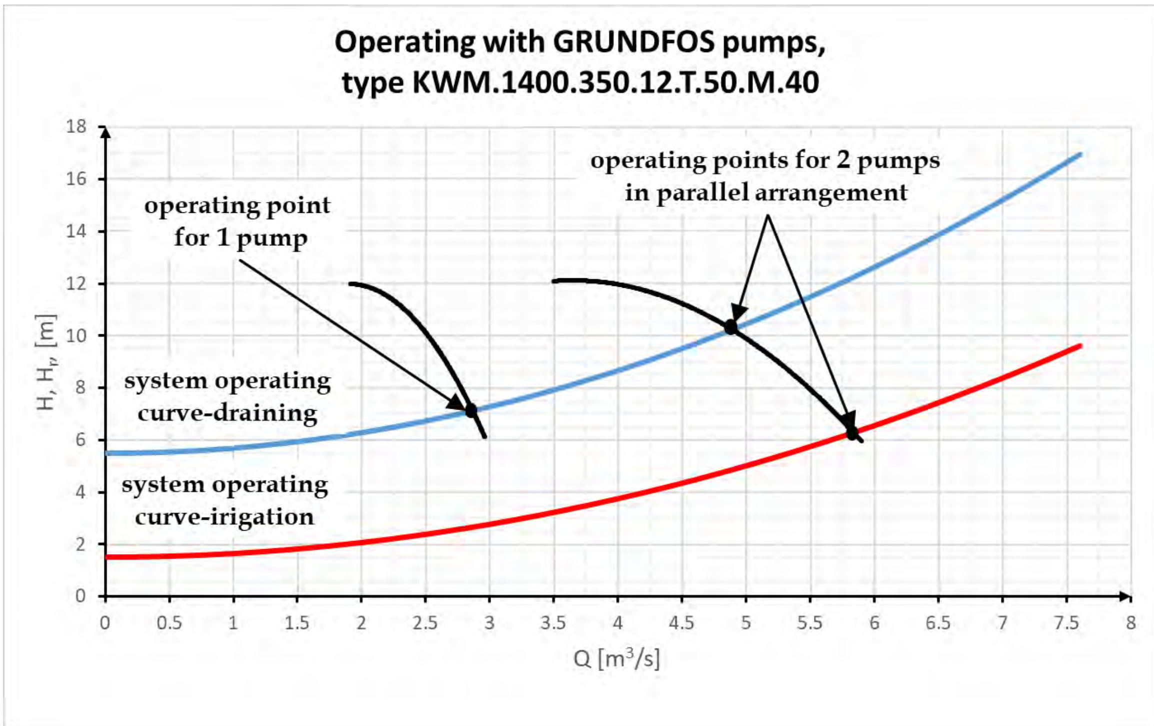

Figure 52. Operating points for the pump Grundfos KWM.1400.350.12.T.50.M.40, single and parallel operation.

The fourth type of pump, P7105/865/230kW, did not provide a large enough value of the pumping head for the pump when operating for the draining of the canals.

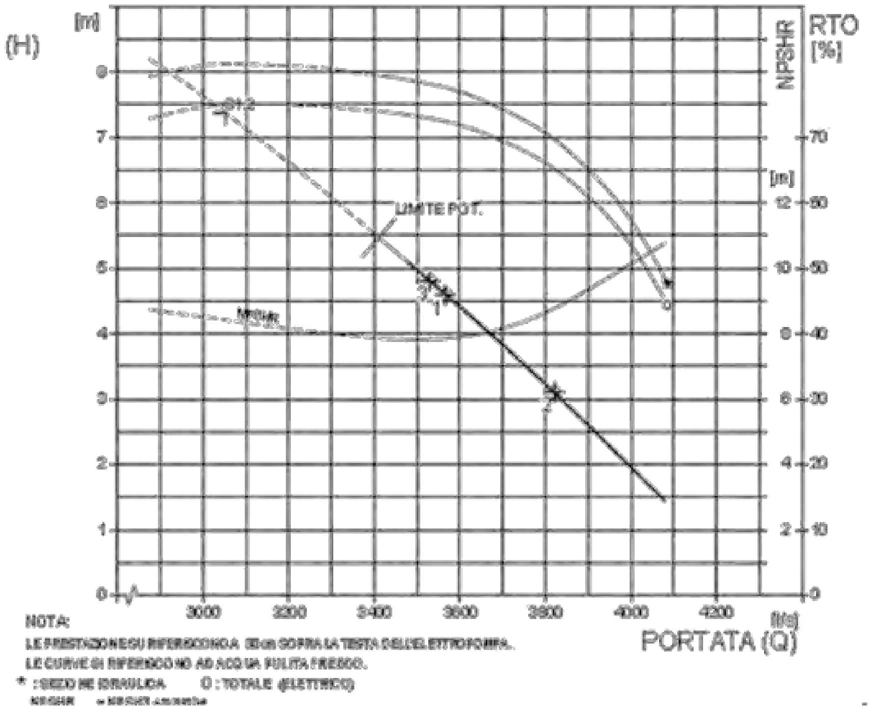

Figure 53. Operating curves for the pump Flygt P7105/865/230kW, provided by the manufacturer.

The fifth analysed scenario, concerning the pump Flygt PL7105/8653-1020, proved to be the best solution which was the chosen one. The pump has the capability to operate at different rotational speed providing the required flow rate with minimum consumption of electrical power, for both operation modes of irrigation and draining.

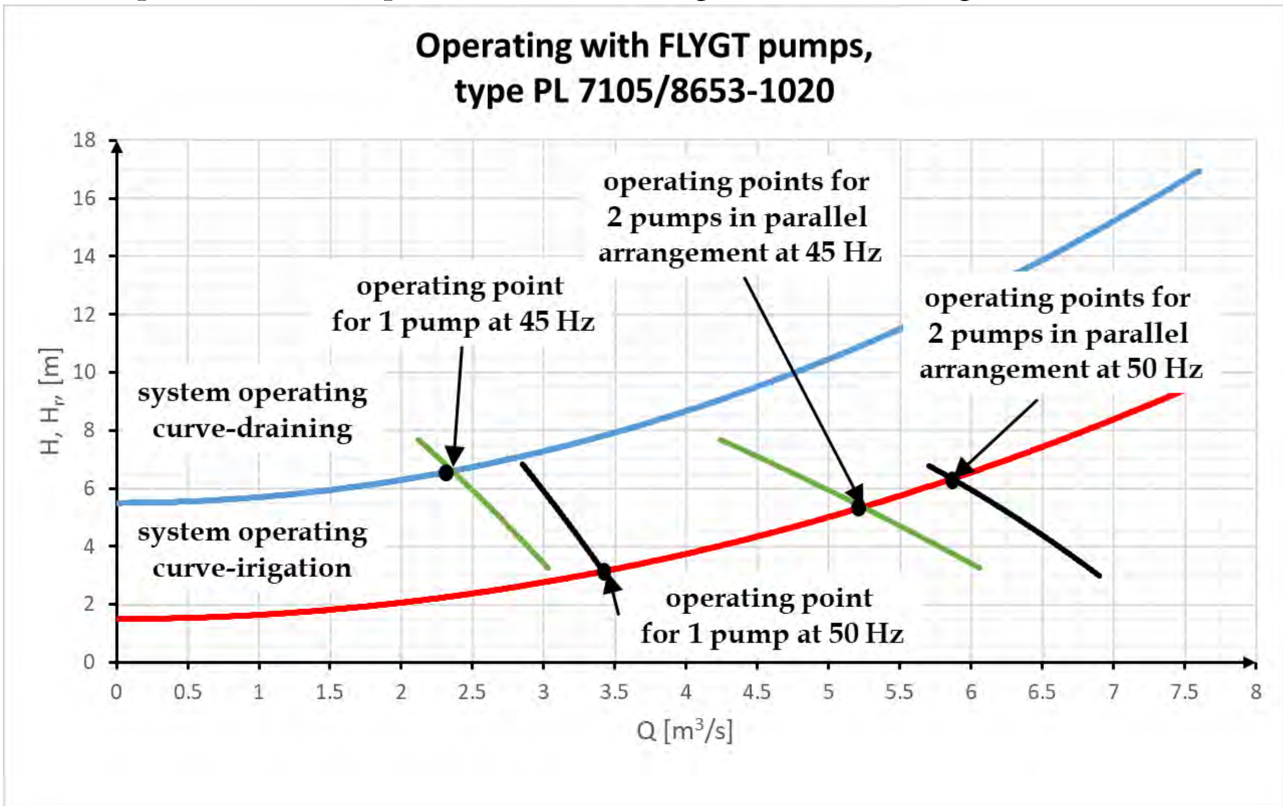

Figure 54. Operating points for the pump Flygt PL7105/8653-1020, single and parallel operation, at different values of the rotational speed.

1.2.2. Scientific achievements in the domain of hydraulic turbines

Another research domain of mine is represented by the investigation of the flow in hydraulic turbines, more precisely the study of a phenomena which appear when the Francis turbines are operating away from the best efficiency point, entitled the vortex rope.

During the years 2013-2016 I was a member of a research grant coordinated by prof.dr.ing. Romeo SUSAN-RESIGA, *Instabilități autoinduse ale curgerii cu rotație în turbine hidraulice la regimuri departe de regimul optim.* My activity consisted in performing numerical simulation of the flow in the draft tube of a Francis turbine, with the aim to find the appropriate numerical set up for modelling this flow phenomena.

The investigations were employed on a well-known geometry of a draft tube from the FLINDT project, where numerical and experimental results were available in order to validate our numerical results.

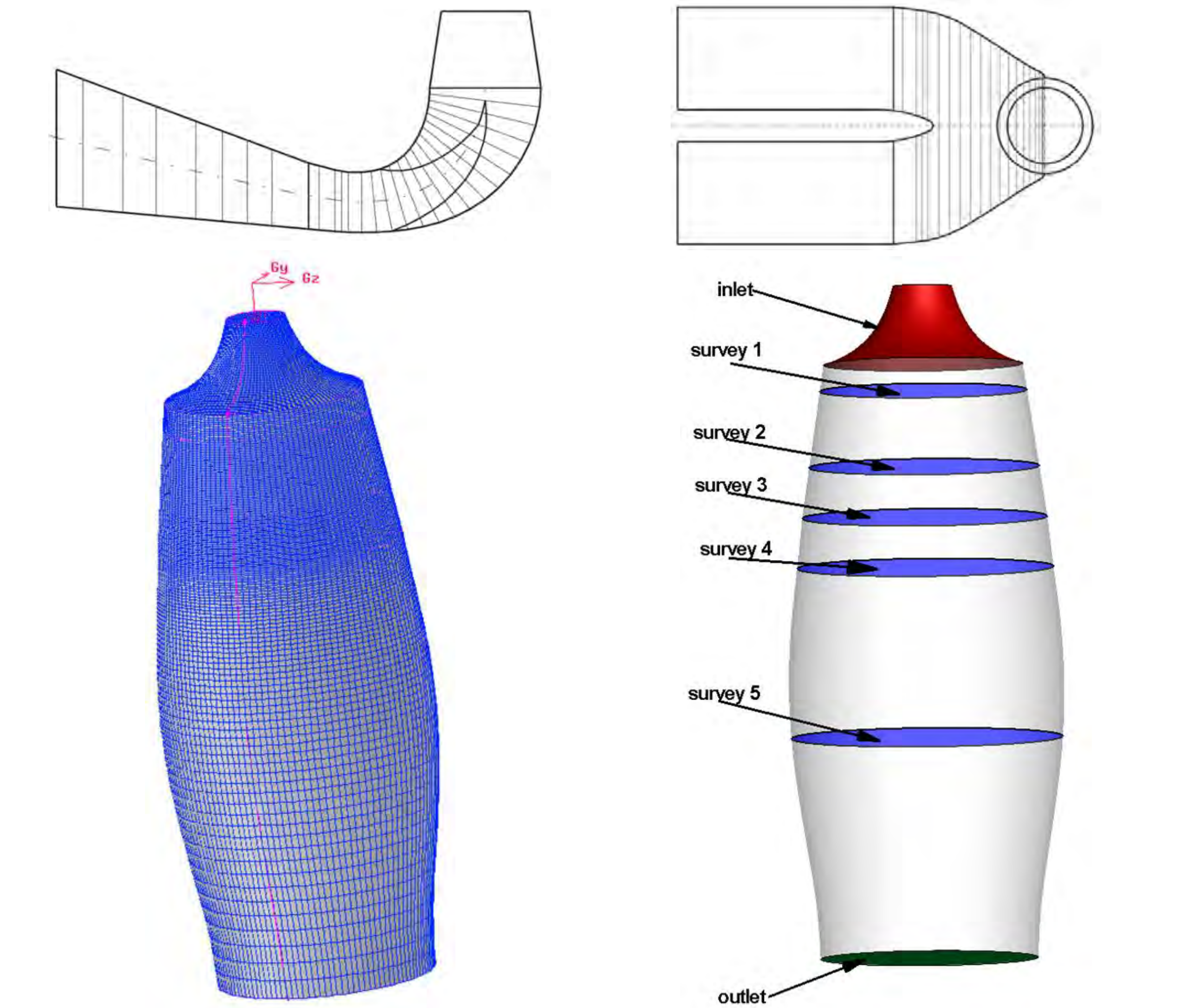

Figure 55. Simplified 3D draft tube from FLINDT project, pressure monitoring sections.

To find the best suited numerical set-up for modelling the evolution of the vortex rope, a great number of cases were analysed, taking into consideration previous results of other researchers, and by changing different numerical set-up parameters we tried to identify how these parameters influence the numerical results:

- turbulence models from the software ANSYS Fluent 6.3 (inviscid, realizable k-ε, Reynolds Stress Model-RSM, Large Eddy Simulation-LES, Detached Eddy Simulation-DES) and later with the software ANSYS Fluent 15, which had implemented a new turbulence model (Scale-Adaptive Simulation-SAS),
- different types of boundary conditions on the outlet section of the domain
- different values for the time step.

In the early phase of our scientific research, the analyse of the numerical results to underline the presence of the vortex rope was performed using iso-surface of constant pressure and velocity, and by monitoring the pressure pulsation in different sections of the draft tube, as all the researchers in the domain were doing.

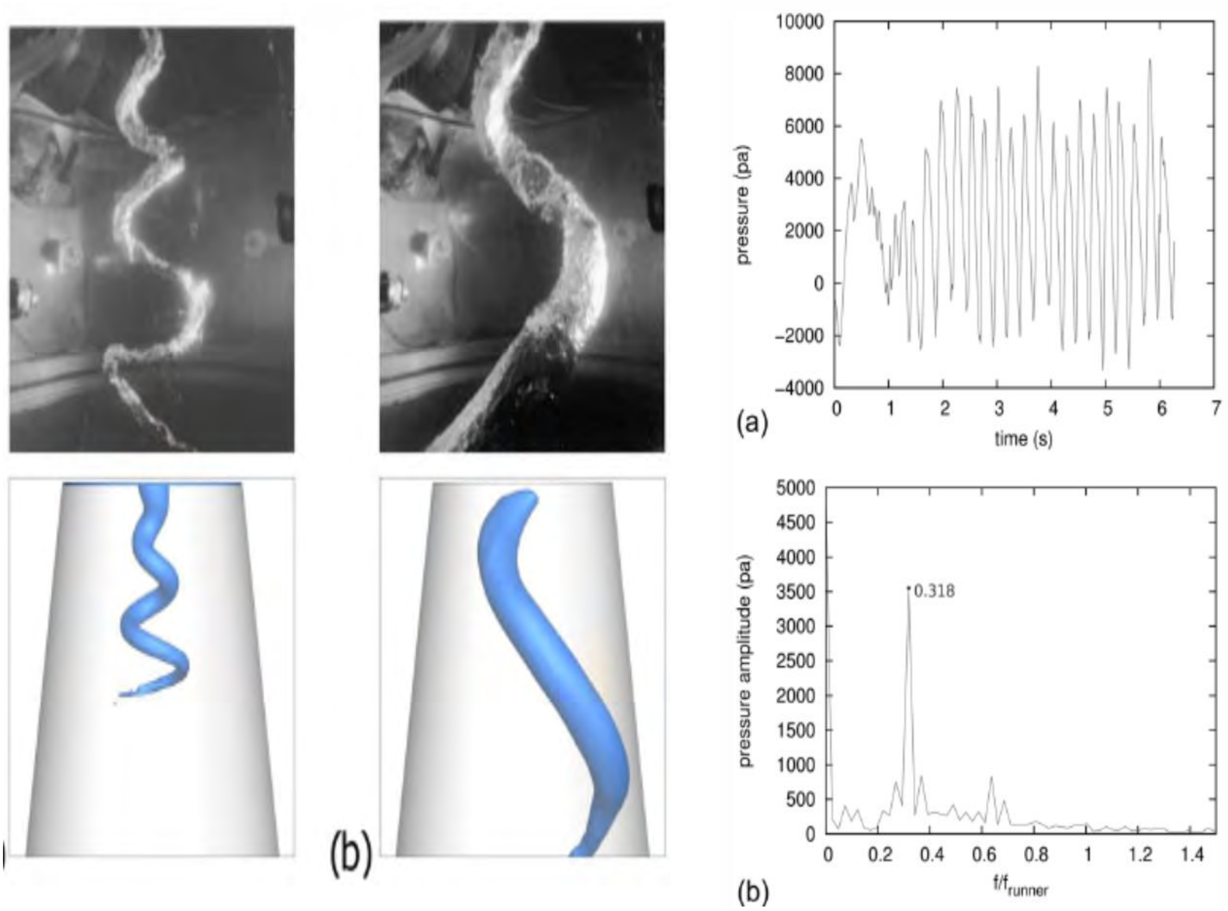

Figure 56. Numerical results of modelling the vortex rope for FLINDT draft tube obtained by Foroutan & Yavuzkurt, [32].

Together with prof.dr.ing. Romeo SUSAN-RESIGA, I applied a new method to underline the presence of the vortex rope, with the help of the vortex core values computed from the hydrodynamic field of the flow by employing the software TECPLOT. Comparing this method of highlighting the presence of the vortex rope with previous methods, it proved to be the most accurate and illustrated the entire filament of the vortex rope.

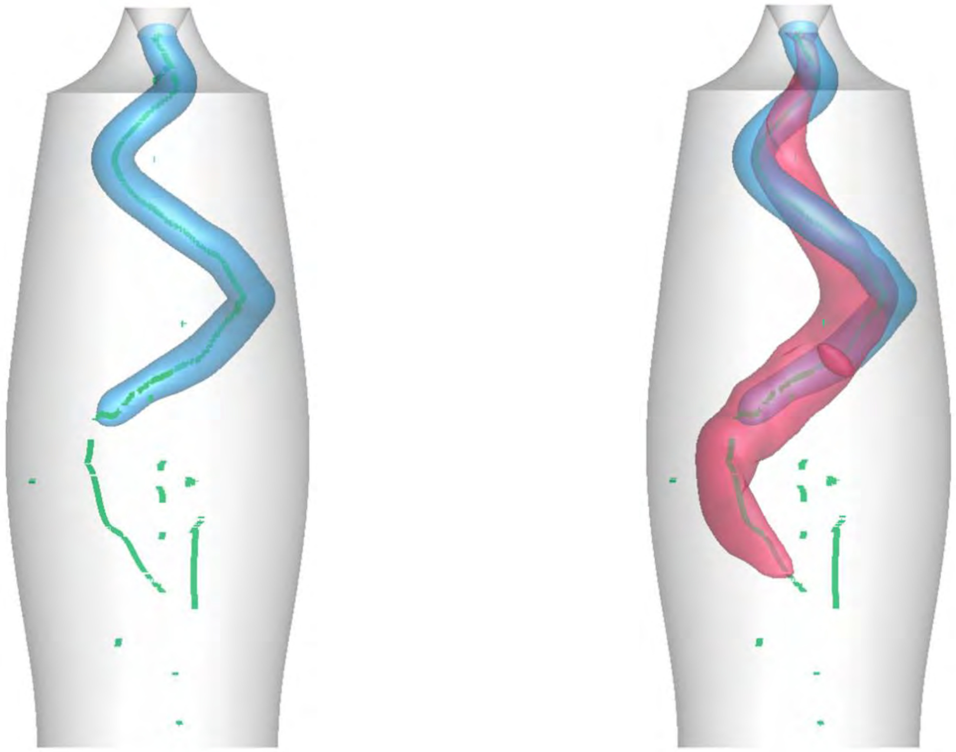

Figure 57. Pressure & velocity iso-surface and vortex core, realizable k-ε turbulence model, Fluent 6.3.

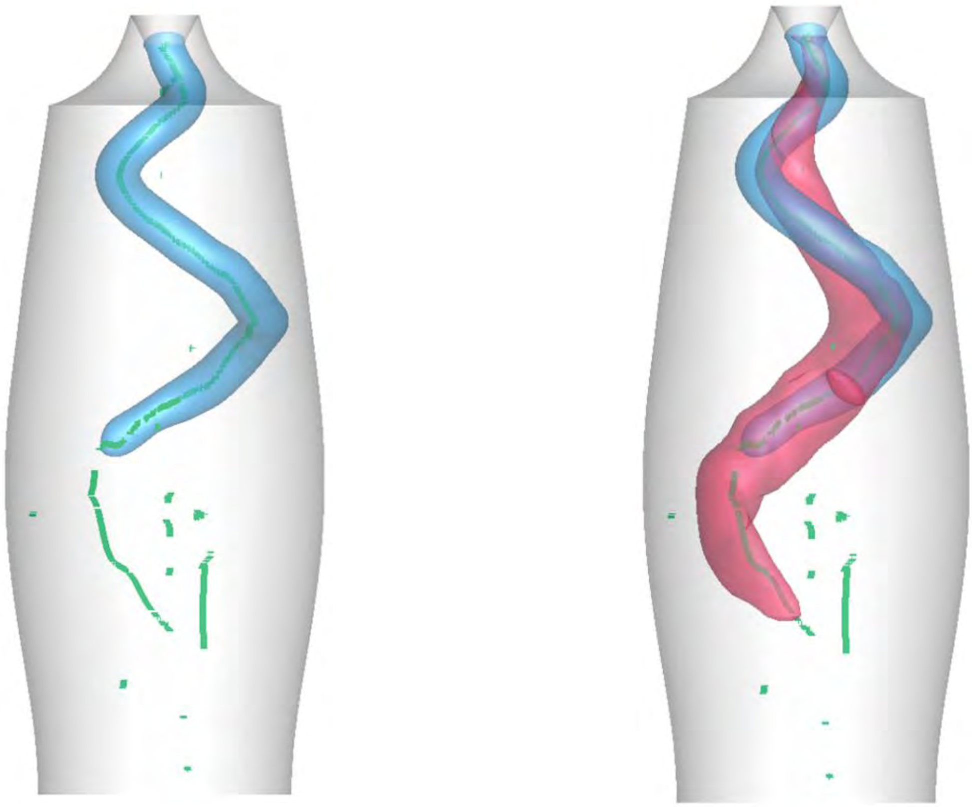

Figure 58. Pressure & velocity iso-surface and vortex core, RSM turbulence model, Fluent 6.3.

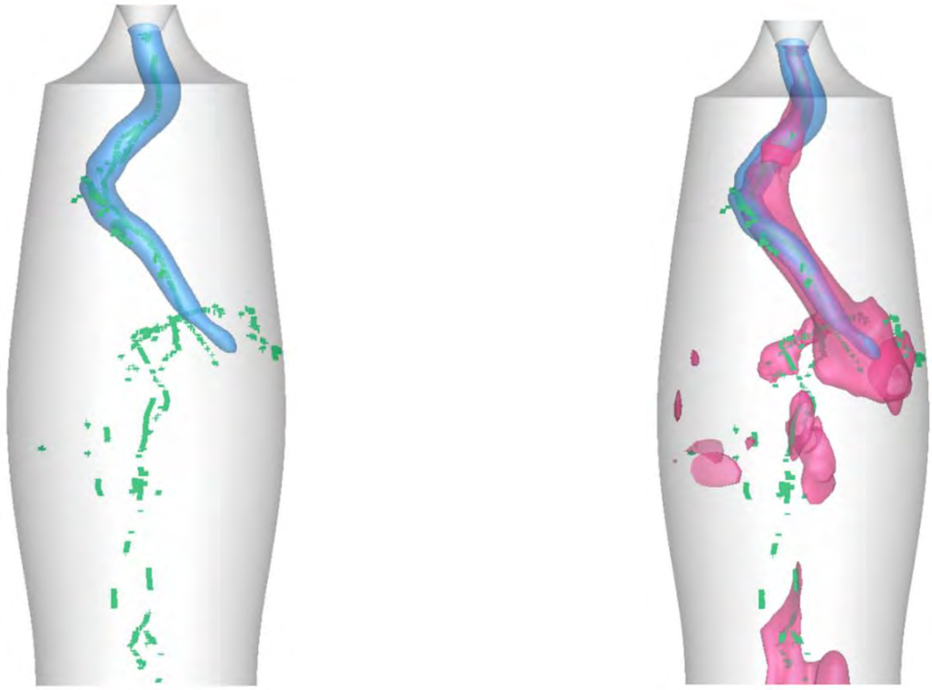

Figure 59. Pressure & velocity iso-surface and vortex core, LES turbulence model, Fluent 6.3.

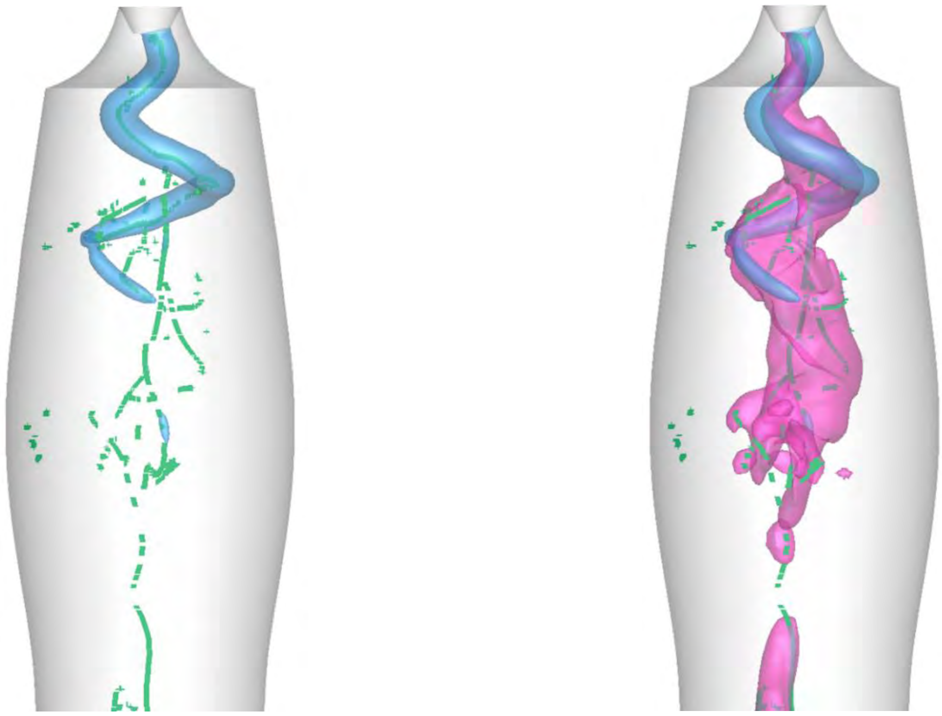

Figure 60. Pressure & velocity iso-surface and vortex core, DES turbulence model, Fluent 6.3.

The presence of the vortex rope is also underlined by the pressure pulsations that appear in the draft tube. This is way pressure monitors were fitted on the draft tube in several sections. The pressure signal was analysed, and the direct Fourier transformation was applied to the pressure signal in order to identify the dominant frequency of the vortex rope. This value was compared to the values obtained by other researchers in order to validate our numerical results.

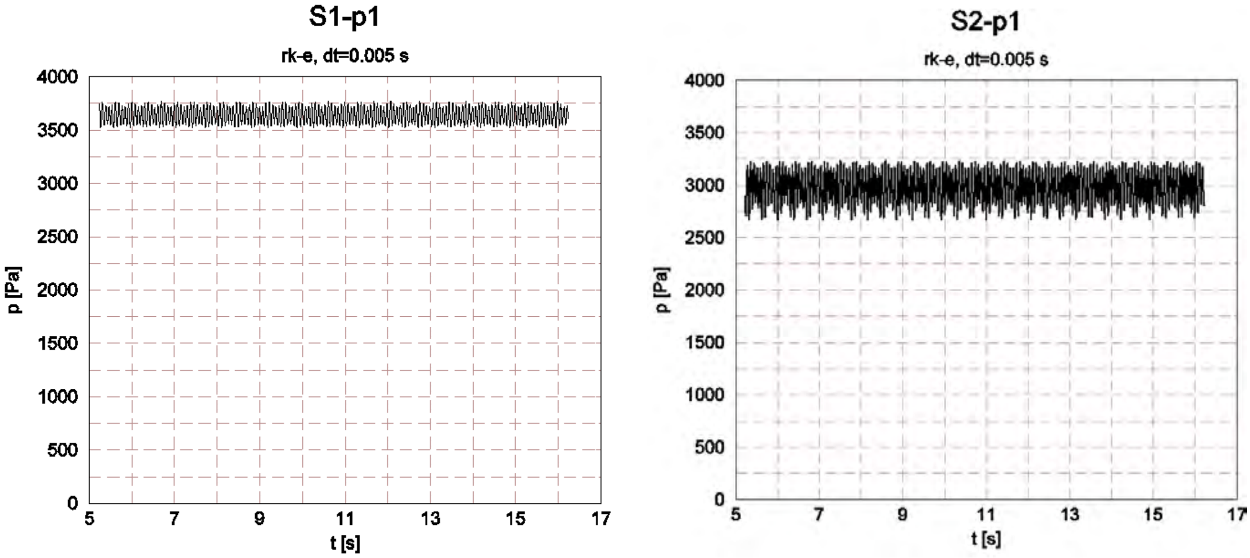

Figure 61. Pressure pulsation, realizable k-ε turbulence model, Fluent 6.3.

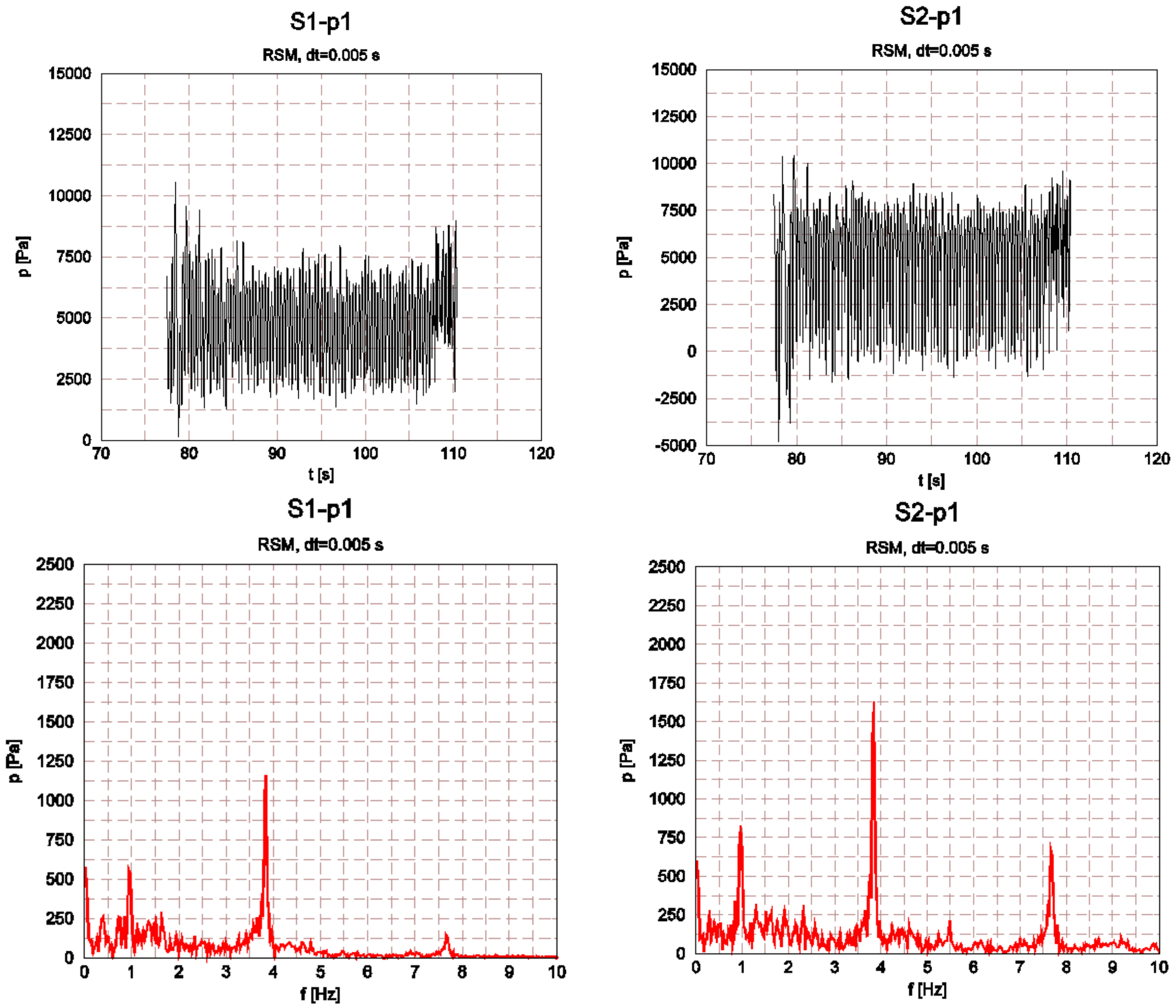

Figure 62. Pressure pulsation, RSM turbulence model, Fluent 6.3.

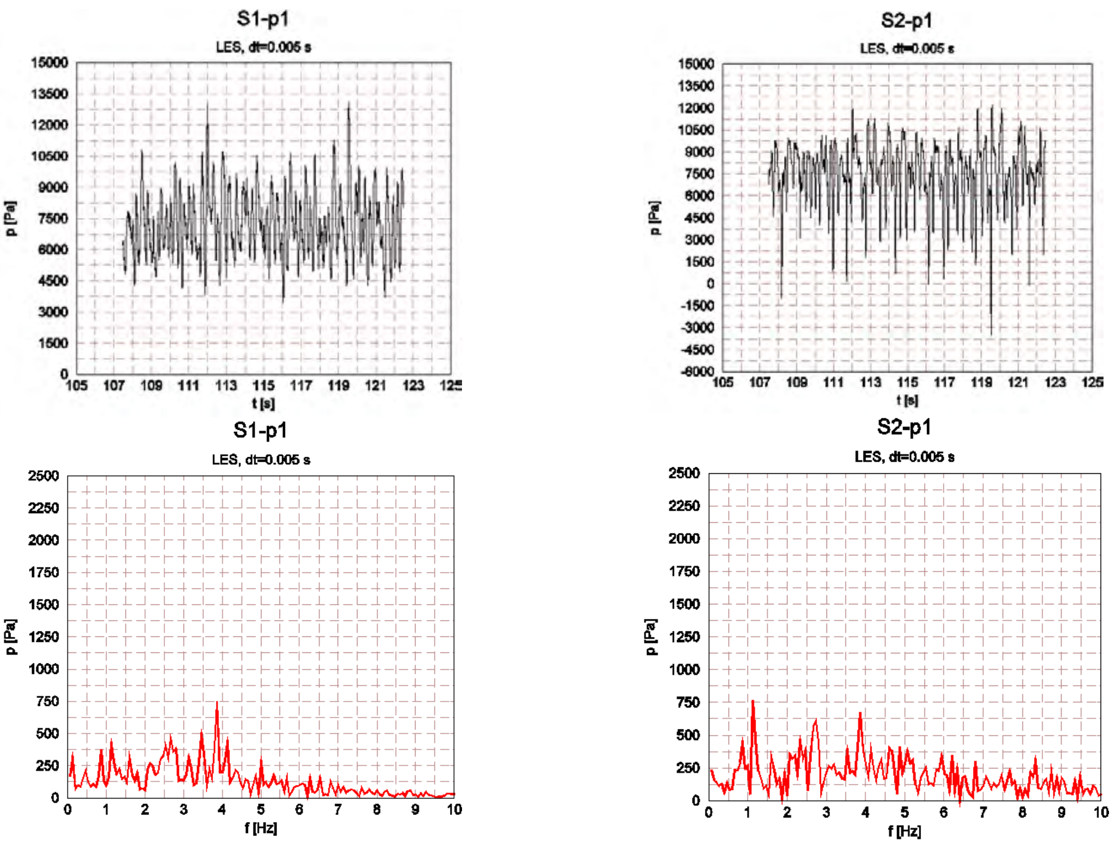

Figure 63. Pressure pulsation, LES turbulence model, Fluent 6.3.

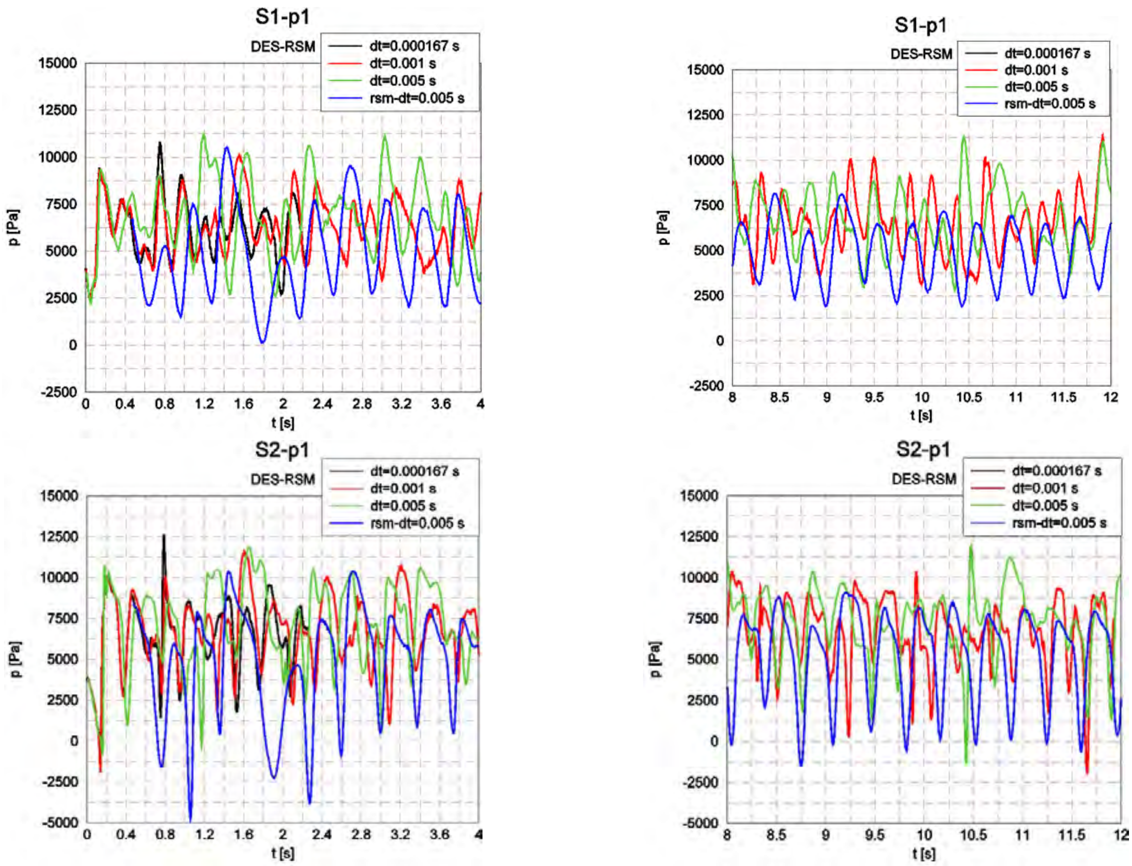

Figure 64. Pressure pulsation, DES vs. RSM turbulence model, for different values of the time-step, Fluent 6.3.

The conclusions for the first rounds of investigation were:

- The numerical simulation should be carried out using unsteady solver starting from a steady solution,
- Using realizable k-ε turbulence model cannot predict the pressure pulsation,
- Good results are obtained using RSM turbulence model,
- Using LES model leads to a long simulation time,
- The value of the time step influences the pressure pulsations,
- Using DES model reduces the simulation time in comparation with LES, but the pressure signal is still noisy,
- Further investigations are needed concerning the use of RSM model.

After this phase of the research, a new version of the software ANSYS Fluent was employed, version 15. This version contained new and improved turbulence models, like SAS. The results obtained with this new turbulence model proved to be the most accurate and not so much time consuming. This turbulence model also offers different options, two of them being investigated: the single SAS model and combination of SAS and RSM model.

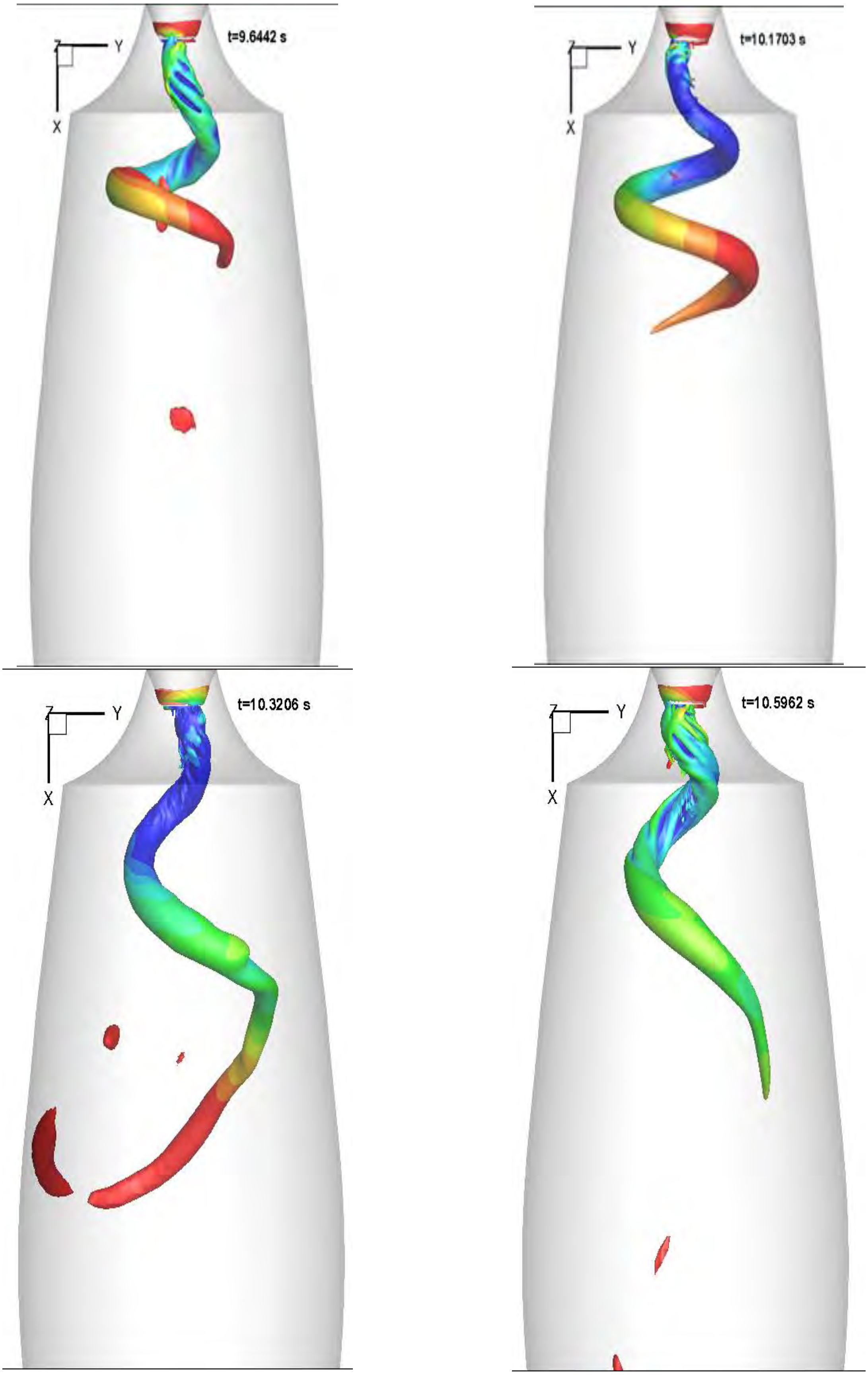

Figure 65. Vortex rope visualization with iso-surface of constant pressure, SAS turbulence model, Fluent 15.

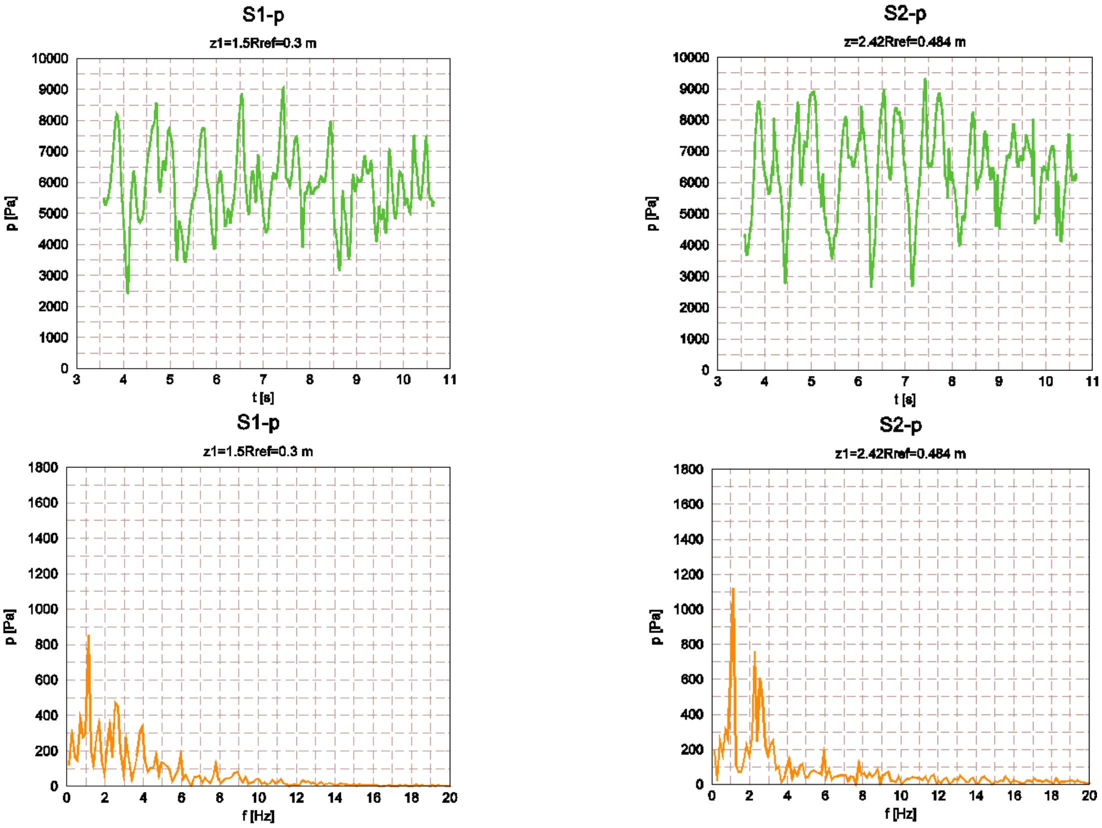

Figure 66. Pressure pulsation, SAS turbulence model, Fluent 15.

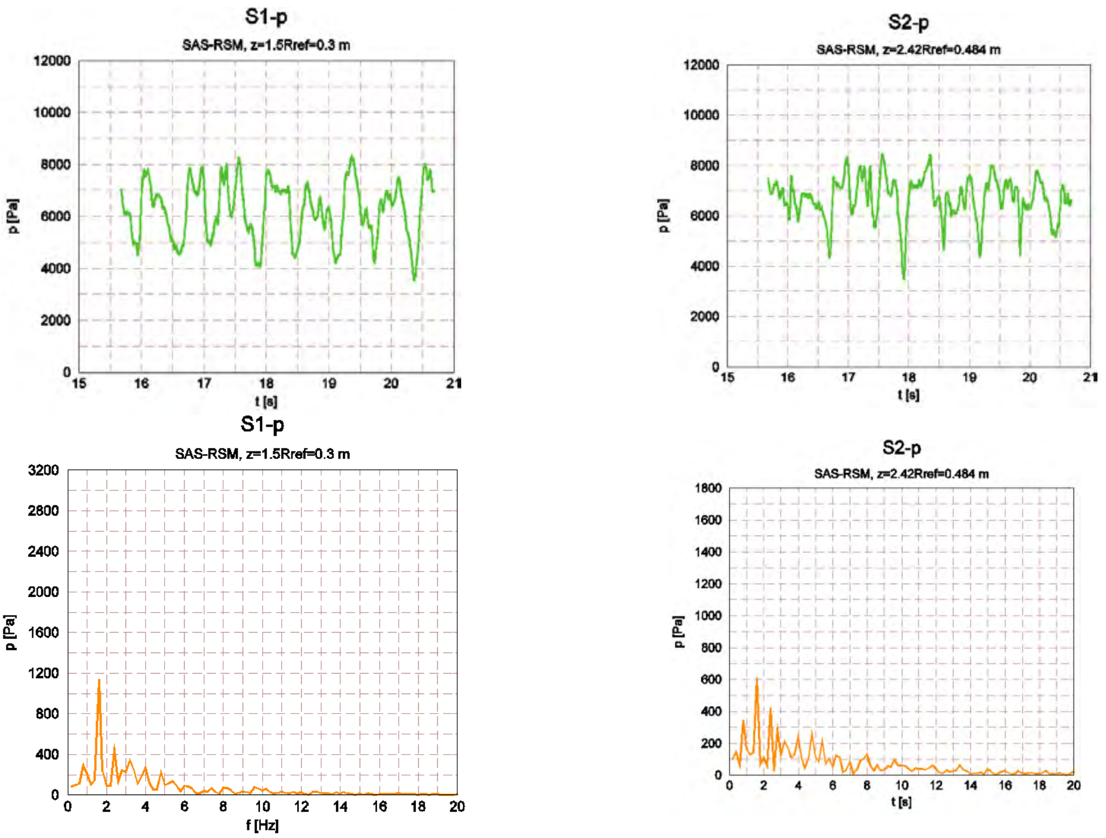

Figure 67. Pressure pulsation, SAS-RSM turbulence model, Fluent 15.

From the analysis of the results and comparing with the results from previous research works we concluded that the following set-up is optimum to simulate the flow in the draft tube in order to capture the presence of the vortex rope:

- On the inlet section the velocity profile is imposed which corresponds to the velocity profile from the outlet section of the Francis turbine runner
- On the outlet we have used a pressure condition, with average pressure specification which allows the pressure on the outlet boundary to vary while maintaining an average equivalent to the specified value in the Gauge Pressure input field. Within this boundary pressure implementation, the pressure variation provides a certain level of non-reflectivity.
- The most accurate turbulence model proved to be the Scale-Adaptive Simulation Method (SAS). An interesting and useful feature of the SAS approach is that for unstable flows the model changes smoothly from a large eddy simulation (LES) model through various stages of eddy-resolution back to a RANS model based on the specified time step.
- The FLUENT 15 setup used in the present investigations uses SIMPLEC for pressure-velocity coupling method. For the spatial discretization we use Least Squares Cell Based for Gradient, Second Order for Pressure, Bounded Central Differencing for the Momentum, Second Order Upwind for Turbulent Kinetic Energy and Specific Dissipation Rate. The transient formulation was set to Bounded Second Order Implicit.
- The total flow time was more than 10 seconds, with a time step of 0.000167 seconds corresponding to the movement of the vortex rope.

Applying the previous mentioned numerical set-up, we tried to explain the origin of the plunging pressure pulsations from the draft tube of a Francis turbine, [33]. Our research attempts to elucidate a rather unexpected feature of the unsteady pressure field resulting from the self-induced instability of the decelerated swirling flow in a straight diffuser. We perform a numerical experiment using an axisymmetric surrogate draft tube, with inlet swirl corresponding to the flow exiting a Francis turbine runner when operating at 70% the best efficiency discharge. The numerical results correctly capture the precession movement of the helical vortex (vortex rope), but they also reveal a complex dynamics of the vortex filament during the precession. We show that the vortex filament is stretching, leading to an elongated rope, followed by a sudden break up and a bouncing back phase. This cycle, with lower frequency that the precession one, appears to be responsible for the plunging (synchronous) pressure fluctuations superimposed over the rotating (asynchronous) pressure field associated with the precession of the vortex rope. As a result, we show that the plunging oscillations are not necessary the result of the interaction between the vortex rope and the draft tube elbow, but they are an intrinsic feature of the helical vortex filament dynamics.

Figure 68 shows the vortex core segments identified with the algorithm implemented in the TECPLOT software. In Fig. 96a) one can easily identify the helical vortex line associated with the precession movement of the vortex rope, as well as other spurious vortex segments further downstream. The vortex segments are coloured by the vorticity magnitude, chosen as indicator of the vortex strength. One can remove the spurious vortex segments simply by setting a threshold for the vortex strengths, thus visualizing only the vortex rope, as shown in Fig. 96b). The correlation with an iso-pressure surface is shown in Fig. 96c). As expected, the iso-pressure surface includes part of the vortex filament, but not all of it. Moreover, the extent of the iso-pressure surface depends on the chosen pressure value, while the vortex filament detection does not require any arbitrary parameter.

a) All vortex filaments b) Blanked vortex filament c) Iso-pressure surface

Figure 68. Vortex filament extraction and correlation with iso-pressure surface, [33].

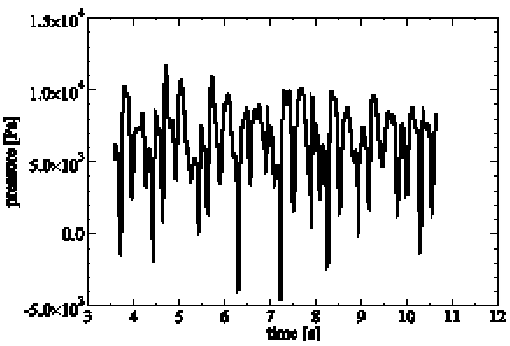

a) Unsteadt pressure at monitor

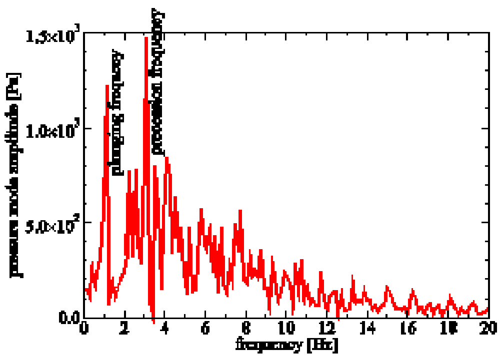

b) Fourier transform of monitor pressure

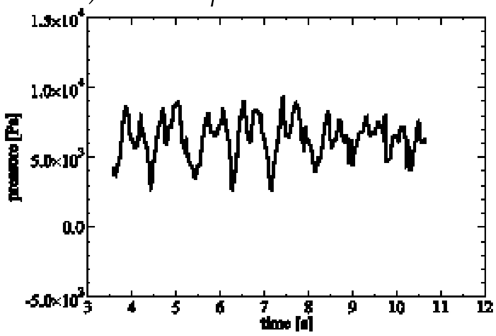

c) Circle-average unsteady pressure

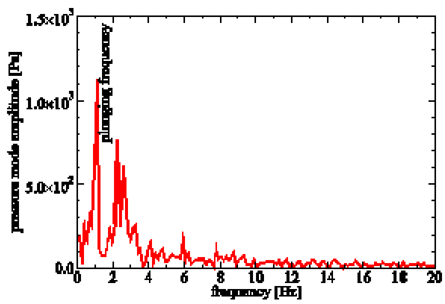

d) Fourier transform circle-average pressure

Figure 69. Unsteady wall pressure and its Fourier transform, [33].

We start our analysis by examining the wall pressure fluctuations recorded at the pressure monitors shown in Figure 55, as well as the average pressure on the wall circle where these monitors are located. When looking at the individual unsteady pressure monitors, the signal shown in Fig. 97a) shows in the Fourier spectrum, Fig. 97b), two distinct peaks: the first one corresponds to the precession frequency of the vortex rope, in agreement with experimental and numerical data from, and the second one, with lower frequency, corresponds to the plunging oscillations. This conclusion is supported by the analysis of the circle-averaged pressure, shown in Fig. 97c), which displays in the Fourier spectrum, Fig. 97d), the unaltered peak at low frequency.

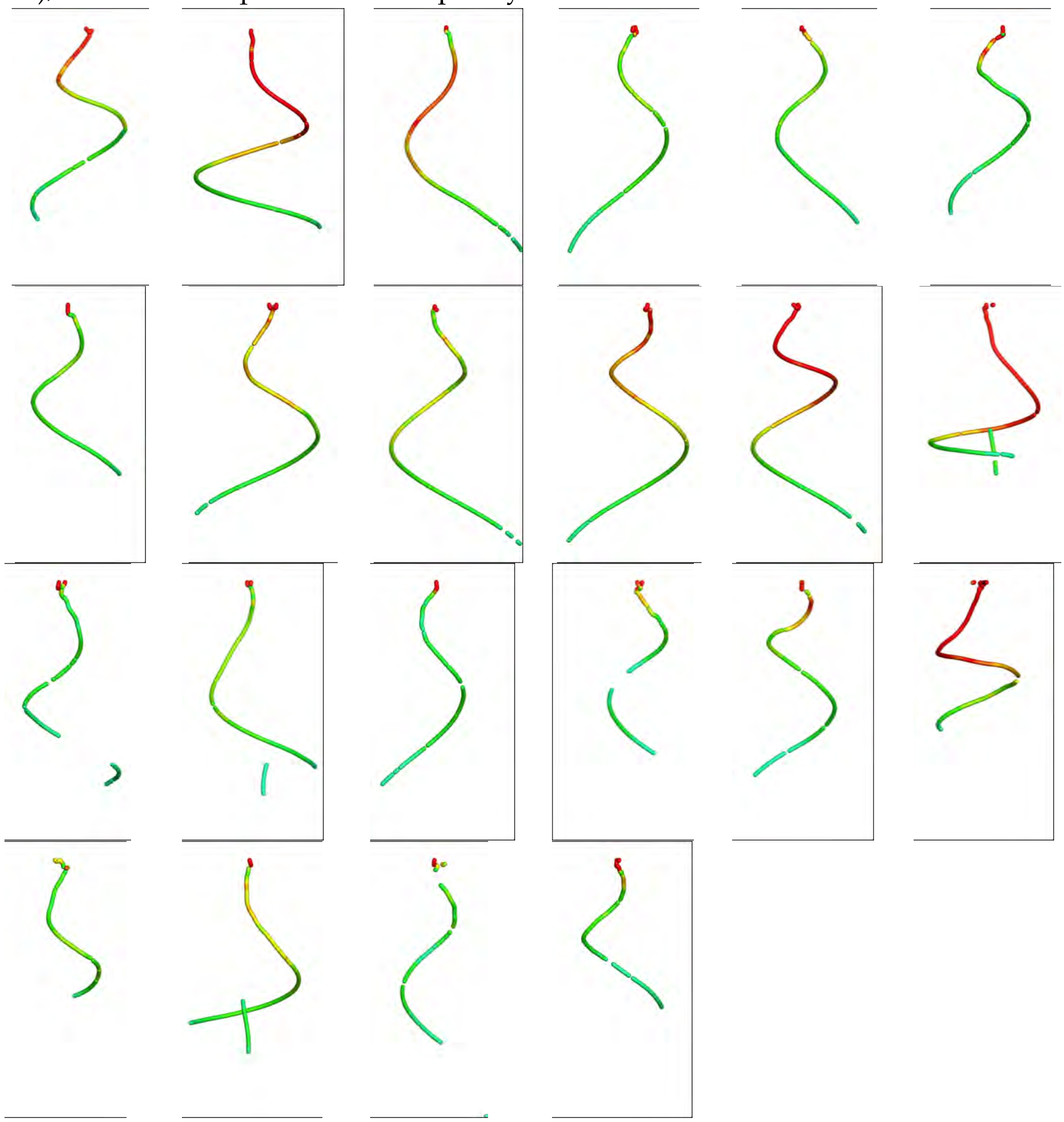

Figure 70. Vortex rope filament dynamics: stretching, breaking, bouncing back sequence, [33].

As a result, we conclude that plunging (synchronous) pressure pulsations occur in the straight axisymmetric geometry as well and are not only the result of the interaction between the precession movement of the vortex rope and the draft tube elbow. To further elucidate the flow mechanism that produces these plunging fluctuations we examine the evolution of the vortex rope filament as shown in Figure 70.

Figure 70 shows significant changes in the vortex rope shape as it rotates with the precession frequency. One can identify an elongation phase, where the pitch increases, and the vortex filament is stretched. Then, at the end of this stretching phase the vortex filament breaks up and the segment attached to the runner crown bounces back reaching a small pitch. The cycle is repeated with a smaller frequency than the precession frequency.

As a result, we conclude that it is this stretching – breaking – bouncing back sequence that leads to the low frequency plunging pressure fluctuations revealed by the Fourier analysis of the unsteady wall pressure signals.

Another research, [12], presented a quantitative approach to describe the precession movement of the vortex rope by properly fitting a three-dimensional logarithmic spiral model with the vortex filament computed from the velocity gradient tensor. We showed that the slope coefficient of either curvature or torsion radii of the helix is a good indicator for the vortex rope dynamics, and it supports the stretching–breaking up–bouncing back mechanism that may explain the plunging oscillations.

The following post-processing procedure is applied in order to obtain a helical vortex filament. First, we select the vortex segments with the vortex core strength within a proper interval. This step removes spurious segments which are not actually related to the helical vortex filament. Second, we order the points for increasing axial coordinate. Third, we compute the arc-length coordinate by successively adding the length of each cell segment, thus obtaining the numerical data, shown with circles in Fig. 99 left. Figure 71 shows a typical fit for the arc-length parameterization of the vortex filament. One can see that the reconstructed three-dimensional logarithmic spiral (green line) closely matches the numerical vortex filament (black line).

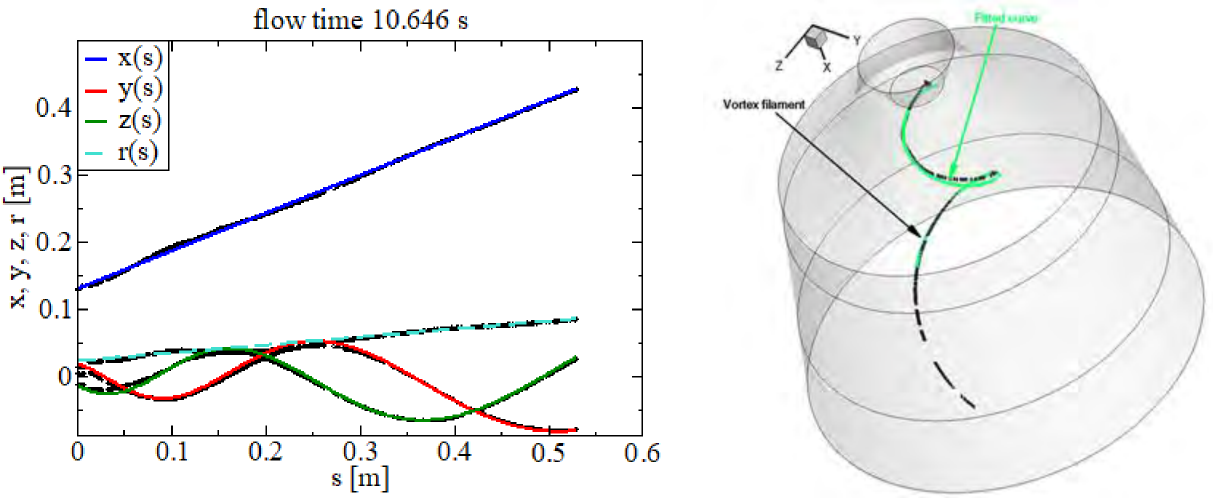

Figure 71. Least-squares fit of numerical data for x(s), y(s), z(s) and the corresponding three-dimensional reconstruction of the vortex filament, [12].

Examples of the resulting fits are further shown in Figure 72, to illustrate the robustness of the approach introduced in this paper. One can see that even when there is a gap in the numerical data, our least-squares approach produced good results.

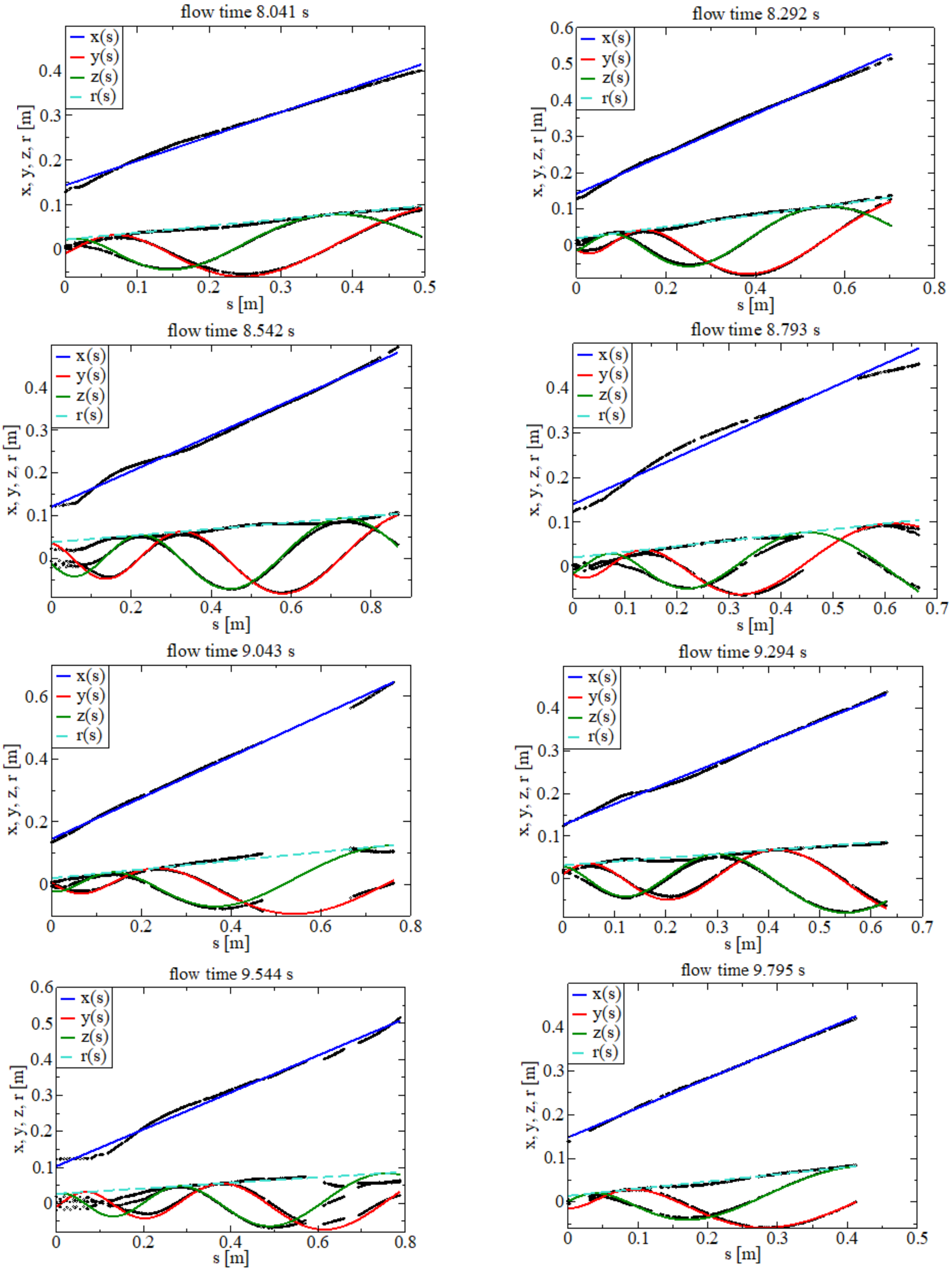

Figure 72. Numerical data (circles) and least-squares fit (solid lines) for the arc-length parameterization x(s), y(s), z(s) of the helical vortex filament. The dashed line corresponds to the computed r(s), [12].

The analysis of the precession angle is shown in Figure 73. The slope of the linear regression (solid red line in Figure 73) provides the average angular speed, with a corresponding precession movement frequency of 3.582 Hz. The corresponding experimental value is 3.75 Hz; thus, we can say that our numerical experiment closely match the measurements with respect to this parameter. However, one can notice in Figure 73 that the precession movement angular speed fluctuates around the average value, indicating that despite the simple problem setup the rope has a more complicated motion.

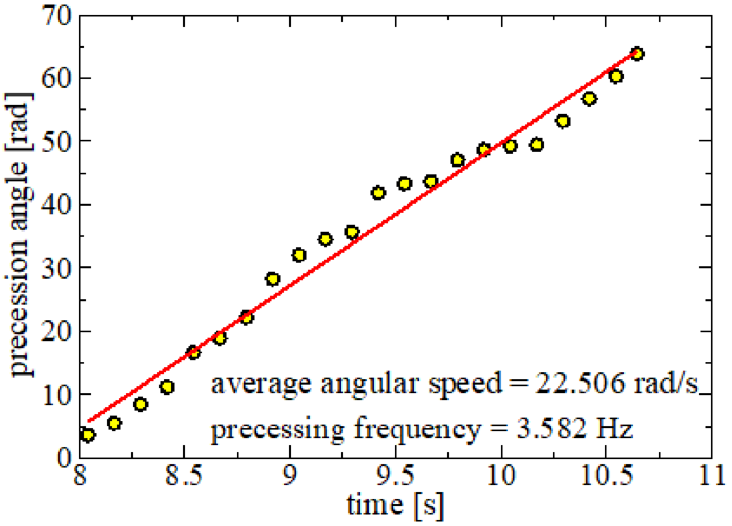

Figure 73. Precession angle versus time. Fit values for c_0 adjusted with multiple of 2π for monotonic increase, [12].

The plot of slope of either curvature or torsion radii in Figure 74 reveals low frequency changes in both curvature and torsion slopes. As a result, one can imagine the helical vortex filament as a spring that is successively elongating and compressing, thus producing the low frequency plunging fluctuations. We conjecture that this behaviour is related to a cycle of vortex stretching–breaking up–bouncing back which is going to be further investigated.

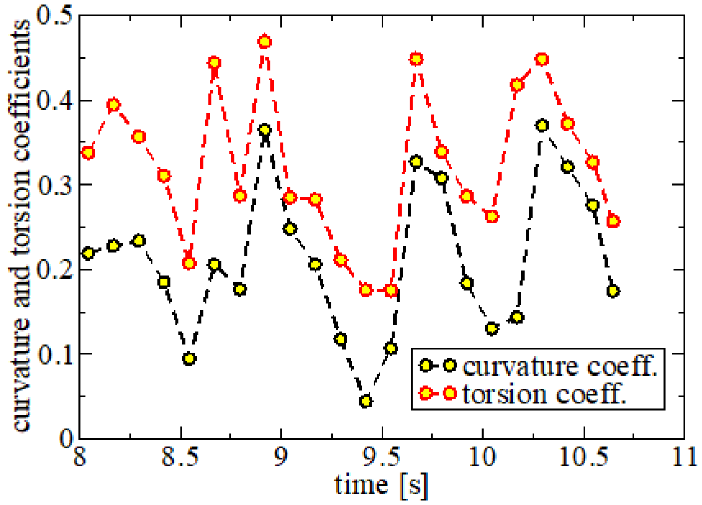

Figure 74. Curvature and torsion coefficients, [12].

After we found a numerical set-up to calculate the vortex rope and we found information about its dynamic, because the presence of the vortex rope affects the operation of the Francis turbine, we focused our research to find solutions for mitigating the vortex rope.

A first method for mitigating the vortex rope that I investigated together with my colleagues, [34] and[18], was a passive control method based on the presence of a diaphragm in the cone of the draft tube. My role in the investigation was to perform the numerical simulation and the data processing. Five cases (one without and four with different types of diaphragms) are numerically investigated for four different values of the inner diameter of the diaphragm: 0.134 m, 0.113 m, 0.1 m and 0.088 m. It is shown that the diaphragm can mitigate the unsteadiness. Moreover, the dynamic-to-static pressure recovery and hydraulic losses in the conical diffuser are computed.

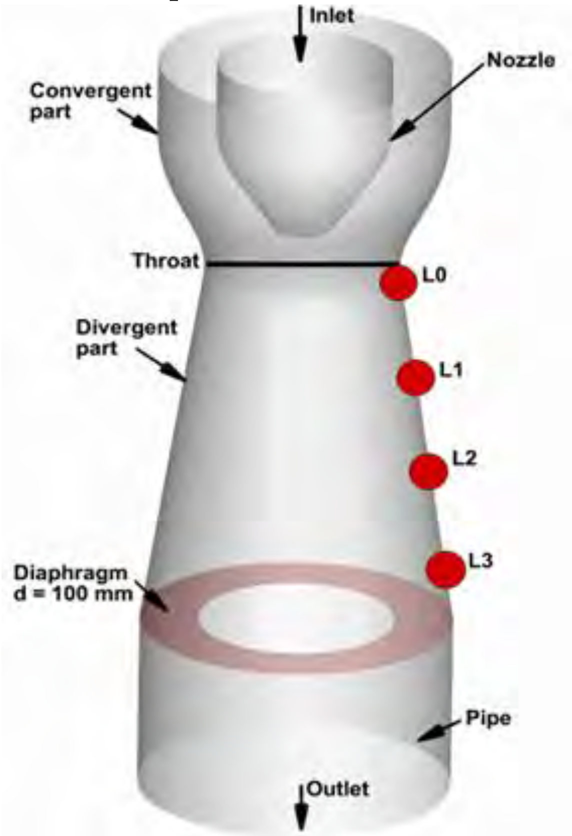

Figure 75. 3D computational domain for the case with diaphragm, [34].

The visualization of the vortex rope is employed with an iso-surface of constant value of the Q-criterion calculated with the following equation:

$$Q = \frac{\Omega^2 - S^2}{2} \qquad (18)$$

where S is the strain rate and Ω is the vorticity rate. The numerical results clearly show that the helical vortex evolves in a straight vortex structure when the diaphragm is employed.

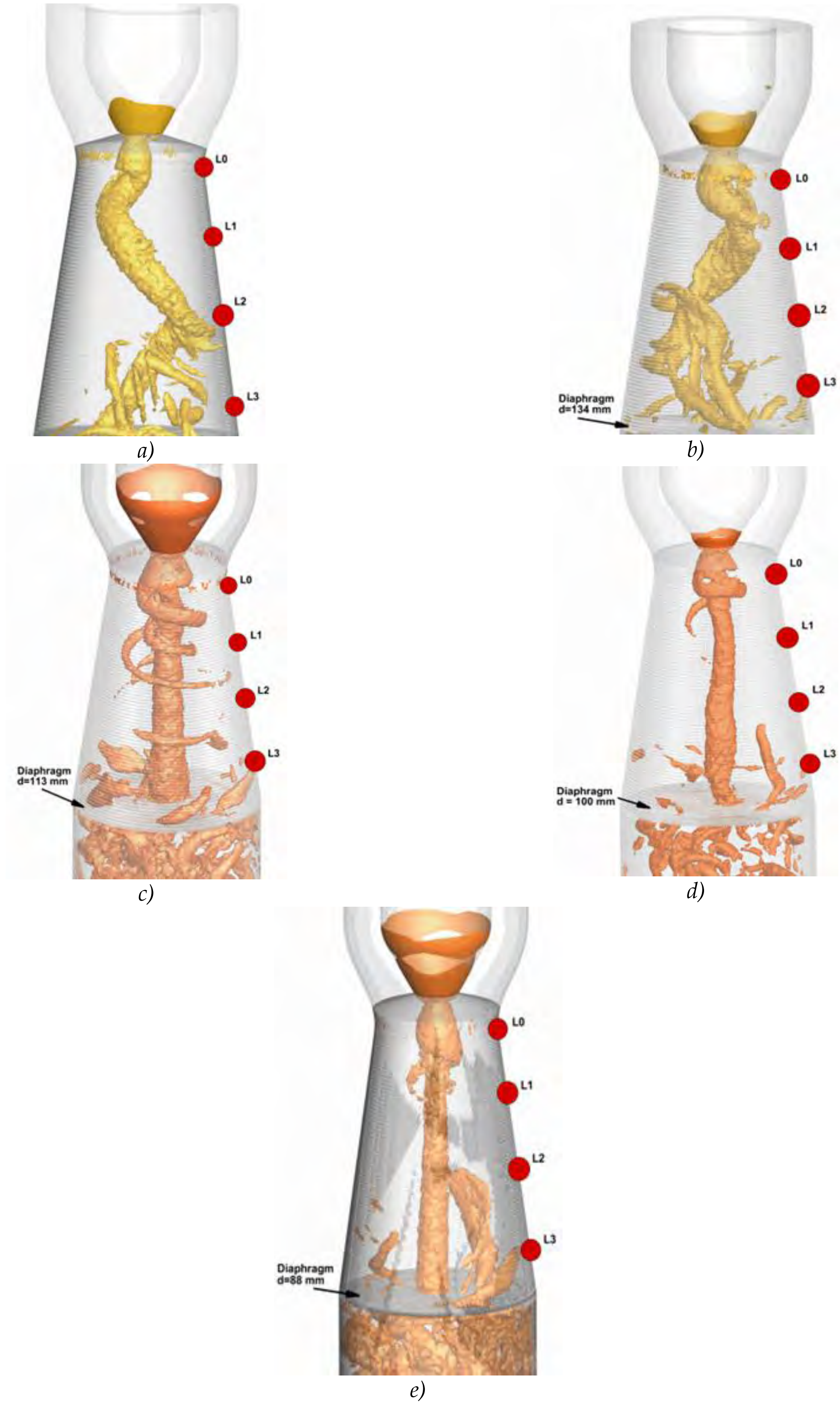

Figure 76. Vortex rope evolution: a) no diaphragm, b) diaphragm d=0.134 m, c) diaphragm d=0.113 m, d) diaphragm d=0.1 m, e) diaphragm d=0.088 m, [34].

As a result, the unsteady pressure signals associated to the helical vortex are mitigated up to 65% in the amplitude and 80% in frequency when the straight vortex is developed. We conclude that the passive method presented has the potential to effectively mitigate the pressure fluctuations in decelerated swirling flow with precession movement of the helical vortex

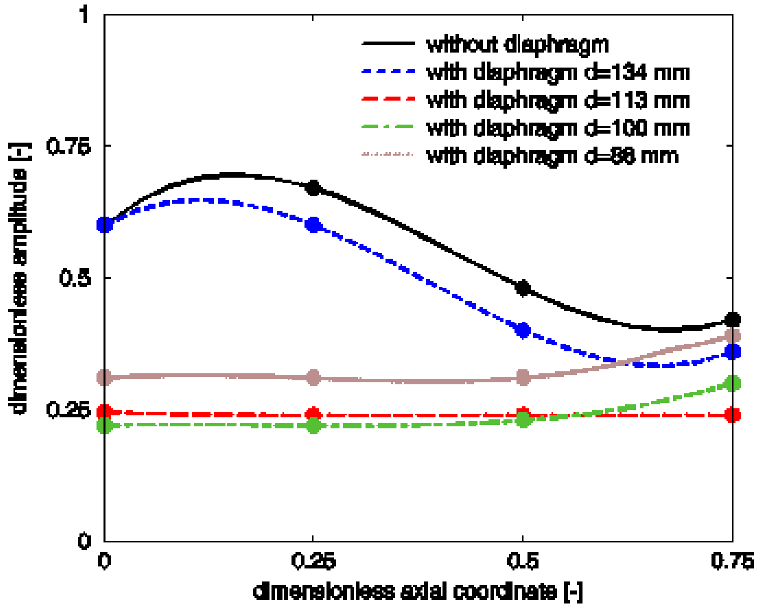

a)

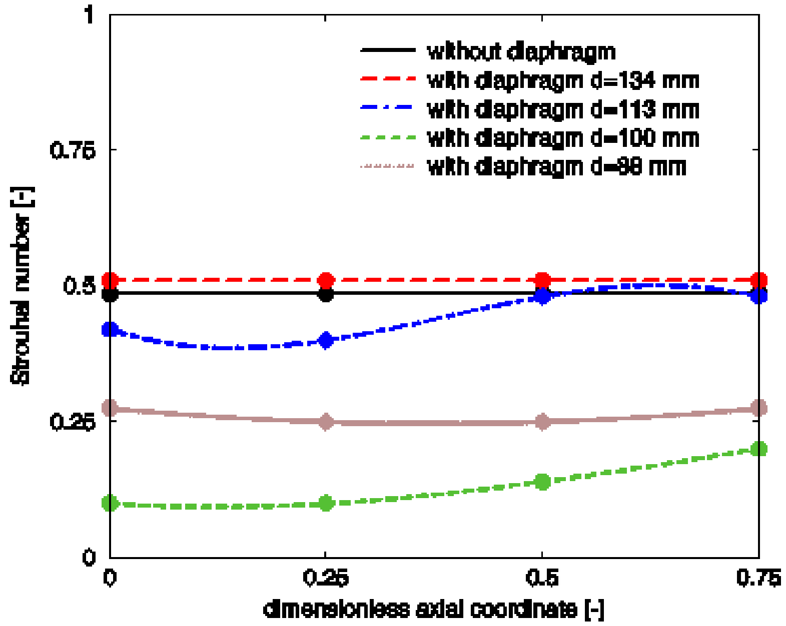

b)

Figure 77. a) Equivalent amplitudes corresponding to pressure taps from the test section domain vs. axial coordinate and b) Strouhal number vs. axial coordinate, [34].

Another new method for the mitigation of the vortex rope was investigated and presented in [22] and [21]. The new method consists in the axial injection of a pulsating water jet along the axis of the conical diffuser of the hydraulic turbines. The aim of our research work was to evaluate the new method with the help of 3D numerical simulation of the flow for different speeds of the vortex generator with and without pulsating jet. The numerical domain is presented in the next figure:

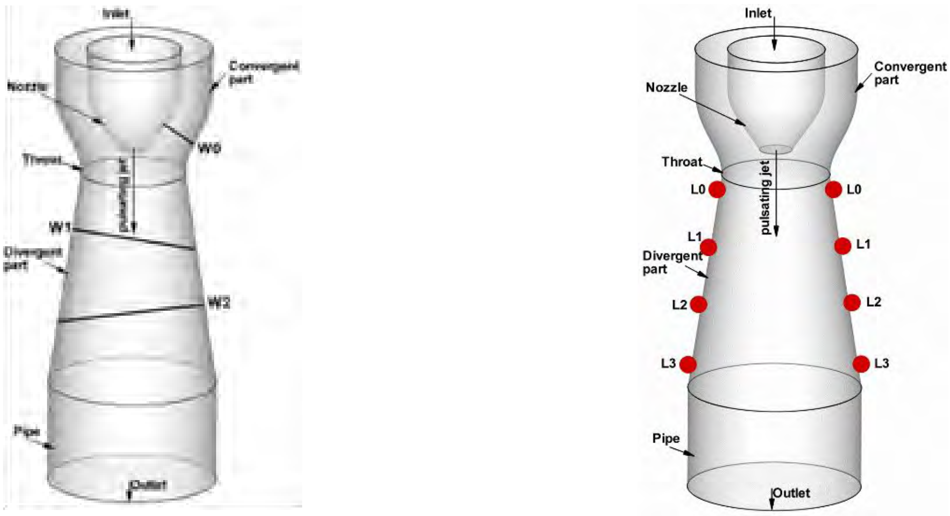

Figure 78. 3D computational domain for the case with pulsating jet, [21].

It is clear that de vortex rope with the associated quasi-stagnant region is well developed for a runner speed of 800 rpm, Figure 79. The meridian velocity profile from both survey axis shows clearly the quasi-stagnant region in the middle of the cone.

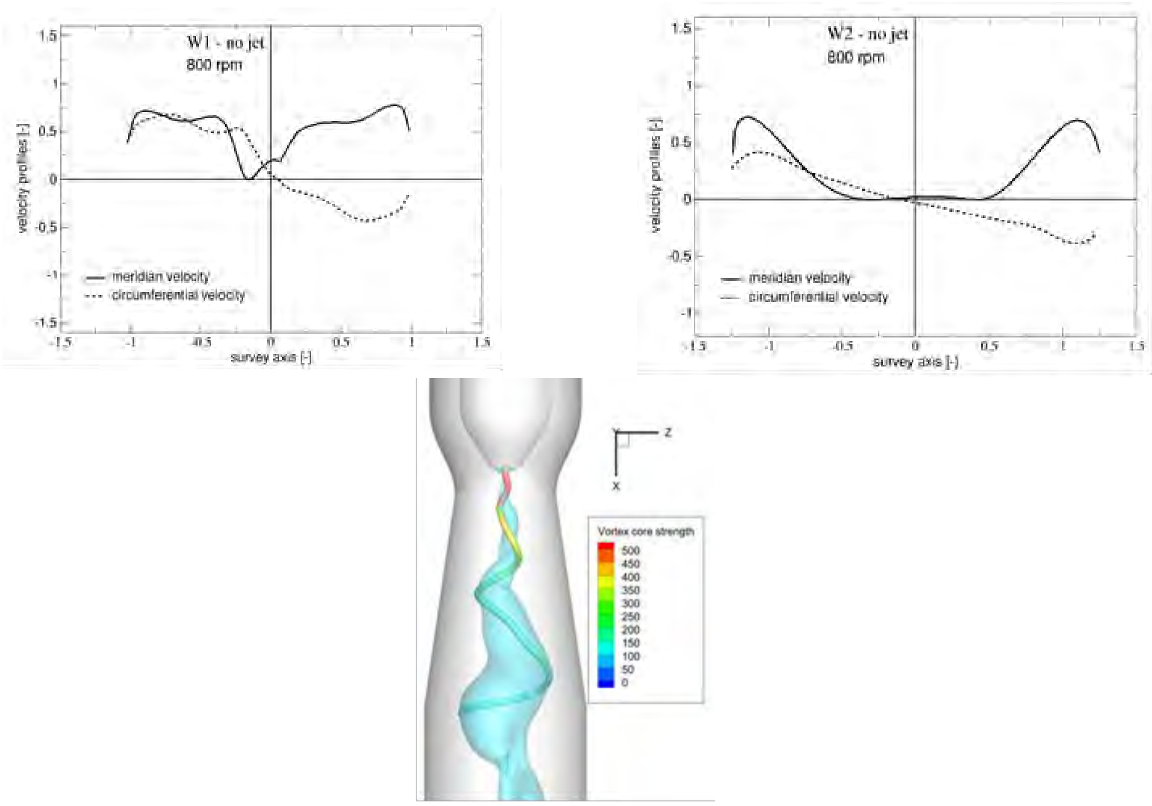

Figure 79. Velocity profiles and vortex core of the swirling flow with no jet for 800 rpm speed of the runner, [21].

Since pulsating water jet is introduced, Figure 80, the vortex rope and associated quasi-stagnant region is mitigated. This fact is clear from the velocity profiles where it exists an excess of meridian velocity on both survey axis. The 600 rpm speed of the runner gives the best efficiency point regime. This is underlined in Figure 81, where quasi-stagnant region still exists but the vortex rope is not present.

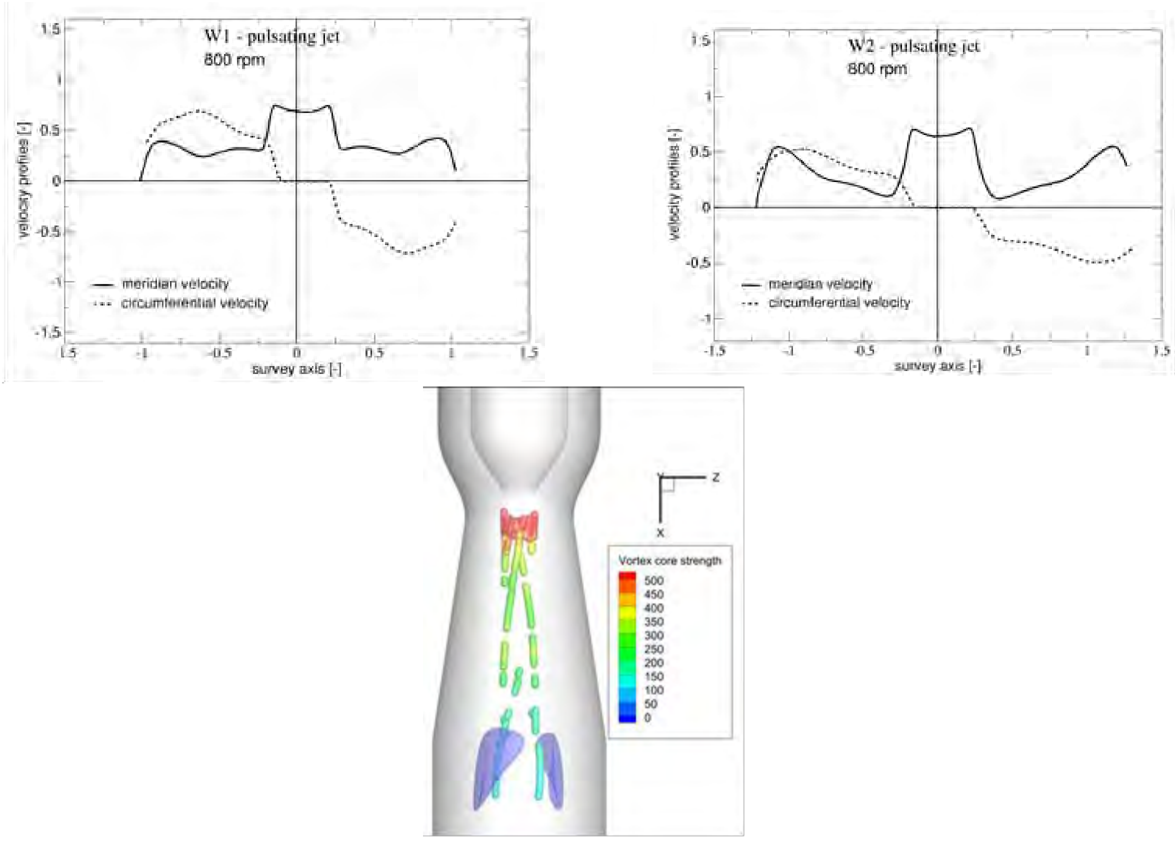

Figure 80. Velocity profiles and vortex core of the swirling flow with pulsating water jet for 800 rpm speed of the runner, [21].

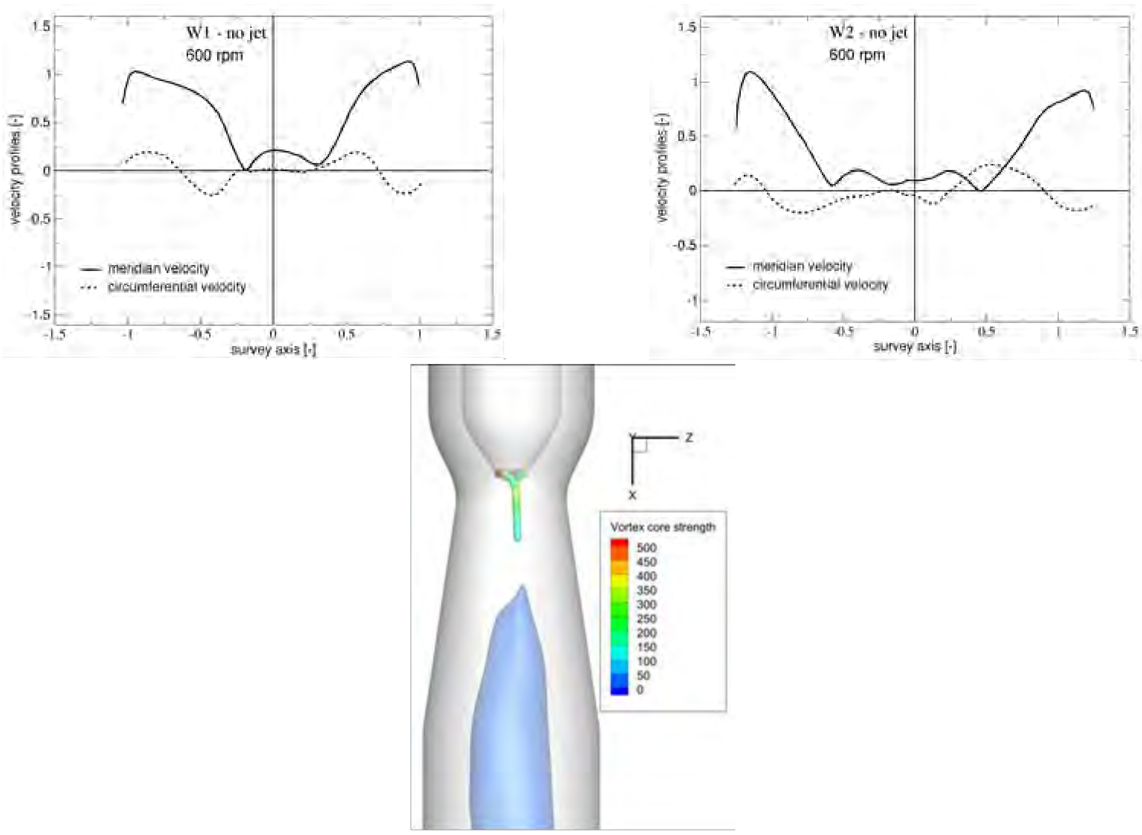

Figure 81. Velocity profiles and vortex core of the swirling flow with no jet for 600 rpm speed of the runner, [21].

If the pulsating jet is introduced, also the quasi-stagnant region is mitigated, Figure 82.

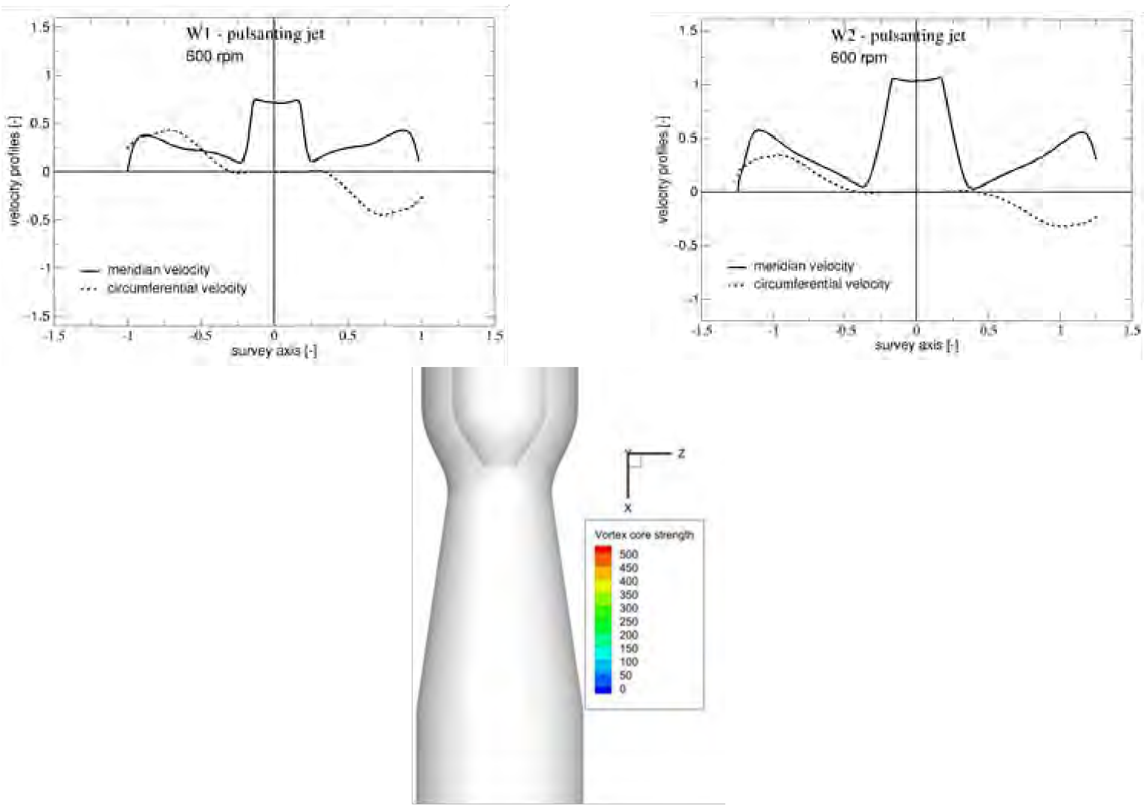

Figure 82. Velocity profiles and vortex core of the swirling flow with pulsating water jet for 600 rpm speed of the runner, [21].

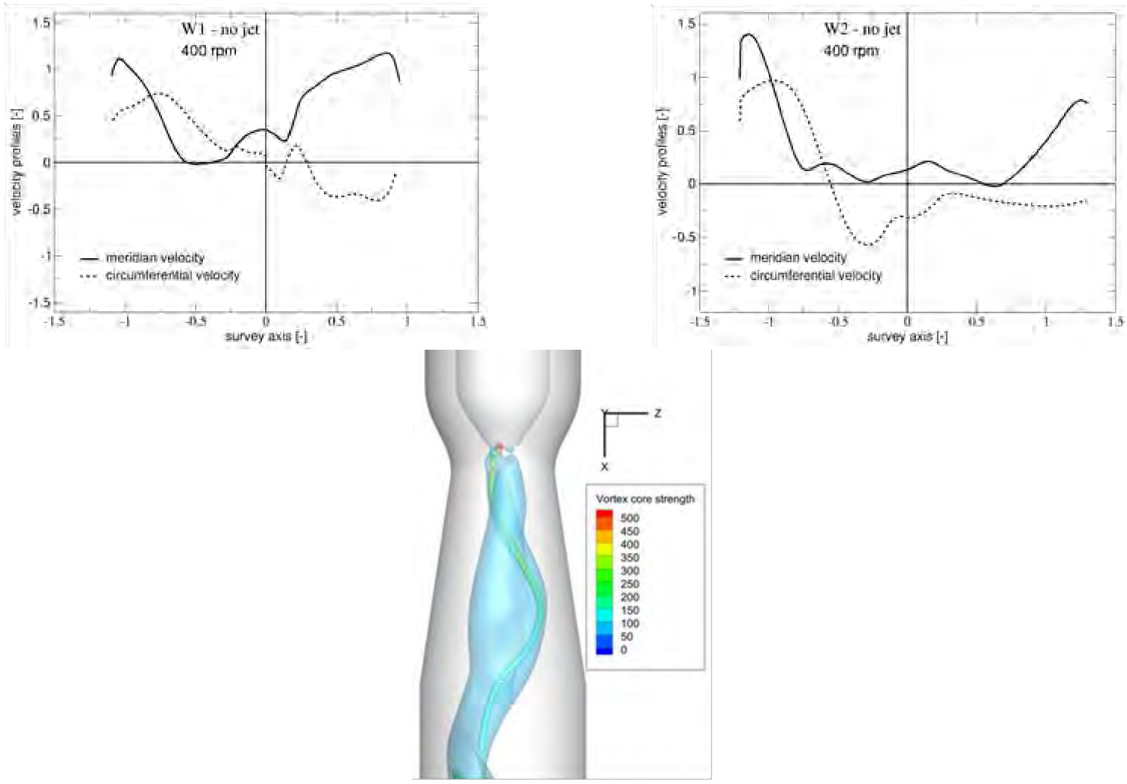

Figure 83. Velocity profiles and vortex core of the swirling flow with no jet for 400 rpm speed of the runner, [21].

Figure 83 shows clearly that the vortex obtained at that regime in the case of the swirl generator, it has changed the shape compared with vortex rope obtained at part load. Anyway, if pulsating jet is introduced the vortex rope is mitigated.

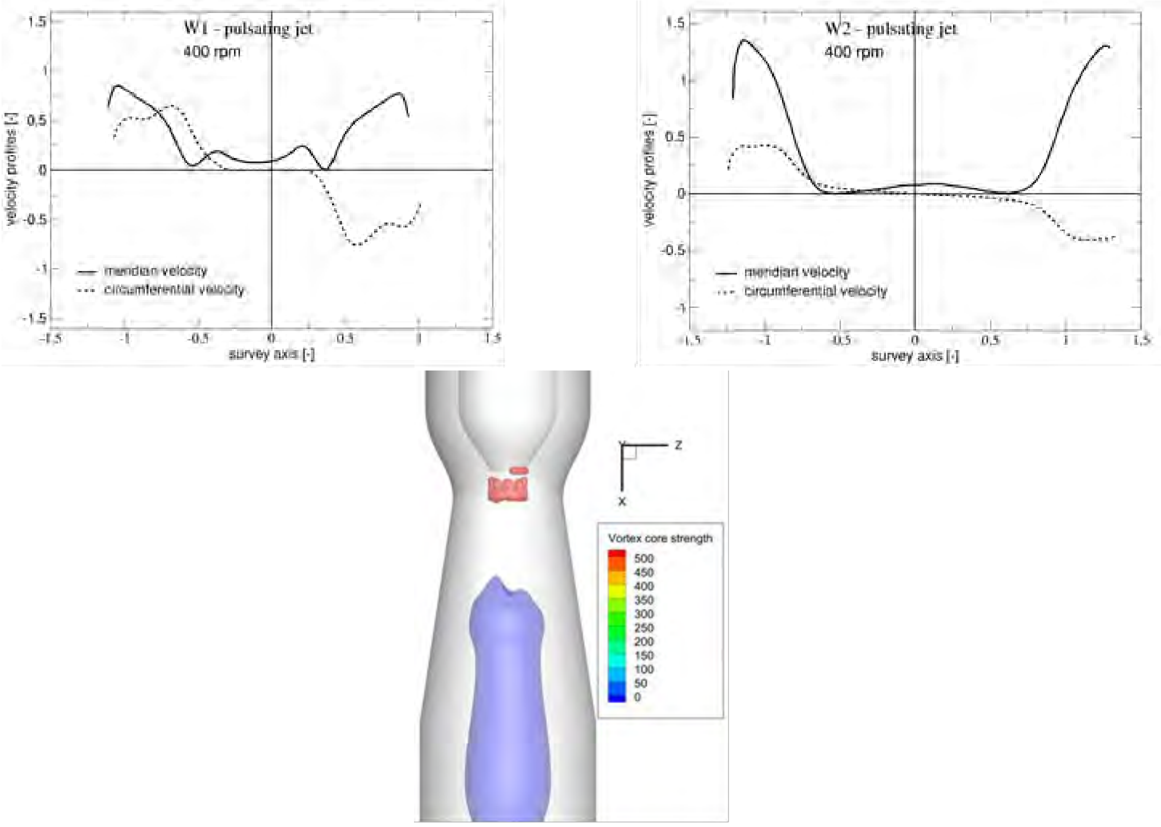

Figure 84. Velocity profiles and vortex core of the swirling flow with pulsating water jet for 400 rpm speed of the runner, [21].

The improvement of the pressure recovery in the draft tube using the pulsating water jet, can be translated for real a turbine as an increase of the overall efficiency at part load regimes, Figure 85.

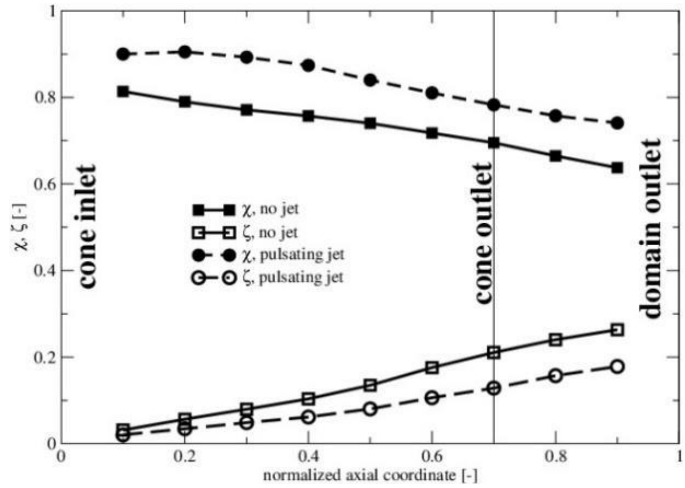

Figure 85. Energy conversion (χ) and the loss coefficient (ζ) along the draft tube cone axis, [22].

Figure 86 shows the pressure fluctuation and the associated Direct Fourier Transform for level L1. It resulted a sudden drop in amplitude (with ~80%), when injecting the pulsating water jet.

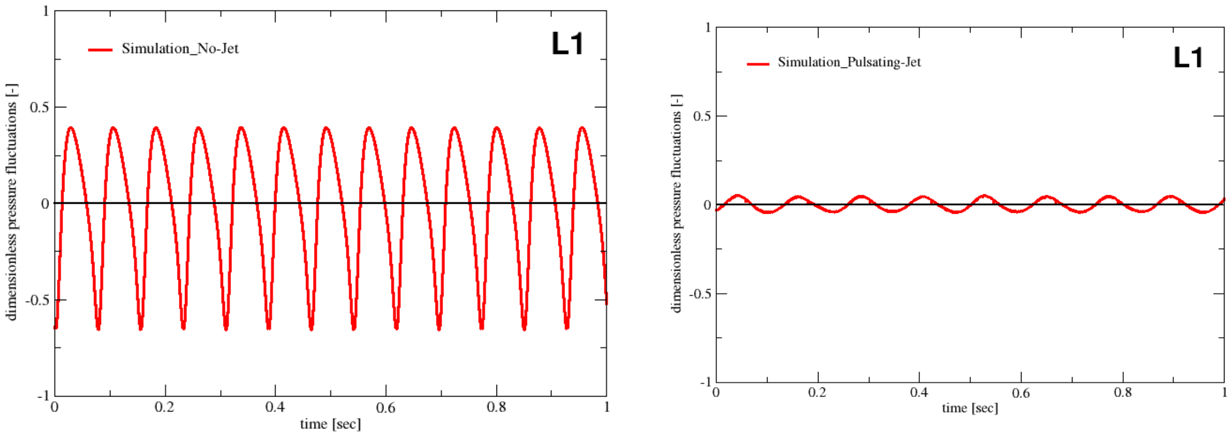

Figure 86. Pressure fluctuation and Fourier spectra for L1 level monitoring at the cone wall without and with pulsating jet, [22].

From Figure 87 it can be observed that the amplitude of the rotating component associated to the vortex rope has a sudden drop up to zero, when the pulsating jet is introduced. Practically, the rotating component associated to the vortex rope is, eliminated. As a result, the vortex rope effect is diminished because the rotating component is negligible. However, the unsteady pressure field reveals only plunging fluctuation with small amplitude compared with the case without pulsating water jet injection. It is clear that, injection of the pulsating water jet, practically changes the ability of the decelerated swirling flows to generate both rotating and plunging fluctuations.

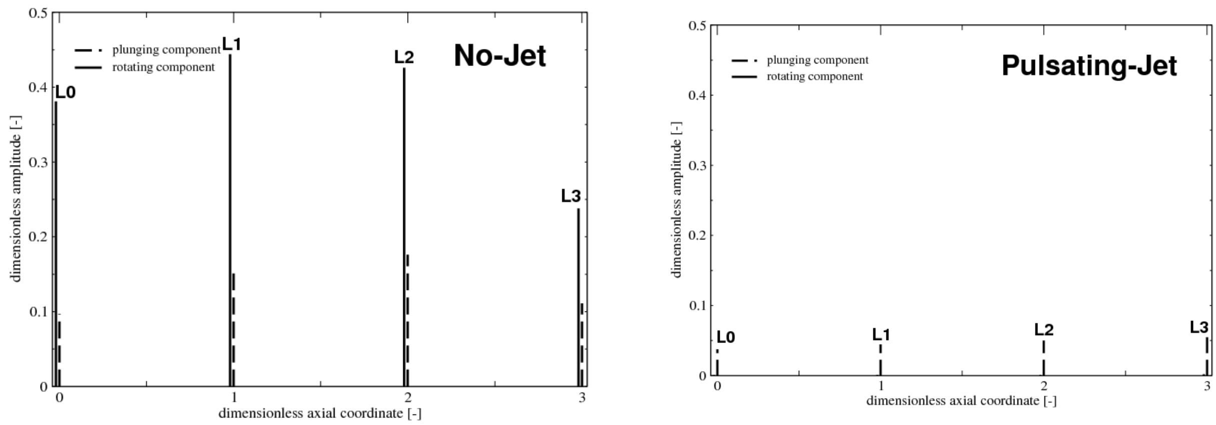

Figure 87. Pressure pulsations distributions along the cone axis without and with pulsating jet, [22].

We had another effective approach to flatten the hill chart of a Francis turbine, while mitigating the instabilities in the draft tube cone by adaptively adjust the swirling flow exiting the runner for variable operating regimes, [16]. As a result, o novel concept of tandem runners is introduced, whereas the classical Francis runner is split into a high-pressure runner (HPR) with a constant speed and a low-pressure runner (LPR) with variable speed. We explore this concept using realistic Francis turbine tandem cascades, with constant and variable transport speed, respectively. Our concept is functionally different from various counter-rotating tandem-runner axial machines such as the bulb turbine, the counter-rotating micro-turbine, or the counter-rotating pump-turbine. Using an additional axial runner in tandem with the main radial-axial runner has also been proposed for a radial-axial pump-turbine (the RAPT concept), but in this case both runners are installed on the same shaft and rotate with the same speed.

The swirling flow exiting the runner, usually optimized for a peak overall efficiency with corresponding minimum draft tube losses, dramatically departs from the optimum configuration at off-design operating points with abrupt increase in draft tube hydraulic losses and severe flow instabilities. In order to keep the swirl ingested by the draft tube optimal no matter the operating regime we introduce a variable speed runner, coloured in red in Figure 88, with the speed correlated with the operating point. As a result, the turbine will have:

- a high-pressure runner (HPR), with constant speed, like the regular Francis turbine runner; the HPR generates the whole turbine power at design operating point, and most of the power at part load,
- a low-pressure runner (LPR), with variable speed, that generates a fraction of total turbine power at part load; the LPR is design to work at runaway speed at the turbine design operating point, where it generates no power at all.

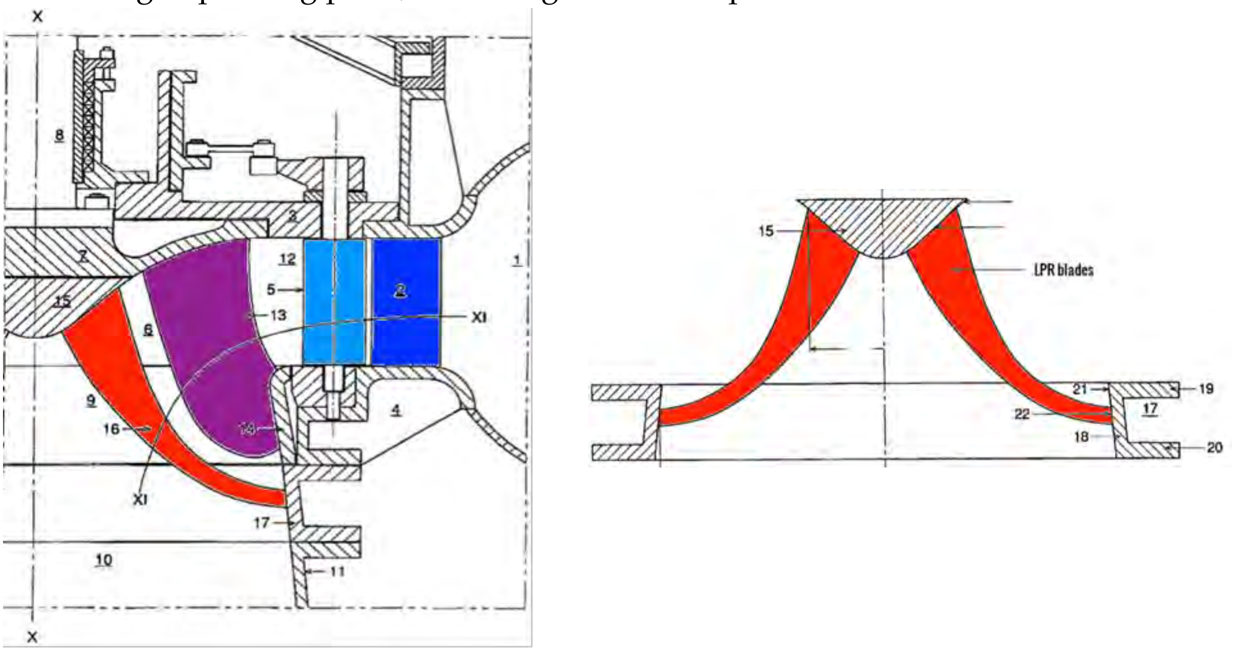

Figure 88. Meridian cross section through a Francis turbine (left) with an exit stay apparatus. A conventional Francis turbine with stay vanes and guide vanes (shown in blue) and a runner (shown in magenta) is fitted with an Exit Stay Apparatus (shown in red). The blades of the Exit Stay Apparatus (right picture) have their own stationary crown and a crown (flange) secured to the turbine discharge ring and to the draft tube cone, [16].

In order to illustrate the operation of the tandem runner turbine, we will examine the basic problem of two hydrofoil cascades working in tandem, with different tangential speeds. We consider a realistic cascade as obtained by intersecting the Francis runner with an axisymmetric stream surface in the crown neighbourhood, and further projecting it into the conformal plane.

The analysis domain, Figure 89, corresponds to a periodic strip with three hydrofoils for the upstream cascade (corresponding to the HPR) and two hydrofoils for the downstream cascade (originating from the LPR).

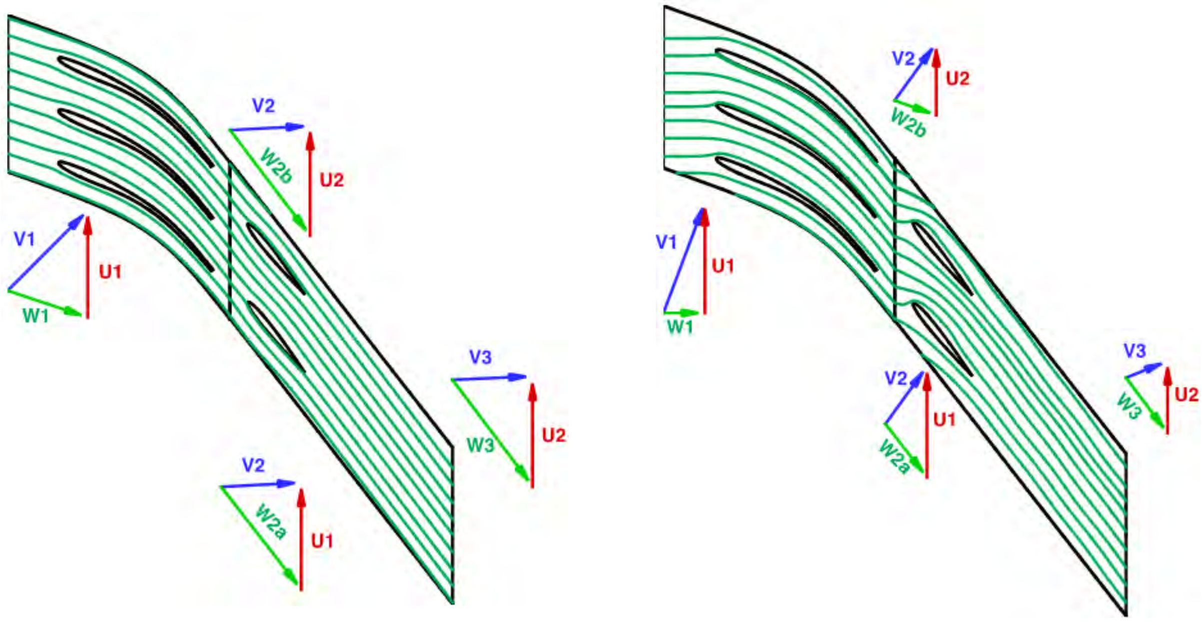

a) *b)*

Figure 89. Flow kinematics for tandem cascades: a) at the rated operating point, b) at half discharge from rated point, [16].

Figure 89.a shows the flow kinematics, i.e. the streamlines for the relative flow and the velocity triangles at the rated operating point. The upstream flow, in reality provided by the turbine distributor, has an absolute velocity with axial component v_{1axial}=3.0 m/s and tangential component v_{1tang}=3.0 m/s for an absolute flow angle of 45°. The transport velocity for the upstream cascade is u_1=4.0 m/s resulting in an optimum angle of attack for the relative velocity $\vec{w}_1$. The absolute flow exiting the upstream cascade, $\vec{v}_2$ is practically axial, with negligible tangential component. The pitch angle for the downstream cascade corresponds to the angle of the relative velocity, $\vec{w}_{2a}$. However, when examining the flow into the downstream cascade we noticed that the transport velocity should be slightly adjusted to u_2=4.1 m/s to correspond to the runaway speed, with disappearing tangential force. This is why the relative velocity entering the downstream cascade, $\vec{w}_{2b}$, has a slightly different angle with respect to $\vec{w}_{2a}$. At this operating point there is no relative flow deflection in the downstream cascade, thus $\vec{v}_3 \simeq \vec{v}_2$, or to be more precise v_{2tang}=0.156 m/s and v_{3tang}=0.132 m/s.

The partial discharge regime shown in Figure 89.b corresponds to half discharge and the same head. As a result, the inlet velocity components are v_{1axial}=1.5 m/s and v_{1tang}=4.0 m/s, resulting in the same velocity magnitude as in the previous case, as it should be when operating the turbine at constant head. As a result, the relative velocity $\vec{w}_1$ becomes axial, with a positive angle of attack for the upstream cascade. The transport velocity for the upstream cascade is kept u_1=4.0 m/s, since the high-pressure runner works at the synchronous generator speed. In this case, the absolute flow exiting the upstream cascade, $\vec{v}_2$, has a large tangential component v_{2tang}=2.07 m/s. It is this high level of swirl, compared to the discharge velocity, that is ingested by the draft tube further increasing the hydraulic losses the triggering the flow self-induced instabilities. The recuperative braking of the downstream cascade down to u_2=2.6 m/s practically recovers this swirl excess leaving v_{3tang}=0.6 m/s at the draft tube inlet. The relative streamlines in Figure 89.b clearly show the loading of the downstream cascade. Note that at the interface the relative streamlines have an angular point corresponding to the change in the transport velocity from u_1=4.0 m/s to u_2=2.6 m/s.

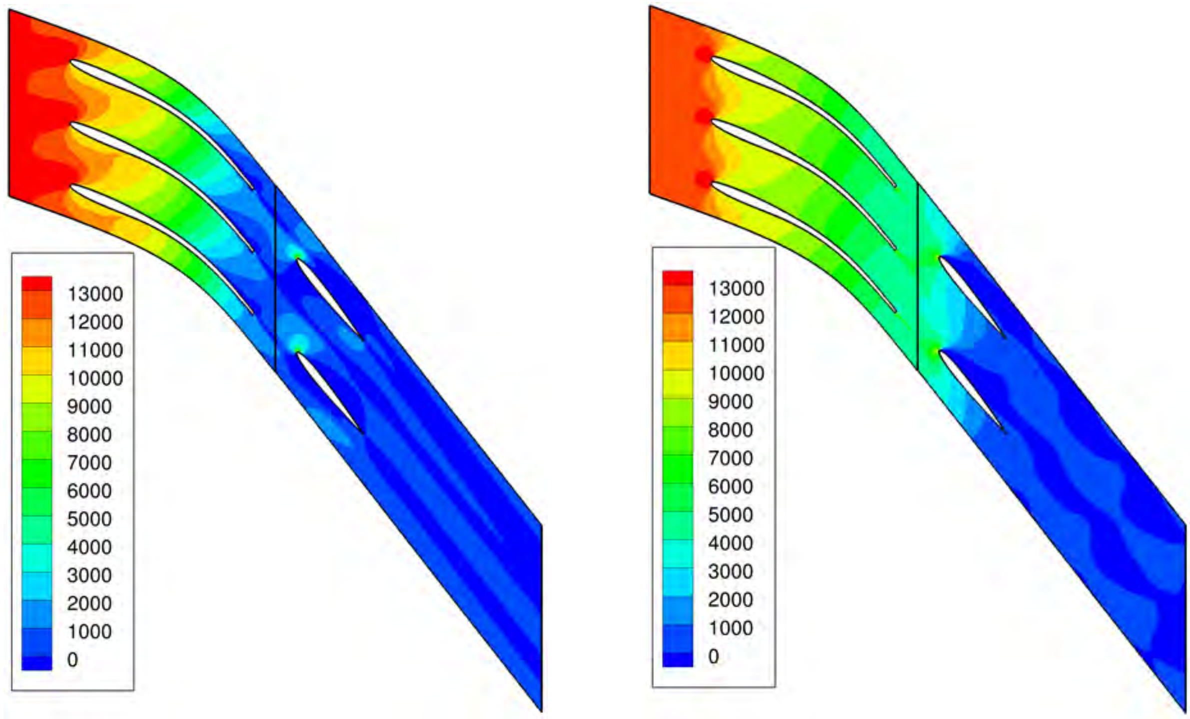

a) b)

Figure 90. a) Total pressure at rated operating point. Energy conversion only in the upstream cascade, b) Total pressure at half the discharge and the same head as the rated point. Both cascade extract energy from the fluid, [16].

From the dynamic point of view, we show in Figure 90 the variation of the total pressure (mechanical energy per unit volume) through the two tandem cascades. According to Figure 90.a, at the rated operating point the whole energy conversion takes place in the upstream cascade, i.e. the high-pressure runner with synchronous speed. The low-pressure runner practically does not extract energy from the fluid since it is rotating at its runaway speed, practically equal by design to the synchronous speed.

At partial (50%) discharge, however, both runners contribute to the energy conversion, while keeping the same turbine head. The total pressure decreases in the downstream cascade accounts for the recuperative braking that kicks in at part load. The values of the total pressure, as shown in Figure 90, simply illustrate the fact that both operating points have the same total pressure drop, or constant turbine head, but the actual value of the head is irrelevant for the present discussion. We recall at this point the main difference with respect to the Stay Vane Apparatus, where the downstream cascade is fixed, thus acting as a stator in an attempt to convert the excess or swirl into static pressure. However, the recuperative runner proposed in this paper contributes to the full hydraulic energy conversion in the turbine, while keeping the optimum swirl at draft tube inlet.

The main advantage of employing a recuperative braking low-pressure runner is that the swirling flow ingested by the draft tube has an optimum configuration within a wide range of operating regimes. As a result, for high specific speed Francis or propeller turbines the draft tube losses are kept to a minimum thereby flattening the efficiency hill chart. In addition, the flow instabilities in the draft tube are altogether avoided by providing a stable swirl configuration at the draft tube inlet within the whole turbine operating range. The resulting efficient and smooth operation of the hydraulic turbine ensures the robust flexibility required by the integration of the new and highly fluctuating renewable energy sources.

Another investigated method is that the swirling flow ingested by the draft tube of a Francis turbine operated far from the best efficiency point can be altered by a runaway runner installed at the inlet of the discharge cone, in the neighbourhood of the turbine throat, [19]. In order to design such a runner, one must first determine the necessary changes in the swirling flow configuration which mitigate the vortex rope without affecting the turbine operating point. Let us examine the flow with vortex rope using two different models. The first one corresponds to the axisymmetric swirling flow and the second one is the full 3D unsteady turbulent flow. Figure 91 shows the numerical results for the axial and tangential profiles in the survey section, together with the experimental data measured with Laser Doppler Velocimetry. The experimental data are time averaged, while the 3D numerical data are circumferentially averaged. There is a good agreement between 2D/3D numerical data and the experimental ones particularly in the annular region of the main flow which is relevant for the following developments in this paper.

As shown in Figure 92, the axisymmetric streamline pattern indicates the development of a central stagnant region in the upstream diverging part of the diffuser, with the actual vortex rope wrapped around this region. The actual three-dimensional vortex rope is shown in Figure 93, being visualized both as a vortex filament (using the eigenvalues of the velocity gradient tensor) and as an iso-pressure surface (as it is conveniently done for engineering simulations). One can observe that the stagnant region shown in Figure 92 is abruptly closing further downstream and the flow at the outlet section shows no vortex breakdown, with positive axial velocity. Observing that the outlet section has approximately the same diameter as the survey section, one could consider a flow configuration similar to the outlet one but immediately downstream the survey section. In other words, a runaway runner (which has zero net torque) installed in the region of the survey section should ingest the residual swirl as exiting the turbine runner and modify it to resemble the swirl in the outlet section of the diffuser, while keeping the same overall fluxes of the moment of momentum and total pressure, i.e. unchanging the turbine operating point.

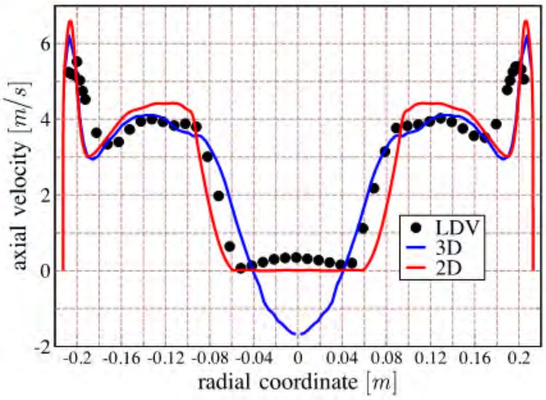

a)

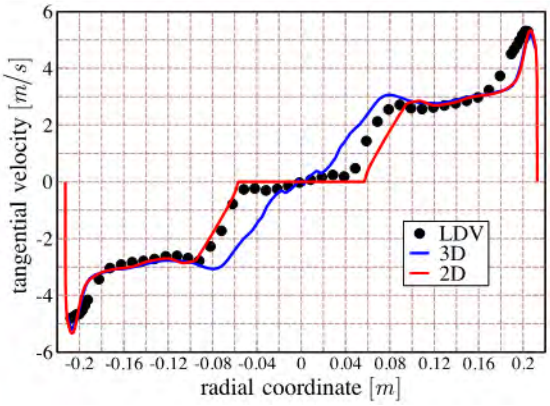

b)

Figure 91. The computed velocity in the survey section compared with experimental data: a) axial velocity, b) tangential velocity, [19].

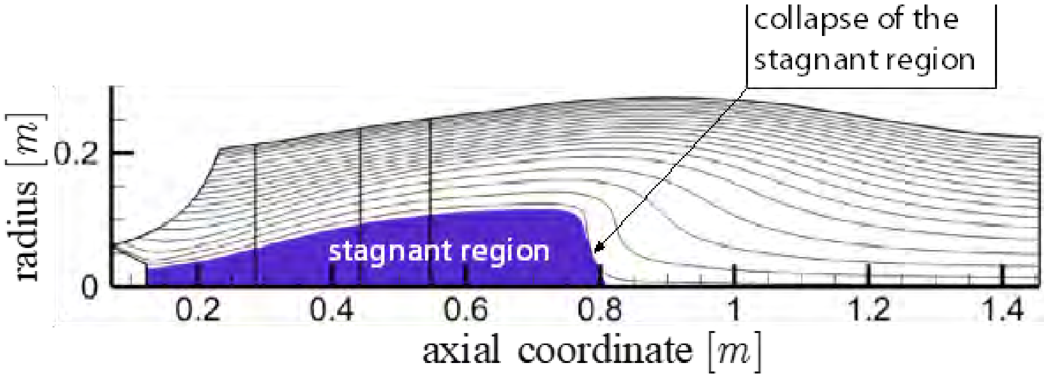

Figure 92. Streamlines for the axisymmetric swirling flow and the stagnant region developed in the conical section, [19].

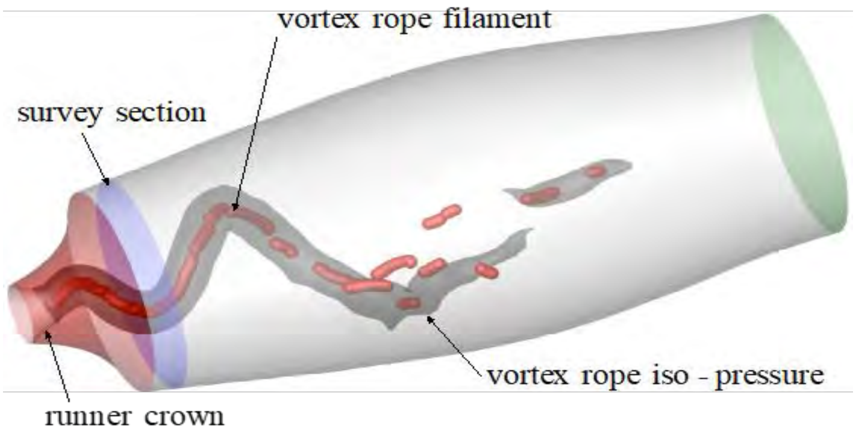

Figure 93. Vortex rope for the unsteady 3D flow simulation in the axisymmetric diffuser. The rope is identified both through its central vortex filament and an iso-pressure surface, [19].

The Euler equation for steady axisymmetric flows shows that both the moment of momentum $\left(rV_u\right)(\Psi)$ and total pressure $p_{tot}(\Psi)$ are functional dependencies only on the stream function, as shown in Figure 94, respectively.

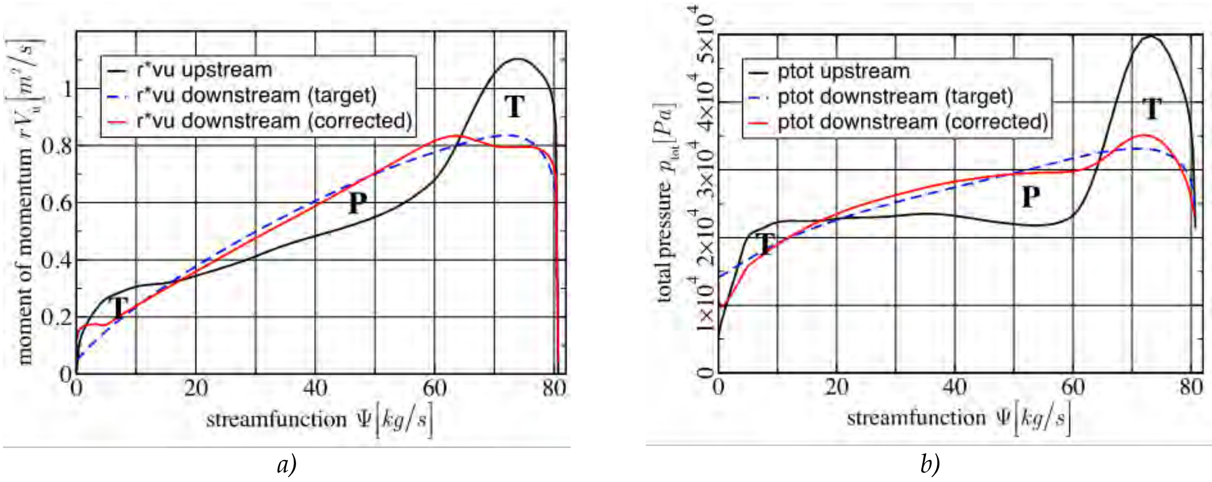

Figure 94. Functional dependencies: a) $(rV_u)(\Psi)$, b) $p_{tot}(\Psi)$, [19].

The black lines correspond to the swirl at the survey section and the blue dashed lines correspond to the swirl at the outlet section, with a slight vertical shift to compensate the viscous losses, thereby preserving the fluxes. Wherever either p_{tot} or rV_u decreases one has the behaviour of a turbine (denoted as T), otherwise it acts as a pump (the P region). The algebraic sum of areas T and P vanishes.

The actuator disc model, which is a surrogate for the runaway runner, is implemented in ANSYS-Fluent commercial CFD code using the "Fan Model" for the 3D unsteady turbulent flow simulation. The survey section is changed from interior-type to fan-type, and the radial profiles for the downstream tangential velocity and the static pressure jump (as required by the Fluent fan model) are prescribed. The static pressure jump is computed from the total pressure jump, Figure 94.b, by subtracting the dynamic pressure jump. Both the axial and radial velocity components are considered continuous across the actuator disc, although a refined methodology could consider a jump in the radial profile as well by employing the full actuator disc theory.

After the survey section shown in Figure 93 is replaced by the actuator disc (modelled as fan in ANSYS Fluent as shown in the previous section) the unsteady 3D flow significantly changes after a short period of time of 0.1 s (the time step of the numerical simulation is 0.2 ms). In this incipient stage, Figure 95, the well-structured vortex rope from Figure 93 is on one hand already significantly attenuated and on the other hand it breaks down in many vortex segments. The main result of the research is illustrated in Figure 96, at 0.5 seconds later that the flow-field shown in Figure 95. One can see that the initial vortex rope from Figure 93 is practically mitigated, with the well-developed vortex filament broken down in a cloud of small vortex filaments. The flow region with such fragmented small vortices has a higher turbulence intensity but it no longer generates the high amplitude low frequency pressure fluctuations as the precession vortex rope. It is expected that later on the swirling flow in the diffuser becomes even more stable, with an additional benefit of reducing the hydraulic losses and increasing the pressure recovery efficiency.

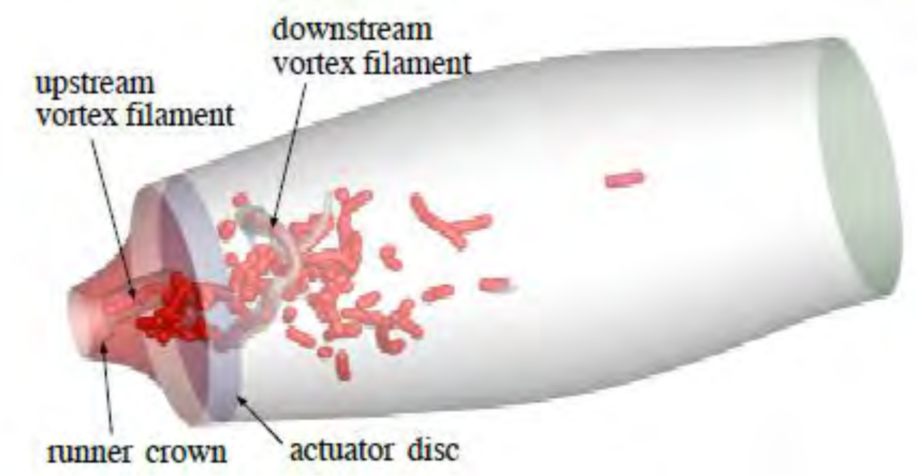

Figure 95. Incipient stage of mitigating the vortex rope, [19].

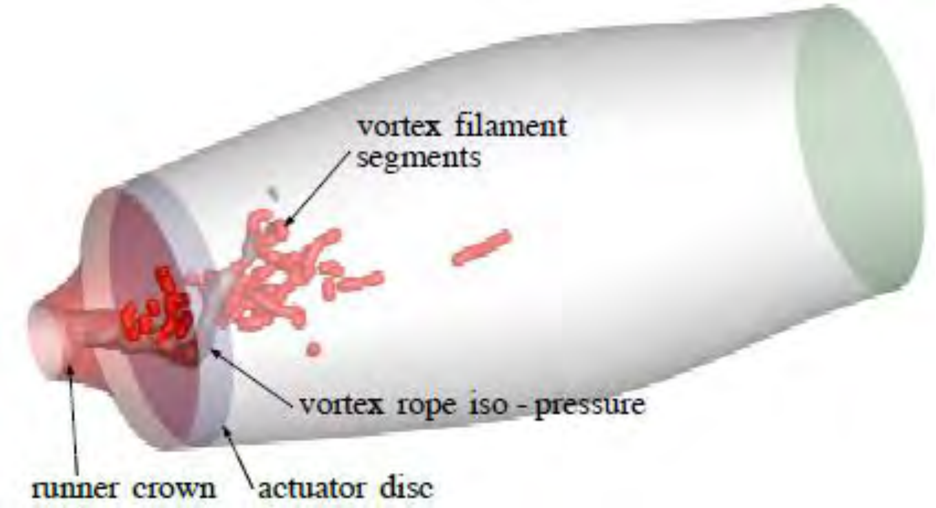

Figure 96. Advanced stage of mitigating the vortex rope, [19].

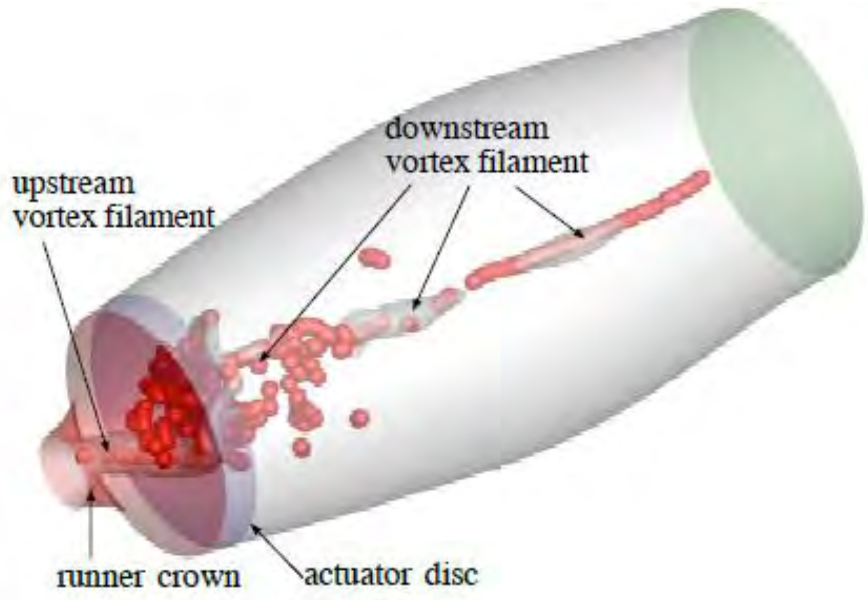

Figure 97. Final stage of mitigating the vortex rope, [19].

The stabilized configuration of the swirl downstream the actuator disc is shown in Figure 97 after 5 seconds flow time (25,000 time-steps). One can see that the swirling flow is practically stabilized to a quasi axi-symmetrical configuration, with an effective mitigation of the vortex rope. Upstream the actuator disc, the precession vortex still develops, but the rather small re-balancing of the total pressure from the axis to the wall, as shown in Figure 94.b, effectively removes the swirling flow instability. The downstream vortex filament is practically aligned to the axis, and there are no more pressure fluctuations as induced by initial precession helical vortex shown in Figure 93.

One can consider this numerical investigation as a successful demonstrator of the runaway runner concept for swirl stabilization.

Another research subject, [20], is represented by a methodology for designing the stator and rotor blades for an axial expansion turbine, with optimisation procedure with respect to cavitation behaviour. The resulting stator-rotor thin blades tandem is analysed using unsteady, incompressible and inviscid flow simulation in order to validate the quasi-analytical design method and associated computer code. Finally, thickness is added to the thin blade (camber line) to ensure structural integrity and the resulting configuration is analysed in turbulent flow.

Fluids from many industrial processes are often released via pressure regulators or valves thus dissipating (wasting) their hydraulic energy excess. The overall efficiency of the process can be improved by recovering the hydraulic energy, as mechanical then electrical energy, through modular axial-expansion turbines (AXENT) which were developed in the last decades. Their main advantage over other turbines is that they do not generate a significant pressure surge in the event of a power failure or blocking of the machine, having thus no negative impact on the process by their installation.

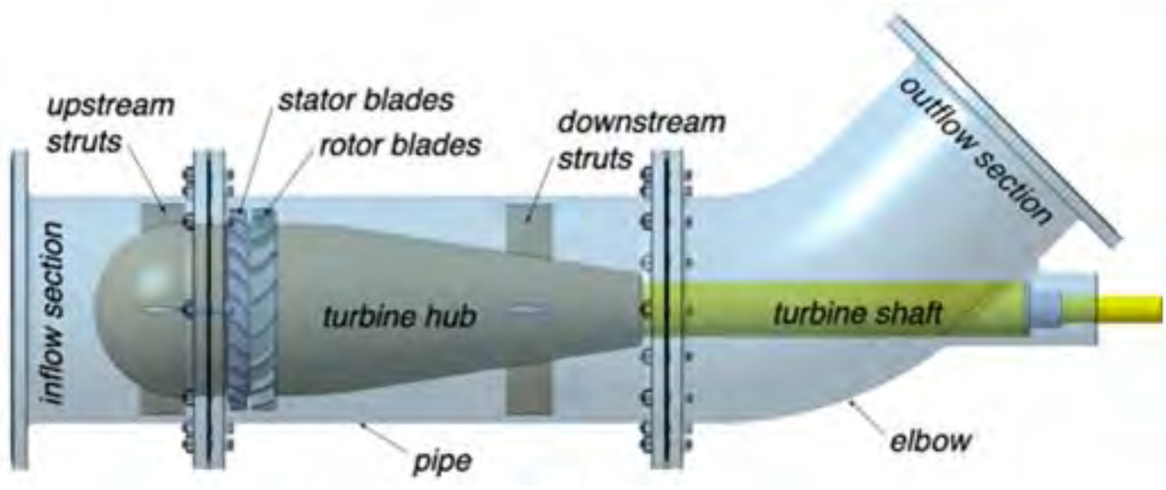

Figure 98. Typical axial expansion turbine for energy recovery, [20].

Figure 98 shows a sketch of an axial expansion turbine for energy recovery. The incoming pipe flow is accelerated in the annular space between the hub and the pipe, where the stator and rotor blade rows are located. Further downstream the flow is decelerated practically back to the upstream discharge velocity, and the elbow allows the shaft to be connected to the electrical generator. The goal of this paper is to present a methodology for designing and optimizing the blades. The employed methodology uses a quasi-analytical approach for blade design, with a specific parameterization of the blade loading distribution.

The design of the thin hydrofoil cascade has the following data input:

- upstream flow direction,
- downstream flow direction,
- spacing,
- blade loading distribution from leading edge to trailing edge.

In order to design the cascades for both stator and rotor blades we first choose a parameterization of the loading function as:

$$g(x,\lambda_1,\lambda_2,\lambda_3) = erf(\lambda_1 x)\cdot erf(\lambda_2(1-x))\cdot(1+\lambda_3 x) \tag{19}$$

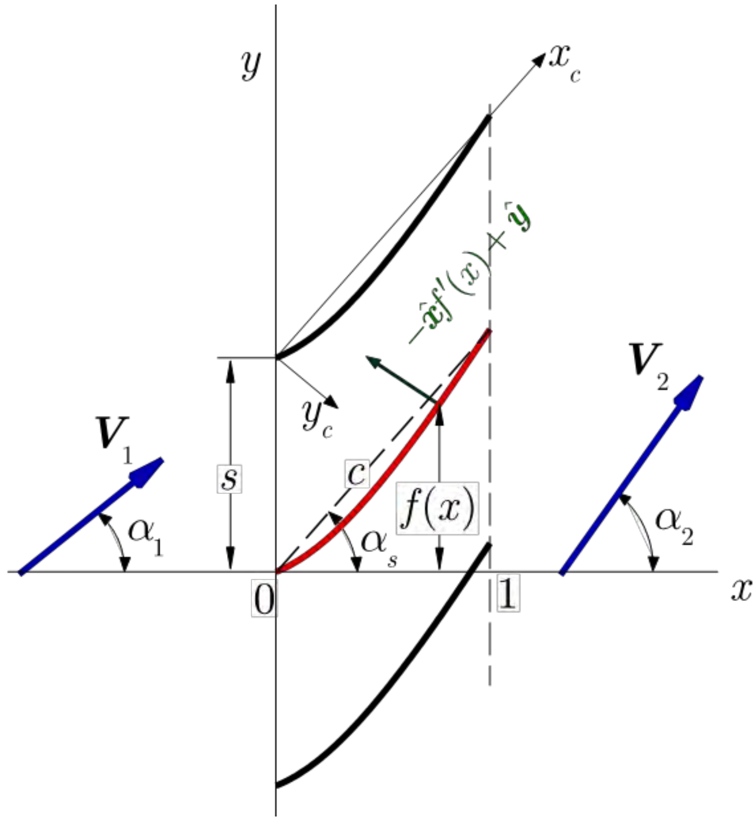

Figure 99. Thin hydrofoil cascade design, [20].

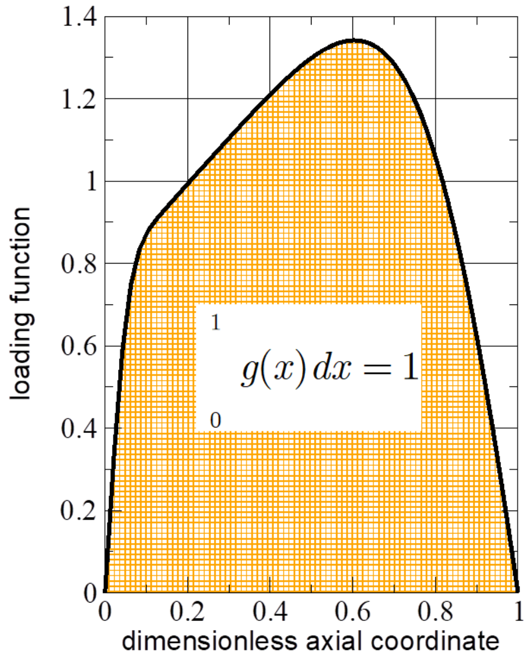

Figure 100. Initial blade loading, [20].

The optimization procedure for the thin blade design uses the maximum velocity on the blade as the objective function to be minimized by automatically adjusting the three parameters in (19) with the BOBYQA (Bound Optimization By Quadratic Approximation) algorithm for bound constrained optimization without derivatives, so ensuring the best cavitation behaviour.

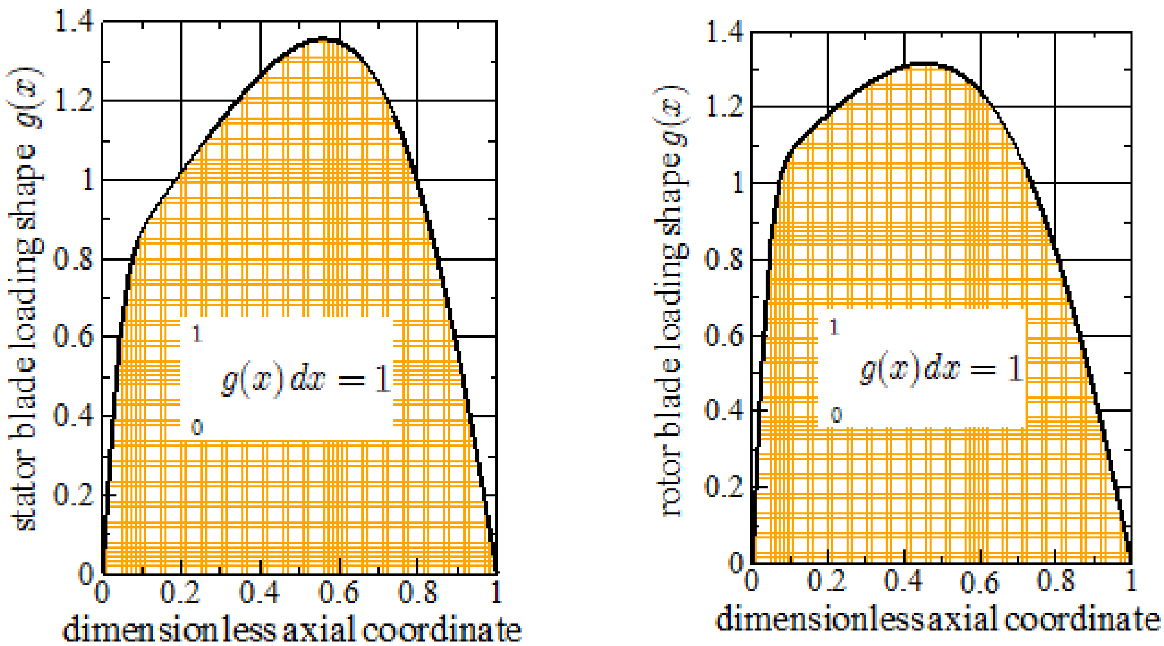

Figure 101. Stator (left) and rotor (right) optimum blade loading shape, [20].

The design process leads to the following results:

- the shape of the thin hydrofoil (camber line)
- pressure distribution on the blade

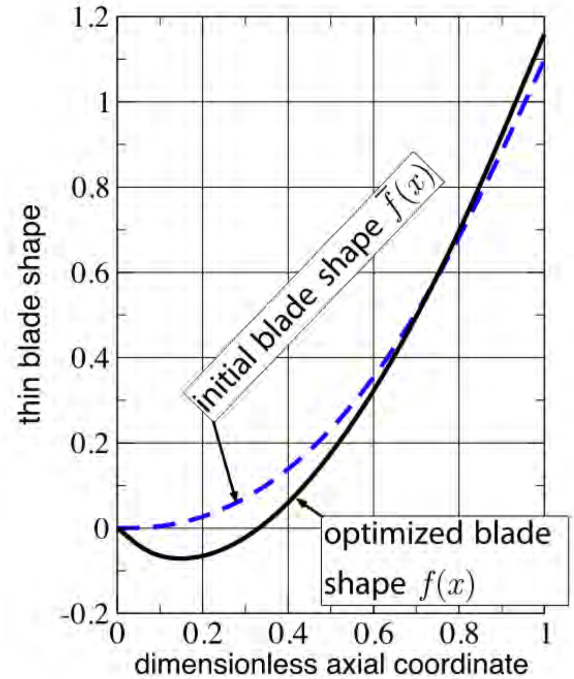

Figure 102. Camber line of the blade, [20].

The in-house design code developed is validated by a numerical simulation of the tandem stator-rotor cascade flow using the FLUENT expert code. The 2D unsteady, incompressible and inviscid flow is solved simultaneously for the stator and rotor periodic domains, Figure 103, using the sliding mesh technique. While the stator domain is fixed, the rotor is moving with the transport velocity u. The velocity triangles at the stator-rotor interface and rotor outlet, respectively, are shown in Figure 103. Note that the flow upstream the stator, as well as downstream the rotor, is axial at the design operating point. At off design regimes there will be a residual swirl downstream the rotor. The streamlines for the absolute stator flow and relative rotor flow, respectively, Figure 103, show the shock-free flow at the leading edge of the blades.

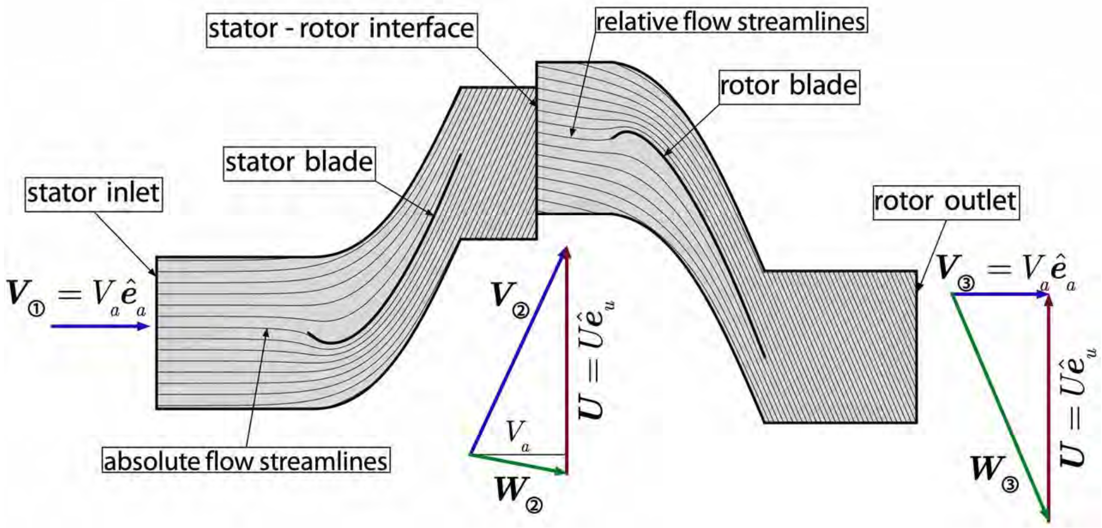

Figure 103. Flow kinematics of stator-rotor tandem cascades. Streamlines for the absolute stator flow and for the relative rotor flow. Velocity triangles upstream and downstream the rotor cascade, [20].

The actual validation of the design code is done by comparing the pressure coefficient on the blades obtained from the theoretical velocity distribution with the directly computed values in FLUENT using the pressure values on the blades.

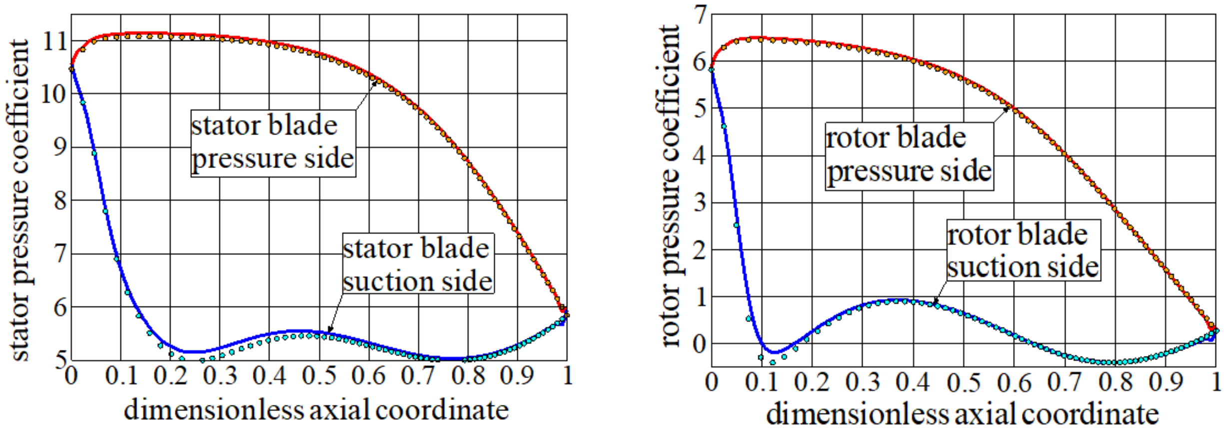

Figure 104. Stator (left) and rotor (right) pressure coefficient. The circles correspond to the theoretical values computed from the design code and the solid lines are from the FLUENT numerical solution, [20].

The thin blade design methodology provides the camber line of the blade. For real blades thickness must be added to the camber line to ensure structural integrity. For the present research we have adopted the YS-900 symmetric hydrofoil thickness distribution for the blade thickness in the tangential direction. The thickness function is scaled-up for a maximum of 10% blade blockage at 52.5% axial width from the leading edge. The corresponding thick stator and rotor blades are shown in Figure 105.

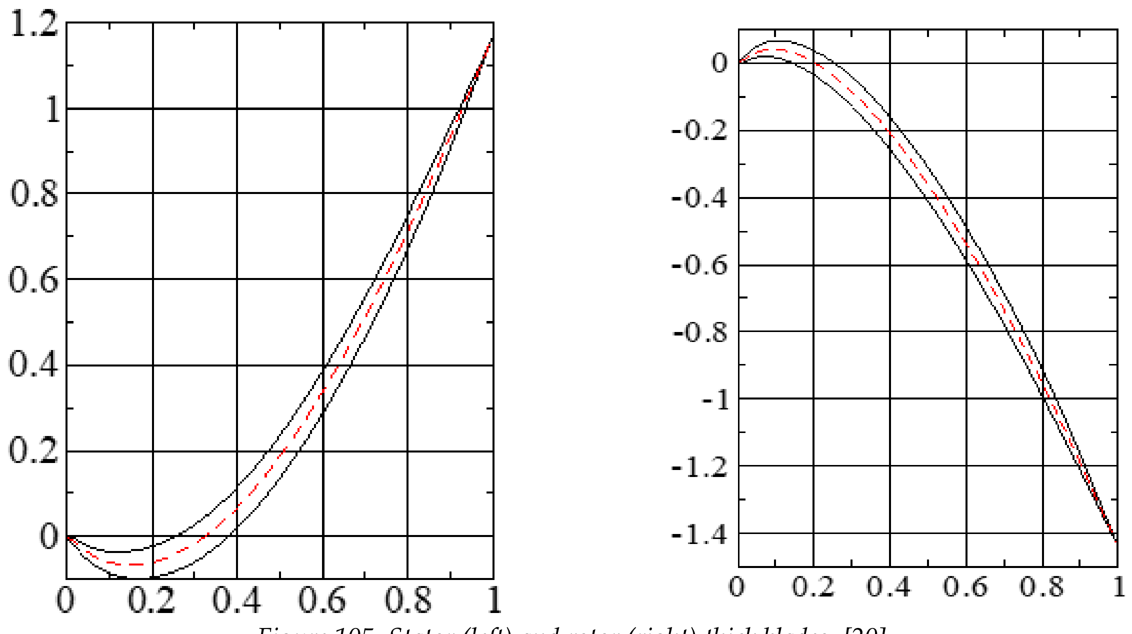

Figure 105. Stator (left) and rotor (right) thick blades, [20].

Finally, the thick blades rotor-stator cascades are investigated in viscous flow simulation, using the Spalart and Allmaras turbulence model. Figure 106 shows the total pressure distribution obtained in this case, as an illustration of the specific hydraulic energy evolution in the bladed region. In the section of the stator blades the total pressure practically remains constant, except the boundary layers and subsequent wakes of the stator blades. The axial gap between the stator and the rotor is chosen equal to the stator spacing.

Within the rotor blades row the total pressure decreases corresponding to the conversion of hydraulic energy in mechanical energy. Also, the total pressure has an increase at the leading edge (red spots) as usual in turbine cascades.

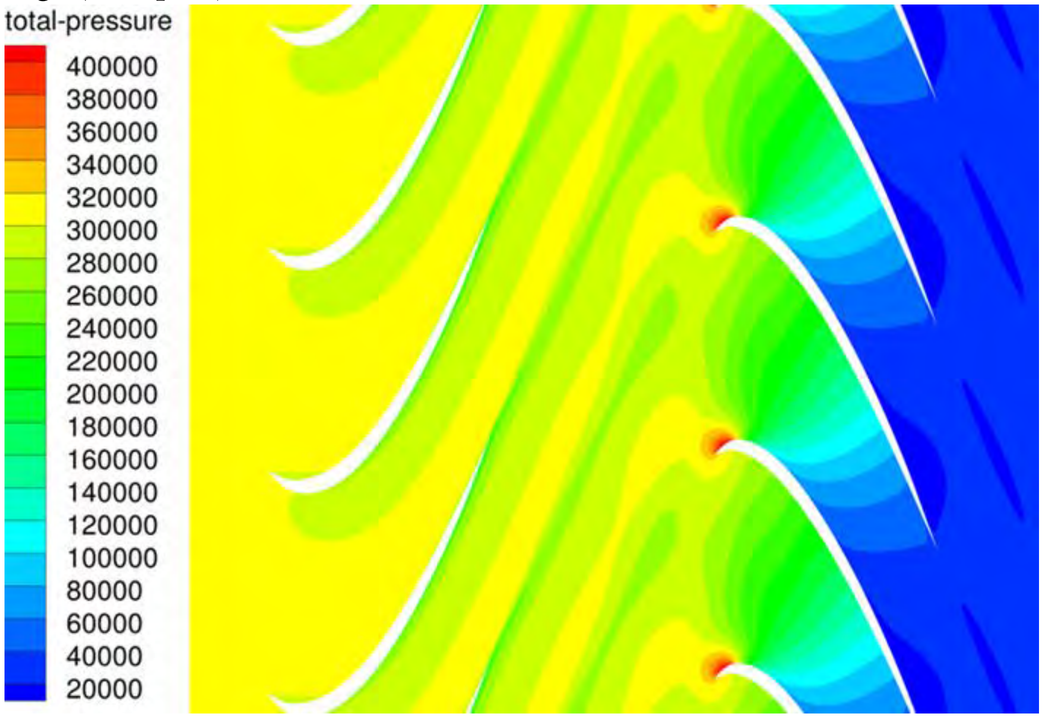

Figure 106. Total pressure in the stator and rotor blade cascades, [20].

The present methodology practically eliminates the classical trial-and-error direct approach, providing an optimized configuration customized to the specific process served by the energy recovery turbine.

The most recent activity in the domain od hydraulic turbines was performed in the year 2021 when I was part of a team of experts from Politehnica University Timisoara. We participated to the hearings of International Court of Arbitration in Zurich as technical experts representing S.P.E.E.H. Hidroelectrica S.A. in a case of arbitration between Andritz Hydro GMBH (Germany) and Andritz Hydro GMBH (Austria) and Hidroelectrica concerning the rehabilitation of the hydroelectric power plant Portile de Fier 2.

1.2.3. Scientific achievements in the domain of chemical reactors

The research in the domain of chemical reactors was motivated by the fact that the company Oltchim S.A. required a study concerning an existing chemical reactor that operated with a liquid-liquid mixture and intended to operate with a two-phases liquid-solid suspension. Although it looked like this type of research should be performed by chemical engineers, it proved to be more like a task to be performed by mechanical engineers specialised in hydraulic machines. That is because the operation of the stirring mechanism from the chemical reactor is very similar to the operation of an axial pump.

My role in this research project was to establish the proper set-up for the numerical investigation, to perform the numerical simulation and to process and analyse the results.

A part of the results obtained from this study were presented in three scientific papers, published in ISI indexed journal, [9], [7] and [8].

The main research activities focused on following directions:

- analysing the performances of the existing stirring mechanism
- designing a new impeller for a new stirring mechanism
- analysing the performances of the new impeller
- finding and analysing the best solution (position, number of impellers) for the new impeller
- designing a simplified version of the new designed impeller
- testing the performances of the new simplified impeller
- supervising the implementation of the new stirring mechanism in the chemical reactor

The main idea behind this research work is to develop a tractable and robust numerical approach for design and assessment of mixing impellers, beyond the rather classical approach of selecting on-the-shelf impellers based on empirical correlations. In the chemical industry are very common the employment of stirred reactors containing liquid and solid phases, to obtain chemical products from the reaction between the solid phase component and the liquid phase component. The quality of the finite chemical product is determined by the fact that the solid particles must remain in suspension in-side the liquid phase as long as possible, so that the chemical reaction to take place. The sedimentation of the solid particles must be prevented by the stirring mechanism and must ensure a homogenous distribution of the solid particles in all the volume of liquid. Another important aspect for obtaining a quality product from the chemical reaction in-side the reactor, is to prolong the contact time between the solid particles and the liquid phase, and the impeller plays a major role in this matter. The quality of the suspension of the solid particles generated by the impeller can be characterized by several parameters such as solid particles distribution, cloud height and suspension velocity.

The hydrodynamics of the flow process inside the stirred tanks are complex, three-dimensional and turbulent. The efficiency of the mixing process that takes place in-side the reactor depends on the interaction between the solid particles and the liquid, the geometry of the reactor, the design and position of the impeller.

The original impeller was designed for the preparation of a chemical product with a prescribed composition. The present study aims at finding, using a numerical simulation analysis, if the performance of the original impeller is suitable for obtaining a new chemical product with a different composition. The Eulerian multiphase model has been employed along with the renormalization (RNG) k–ε turbulence model to simulate the liquid–solid flow with free surface in a stirred tank. A sliding mesh approach was used to model the impeller rotation with the commercial CFD code, FLUENT 16. A schematic representation of the investigated stirred reactor is presented in Figure 107. Initially the reactor and its stirring mechanism was developed to work only with liquid phase components, but a reconversion of its use is needed. After analysing the results obtained and judging the impeller performances from the point of view of solid particles distribution, a decision will be taken if the impeller will be kept, or another type of impeller is needed in order to ensure the prescribed solid particle distribution.

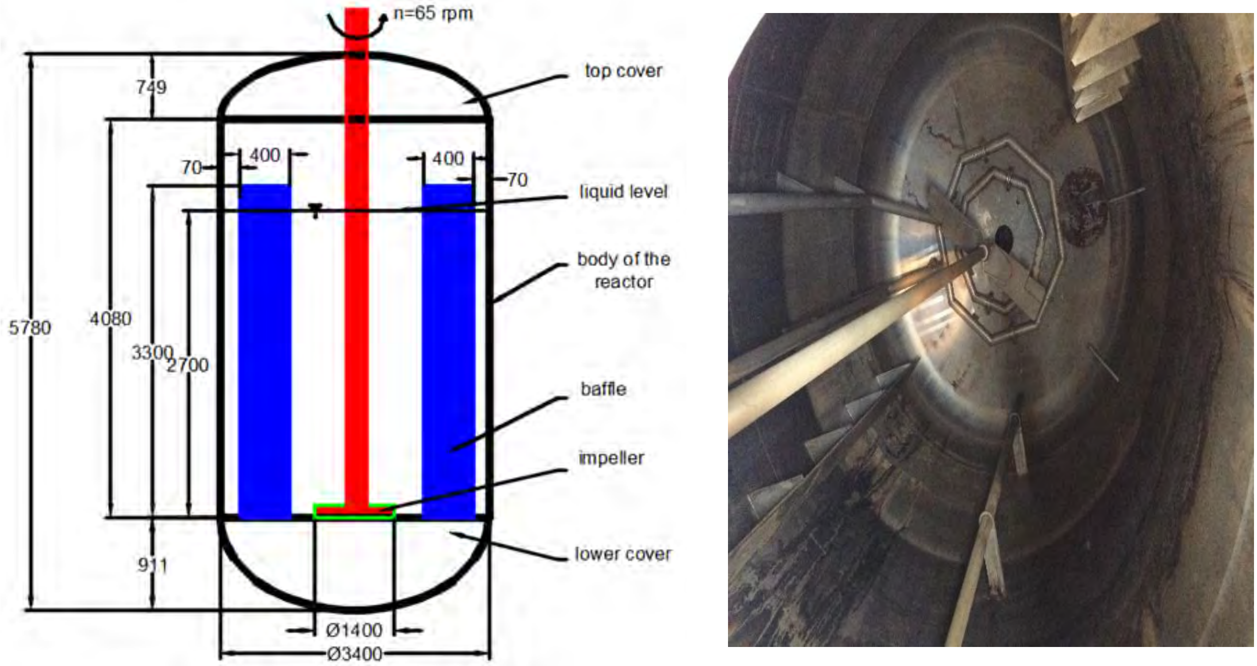

Figure 107. Schematic representation of the stirred reactor, [9].

Geometry reconstruction of the industrial stirred reactor and its meshing have been performed with the software Gambit 2.4. The mesh consists of approximately 1.1 million tetrahedral elements. As regards the mesh quality, we have been restricted to use tetrahedral mesh elements due to a greater number of recommendations from previous case studies. For our numerical investigation, a very high quality of mesh (skewness < 0.6) has been ensured throughout the computational domain. For chemical multi-phase reactions, the hydrodynamic plays a major role in the mixing of the two phases and in the mass transfer. The impact of the hydrodynamic field upon the performances of an industrial stirred reactor is determined by the specific geometry of the reactor. For reactors operating with a two-phase flow, solid and liquid, is recommended to monitor the solid particles distribution and to check if the distribution is in line with prescribed condition of the chemical process. For certain chemical reactions it is mandatory that the solid particles to float inside the liquid phase close to the lower part of the reactor. For other situations, like in the case we analyse, it is required that the solid particles to be distributed uniformly throughout the entire liquid phase volume.

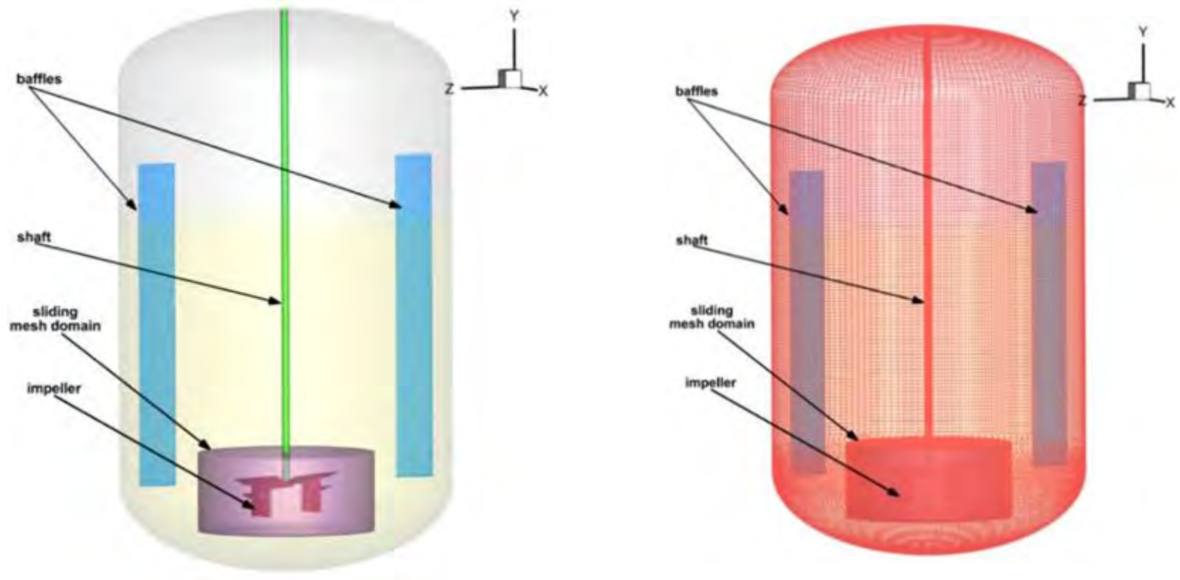

a) b)

Figure 108. Computational domain: (a) Components of the reactor; (b) Mesh of the computational domain, [9].

There are two cases studied in this research and the results analysed: the first case considers that the solid particles are already settle at the bottom of the reactor before the impeller starts to rotate, Figure 109.a, and for the second case it was considered that the solid particles are all in suspension when the impeller starts to rotate, Figure 109.b. In the first two rows of pictures from Figure 109 is represented the distribution of the volume fraction of the solid phase in the entire 3D reactor and on a vertical plane.

The most relevant quantitative representation for the analysis of the performance of the stirring mechanism is represented by the histogram of the distribution of the volume fraction of the solid phase. Thereby, the initial state with the homogenous distribution of the solid phase in the entire volume of the liquid phase corresponds to an optimum solid volume concentration of 18.2 %, Figure 109.b. For the first case, Figure 109.a, where the solid phase is completely sedimented in the lower part of the reactor, the solid volume concentration has a value of 63%, and the rest of 42% of the entire volume of liquid contains no solid phase. The analysis of the volume fraction of the solid phase distribution presented in Figure 110 underlines the fact that the rotation of the impeller did not avoid the sedimentation of the solid phase on the bottom of the reactor for both analysed situations. It results that the first situation analysed, Figure 110.a, is the most unfavourable situation from the point of view of solid phase sedimentation. The histograms of the distribution of the volume fraction of the solid phase presented in Figure 110 confirms that this impeller is not perform properly. In the first case, Figure 110.a, almost 40% of the volume of the liquid phase does not contain solid particles, and for the second case, Figure 110.b, almost 23% of the volume of the liquid phase does not contain solid particles.

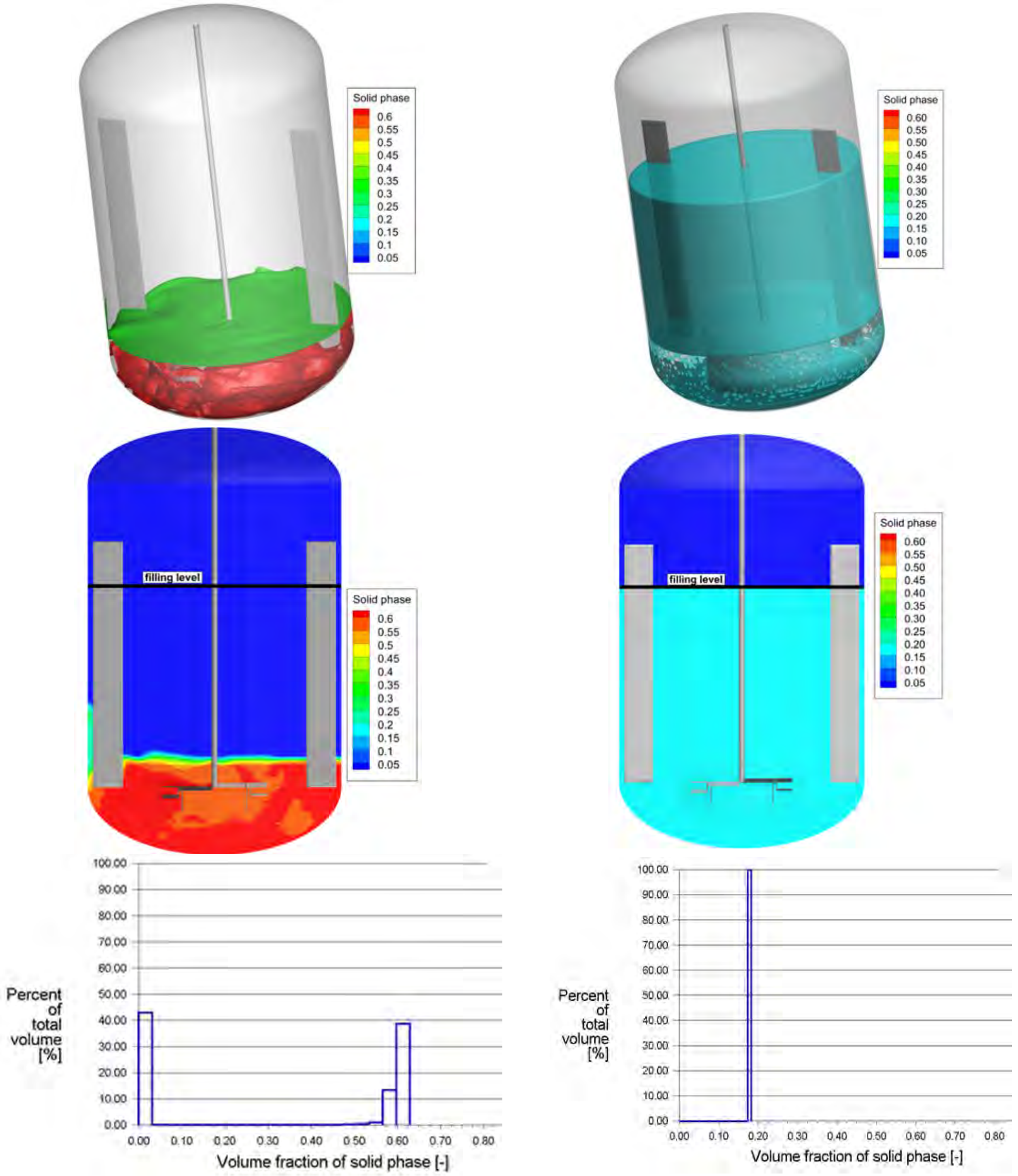

a) b)

Figure 109. Initial state of the volume fraction distribution of the solid phase: (a) flow started from solid phase fully sedimented; (b) flow started from solid phase dispersed in the entire volume of liquid, [9].

By analysing the first two pictures from Figure 110, it results that it is the best option to start the operation of the stirring mechanism when the solid phase is not completely sedimented on the lower part of the reactor. Even for this situation the impeller does not avoid the sedimentation of a consistent part of the solid phase on the bottom of the reactor.

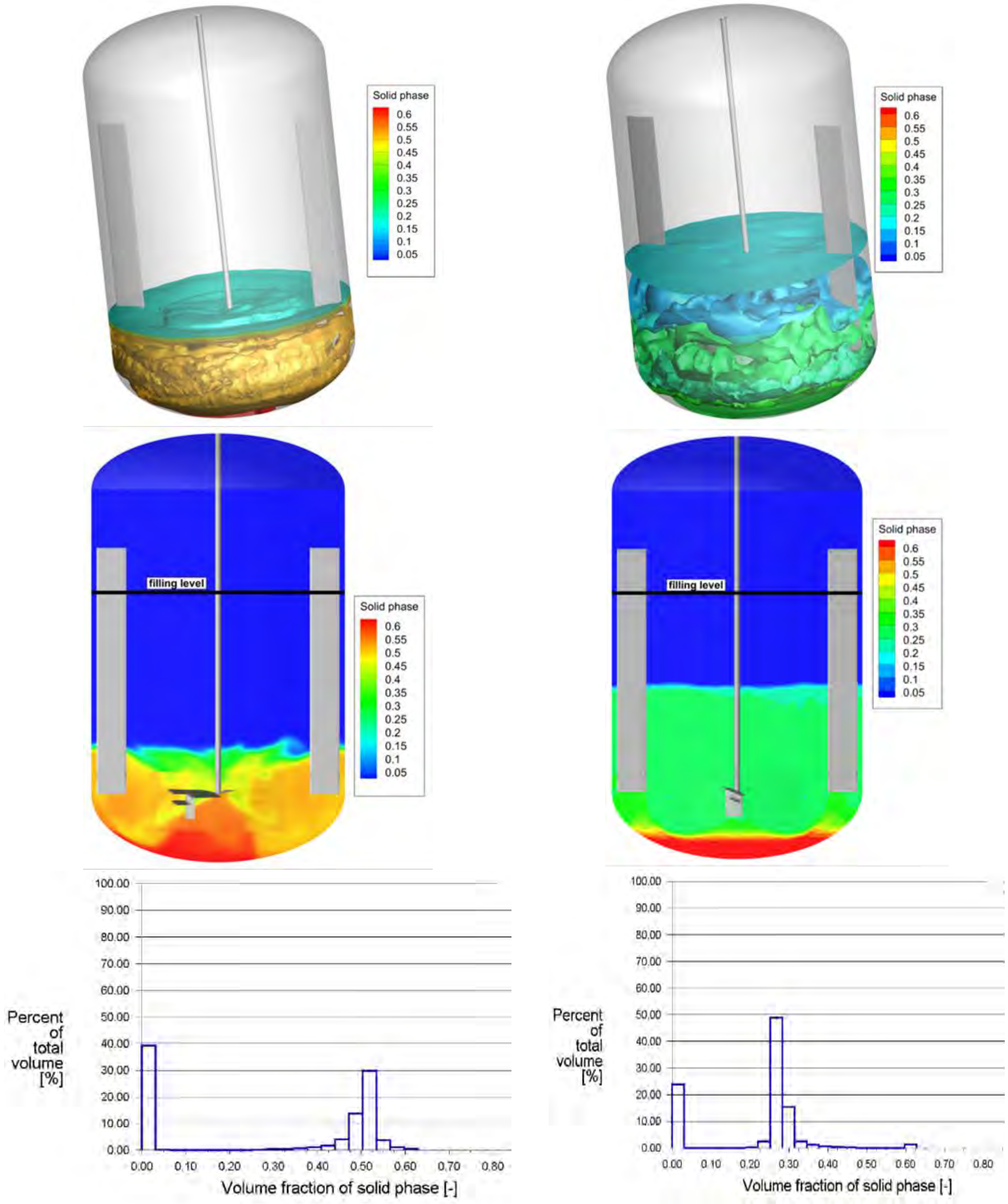

a) *b)*

Figure 110. Final state of the volume fraction distribution of the solid phase: (a) flow started from solid phase fully sedimented; (b) flow started from solid phase dispersed in the entire volume of liquid, [9].

The investigation of the hydrodynamic performance of the impeller is based on the velocity vector distribution of the liquid phase, in order to analyse the flow pattern.

In Figure 111 is presented the velocity vector distribution of the liquid phase on two vertical planes, the upper two pictures, and on one horizontal plane, the lower two pictures. It can be observed that there are generated two vortexes between the impeller and the two baffles, where the liquid is pushed towards the bottom of the reactor and then it goes upwards. The hydrodynamic field of the liquid generated by the impeller did not prove to be adequate to maintain the solid phase suspended off the bottom of the reactor.

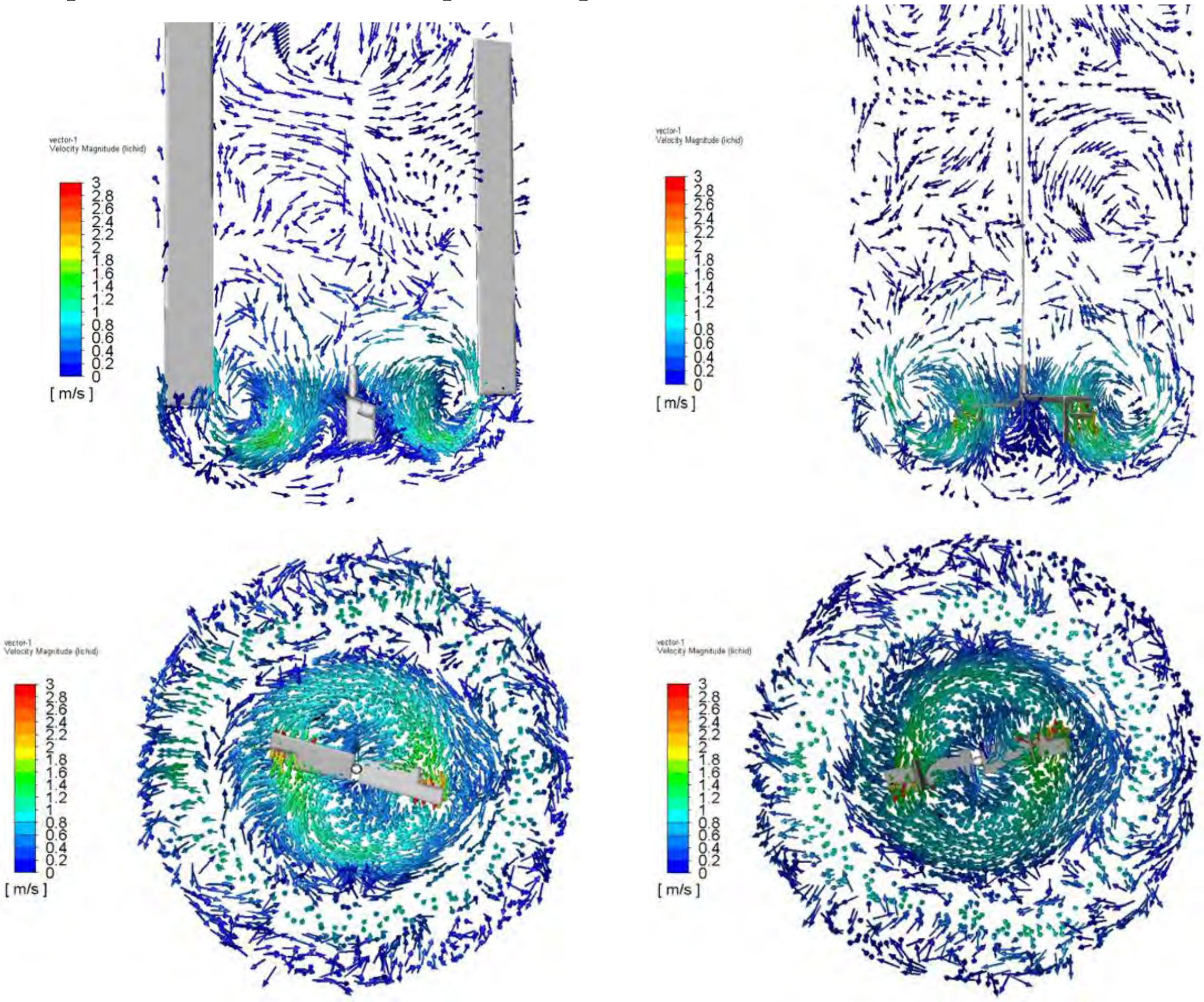

Figure 111. Velocity vector distribution of liquid phase, [9].

From the analysis of these entire data, for both investigated cases, it resulted that the original two blade impeller is not able to generate a hydrodynamic field that would keep the entire solid phase in suspension. At the end of the flow time, a part of the solid phase was sedimented on the bottom of the reactor. The volume fraction of the solid phase sedimented was larger for the first case investigated, proving that the impeller is not able to lift the already sedimented solid phase. Even when the simulation is stated with a homogeneous solid suspension and unacceptable sedimentation still occurs.

As a result, a proper stirring of the liquid-solid suspension requires a new design for the impeller able to generate a suitable flow that prevents the sedimentation which hinders the chemical reaction.

Further investigations were employed, the two-blade original impeller is replaced with a new three-blade design. The new impeller shows clear improvements in mixing a liquid-solid suspension, while keeping the shaft power practically at the same level. As a result, a practically homogenous liquid-solid mixture is obtained, thus ensuring the required quality of the final product. In Figure 112 is represented the new designed impeller versus the initial one: the original one that was initially fitted to the stirring mechanism of the industrial reactor, Figure 112.a, and the one designed by our research team, Figure 112.b. The impeller designed by our research team, has a smaller diameter than the original one, the diameter of the new impeller is 1.2 m, while the diameter of the original one was 1.4 m. Also, the new impeller has three blades instead of two, as the original impeller had. The new designed impeller was fitted to the stirring mechanism in the same position, regarding the bottom of the reactor, as the original impeller.

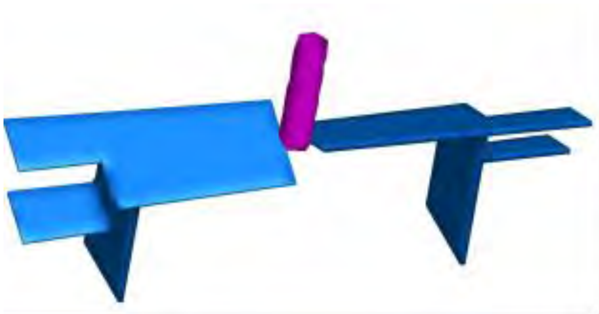

a)

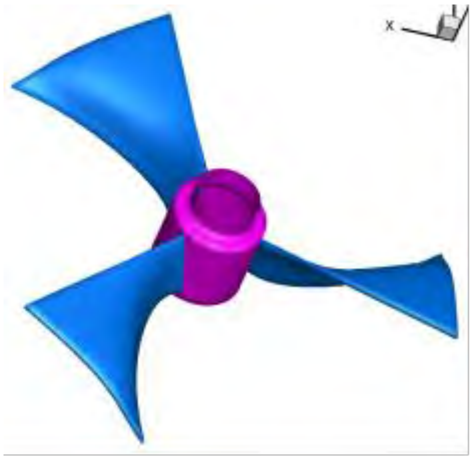

b)

Figure 112. Schematic representation of the two impellers: (a) original; (b) new design, [7].

From analysing Figure 113, it results that the new impeller is performing better than the original one. The volume fraction of the liquid containing no solid particles has decreased from 25% to 20% as shown by the histograms. Also, the new impeller completely prevents the sedimentation of the solid phase on the lower part of the reactor as can be seen from the distribution of the volume fraction of the solid phase on the vertical plane and from the histogram, Figure 113.b.

To underline the better performance of the new impeller regarding the original one, the distribution of the velocity components is analysed. Analysing the flow field generated by the original impeller it can be observed, from Figure 115.c, Figure 117.c and Figure 119.c, that dead zones exist right below the impeller and that is the reason why the original impeller did not prevent the sedimentation of the solid particles.

From the analysis of the velocity components distribution, it results that the new impeller generates a much stronger mixed axial-radial flow than the original impeller. This flow pattern developed by the new impeller has the form of a jet which spreads radially as it progresses towards the base of the reactor, entraining liquid adjacent to the impeller. After hitting the bottom wall of the reactor, part of the axial momentum gets converted to radial component along the base towards the side walls of the reactor. Because of this flow pattern, with no dead zones, there is no sedimentation of the solid phase when the new impeller is operating.

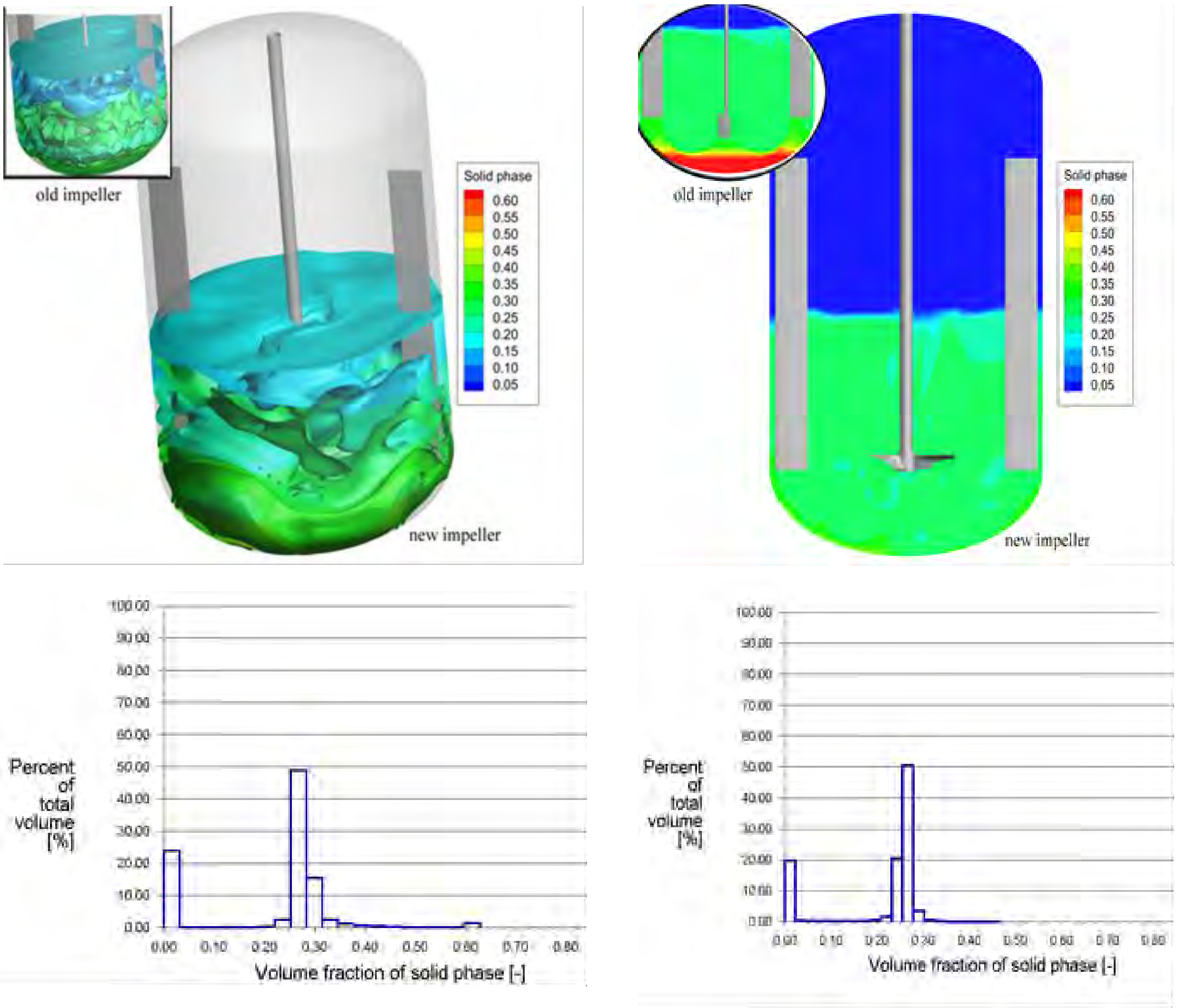

a) *b)*

Figure 113. Final state of the volume fraction distribution of the solid phase: (a) old impeller; (b) new impeller, [7].

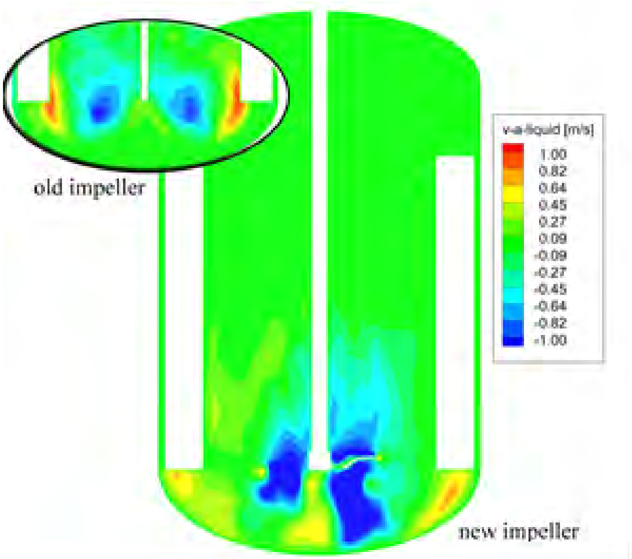

Figure 114. Axial velocity distribution of liquid phase, old impeller vs. new impeller, [7].

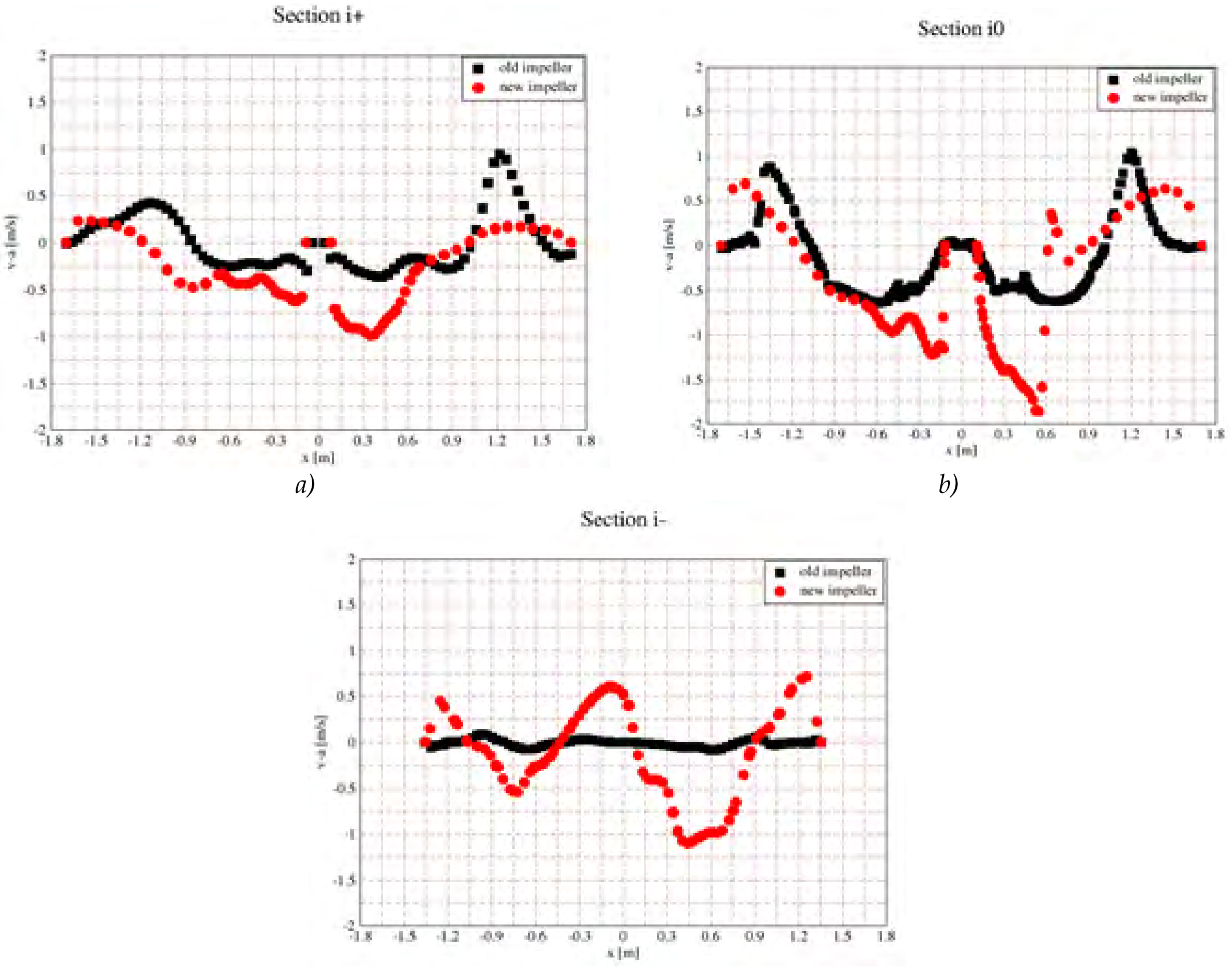

Figure 115. Axial velocity distribution of liquid phase at various axial levels, old impeller vs. new impeller: (a) above impeller; (b) impeller level; (c) under impeller, [7].

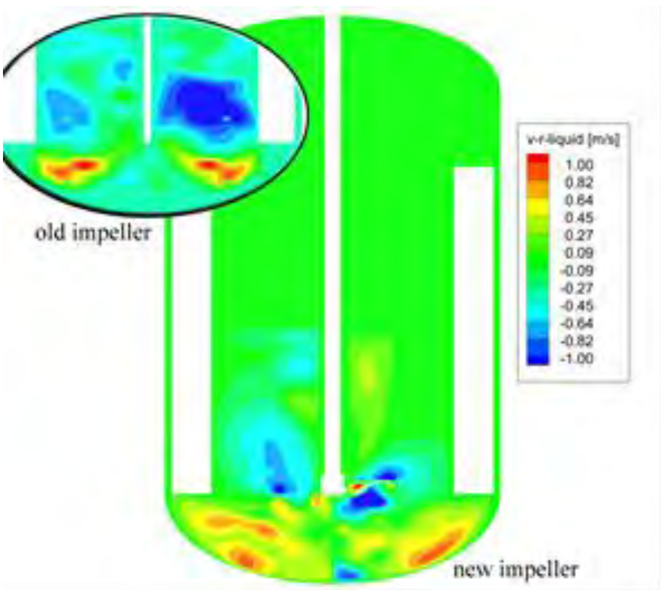

Figure 116. Radial velocity distribution of liquid phase, old impeller vs. new impeller, [7].

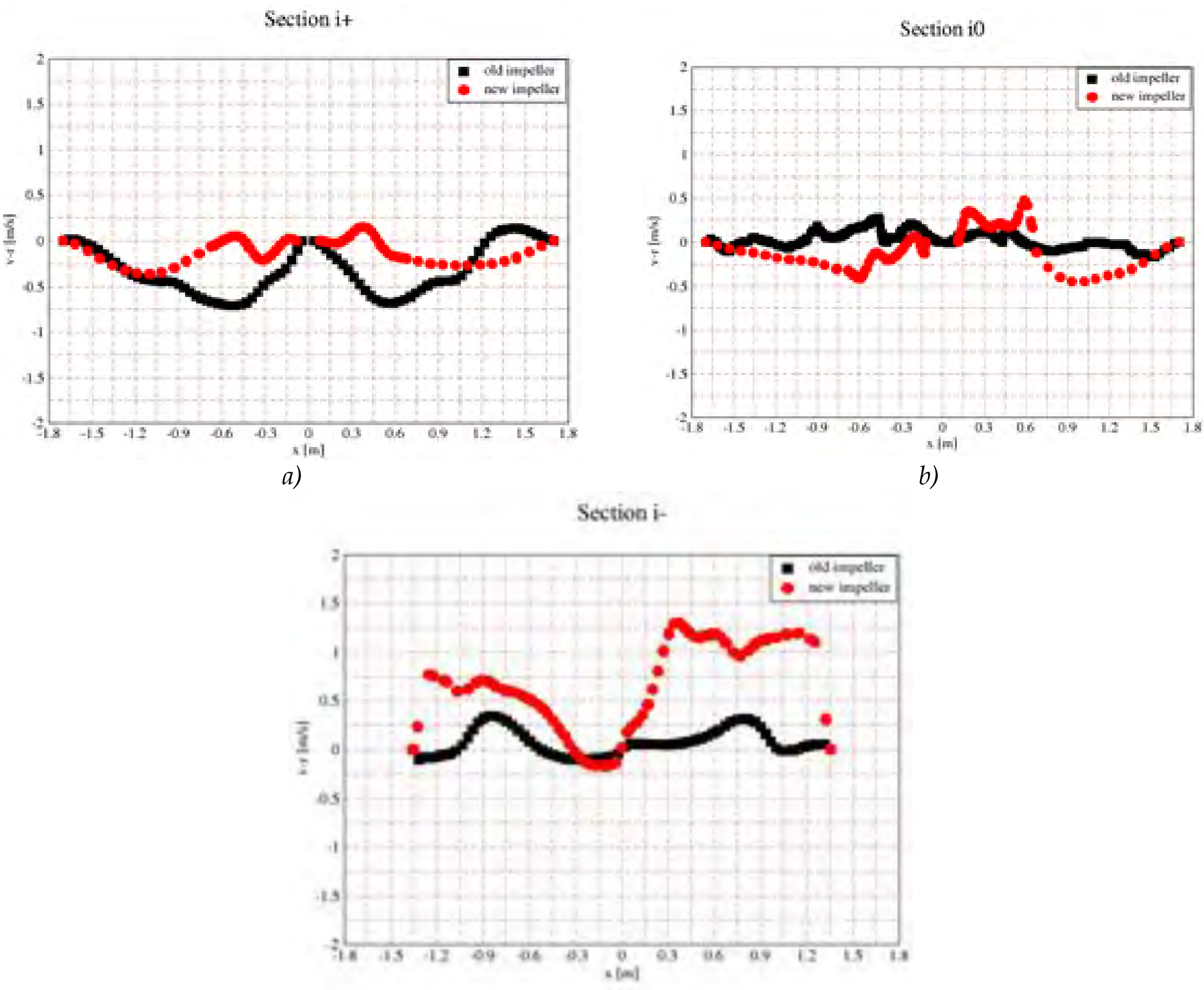

Figure 117. Radial velocity distribution of liquid phase at various axial levels, old impeller vs. new impeller: (a) above impeller; (b) impeller level; (c) under impeller, [7].

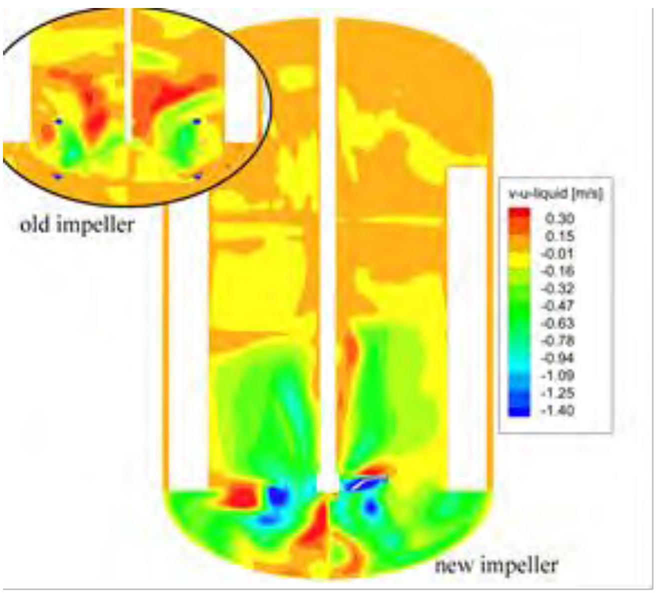

Figure 118. Tangential velocity distribution of liquid phase, old impeller vs. new impeller, [7].

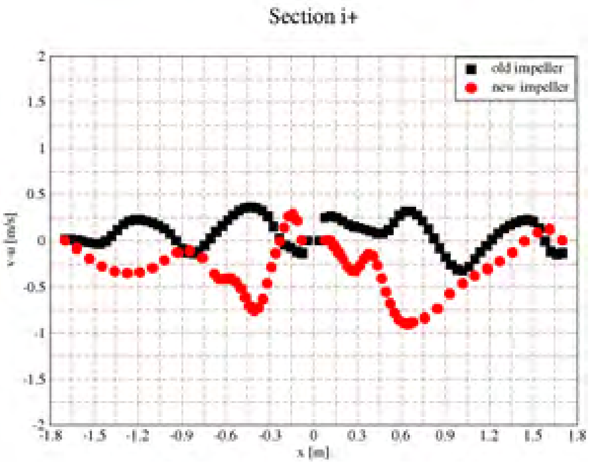

a)

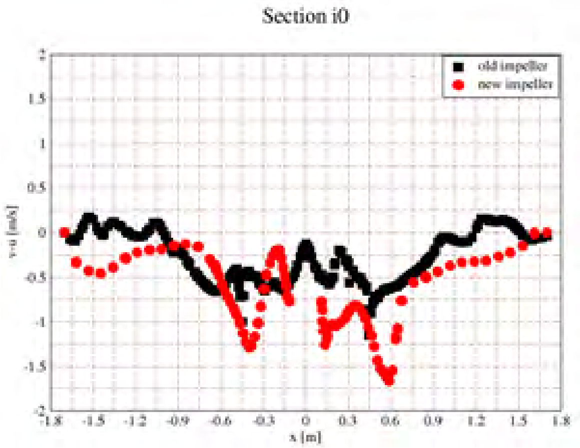

b)

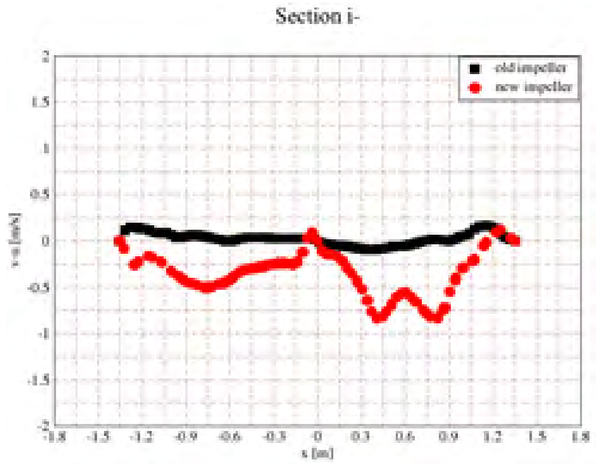

c)

Figure 119. Tangential velocity distribution of liquid phase at various axial levels, old impeller vs. new impeller: (a) above impeller; (b) impeller level; (c) under impeller, [7].

A calculation was performed to check if the existing electrical motor, that drives the stirring mechanism, can pro-vide sufficient power for the new impeller. The electrical motor generates a power of 3.6 kW and the power needed by the new impeller to operate, has the value of 2.32 kW. It results that the existing electrical motor can be used to drive the stirring mechanism fitted with the new impeller, so no supplementary cost is generated. To compare the performances of the two impellers from the point of view of consumption of power is recommended to calculate the power number, N_P, with the following equation:

$$N_P = \frac{P}{\rho_l \cdot n^3 \cdot d^5} \tag{20}$$

The value of the power number for the original impeller is 0.43 and for the new designed impeller is 1.06. Although the power number for the new designed impeller is higher than the original impeller, the hydrodynamic performances are superior.

Although is performing better than the original impeller, the new impeller is not operating at is best, because there is still a consistent volume of liquid, 20%, with no solid particles in it. This means that the part of the volume of liquid with no solid particles in it will be wasted, because no chemical reaction will take part in that region of the reactor.

A new solution was analysed, consisting in fitting on the existing stirring mechanism two new designed impellers operating in tandem. A schematic representation of the investigated stirred reactor is presented in Figure 120, where the two new designed impellers are fitted on the stirring mechanism. The two impellers have three blades each and operate at the same rotational speed of 65 rpm. The lower impeller is positioned in the same place, regarding the lower cover of the reactor, as the original impeller. The upper impeller is positioned at a distance equal with the diameter of the impeller, regarding the position of the lower impeller.

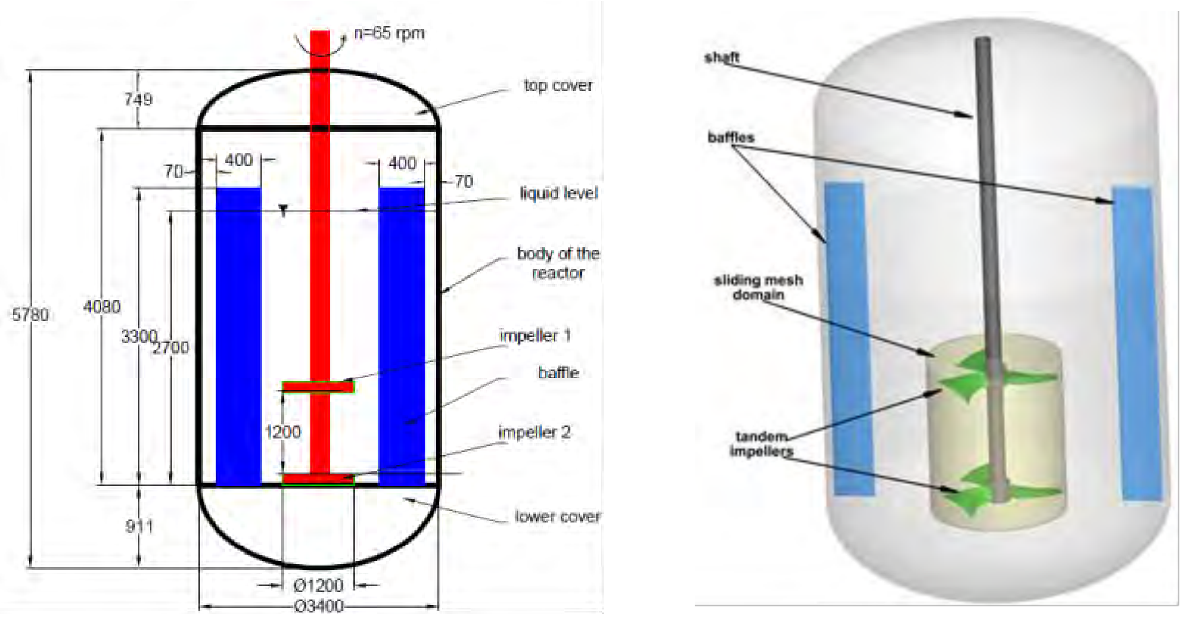

Figure 120. Schematic representation of the industrial reactor with original stirring mechanism fitted with the two new de-signed impellers, [8].

The results presented in the next figures correspond to the operation of the single new designed impeller and the operation of the two new designed impellers in tandem. For both cases, the initial state of the flow corresponds to the homogeneous distribution of the volume fraction of the solid phase in the entire volume of liquid. As it resulted from our previous research work, this is the most favourable situation for the best operation of the reactor. From analysing the distribution of the solid phase inside the industrial reactor, Figure 121, it results that by using two new designed impellers in tandem, a better homogenization of the liquid-solid mixture is obtained. Also, the level of the liquid that contains a low loading of solid particles is reduced to an acceptable value and the sedimentation of the solid particles in the lower part of the reactor is avoided. From comparing the two histograms presented in Figure 3a and Figure 121.b, it clearly results that the volume of liquid containing no solid particles has decreased from 20% to a value of ap-proximately 13%. This value might be even lower because the numerical simulation of the flow did not take in consideration the lift effect of the gas bubbles developed during the chemical reaction upon the solid particles. The stirring mechanism fitted with the two impellers in tandem manage to prevent the sedimentation of the solid particles on the lower cover of the reactor as it results from analysing all the distributions presented in Figure 121.

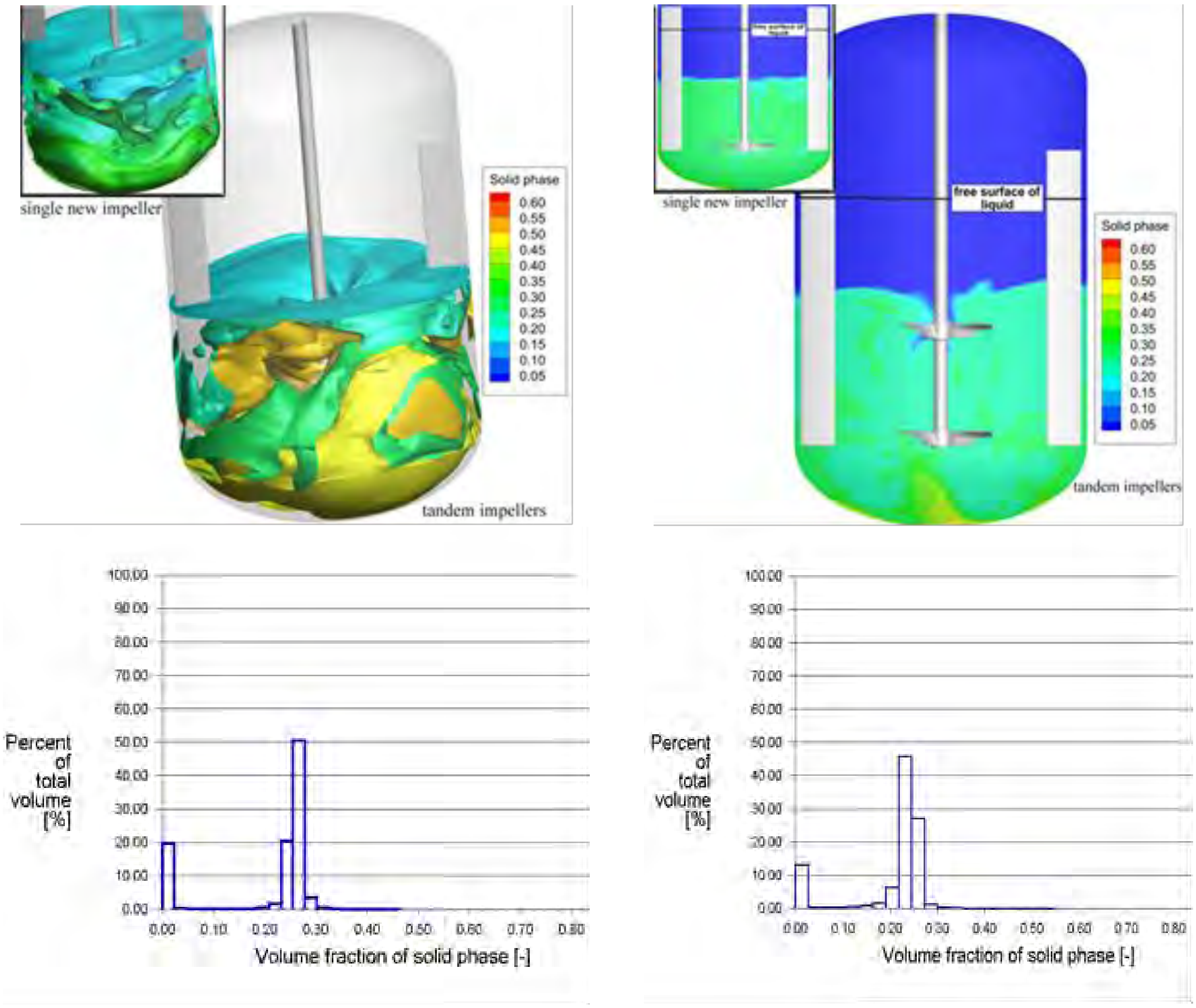

a) *b)*

Figure 121. Final state of the volume fraction distribution of the solid phase, instantaneous results: (a) single new impeller; (b) new impellers in tandem, [8].

To underline the causes for different performances of the stirring mechanism for both cases, once equipped with one impeller and once with two impellers in tandem, the distribution of the velocity components, axial, *v-a*, [m/s], radial, *v-r*, [m/s], and tangential *v-u*, [m/s], are plotted on a vertical plane through the middle of the reactor and on three axial planes situated above (y+), at the impellers level (y0) and below the impellers (y-). From the analysis of the velocity components distribution presented in Figure 122 to Figure 127, it results that the solution with two new designed impellers operating in tandem generates a much more suited hydrodynamic field for a better mixing of the liquid and solid phase. That is the explanation for the fact that only a small amount of the total volume of liquid remains without solid particles inside. Also, the better hydrodynamics of the tandem impellers leads to no sedimentation of the solid particles on the lower cover of the industrial reactor.

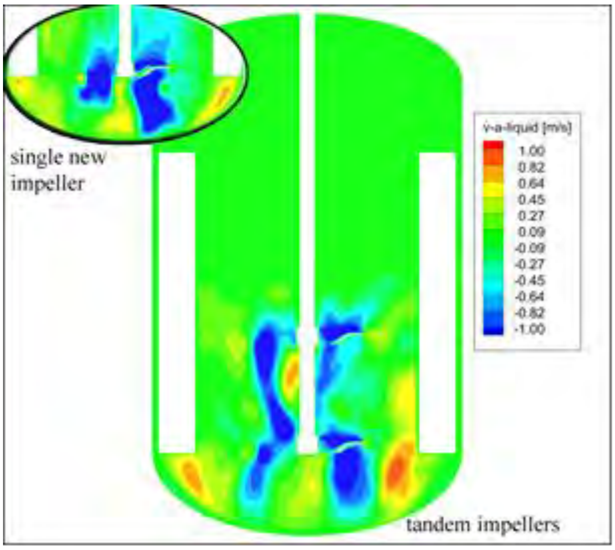

Figure 122. Axial velocity distribution of liquid phase, single new impeller vs. new impellers in tandem, instantaneous results, [8].

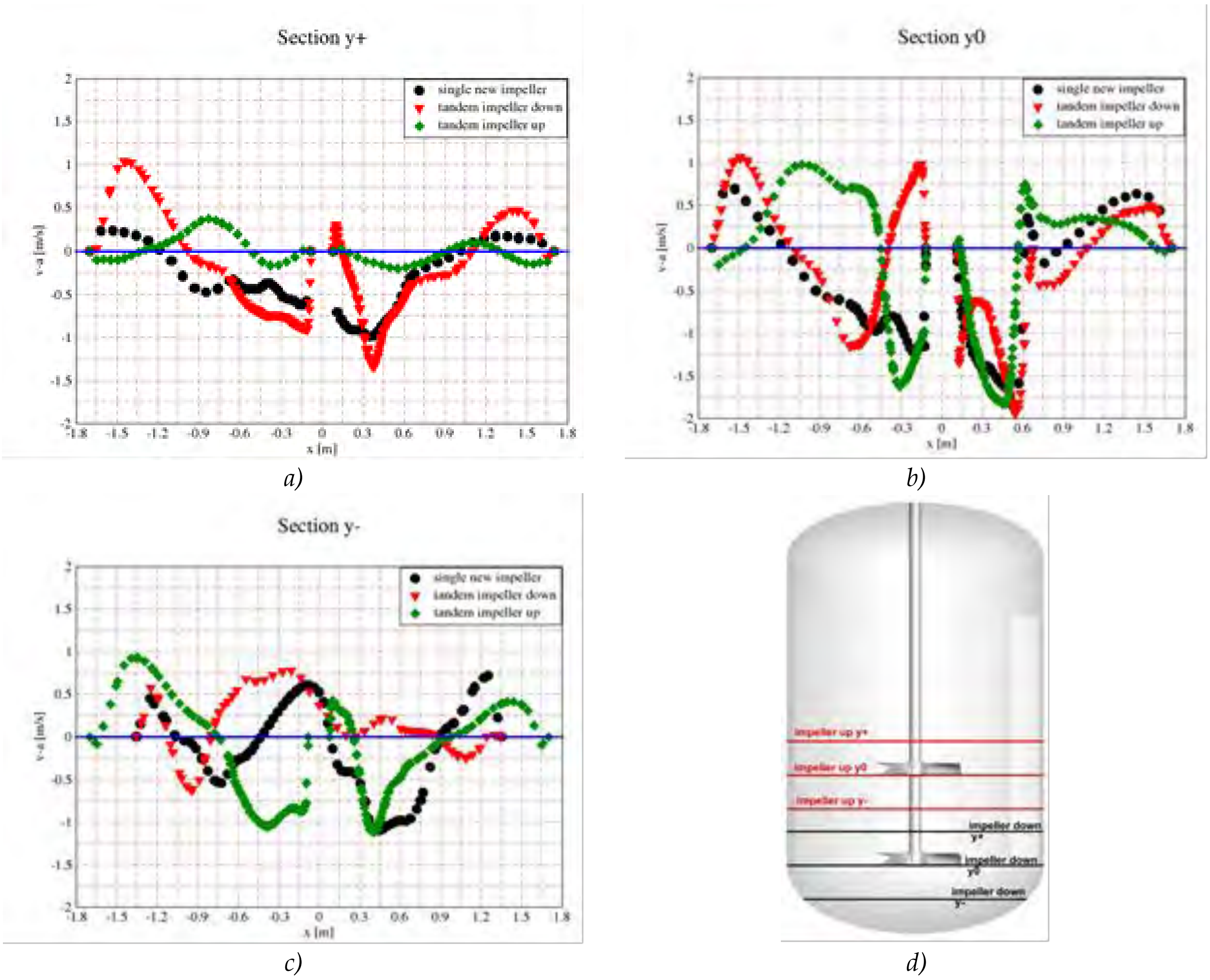

Figure 123. Axial velocity distribution of liquid phase at various axial levels, single new impeller vs. new impellers in tandem, instantaneous results: (a) above impeller; (b) impeller level; (c) under impeller; (d) axial levels position, [8].

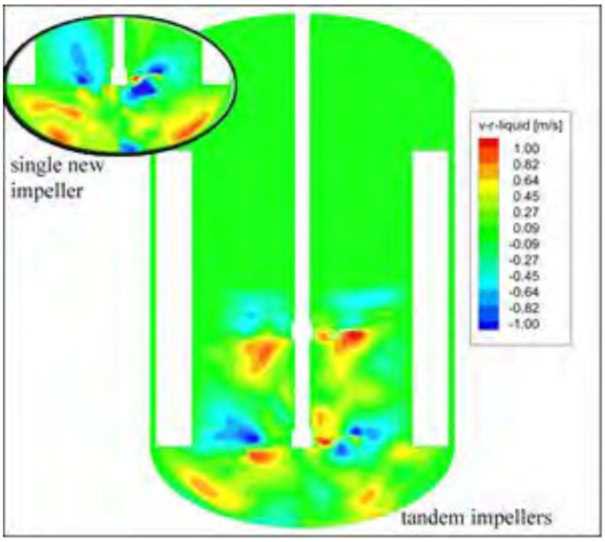

Figure 124. Radial velocity distribution of liquid phase, single new impeller vs. new impellers in tandem, instantaneous results, [8].

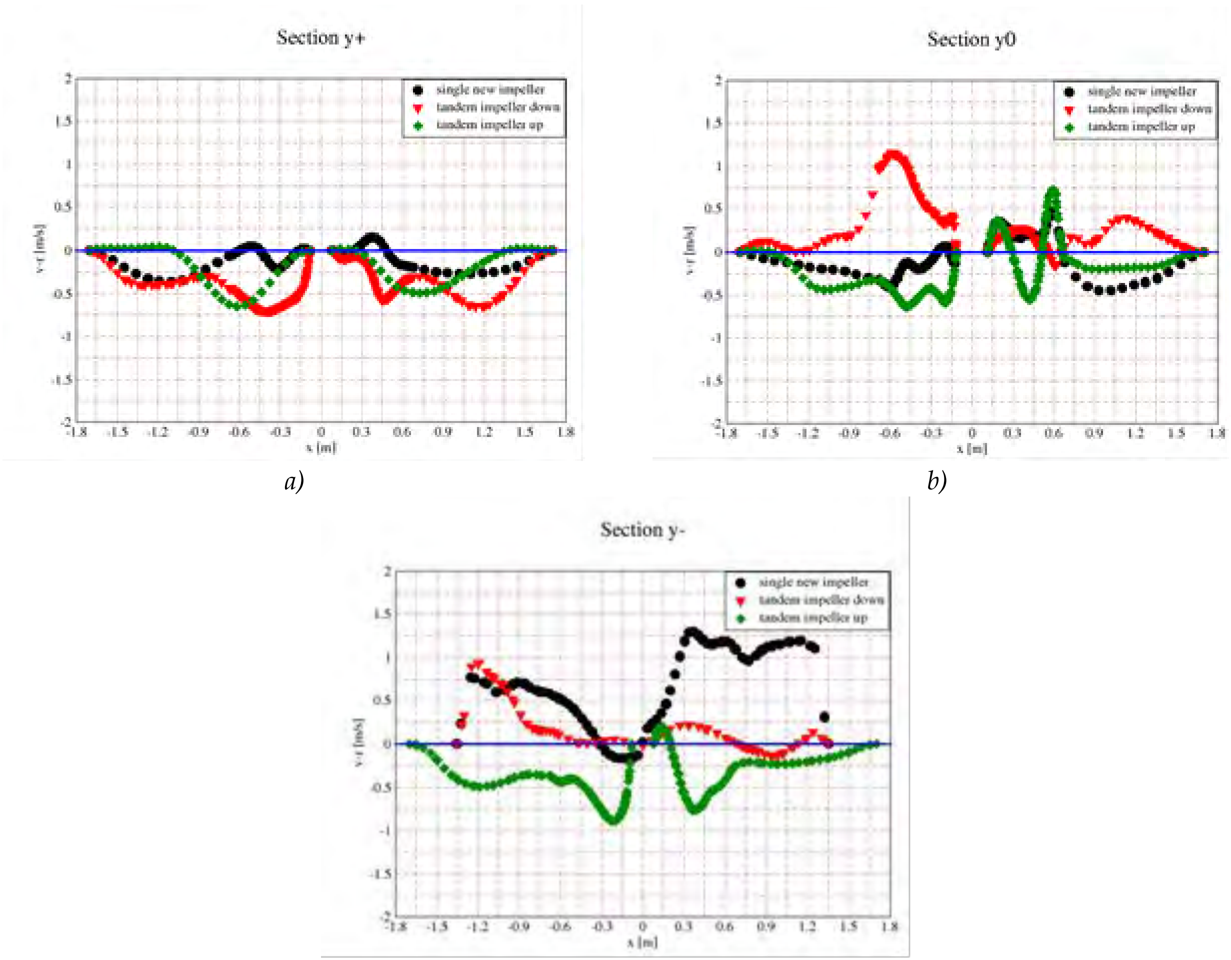

c)

Figure 125. Radial velocity distribution of liquid phase at various axial levels, single new impeller vs. new impellers in tandem, instantaneous results: (a) above impeller; (b) impeller level; (c) under impeller, [8].

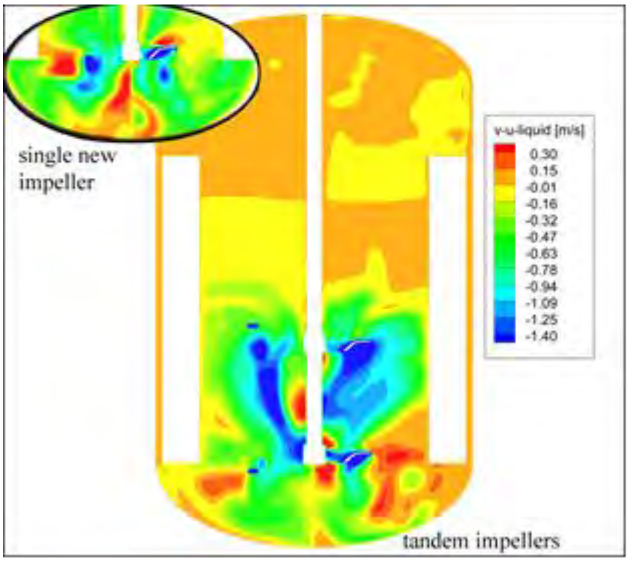

Figure 126. Tangential velocity distribution of liquid phase, single new impeller vs. new impellers in tandem, instantaneous results, [8].

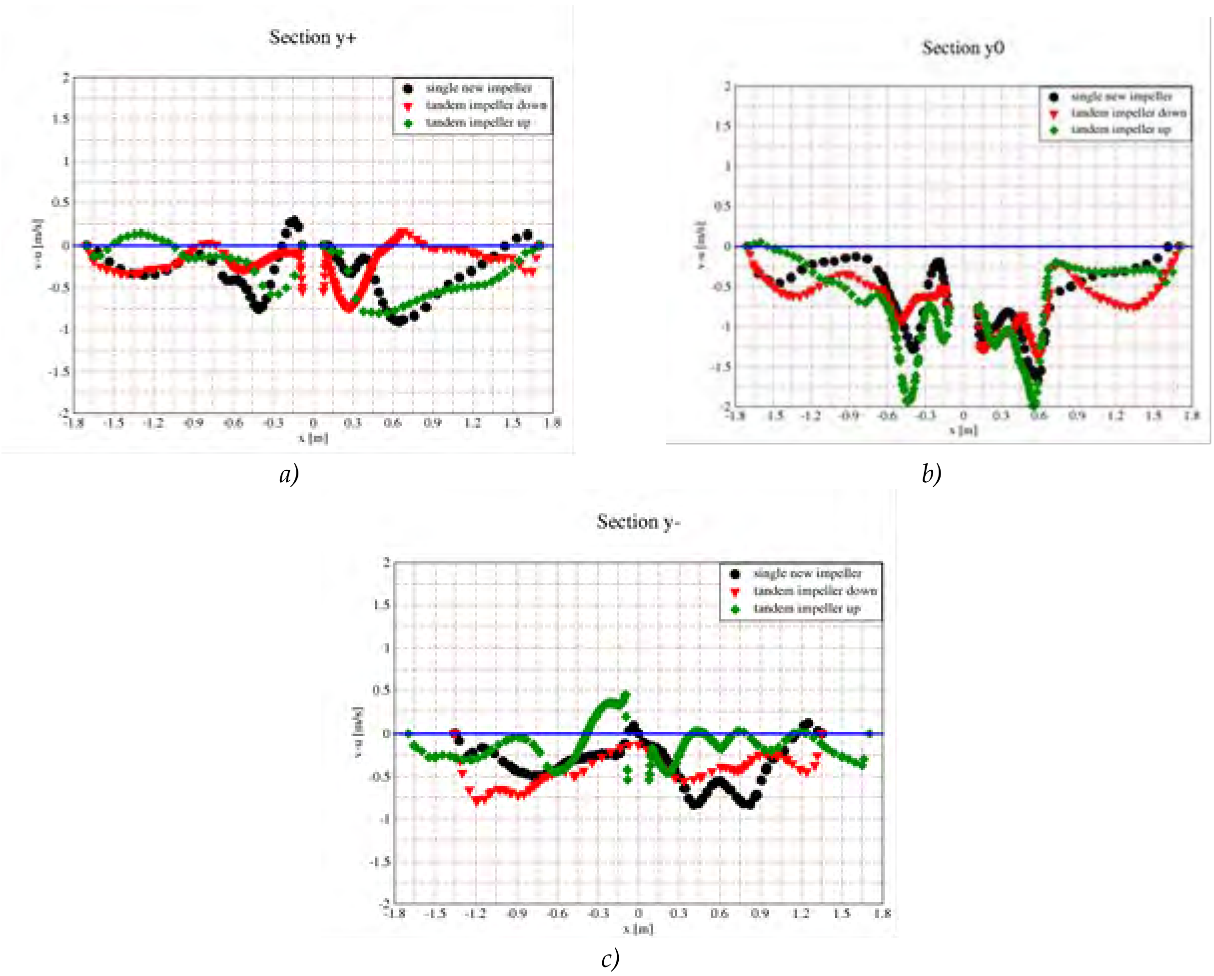

Figure 127. Tangential velocity distribution of liquid phase at various axial levels, single new impeller vs. new impellers in tandem, instantaneous results: (a) above impeller; (b) impeller level; (c) under impeller, [8].

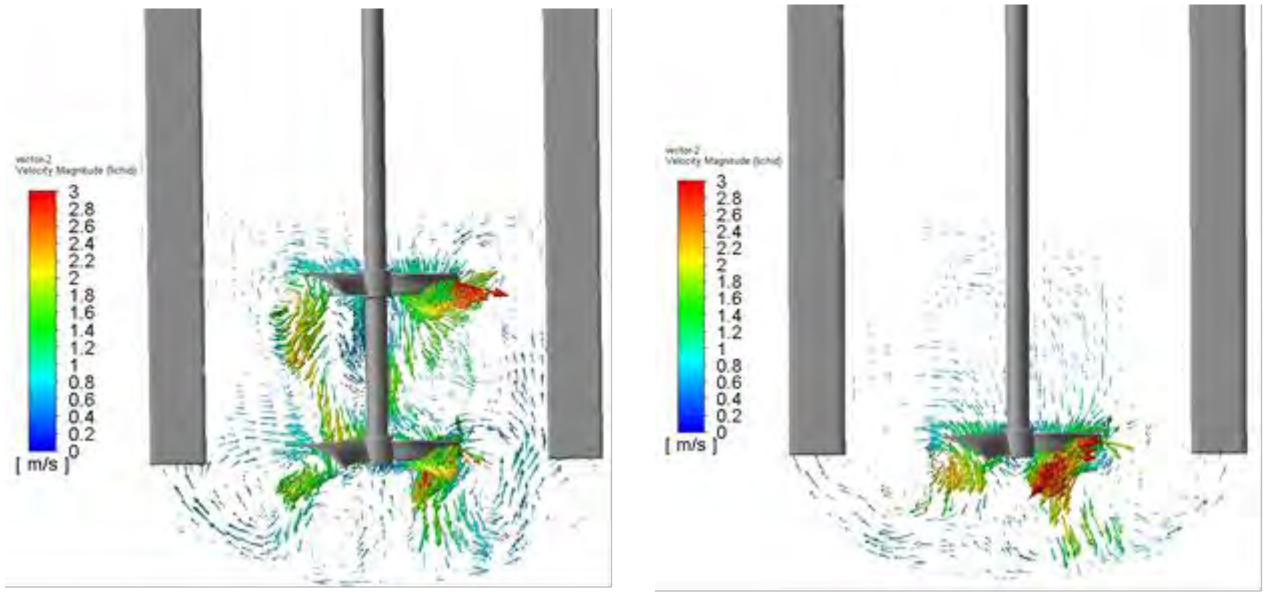

a) b)

Figure 128. Distribution of the velocity vectors of the liquid phase on an axial plane, instantaneous results: (a) new impellers in tandem, (b) single new impeller, [8].

In Figure 128 is presented a comparation of the distribution of the velocity vectors, corresponding to the liquid phase which are coloured as a function of the velocity magnitude of the liquid phase. The employment of the upper impeller leads to the better performance of the stirring mechanism and the quantity of liquid without any solid particles is de-creasing. The better performance is determined by the fact that, when employing the tandem of impellers, the flow at the side of the reactor is much stronger and it is extending well above the position of the lower impeller. The vertical flow generated by the tandem of impellers, pushes the solid particles further up into the reactor ensuring that a smaller volume of the liquid is depleted of solid particles.

It is shown that the tandem impeller configuration examined in this paper is definitely superior in terms of mixing capabilities compared with a single impeller. While sedimentation of the solid phase is practically mitigated, the tandem configuration reduces the fraction of liquid phase depleted from solid particles, at the minimal additional expanse in terms of power consumption. The power needed by the two impellers to operate in tandem was calculated and has the value of 3.45 kW. Although the existing electrical motor generates a power of 3.6 kW, in order for the solution with two impellers in tandem to perform at its best, a replacement of the existing electrical motor is recommended. The new electrical motor should operate at the same rotational speed as the existing one and should provide a power in the range of 4.5 to 5 kW.

Because the shape of the blades of the impeller is to complex and for manufacturing such an impeller the costs would be too significant, a simplified version of the impeller was manufactured.

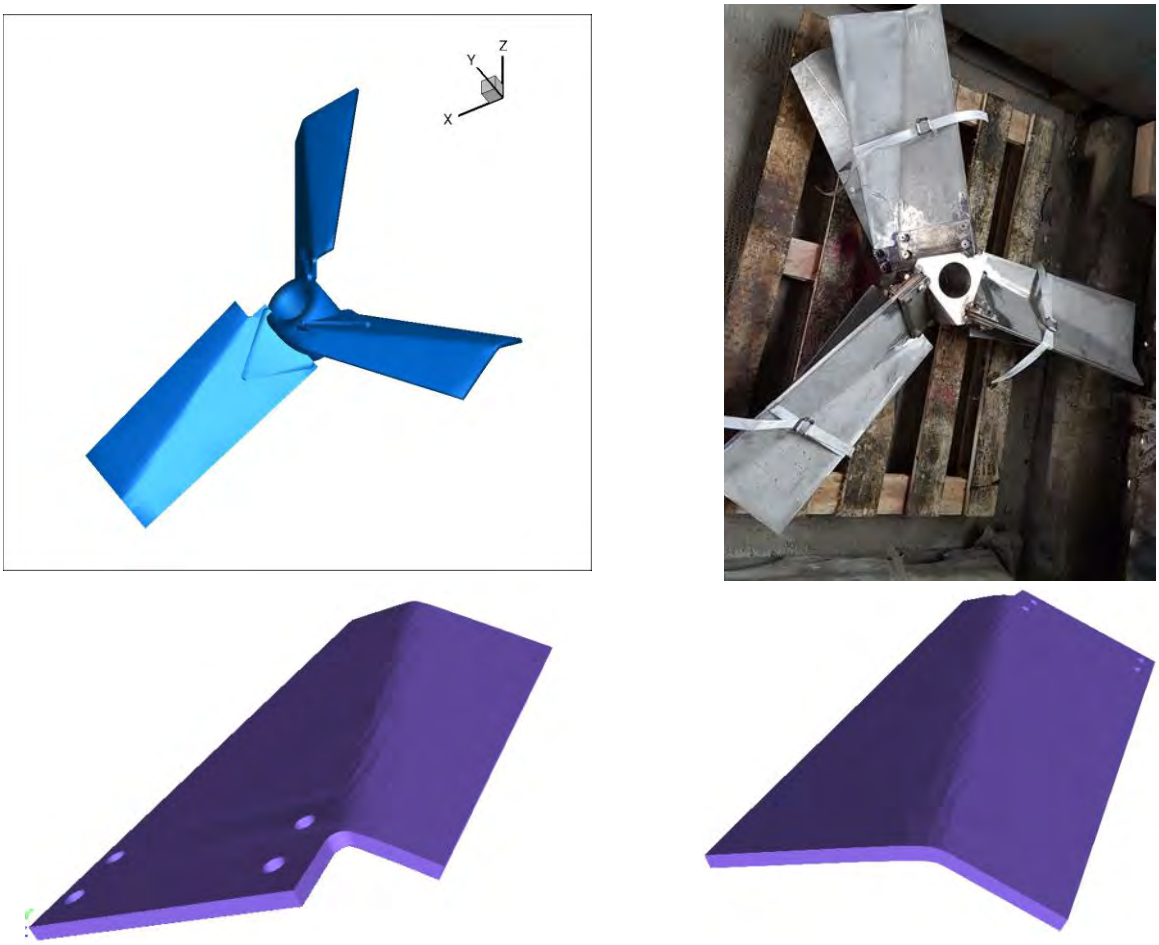

Figure 129. Simplified version of the new impeller.

The final solution for the impeller with detachable blades was imposed by the diameter of the access zone of the chemical reactor. In this case the diameter of the access zone was 600 mm and the diameter of the two impellers was 1200 mm. The components of the impeller, the hub and the three blades, were introduced separately in the reactor and the assembling process of the impeller took place inside the reactor.

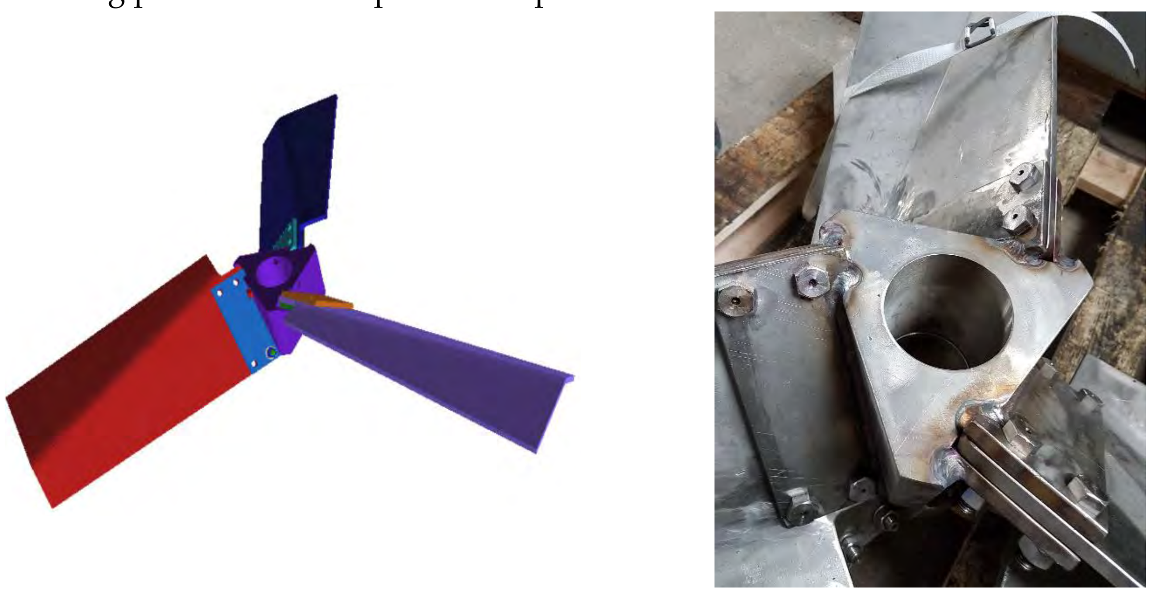

Figure 130. Components of the simplified version of the new impeller.

The simplified version produces the same hydrodynamic field, and this solution was implemented in the existing industrial reactor.

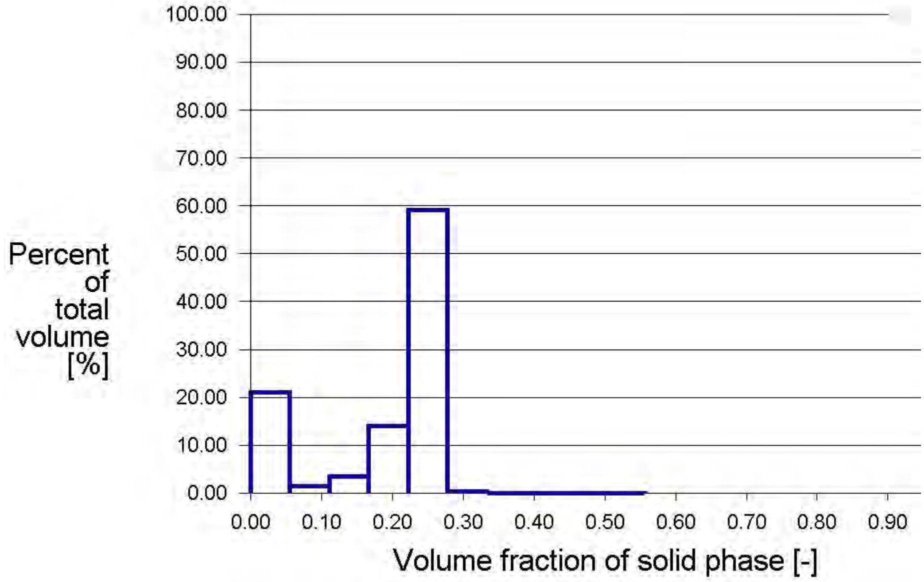

Figure 131. Performance analysis of the simplified version of the new impeller, operating in tandem.

The tests performed on the reactor fitted with the simplified tandem of impellers showed that no solid particles were sedimented on the lower part and that the final chemical product has the required properties.

Figure 132. The simplified version of the new designed impeller, in tandem, fitted on the stirring mechanism of the chemical reactor.

1.2.4. Scientific achievements in the domain of flow around heated elements

Another scientific domain where I performed research work is represented by the domain of the air flow around heated elements.

Along my research activity I was involved in research contracts, as and member of the research team, that investigated the air flow around heated elements. My role in that research was to perform the numerical simulation of the flow and to process the results.

A first subject of research includes the numerical simulation and analysis for a dryer heating system with two configurations. This system has electrically heated wires in a rectangular channel of variable cross-section. Operating regimes correspond to six steady pressure-driven air flow, with heat convection and radiation. For all boundaries we consider finite thickness and appropriate physical material properties (density, conduction, specific heat). The numerical results of this investigation include velocity, pressure, and temperature fields as required by the beneficiary. The purpose of the investigation is to simulate and analyse the air flow in the heating system, taking into account the wires heat power and associated heat transfer through convection and radiation.

The computational domains for the two configurations are presented next:

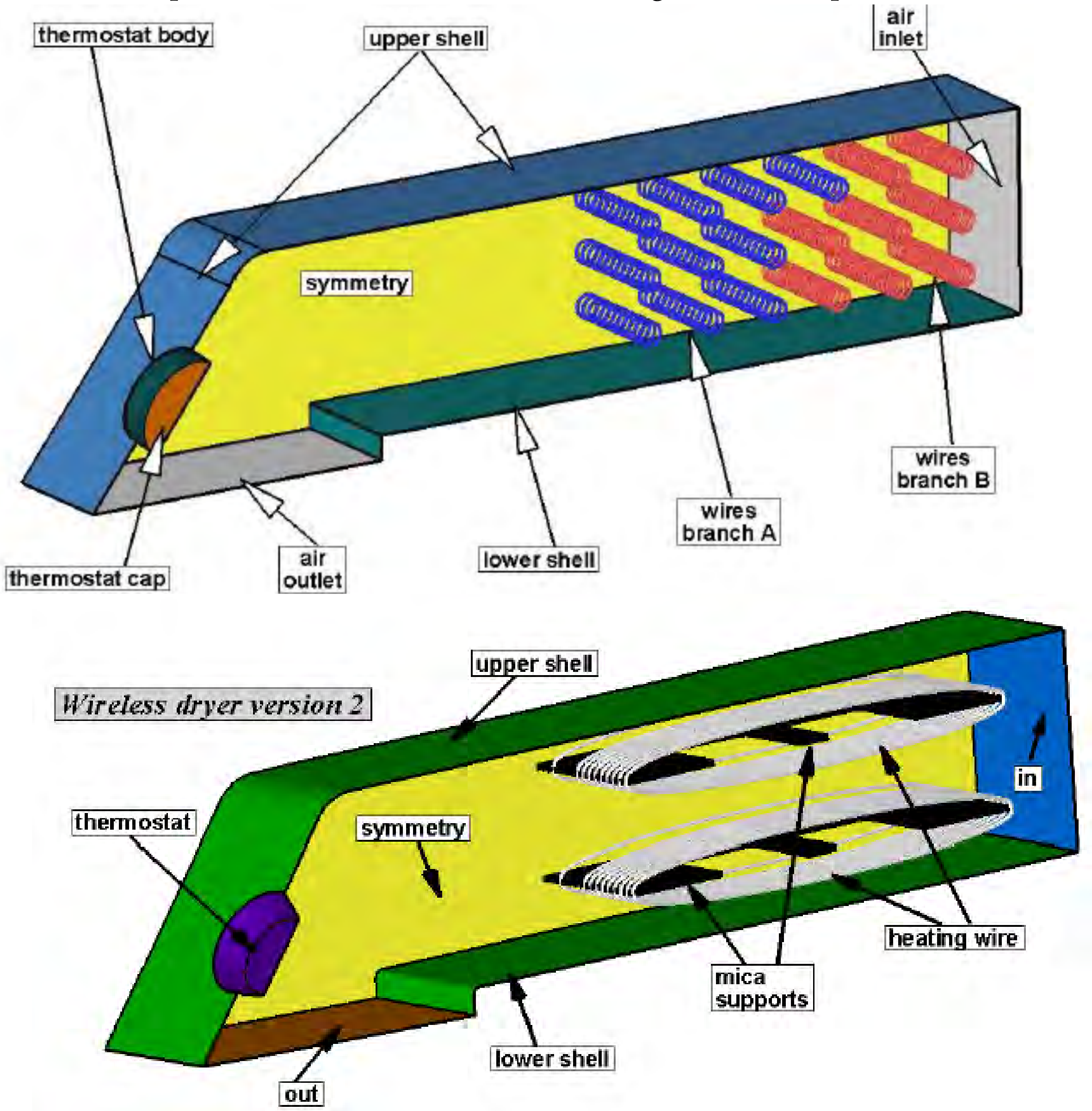

Figure 133. 3D computational domain for the dryer heating system, two configurations.

From the numerical analysis it resulted the values for the pressure drop across the domain and for the thermostat cap average temperature for the 6 investigated ai flow rates, presented in the next two figures. For both types of geometry, the highest value of the total pressure drop, the equivalent of hydraulic losses, is observed at the highest value of the air flow rate. From the temperature curve it results that the temperature on the thermostat cap decreases abruptly as the air flow rate increases.

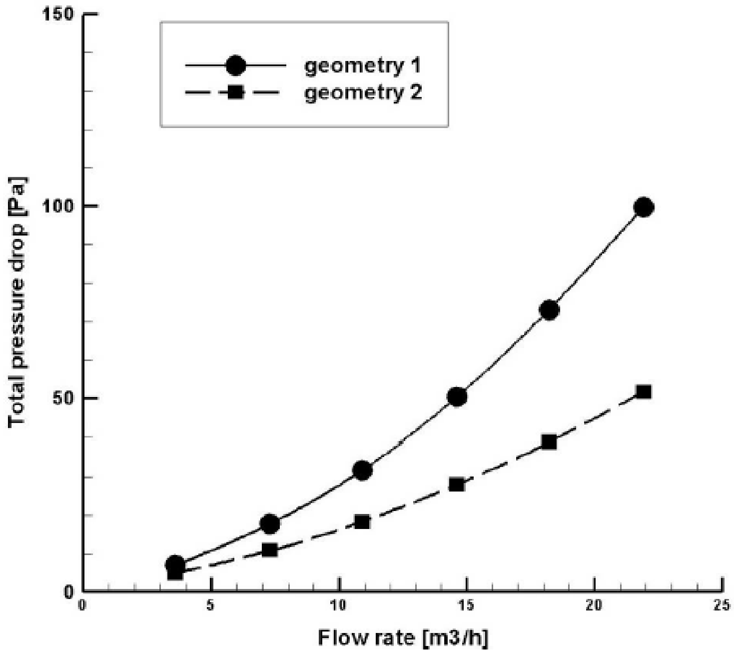

Figure 134. Pressure difference across the domain vs. flow rate.

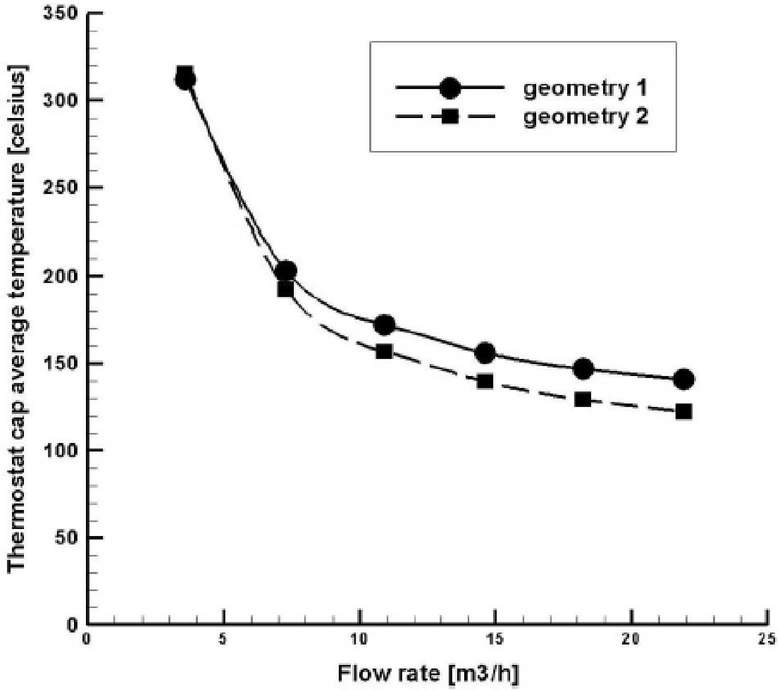

Figure 135. Thermostat cap average temperature distribution for the investigated flow rates.

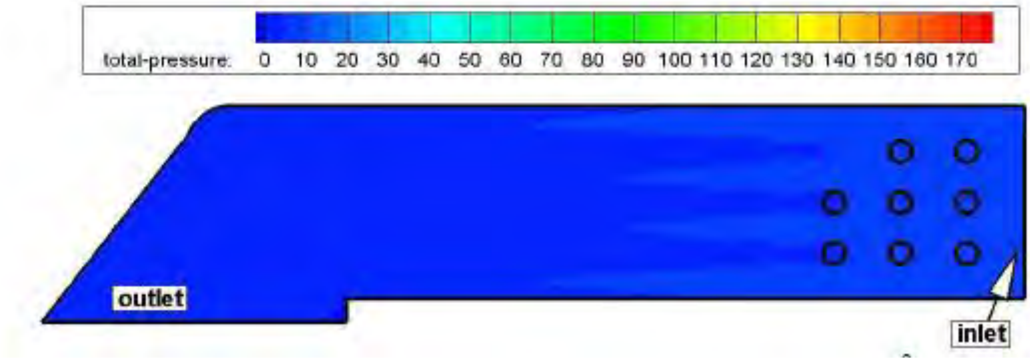

Figure 136. Total pressure map at 3.6 m³/h air flow rate.

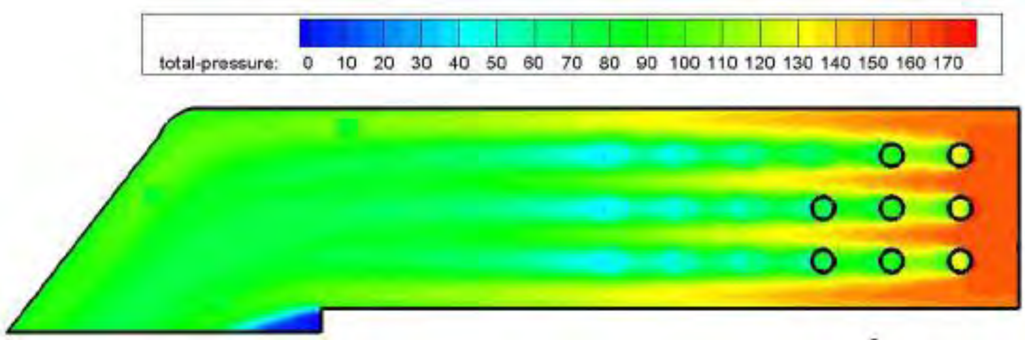

Figure 137. Total pressure map at 21.9 m³/h air flow rate.

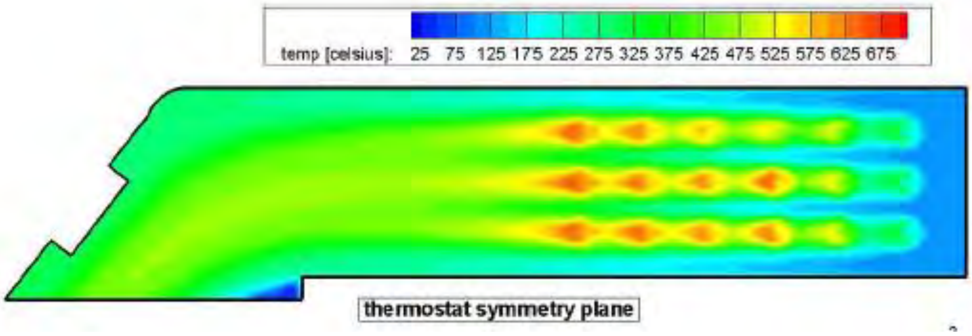

Figure 138. Temperature map at 3.6 m³/h air flow rate.

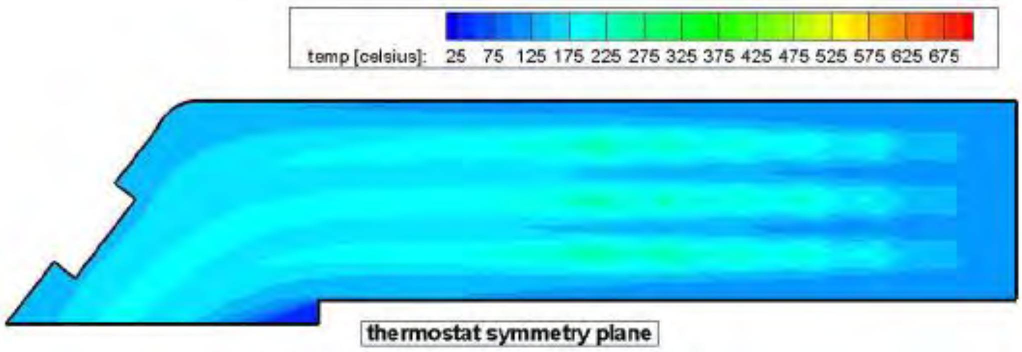

Figure 139. Temperature map at 21.9 m³/h air flow rate.

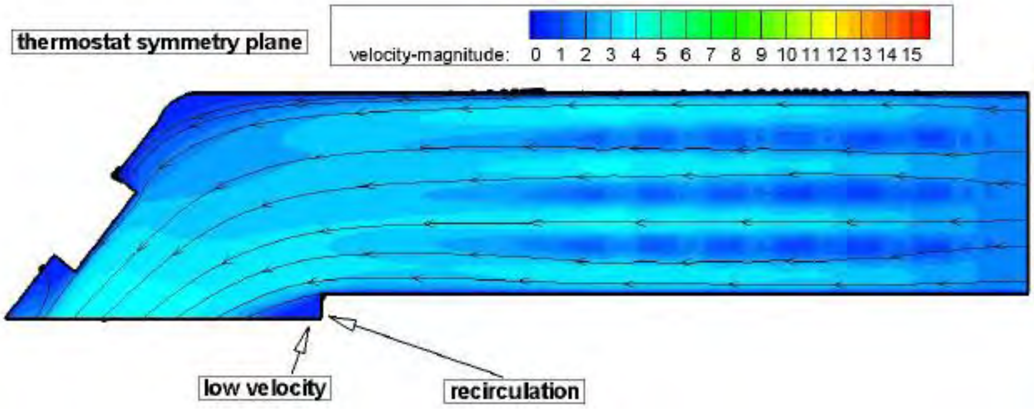

Figure 140. Velocity magnitude map and streamlines distribution at 3.6 m³/h air flow rate.

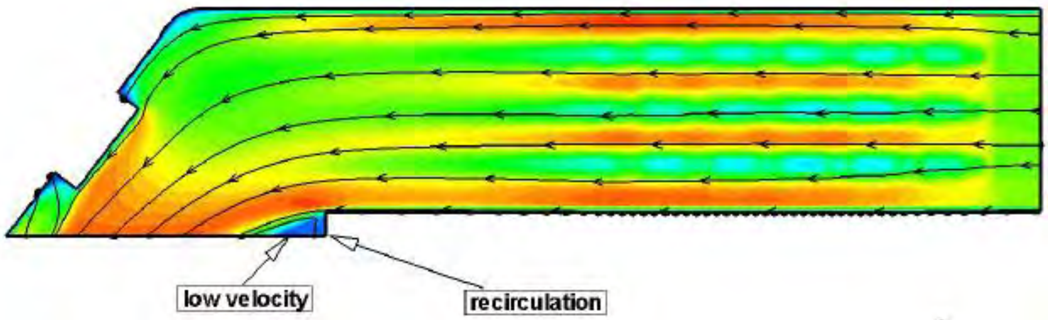

Figure 141. Velocity magnitude map and streamlines distribution at 21.9 m³/h air flow rate.

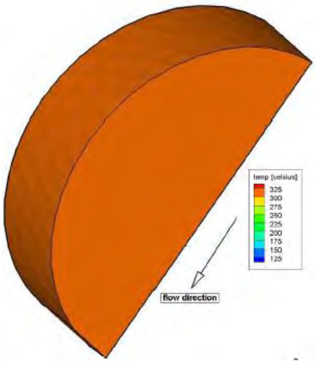

Figure 142. Temperature map for thermostat cap at 3.6 m³/h air flow rate.

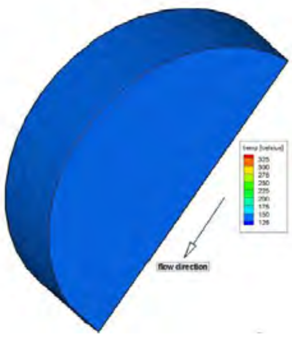

Figure 143. Temperature map for thermostat cap at 21.9 m³/h air flow rate.

In order to explain the temperature differences in vicinity of the sharp corner in the outlet section, it is presented some detail regarding the flow separation, temperature and velocity map and particle traces. The flow in a sudden-expansion channel is characterized by two flow regions: the corner recirculation zone and the central jet. The recirculation zone results from flow separation due to the abrupt changes of the boundary geometry introduced by the sudden expansion step.

The variation of the pressure distribution can be interpreted directly in the context of the mean streamline pattern shown in above mentioned Figures. Separation of flow can also contribute to pressure loss. A strong shear layer at the interface of the separation region and the central jet creates additional viscous losses. For the sudden expansion flow the reattachment length increases with the Reynolds number (inlet velocity in our case). The flow with high temperature is concentrated in the central jet, and in the vicinity of the sharp corner we have a recirculation zone characterized by low velocity and low temperature.

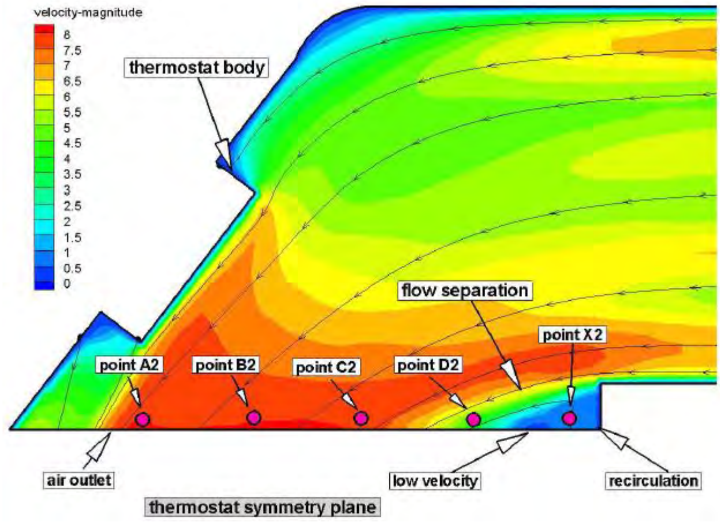

Figure 144. Temperature map for thermostat cap at 21.9 m³/h air flow rate.

In order to improve the temperature distribution along the outlet section, it is recommended to change the sharp corner with a smooth shape in accordance with the flow separation line.

In the following figures it is presented the temperature and pressure distribution on the domain and on the thermostat cap, for the second geometry and only for the minimum and maximum air flow rate.

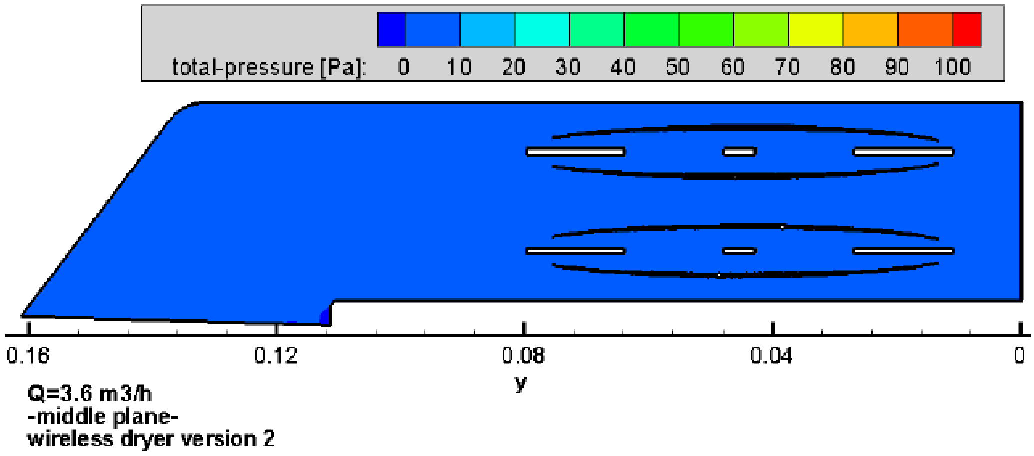

Figure 145. Total pressure map at 3.6 m³/h air flow rate.

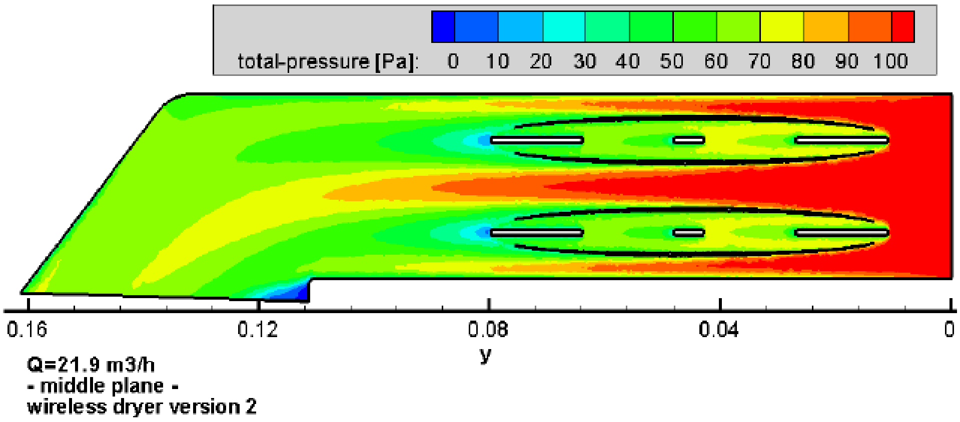

Figure 146. Total pressure map at 21.9 m³/h air flow rate.

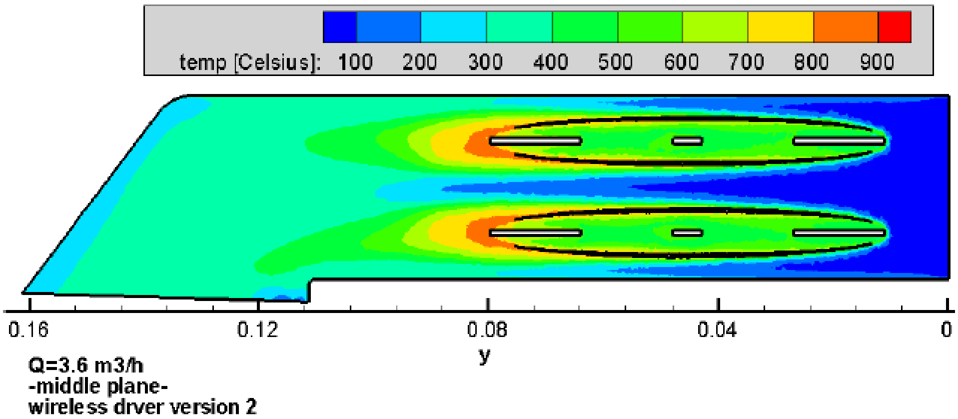

Figure 147. Temperature map at 3.6 m³/h air flow rate.

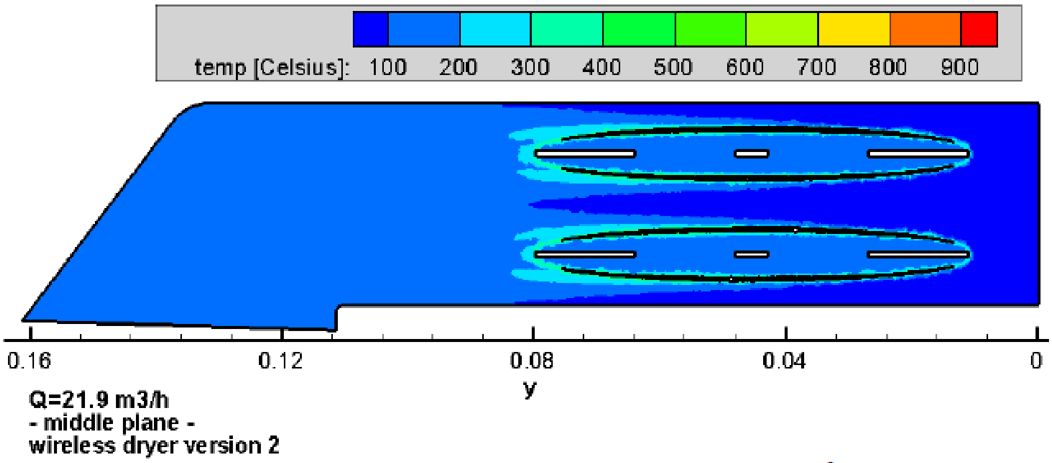

Figure 148. Temperature map at 21.9 m³/h air flow rate.

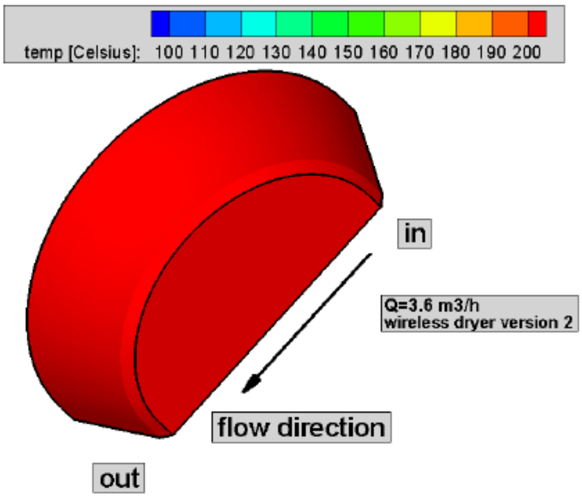

Figure 149. Temperature map for thermostat cap at 3.6 m³/h air flow rate.

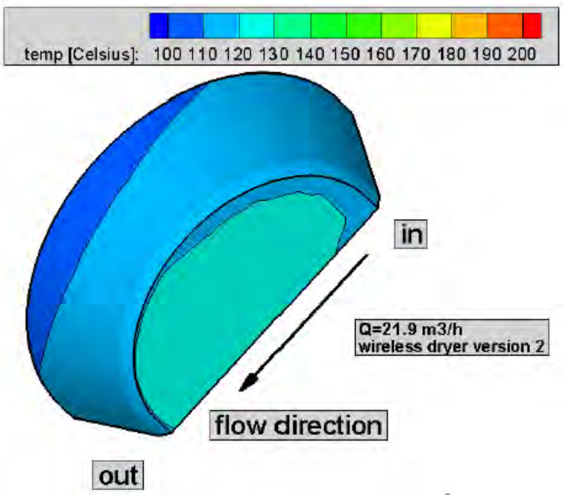

Figure 150. Temperature map for thermostat cap at 21.9 m³/h air flow rate.

From analysing the temperature and total pressure distribution on the domain it results that the second type of the geometry had the best operating characteristics.

Another research in the domain of thermal flow was represented by the analysis of the operation of a radiator which was part of a street lightning corp. Our analysis focused on determining the temperature distribution for the radiator for different values of the length and of the ambient temperature.

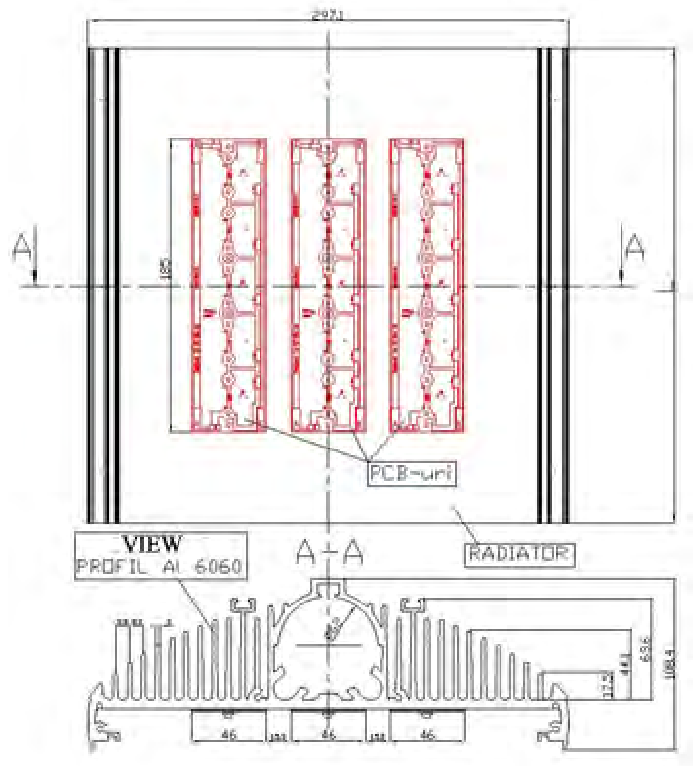

Figure 151. Radiator from a street lighting body with 3 modules, each module with 5 LED.

Several cases were investigated, for three different values of the length of the radiator and for eight different values of the ambient temperature, starting from 20°C and up to 55°C.

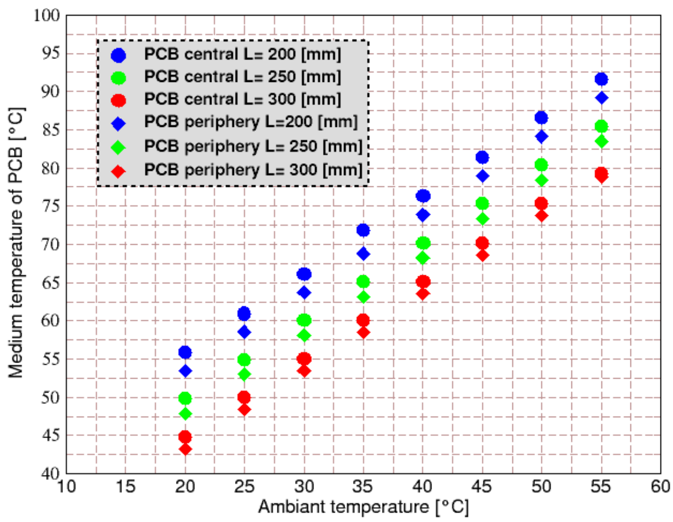

Figure 152. PCB average temperature, central and lateral section, vs. ambient temperature for three different lengths of the radiator.

From analysing the temperature evolution on the PCB sections, it results that the minimum values are achieved for the radiator with the highest value of the length. For this case the average temperatures on the two sections had similar values.

A temperature distribution on a cross-section of the radiator with the highest value of the length, for three different values of the ambient temperature, is presented in the next figures.

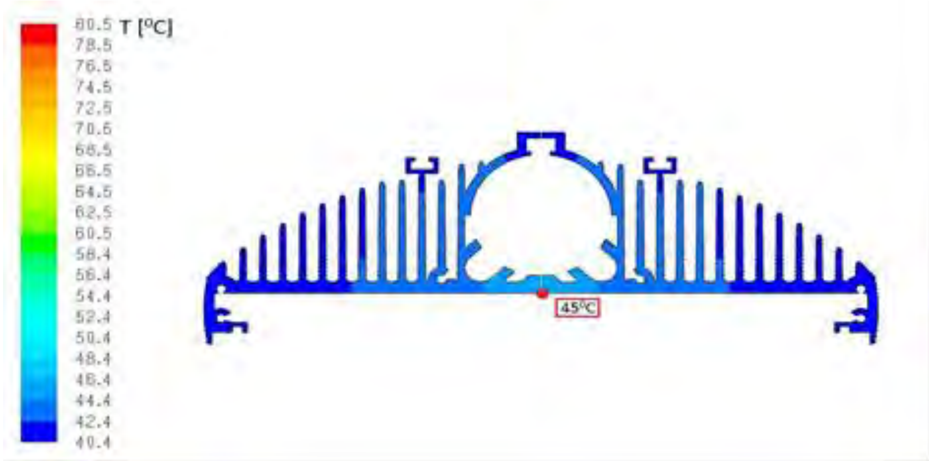

Figure 153. Temperature distribution for the radiator with L=300 mm, for ambient temperature of 20°C.

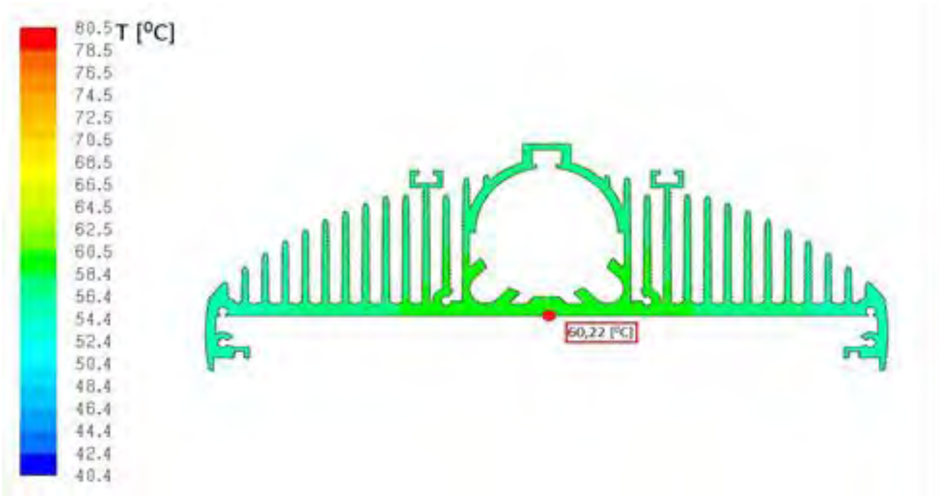

Figure 154. Temperature distribution for the radiator with L=300 mm, for ambient temperature of 35°C.

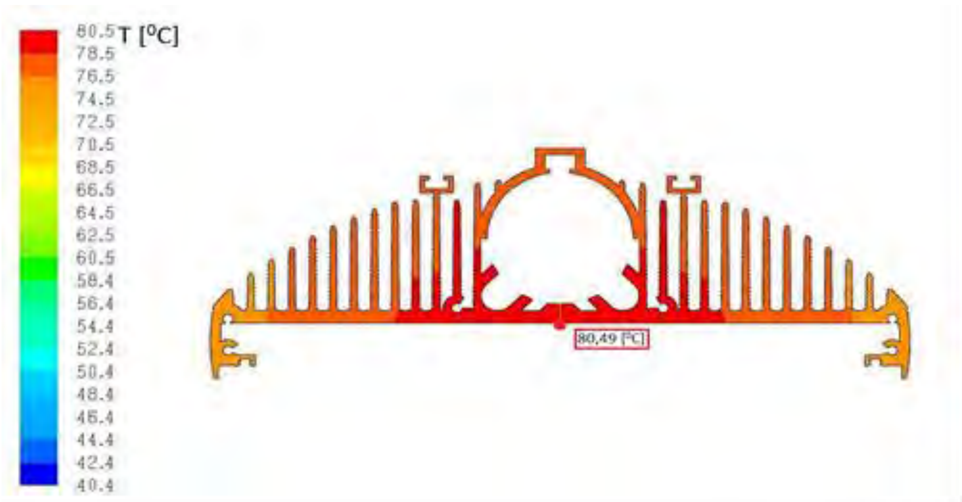

Figure 155. Temperature distribution for the radiator with L=300 mm, for ambient temperature of 55°C.

Another research subject of mine focuses on numerical analysis of temperature field into a magneto-rheological clutch, [24]. The magneto-rheological fluid is used for a clutch operated at different speeds and the clutch application was developed due to the magnetic control and fast response.

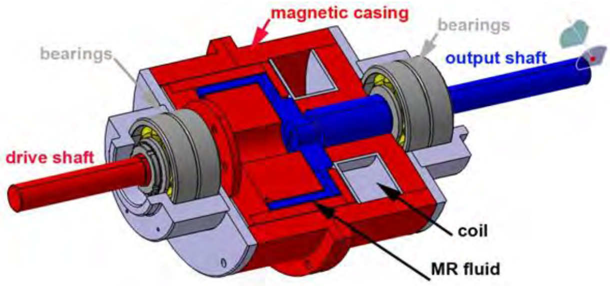

Figure 156. 3D view of the investigated magneto-rheological clutch, [24].

The 2D axi-symmetric computational domain corresponds to the experimental magneto-rheological clutch. The numerical simulations have been performed for seven values of the rotational speed without taking into consideration the magnetic field.

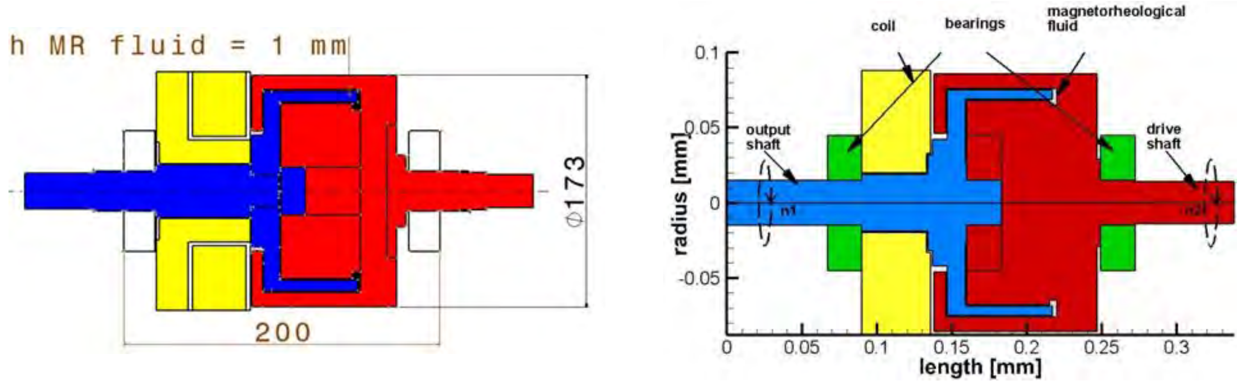

Figure 157. Sketch of the MR clutch (left) and numerical domain of the clutch for numerical simulation (right), [24].

The temperature map for magneto-rheological clutch is computed and then the temperature value obtained for the outside casing wall is validated against experimental data.

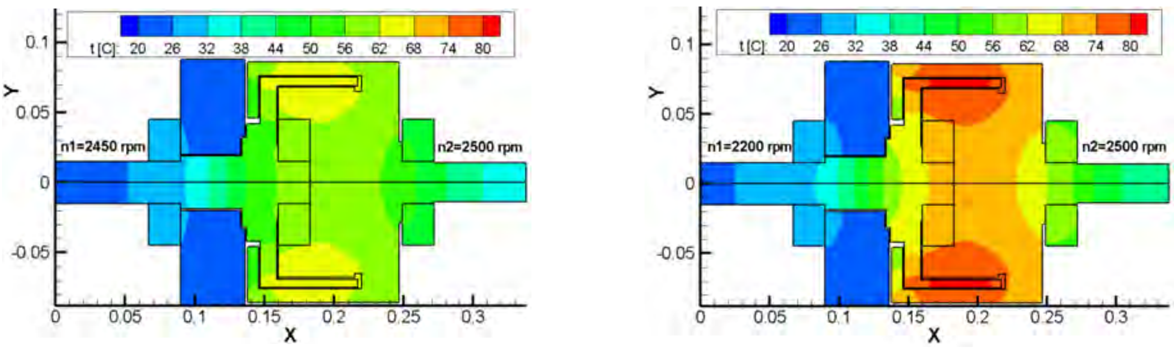

Figure 158. Temperature distribution for smallest (Dn = 50 rpm) and largest (Dn = 300 rpm) speed values, [24].

In both cases it can be observed that the main heating source is associated to MR fluid viscosity. A maximum temperature value of 67.68 °C is obtained inside the MR fluid for the rotational speed difference of 50 rpm. For this case the rheological behaviour of the MR fluid corresponds to the prescriptions of the manufacturer.

2. Overview of author's professional, academic and scientific plans

2.1. Professional and academic plans

Considering my expertise obtained along my career, the research domains for which I will propose PhD themes will be:

- numerical and experimental investigation of the operation of hydraulic pumps
- numerical and experimental investigations of the operation of hydraulic turbines
- numerical and experimental investigation of the flow around heated elements

My experience in coordinating a research team, obtained from the activity of coordinating 1 grant and 2 research projects with industrial partners and from being a member of the research team for 30 research grants and contracts, will be very helpful in coordinating the research activity of the PhD students. Also, my experience in coordinating more than 50 students in defending their Bachelor and Master thesis will be of great importance in my work of coordinating the research activity of the PhD students.

The existing research laboratories (Fluid Mechanics, Hydraulic Machines and Numerical Simulation) in the development of which I was involved, will constitute an excellent infrastructure for the research activity of the PhD students. In order to develop furthermore the existing infrastructure, I will be involved in the development of the new Centre of Excellence in Turbomachines that will be developed by Politehnica University Timisoara in partnership with S.P.E.E.H. Hidroelectrica S.A. and will represent an investment of approximately 2.000.000 Euro. This new research facility will be one of the modern and complex laboratories from this part of Europe. Many research themes for PhD students will be available after the commissioning of this laboratory.

Also, the existing Laboratories for Numerical Simulation will be upgraded with new software for numerical simulation provided by ANSYS and new high-performance computers, and I will be involved in this upgrading process.

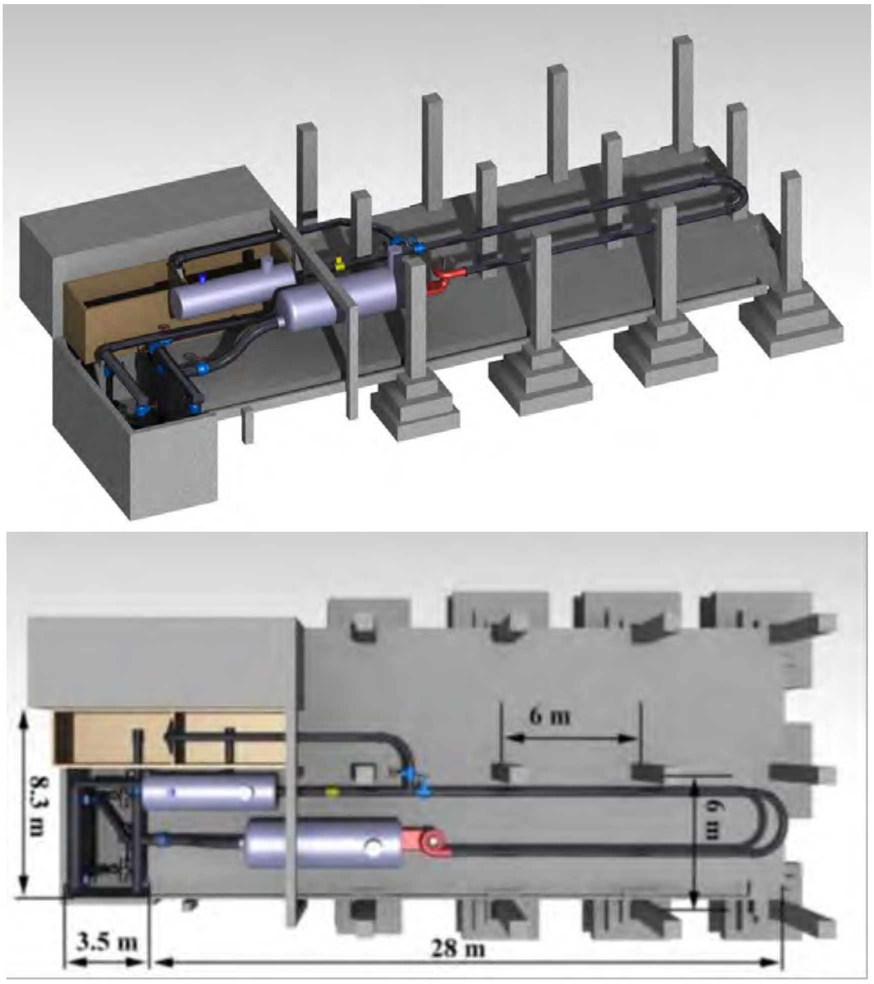

Figure 159. Modern test rig for the study of the operation of turbine models

My activity of coordinating Bachelor's and Master's thesis will lead to attracting students to continue their education by following the PhD study in the domain of Mechanical Engineering.

I will continue and I will intensify my collaboration with my colleagues from other universities form Romania:

- Politehnica University Bucharest,
- Technical University of Civil Engineering Bucharest,
- Technical University from Cluj,
- "Dunărea de Jos" University of Galati.

At the international, level I will consolidate and extended my collaboration with universities from Europe:

- Stuttgart University,
- Brno University of Technology,
- HES-SO Valais-Wallis Sion.

I will also intend to maintain my collaboration with industrial partners such as:

- S.P.E.E.H. Hidroelectrica S.A.,

- S.C. Colterm S.A.,
- S.C. Aquatim S.A.,
- S.C. Oltchim S.A.,
- S.C. Zoppas Industries S.A.

All these collaborations with colleagues from other universities and industrial companies will aim to offer for the PhD students a consistent number of research themes and access to additional research infrastructure.

I intend to involve the PhD students in my future research grants and research projects with industrial partners in order to gain more research experience and knowledge and a supplementary income.

2.2. Scientific plans

The international and national trend is to try to lower the carbon emission especially by trying to produce electrical energy from hydraulic resources and implementing the cars that are driven only by electric motors. In the near future, because of the number of electric cars will increase, the demand for the electrical energy will also increase. In order to generate more electric power from green resources, the existing hydropower plants will have to be refurbished and new hydropower plants have to be developed.

The main research subjects that will derive from these trends will be:

- operating the hydraulic machines on a wide range domain with high efficiencies values
- avoiding cavitation phenomena and its effects
- solutions for wide range operation of the hydraulic machines
- solutions for cooling off the components of the electrical motors

The above presented research directions, which are similar with my research domains for which I gained expertise during my activity, will generate a great number of research subjects for the PhD students from the domain of Mechanical Engineering.

I intend to apply for research grants and to continue to obtain research projects with the industrial companies, so that the research work performed by the PhD students to have practical application. The results that will be obtained from the research process will be presented at international conferences and will be published in international journals with impact factor.

Bibliography

[1] A. Stuparu, “Modelarea numerică și experimentală a curgerii în pompele centrifuge,” PhD. Thesis, Universitate Politehnica Timișoara, Timișoara, 2009.

[2] A.-C. Stuparu and A. Bosioc, *Pompe centrifuge*. Timişoara, Romania: Editura Politehnica, 2021.

[3] A.-C. Stuparu and L. E. Anton, *Hidrodinamica*. Editura Orizonturi Universitare, 2018.

[4] L. E. Anton, A. Baya, and A.-C. Stuparu, *Măsurarea și monitorizarea mărimilor hidraulice în timp real*. Editura Orizonturi Universitare, 2009.

[5] L. E. Anton, A. Baya, T. Miloș, and A.-C. Stuparu, *Hidrodinamică experimentală*. Editura Orizonturi Universitare, 2007.

[6] L. E. Anton *et al.*, *Mecanica fluidelor, mașini hidraulice și acționări. Aplicații de calcul*. Timișoara, Romania: Editura Orizonturi Universitare, 2004.

[7] A.-C. Stuparu, R. F. Susan-Resiga, and C. Tănasă, “CFD Assessment of the Hydrodynamic Performance of Two Impellers for a Baffled Stirred Reactor,” *Applied Sciences-Basel*, vol. 11, no. 11, p. 13, 2021, doi: 10.3390/app11114949.

[8] A.-C. Stuparu, R. Susan-Resiga, and A. Bosioc, “Improving the Homogenization of the Liquid-Solid Mixture Using a Tandem of Impellers in a Baffled Industrial Reactor,” *Applied Sciences-Basel*, vol. 11, no. 12, p. 11, 2021, doi: 10.3390/app11125492.

[9] A.-C. Stuparu, R. Susan-Resiga, and A. Bosioc, “CFD Simulation of Solid Suspension for a Liquid-Solid Industrial Stirred Reactor,” *Applied Sciences-Basel*, vol. 11, no. 12, p. 15, 2021, doi: 10.3390/app11125705.

[10] A. Stuparu, A. Baya, A. Bosioc, L. Anton, and D. C. Moș, “Experimental investigation of a pumping station from CET power plant Timisoara,” in *IOP Conference Series: Earth and Environmental Science, Proceeding of 29th IAHR Symposium on Hydraulic Machinery and Systems*, Kyoto, Japan, 2018, vol. 240, p. 10.

[11] A. Stuparu, A. Baya, A. Bosioc, L. Anton, and D. C. Moș, “Modelling the operation curves of two similar high power centrifugal pumps,” in *PROCEEDINGS OF THE INTERNATIONAL CONFERENCE ON NUMERICAL ANALYSIS AND APPLIED MATHEMATICS 2017 (ICNAAM-2017)*, Thessaloniki, Grecee, 2017, vol. 1978, p. 4.

[12] A. Stuparu and R. Susan-Resiga, “The Complex Dynamics of the Precessing Vortex Rope in a Straight Diffuser,” Grenoble, France, 2016, vol. 49, p. 082013. doi: 10.1088/1755-1315/49/8/082013.

[13] A.-C. Stuparu and S. Holotescu, “Influence of Geometry on the Position and the Intensity of Maximum Kinetic Energy in a Combustion Chamber,” *DIFFUSION IN SOLIDS AND LIQUIDS*, vol. 312–315, pp. 725–730, 2011, doi: 10.4028/www.scientific.net/DDF.312-315.725.

[14] A.-C. Stuparu and S. Holotescu, “Numerical simulation of the 3D unsteady turbulent flow in a combustion chamber,” *Central European Journal of Engineering*, vol. 1, no. 2, pp. 189–194, Jun. 2011, doi: 10.2478/s13531-011-0014-9.

[15] A. Stuparu, R. Susan-Resiga, L. E. Anton, and S. Muntean, “Numerical investigation of the cavitational behaviour into a storage pump at off design operating points,” Timișoara, Romania, 2010, vol. 12, p. 012068. doi: 10.1088/1755-1315/12/1/012068.

[16] R. F. Susan-Resiga, C. Popescu, R. Szakal, S. Muntean, and A. Stuparu, “A benchmark test case for swirling flows: design of the swirl apparatus, experimental data, and numerical challenges,” presented at the 29th IAHR Symposium on Hydraulic

Machinery and Systems, Kyoto, Japan, 2018. [Online]. Available: http://www.iahrkyoto2018.org/

[17] R. F. Susan-Resiga, S. Muntean, A. Stuparu, A. I. Bosioc, C. Tanasa, and C. Ighisan, "A variational model for swirling flow states with stagnant region," *Eur J Mech B-Fluid*, vol. 55, no. 1, pp. 104–115, Jan. 2016, doi: 10.1016/j.euromechflu.2015.09.002.

[18] C. Tanasa, R. Susan-Resiga, S. Muntean, A. Stuparu, A. Bosioc, and T. Ciocan, "Numerical Assessment of a Novel Concept for Mitigating the Unsteady Pressure Pulsations Associated to Decelerating Swirling Flow with Precessing Helical Vortex," *Aip Conf Proc*, vol. 1702, 2015, doi: 10.1063/1.4938798.

[19] R. F. Susan-Resiga, S. Muntean, A. Bosioc, and A. Stuparu, "Stabilisation of the swirl exiting a Francis runner far from the best efficiency point," presented at the 30th Symposium on Hydraulic Machinery and Systems IAHR2020, Lausanne, Switzerland, 2020.

[20] O. V. Nemet, A. C. Stuparu, and R. Susan-Resiga, "Design and Optimization of an Axial Expansion Turbine for Energy Recovery," presented at the 9th International Conference on Energy and Environment, Timișoara, Romania, 2019. doi: 10.1109/CIEM46456.2019.8937649.

[21] C. Tanasa, A.-C. Stuparu, A. Bosioc, and R. Susan-Resiga, "Numerical Analysis of Pulsating Water Jet Method for Mitigating the Vortex Rope," Politehnica Univ Timisoara, Timisoara, ROMANIA, 2019, pp. 423–428.

[22] C. Tanasa, A.-C. Stuparu, C. Stroita, C. Popescu, and R. Susan-Resiga, "3D Numerical Analysis of Pulsating Water Jet in the Draft Tube Cone of Hydraulic Machinery," in *PROCEEDINGS OF THE INTERNATIONAL CONFERENCE OF COMPUTATIONAL METHODS IN SCIENCES AND ENGINEERING 2019 (ICCMSE-2019)*, Rhodes, Grrece, 2019, vol. 2186. doi: 10.1063/1.5138117.

[23] R. F. Susan-Resiga, A. Stuparu, and S. Muntean, "Francis turbine with tandem runners: a proof of concept," presented at the 29th IAHR Symposium on Hydraulic Machinery and Systems, Kyoto, Japan, 2018. [Online]. Available: http://www.iahrkyoto2018.org/

[24] A. Bosioc, A. Stuparu, and R. Susan-Resiga, "Numerical Analysis of Temperature and Torque in A Magneto-Rheological Clutch," in *PROCEEDINGS OF THE INTERNATIONAL CONFERENCE ON NUMERICAL ANALYSIS AND APPLIED MATHEMATICS 2016 (ICNAAM-2016)*, Rhodes, Grrece, 2016, vol. 1863, p. 4.

[25] A. Stuparu, R. Susan-Resiga, L. E. Anton, and S. Muntean, "A New Approach in Numerical Assessment of the Cavitation Behaviour of Centrifugal Pumps," *International Journal of Fluid Machinery and Systems*, vol. 4, no. 1, pp. 104–113, 2011, doi: 10.5293/IJFMS.2011.4.1.104.

[26] L. Anton, "Îmbunătățirea caracteristicilor cavitaționale la pompele cu impulsor," PhD. Thesis, Universitatea Politehnica Timișoara, Timișoara, 1994.

[27] L. Anton, A. Stuparu, and A. Baya, "Numerical and Experimental Investigation of the Flow into an Inducer," *Scientific Bulletin of the „Politehnica" University Of Timisoara, Transactions on Mechanics*, vol. 53, no. 67, pp. 227–232, 2008.

[28] L. Anton, A. Stuparu, S. Muntean, and A. Baya, "3D Numerical Simulation of the Turbulent Flow in an Inducer," in *Annals of DAAAM for 2008 & Proceedings of the 19th International DAAAM Symposium „Intelligent Manufacturing & Automation: Focus on Next Generation of Intelligent Systems and Solutions"*, Trnava, Slovakia, 2008, vol. 19, pp. 21–22.

[29] A. Stuparu, S. Muntean, A. Baya, and L. Anton, "Numerical Investigation of the Flow in a Straight and Bended hydrofoil Cascade of an Inducer," in *Annals of DAAAM for 2008 & Proceedings of the 19th International DAAAM Symposium „Intelligent Manufacturing & Automation: Focus on Next Generation of Intelligent Systems and Solutions*, Trnava, Slovakia, 2008, vol. 19, pp. 1327–1328.

[30] A. Stuparu, S. Muntean, and L. Anton, "Validation of the 2D numerical invetigation methodology of the turbulent flow into an inducer with the 3D computation," Budapest, Hungary, 2009, pp. 736–742.

[31] J. F. Gülich, *Centrifugal Pumps*, 3rd ed. Springer, 2014.

[32] H. Foroutan and S. Yavuzkurt, "Flow in the Simplified Draft Tube of a Francis Turbine Operating at Partial Load—Part II: Control of the Vortex Rope," *J. Appl. Mech*, vol. 81, no. 6, pp. 061011-061011–7, Mar. 2014, doi: 10.1115/1.4026818.

[33] A.-C. Stuparu and R. Susan-Resiga, "THE ORIGIN OF THE PLUNGING PRESSURE FLUCTUATIONS FOR A SWIRLING FLOW WITH PRECESSING VORTEX ROPE IN A STRAIGHT DIFFUSER," Ljubljana, Slovenia, 2015, p. 8.

[34] C. Tănasă, R. Susan-Resiga, S. Muntean, A. Stuparu, A. Bosioc, and T. Ciocan, "Numerical assessment of a new passive control method for mitigating the precessing helical vortex in a conical diffuser," presented at the The 16th International Conference on Fluid Flow Technologies, Budapest, Hungary, 2015.

[35] Bălan, C., *Lecții de mecanica fluidelor*, Editura Tehnică, București, 2003.

[36] Georgescu, S. C., Georgescu, A., Dunca, G., *Stații de pompare. Încadrarea turbopompelor în sisteme hidraulice*, Editura Printech, București, 2005.

[37] Hașegan, L., Anton, A., *Machines hydrauliques*, Editura Matrix Rom, București, 2001

[38] Robescu D., Roman, P., Stamatoiu, D., *Pompe și stații de pompare*, Litografia Institutului Politehnic București, 1989.

[39] Gyulai, F., *Pompe, ventilatoare, compresoare*, Vol I şi II, Lito. Univ. Politehnica, Timişoara, 1988.

[40] Miloş, T., *Pompe şi ventilatoare centrifuge şi axiale*, Editura Politehnica Timişoara, 2009.

[41] Anton, A., Perju, S., *Monitoring the main parameters of a water supply pumping station over ten years*, Transactions on Mechanics, Scientific Bulletin of the Politehnica University of Timisoara, vol. 49, nr. 63, Special Issue Proc. On 6th International Conference on Hydraulic MAchinery and Hydrodynamics, 2004.

[42] Anton, I., *Cavitația*, vol. I, Editura Academiei Române, Bucureşti, 1984, 1985.

[43] Anton, I., *Cavitația*, vol. II, Editura Academiei Române, Bucureşti, 1985, 1985.

[44] Anton, I., *Sarcina maximă de aspirație la pompe. Curbe caracteristice de cavitație, Studii şi cercetări ştiințifice*, Baza Academiei, Tom IV, nr.1-2, Timişoara, 1954.

[45] Anton, L. E., Miloş T., *Pompe centrifuge cu impulsor*, Editura Orizonturi Universitare, Timişoara, 1998.

[46] Anton, L. E., Baya, A., *Mecanica fluidelor, maşini hidraulice şi acționări*, Editura Orizonturi Universitare, Timişoara, 2002.

[47] Li, S. C., 2000, "Cavitation of Hydraulic Machinery," Imperial College Press.

[48] Singhal, A.K., Li, H.Y., Athavale, M.M., Jiang, Y., 2001, "Mathematical basis and validation of the full cavitation model," ASME FEDSM'01, New Orleans, Louisiana.

[49] Susan-Resiga, R., Muntean, S., Bernad, S., and Anton, I., 2003, “Numerical investigation of 3D cavitating flow in Francis turbines,” in Proceedings of the International Conference on Modelling Fluid Flow (CMFF03), Budapest, Hungary. Vol. 2, pp. 950-957.
[50] Hirschi, R., Dupont, P. H., Avellan, F., Favre, J.-N., Guelich, J.-F., and Parkinson, E., 1998, “Centrifugal pump performance drop due to leading edge cavitation: numerical predictions compared with model tests,” Journal of Fluids Engineering, Vol. 120, No. 6, pp. 705-711.
[51] Pouffary, B., Patella, R.F., Rebound, J.-L., Lambert, P.-A., 2008, “Numerical Simulation of 3D Cavitating Flows: Analysis of Cavitation Head Drop in Turbomachinery,” Journal of Fluids Engineering, Vol. 130, pp. 061301-1 – 061301-10.
[52] Gonzalo Flores, N., Goncalves, E., Fortes Patella, R., Rolland, J., and Rebattet, C., 2008, “Head Drop of a Spatial Turbopump Inducer,” Journal of Fluids Engineering, Vol. 130, Paper 111301.
[53] Ait-Bouziad, Y., 2006, “Physical Modelling of Leading Edge Cavitation: Computational Methodologies and Application to Hydraulic Machinery,” PhD Thesis, EPFL, Lausanne, Switzerland.
[54] Keck, H., Sick, M., 2008, “Thirty years of numerical flow simulation in hydraulic turbomachines”, in Acta Mech, 201, 211-229.
[55] Braembussche, R.A., 2006, “Flow and loss mechanisms of centrifugal pumps”, in Design and analysis of high speed pumps, Educational Notes RTO-EN-AVT, Paper 12, pp.12-1—12-26, Neuilly-sur-Seime, France.
[56]] K. Ashihara, A. Goto, 2002, ”Effects of Blade Loading on Pump Inducer Performance and Flow field”. Proceedings of ASME FEDSM2002: ASME 2002 Fluid Engineering Division Summer Meeting, July 14 – 18, 2002, Montreal, Quebec, Canada.
[57] K. Ashihara, A. Goto, K. Kamijo, H. Yamada, M. Uchiumi, 2002, ”Improvements of Inducer Inlet Backflow Characteristics Using 3-D Inverse Design Method”, American Institute of Aeronautics , 4158.
[58] Dörfler P., Sick M. and Coutou A., 2013, ”Flow-Induced Pulsation and Vibration in Hydroelectric Machinery”, Springer Verlag London, Ch. 2 – Low-Frequency Phenomena in Swirling Flow, pp 33-67, DOI: 10.1007/978-1-4471-4252-2_2.
[59] Dörfler P., Ruchonnet N., 2012, ”A statistical method for draft tube pressure pulsation analysis”, IOP Conference Series: Earth and Environmental Science, 15(6), p. 062002, DOI: 10.1088/1755-1315/15/6/062002.
[60] Ciocan G .D., Iliescu M. S., Vu T. C., Nennemann B., Avellan F., 2007, ”Experimental Study and the Numerical Simulation of the FLINDT Draft Tube Rotating Vortex”, Journal of Fluids Engineering – Transactions of the ASME, 129(2), pp 146-158, DOI: 10.1115/1.2409332.
[61] Iliescu M. S., Ciocan G. D., Avellan F., 2008, Analysis of the Cavitating Draft Tube Vortex in a Francis Turbine Using Particle Image Velocimetry Measurements in Two-Phase Flow”, Journal of Fluids Engineering – Transactions of the ASME, 130(2), p 0211105, DOI: 10.1115/1.2813052.

[62] Susan-Resiga R., Muntean S., Stein P. and Avellan F., 2009, ”Axisymmetric Swirling Flow Simulation of the Draft Tube Vortex in Francis Turbines at Partial Discharge”, International Journal of Fluid Machinery and Systems, 2(4), pp 295-302, DOI: 10.5293/IJFMS.2009.2.4.295.
[63] Kuibin P. A., Okulov V. L., Susan-Resiga R. and Muntean S., 2010, ”Validation of mathematical models for predicting the swirling flow and the vortex rope in a Francis turbine operated at partial discharge”, IOP Conference Series: Earth and Environmental Science, 12(1), p 012051, DOI: 10.1088/1755-1315/12/1/012051.
[64] Kuibin P, A,, Susan-Resiga R, and Muntean S., 2014, ”A model for precessing helical vortex in the turbine discharge cone”, IOP Conference Series: Earth and Environmental Science, 22(2), p 022024, DOI: 10.1088/1755-1315/22/2/022024.
[65] Ciocan G. D. and Iliescu M. S., 2007, ”Vortex Rope Investigation by 3D-PIV Method”, 2nd IAHR International Meeting of the Workgroup on Cavitation and Dynamic Problems in Hydraulic Machinery and Systems (Scientific Bulletin of the Politehnica University of Timișoara – Transactions on Mechanics, 52(6), pp. 159-172).
[66] Ciocan G. D., Iliescu M. S., 2008, ”3D PIV Measurements in Two-Phase Flow and Rope Parametrical Modeling”, Proc. 24th IAHR Symp. Hydraulic Machinery and Systems Foz do Iguassu, Brasil.
[67] Menter F. R., Egorov Y., 2010, ”The Scale-Adaptive Method for Unsteady Turbulent Flow Predictions. Part 1: Theory and Model Description Flow”, Turbulence and Combustion, 85(1), pp 113-138 DOI: 10.1007/s10494-010-9264-5.
[68] Egorov Y., Menter F. R., Lechner R. and Cokljat D., 2010, ”The Scale-Adaptive Method for Unsteady Turbulent Flow Predictions. Part 2: Application to Complex Flows Flow”, Turbulence and Combustion, 85(1), pp 139-165, DOI: 10.1007/s10494-010-9265-4.
[69] Haimes R. and Kenwright D., 1999, ”On the Velocity Gradient Tensor and Fluid Feature Extraction”, 14th Computational Fluid Dynamics Conference, AIAA-99-3288, DOI: 10.2514/6.1999-3288.
[70] Haimes R. and Kenwright D., 2000, ”FX Programer's Guide”, Massachusetts Institute of Technology.
[71] Muntean S., Drăghici I., Gînga G., Anton L.E., Baya A., 2015, ”Hydrodynamic design of a storage pump impeller using inverse method and experimental investigation of the global performances”, WasserWirtschaft Extra, 1, pp. 28 – 32
[72] Muntean S., Škerlavaj A., Drăghici I., Anton L.E.,2015, ”Numerical analysis of the flow non-uniformity generated by symetrical suction elbows of the large storage pumps”, Proc. 6th IAHR Int. Meeting of the Workgroup on Cavitation and Dynamic Problems in Hydraulic Machinery and Systems, Ljubljana, Slovenia. pp. 1-8.
[73] Muntean S., Bosioc A.I., Drăghici I., Anton L.E., 2016, ”Hydrodynamic analysis of the flow field induced by a symmetrical suction elbow at the pump inlet”, IOP Conference Series - Earth and Environmental Science, 49(3), 032014.
[74] Drăghici I., Muntean S., Bosioc A.I., Anton L.E., 2014, ”LDV measurements of the velocity field on the inlet section of a pumped storage equipped with a symmetrical

suction elbow for variable discharge values”, IOP Conf. Series: Earth and Environmental Science, 22, 032017, pp. 1-9.

[75] Drăghici I.A., Muntean S., Bosioc A.I., Gînga G., Anton L.E., 2016, ”Unsteady pressure field analysis at pump inlet equipped with a symmetrical suction elbow”, Proc. of the Romanian Academy Series A: Mathematics, Physics, Technical Sciences, Information Sciences, 17(3), pp. 237-244.

[76] Gînga G., Stanciu I.R., Muntean S., Baya A., Anton L.E., 2012, ”3D numerical flow analysis and experimental validation into a model impeller of a storage pump”, Proc. 15th Int. Conf. on Fluid Flow Technologies, Budapest, Hungary, pp. 804 – 811.

[77] Rakusch C., Senn F., Guggenberger M. and Jaberg H., 2016, ”A new measurement and data acquisition system for field acceptance tests using thermodynamic method”, Proc. of IGHEM (Linz), p 554.

[78] Lanzersdorfer J., Schmidt M. and Pichler J., 2016, ”Flow rate evaluation in parallel pump arangements: two case studies”, Proc. of IGHEM (Linz), p 545.

[79] Larreategui A. and Walsh J. T., 2014, ”Improving the accuracy on the efficiency measurements in the acceptance tests of hydraulic machines: a nice lesson for manufacturers, utilities, engineers and independent testers”, Proc. of IGHEM (Itajuba), p 384,

[80] Schwery A., Abgottspon A. and Staubli T., 2012, ”Field and laboratory experience with a clamp-on accoustic transit time flow meter”, Proc. of IGHEM (Trondheim), p 357.

[81] Cote E. and Proulx G., 2012, ”Experiments with thermodynamic method”, Proc. of IGHEM (Trondheim), p 361.

[82] Brekke H., 2012, ”A proposal for improving the thermodynamic method”, Proc. of IGHEM (Trondheim), p 362.

[83] Rau T. and Eissner M., 2012, ”Comparison of discharge measurements-thermodynamic to US clamp-on, stationary US and needle opening curve”, Proc. of IGHEM (Trondheim) p 363.

[84] Papa F., Radulj D., Karney B. and Robertson M., 2013, ”Pump energy efficiency field testing & benchmarking in Canada”, Proc. of Asset management for enhancing energy efficiency in water and wastewater systems, (Marbella).

[85] Cartright S. and Eaton B., 2009, ”Investigating energy savings in pumps and pumping system by the thermodynamic method”, Proc. of Pumps: Maintenance, Design, and Reliability Conference – IDC Technologies.

[86] Robertson M. and Rhodes I., 2008, ”Optimising and verifying energy savings in pumps and pumping”, Proc. of the 4th International Conference on Water and Wastewater Pumping Stations (Cranfield)

[87] Muhirwa A., Cai W.-H., Su W.-T., Liu Q.Z., Binama M., Li B. and Wu J., 2020, ”A review on remedial attempts to counteract the power generation compromise from draft tubes of hydropower plants”, Renewable Energy, 150, 743-764.

[88] Pasche S., Avellan F. and Gallaire F., 2019, ”Optimal Control of Part Load Vortex Rope in Francis Turbines”, J. Fluids Eng., 141, 081203.

[89] Ardelean T., Susan-Resiga R. F. and Muntean S., 2019, ”Vortex Breakdown in Decelerated Swirling Flows”, 9th Int. Conf. Energy and Environment, paper 013.
[90] Davidson, L., 2006, ”Evaluation of the SST-SAS model: channel flow, asymmetric diffuser and axi-symmetric hill”, European Conference on Computational Fluid Dynamics ECCOMAS CFD.
[91] Davidson, L., 2007, ”The SAS model: A turbulence model with controlled modeled dissipation”, 20th Nordic Seminar on Computational Mechanics, 2007, Göteborg.
[92] Fouratan, H., Yavuzkurt, S., 2014, ”A partially-averaged Navier-Stokes model for the simulation of turbulent swirling flow with vortex breakdown”, International Journal of Heat and Fluid Flow.
[93] Stein, P., Sick, M., Dörfler, P., White, P., Braune, A., 2006, ”Numerical simulation of the cavitating draft tube vortex in a Francis turbine”, Proc. 23rd IAHR Symposium on Hydraulic Machinery and Systems, 2006, Yokohama, Japan.
[94] R. Rizzo, A. Musolino, F. Bucchi, P. Forte, F. Fredo, 2015, "A multi-gap magnetorheological clutch with permanent magnet", Smart Materials and Structures, 24, 075012.
[95] F. Bucchi, Forte P., Fredo F., 2015, "Temperature Effect on the Torque Characteristic of a Magnetorheological Clutch", Mechanics of Advanced Materials and Structures, 22, 150-158.
[96] A. Bosioc, E. Beja, S. Muntean, I. Borbath, L. Vekas, 2016, "Experimental investigations of MR fluids in air and water used for brakes and clutches", 1st International Conference on Materials Design and Applications, to be published in Advanced Structured Materials – Springer.
[97] Tanasa C., Susan-Resiga R. F., Muntean S. and Bosioc A. I., 2013, ”Flow-Feedback method for mitigating the vortex rope in decelerated swirling flows”, J. of Fluids Eng., 135 (6).
[98] Tanasa C., Muntean S., Ciocan T. and Susan-Resiga R. F., 2016, ”3D Numerical simulation versus experimental assessment of pressure pulsations using a passive method for swirling flow control in conical diffusers of hydraulic turbines”, IOP Conf. Series: Earth and Environmental Science 49.
[99] Tanasa C., Ciocan T. and Muntean S., 2017, ”Numerical Assessment of Pulsating Water Jet in the Conical Diffusers”, AIP Conference Proceedings, 1906.
[100] Paul, E.L.; Atiemo-Obeng, V.A.; Kresta, S.M., *Handbook of industrial mixing,* John Wiley&Sons, Hoboke, NJ, USA, 2004.
[101] Murthy, B.N.; Ghadge, R.S., Joshi, J.B., ”CFD simulations of gas-liquid-solid stirred reactor: Prediction of critical impeller speed for solid suspension”, Chemical Engineering Science 2007, 62, 7184-7195.
[102] Gohel, S.; Joshi, S.; Azhar, M., ”CFD modeling of solid suspension in a stirred tank: Effect of drag models and turbulent dis-persion on cloud height”, International Journal of Chemical Engineering 2012, 2012, 9.

[103] Calvo, S.; Delafosse, A.; Collignon, M.L.; Crine, M.; Toye, D., ″Experimental characterization and modelling of homogeneous solid suspension in an industrial stirred tank″, Advances in Mechanical Engineering 2013, 2013, 9.
[104] Delafosse, A.; line, A.; Morchain, J.; Guiraud, P., ″LES and URANS simulations of hydrodynamics in mixing tank: Comparison to PIV experiments″, Chemical Engineering Research and Design 2008, 86, 1322-1330.
[105] Murthy, B.N.; Joshi, J.B., ″Assessment of standard k-ε, RSM and LES turbulence models in a baffled stirred vessel agitated by various impeller designs″, Chemical Engineering Science 2008, 63, 5468-5495.
[106] Panneerselvam, R.; Savithri, S.; Surender, G.D., ″CFD modeling of gas-liquid-solid mechanically agitated contactor″, Chemical Engineering Research and Design 2008, 86, 1331-1344.
[107] Ochieng, A.; Onyango, M.S., ″CFD simulation of solid suspension in stirred tanks: review″, Hemijska industrija 2010, 64, 365-374.
[108] Kasat, G.R.; Khopkar, A.R.; Ranade, V.V.; Pandit, A.B., ″CFD simulation of liquid-phase mixing in solid-liquid stirred reactor″, Chemical Engineering Science 2008, 63, 3877-3885.
[109] Montante, G.; Micale, G.; Magelli, F.; Brucato, A., ″Experiments and CFD prediction of solid particle distribution height in a vessel agitated with four pitched blade turbines″, Chemical Engineering Research and Design 2001, 79, 1005-1010.
[110] Micale, G.; Grisafi, F.; Rizzuti, L.; Brucato, A., ″CFD simulation of particle suspension height in stirred vessels″, Chemical Engi-neering research and Design 2004, 82, 1204-1213.
[111] Khopkar, A.R.; Kasat, G.R.; Pandit, A.B.; Ranade, V.V., ″Computational fluid dynamics simulation of the solid suspension in a stirred slurry reactor″, Industrial and Engineering Chemistry Research 2006, 45, 4416-4428.
[112] Micale, G.; Montante, G.; Grisafi, F.; Brucato, A.; Godfrey, J., ″CFD simulation of particle distribution in stirred vessels″, Chemical Engineering Research and design 2000, 78, 435-444.
[113] Wadnerkar, D.; Utikar, R.P.; Tade, M.O.; Pareek, V.K., ″CFD simulation of solid-liquid stirred tanks″, Advanced Powder Technology 2012, 23, 445-453.
[114] Montante, G. ; Bakker, A., ″Solid-liquid multiphase flow validation in tall stirred vessels with multiple impeller systems″, Technical notes, 2004.
[115] Hoseini, S.S.; Najafi, G.; Ghobadian, B.; Akbarzadeh, A.H., ″Impeller shape-optimization of stirred-tank reactor: CFD and fluid structure interaction analyses″, Chemical Engineering Journal 2021, 413.
[116] Valizadeh, K.; Farahbakhsh, S.; Bateni, A.; Zargarian, A.; Davarpanah, A.; Alizadeh, A.; Zarei, M., ″A parametric study to sim-ulate the non-Newtonian turbulent flow in spiral tubes″, Energy Science & Engineering 2020, 8(1), 134-149.
[117] De Lamotte, A.; Delafosse, A.; Calvo, S.; Toye, D., ″Identifying dominant spatial and time characteristics for flow dynamics within free-surface baffled stirred-tanks from CFD simulations″, Chemical Engineering Science 2018, 192, 12-142.

[118] Tembely, M.; Alameri, W.S.; AlSumaiti, A.M.; Jouini, M., ”Pore-scale modelling of the effect of wettability on two-phase flow properties for Newtonian and non-newtonian fluids”, Polymers 2020, 12, 22.

[119] Stachnik, M.; Jakubowski, M., ”Multiphase model of flow and separation phases in a whirlpool: Advanced simulation and phenomena visualization approach”, Journal of Food Engineering 2020, 274, 10.

[120] McCraney, J.; Weislogel, M.; Steen, P., ”OpenFOAM simulations of late stage container draining in microgravity”, Fluids 2020, 5(207), 16.

[121] Silva, M.F.; Campos, J.B.L.M.; Miranda, J.M.; Araujo, J.D.P., ”Numerical study of single taylor bubble movement through a microchannel using different CFD packages”, Processes 2020, 8(1418), 16.

[122] He, X.; Xu, H.; Li, W.; Sheng, D., ”An improved VOF-DEM model for soil-water interaction with particle size scaling”, Computers and Geotehnics 2020, 128, 12.

[123] Boffeta, G.; Celani, A.; De Lillo, F.; Musacchio, S., ”The Eulerian description of dilute collisionless suspension”, Europhysics Letters 2007, 78, 14001.